Doctoral Thesis in agreement with the cotutelle contract between:

Université Pierre et Marie Curie

and

Freie Universität Berlin

Positioning nuclei at the periphery of skeletal muscle cells

William Roman

Supervised by Dr. Edgar R. Gomes and Prof. Dr. Simone Spuler

Doctoral Thesis in agreement with the cotutelle contract between:

Université Pierre et Marie Curie

Doctoral School: Ecole Doctorale Complexité du Vivant, U974 Institut de Myologie

And

Freie Universität Berlin

Department of Biology, Chemistry and Pharmacy of the Freie Universität

Laboratory: Max Delbrück Center for Molecular Medicine

Positioning nuclei at the periphery of skeletal muscle cells

William Roman

Supervised by Dr. Edgar Gomes and Prof. Dr. Simone Spuler
Publically presented and defended on September 28th 2016

PhD Jury composed of:
Dr. Edgar R. Gomes (Director of research, thesis co-supervisor)
Prof. Dr. Simone Spuler (Professor, thesis co-supervisor)
Dr. Claudio Franco (Director of research, reviewer)
Dr. Jocelyn Laporte (Director of research, reviewer)
Dr. Vincent Mouly (Director of research, representative of the UPMC)
Prof. Dr. Sigmar Stricker (Professor, representative of the FU)
Dr. Ezequiel Mendoza (FU Post-doc)

Acknowledgements

I thank Dr Edgar Gomes for accepting me in his laboratory and entrusting me with this project. I thank him for scientific and life discussions and for mentoring me all along my degree scientifically and personally.
I thank Dr Simone Spuler for welcoming me in her laboratory and selecting me as part of the myograd PhD program.
I thank Dr Claudio Franco and Dr Jocelyn Laporte for accepting to be the reviewers of my thesis. I thank Dr Vicent Mouly, Prof Dr Sigmar Stricker and Dr Ezequiel Mendoza for accepting to be part of the members of my PhD jury.
I thank the founders of the MyoGrad Programme that made possible this enriching PhD in cotutelle: Prof Dr Simone Spuler, Prof Dr Thomas Voit and Dr Helge Amthor. I thank Susanne Wissler for essential support at the administrative level during all my PhD.
I thank the entire Gomes laborator members over the years:
Dr Sestina Falcone for her training at the start of my degree. Mother figure of my PhD, I thank her for my integration in the laboratory socially and scientifically.
Dr Bruno Cadot for his mentoring and patience. I thank him for his technical insights and captivating scientific ideas. I thank his kindness and his aptitude for keeping calm facing stressful or dangerous situations.
Dr Vincent Gache for being the comic relief of the initial stages of my PhD and for his scientific insights.
Petra Gimpel for her optimism and happiness as well as for her technical help and solutions.
Dr Valerie Vilmont for technical help and for making each day in the laboratory unpredictable.
Dr Yue Jiao for her sunny smile
Dr Jheimmy Diaz for her latin vibes
Jean-François Darrigrand for his lightness and arguably good jokes
Dr Judite Costa for her scientific input, kindness and honesty
Dr Vania Gloria for trying to get used to my jokes
Catia Janota for her energy and making me look organized
Catia Almeida for her happiness, jokes and accent in English
Telma Carrilho for my administrative integration in Portugal
Dr Patrica Costa for her natural and social support
Joao Martins for important technical assistance and pool mentorship
Mafalda Pimentel for scientific and technical help. For social and moral support and for reminding me that there is a life outside the laboratory.

I thank the IMM bio-imaging team (Antonio Temudo, Ana Almeida and Jose Henriques) for their technical assistance.

Table of Contents

Summary

Nuclear movements are important for multiple cellular functions and are driven by forces originating from motor proteins and cytoskeleton. During skeletal myofiber formation or regeneration, nuclei move from the center to the periphery of the myofiber for proper muscle function. Furthermore, centrally located nuclei are found in different muscle disorders. Using theoretical and experimental approaches, we demonstrate that nuclear movement to the periphery of myofibers is mediated by centripetal forces around the nucleus in combination with local changes of nuclear stiffness. The centripetal forces are generated by myofibril contraction, cross-linking and zipping around the nucleus. Local changes of nuclear stiffness are achieved by asymmetric distribution of lamin A/C. Beginning with *BIN1*, a gene mutated in centronuclear myopathies (CNMs), we identified the molecular cascade involved in nuclear movement to the periphery. We show that Amphipysin 2 (*BIN1*) is important for N-WASP recruitment which itself activates the Arp2/3 complex to induce actin polymerization. This cascade is important for nuclear movement to the periphery and transversal triad formation. This pathway is perturbed in certain patients harboring BIN1 mutations as it leads to mis-localized amphiphysin 2. Despite originating from the same pathway, peripheral nuclear movement and transversal triad formation are independent processes. An Arp2/3 complex containing Arpc5L together with γ-actin organize desmin to cross-link and zip myofibrils for nuclear movement whereas an Arp2/3 complex containing Arpc5 together with β-actin is required for transversal triad formation.

Resumé

Les mouvements nucléaires sont importants pour une multitude de fonctions cellulaires et sont induits par des forces produites par des protéines moteurs et le cytosquelette. Lors de la formation et régénération de myofibres, les noyaux migrent du centre à la périphérie de la cellule pour son bon fonctionnement. De plus, certaines maladies musculaires sont caractérisées par une accumulation de noyaux centraux. En utilisant une approche théorique et empirique, nous démontrons que le mouvement de noyaux vers la périphérie des myofibres est induit par des forces centripètes autour des noyaux ainsi que par des changements locaux de rigidité nucléaire. Ces forces centripètes sont générées par la contraction de myofibrilles et par leur réticulation autour des noyaux. Les changements de rigidité nucléaire relèvent d'une asymétrie de la distribution de la lamin A/C. En débutant par *BIN1*, gène muté dans les myopathies centro-nucléés (CNM), nous avons identifié la cascade moléculaire à l'origine du mouvement des noyaux. Nous montrons que l'Amphiphysin 2 (*BIN1*) est indispensable pour le recrutement de N-WASP, activateur du complexe Arp2/3 afin de promouvoir la polymérisation de l'actine. Cette cascade est nécessaire au mouvement des noyaux vers la périphérie et pour la formation de triades transversales. Cet enchainement est perturbé chez certains patients portant des mutations de BIN1 car cela affecte la bonne localisation de l'Amphiphysin 2. Bien que provenant de la même cascade, le mouvement des noyaux vers la périphérie et la formation transversale de triades sont des processus indépendants. Un complexe de Arp2/3 contenant Arpc5L avec la γ-actine organisent la desmine et donc la réticulation des myofibrilles important pour le mouvement nucléaire. En revanche, un complexe de Arp2/3 contenant Arpc5 avec la β-actine est nécessaires à la formation de triades transversales.

Zusammenfassung

Die gerichtete Bewegung von Zellkernen ist für eine Vielzahl von zellulären Funktionen entscheidend und wird durch Kräfte, die von Motorproteinen und dem Zytoskelett erzeugt werden, angetrieben. Während der skelettalen Muskelbildung oder Regeneration, wandern die Zellkerne für den Erhalt einer korrekten Muskelfunktion vom Zentrum zur Peripherie der Muskelfaser. Zentral lokalisierte Zellkerne sind ein Merkmal verschiedener Muskelerkrankungen.

Mit Hilfe theoretischer und experimenteller Methoden zeigen wir, dass die Bewegung von Zellkernen zur Peripherie der Muskelfaser durch zentripetale Kräfte um den Zellkern herum sowie durch lokale Veränderungen der Steifigkeit des Zellkerns vermittelt wird. Die zentripetalen Kräfte werden dabei durch die Kontraktion, Vernetzung und das Zusammenziehen der Myofibrillen um den Zellkern herum generiert. Lokale Veränderungen der Steifigkeit des Zellkerns werden hingegen durch asymmetrische Verteilung der Lamine A/C erzeugt. Ausgehend von *BIN1*, einem Gen, das in Zentronukleären Myopathien (CNMs, für engl. centronuclear myopathies) mutiert ist, haben wir die molekulare Kaskade identifiziert, die in der Bewegung des Zellkerns zur Peripherie involviert ist. Wir zeigen hier, dass Amphiphysin 2 (*BIN1*) entscheidend für die Rekrutierung von N-WASP ist, welches selbst den Arp2/3-Komplex zur Induktion der Aktinpolymerisation aktiviert. Diese Kaskade ist sowohl für die Bewegung des Zellkerns zur Peripherie als auch der transversalen Triadenbildung wichtig. Des Weiteren ist diese Abfolge in einigen Patienten mit *BIN1*-Mutationen gestört, da Amphiphysin 2 mislokalisiert ist. Obwohl die periphere Bewegung des Zellkerns und die transversale Triadenbildung von demselben Signalweg ausgehen, sind es doch zwei voneinander unabhängige Prozesse. Ein Arp2/3-Komplex, der Arpc5L enthält, organisiert zusammen mit γ-Actin Desmin, um Myofibrillen für die Bewegung der Zellkerne zu vernetzen und zusammen zu ziehen. Dahingegen wird ein Arp2/3-Komplex, der Arpc5 enthält, in Kombination mit ß-Actin für die Bildung von transversalen Triaden benötigt.

Introduction

I. Nuclear Movement

The nucleus is often portrayed as a fixed spherical organelle at the center of the cell. However, it was shown that the shape and the position of the nucleus vary across cell types and species. Such variations have steered researchers to explore the biological meaning of this plasticity. The position of the nucleus is relevant for many cellular processes such as cell division, cell migration and differentiation with probably much more to be discovered (Gundersen and Worman, 2013a). The various roles played by nuclear positioning underlie a diverse and complex system involving nuclear movement and anchorage. These processes were shown to be mediated by molecular players and involve the nuclear envelope and the plasma membrane.

I.1 The Nuclear Envelope (NE)

The nucleus is separated from the cytoplasm by two membranes, the outer nuclear membrane (ONM) and the inner nuclear membrane (INM). A complex, called the Linker of Nucleoskeleton and Cytoskeleton (LINC-complex) spans both of these membranes to connect the nucleoskeleton (lamins) and the cytoskeleton (thick, intermediate and thin filaments)(Crisp et al., 2006). The LINC-complex is composed of SUN proteins (Sad1 and Unc-83) and KASH (Klarsicht, Anc1 and Syne homology) proteins. SUN proteins are embedded in the INM to bind lamins and chromatin inside the nucleus whereas KASH proteins are embedded in the ONM bound to SUN proteins on one side, and cytoskeleton on the other. Although 5 genes code the SUN proteins, only two are majorly expressed (SUN1 and SUN2) (Starr and Fridolfsson, 2010). In mammals, five genes code for KASH proteins and are termed nesprins. Four of these five isoforms of nesprins bind different cytoskeletal entities in the cytoplasm. Originally, Nesprin 1 and Nesprin 2 were found to bind actin, Nesprin 3 to bind intermediate filaments and Nesprin 4 to interact with microtubules, however these pairing turned out to be more complex with nesprins being able to bind to more than one type of cytoskeleton (Figure 1)(Luxton et al., 2011)' (Zhang et al., 2001)' (Wilhelmsen et al., 2005)' (Roux et al., 2009).

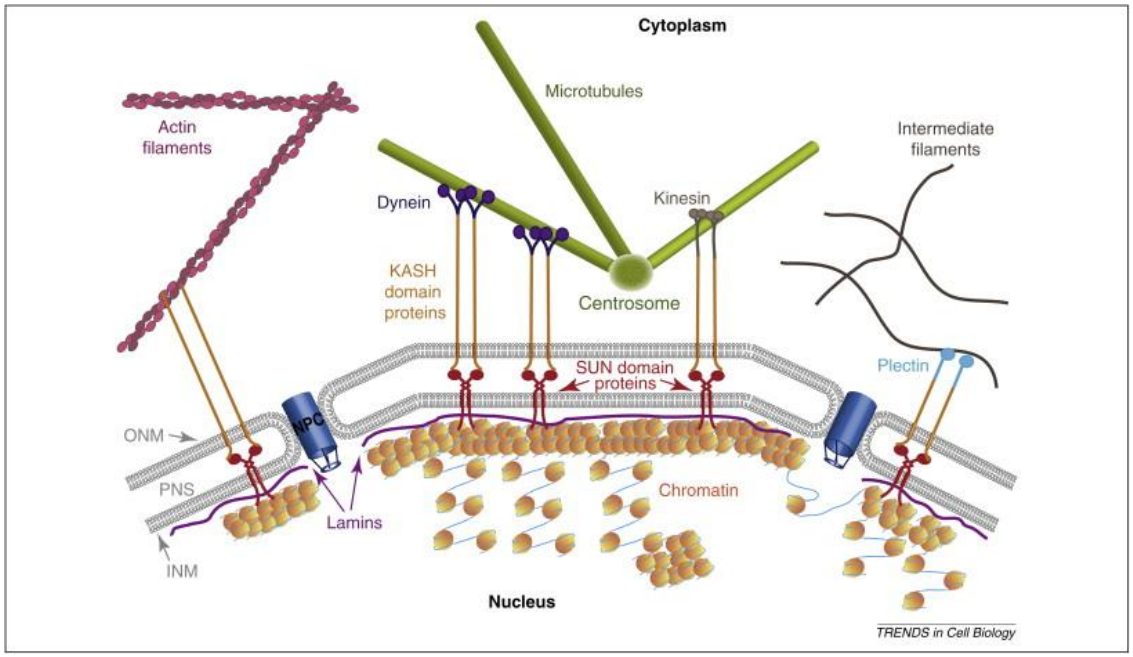

Figure 1. Illustration depicting LINC complexes connecting the nucleus with the cytoskeleton with varying nesprin isoforms and binding different cytoskeleton. Adapted from (Gerlitz and Bustin, 2011)**.**

I.2 Lamins

Lamins are nuclear intermediate filament (IF) proteins and are the major cytoskeleton component of nuclei. Lying just beneath the INM, lamins have been implicated in nuclear dynamics and gene regulation. Humans possess three different lamin genes termed *LMNA* (encoding lamins A which can be spliced to other isoforms, forming lamin A/C), *LMNB1* (encoding lamin B1) and *LMNB2* (encoding lamin B2). The *LMNA* gene is expressed in differentiated cells, while at least one lamin B gene is expressed in every somatic cell in the body (Gruenbaum and Medalia, 2015). Lamin A/C and Lamin B form different networks *in vivo* despite their ability to dimerize *in vitro*. It was however recently shown that these two networks interact (Shimi et al., 2008). Lamins share a similar structure to other IFs as they are constituted of a short N-terminal (head) domain, a central (rod) domain composed of four α-helical domains (coils 1A, 1B, 2A, and 2B) that are separated by linker regions (L1, L12, and L2), and a globular C-terminal (tail) domain that contains lamin-specific motifs, including a nuclear localization signal, an immunoglobulin (Ig) fold motif, and a C-

terminal CaaX motif (Gruenbaum and Foisner, 2015). Lamin A and B differ in their post-translational processing and binding partners (Figure 2) (Simon and Wilson, 2013).

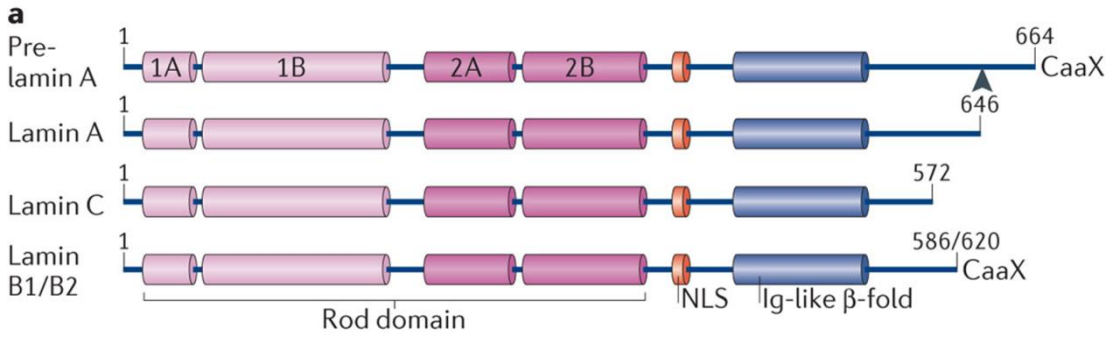

Figure 2. Illustration depicting the different lamin isoforms.
Adapted from (Burke and Stewart, 2012).

Study of the A- and B- type lamins has revealed that these isoforms play different roles in the cell. Lamin A is found to be mostly expressed in differentiating cells and is not expressed in embryonic stem cells or the nervous system (Davidson and Lammerding, 2014) (Jung et al., 2012). On the other hand, B-type lamins are expressed in all cell types and found to be necessary for organogenesis (Kim et al., 2011). Lamin B may therefore be more crucial for development and more specifically for the establishment of the central nervous system. This could explain why most lamin mutations are found in *LMNA* rather than *LMNB1* or *LMNB2* as mutations in these two latter genes may be lethal early on in development.

Secondly, Lamin A/C deficient nuclei were more prone to breakage (Vos et al., 2011) and deformability (Lammerding et al., 2004a) than lamin B (Lammerding et al., 2006). This suggests that lamin A/C is more important for nuclear rigidity. This is reinforced by the fact that there is a strong correlation between the ratio of lamin A/lamin B and tissue stiffness (Swift et al., 2013).

Lamins are also involved in nuclear positioning. They are part of the LINC complex through their interaction with SUN proteins and therefore participate in linking the nucleus to the cytoskeleton (Ostlund et al., 2009). It was shown that Lamin A mutations found in muscle disorders prevents the binding to TAN lines and thus nuclear movement (Folker et al., 2011). Lamin B1 deficient nuclei were observed to rotate extensively suggesting a role of lamin B1 for nuclear anchoring (Ji et al., 2007) whereas

lamin B2 deficient neurons were unable to migrate possibly due to defects in nuclear translocation (Coffinier et al., 2010).

The disruption of the nucleo-skeletal coupling may also have other ramifications. Lamins are in direct contact with chromatin and are therefore involved in signal transduction from the cytoplasm. Lamin A deficient cells have an attenuated response to mechanical or cytokine simulations with decreased NF-kappaB transcription (Lammerding et al., 2004a). Lamin A/C also binds to transcription factors such as c-Fos, ERK1/2, SREBP1, and pRb and may therefore have a direct role on gene expression, independent of cytoskeleton mechano-transduction (Simon and Wilson, 2013).

I.3 The Cytoskeleton

The cytoskeleton is segmented into three types of filaments: thick, intermediate and thin. The versatility of these filaments permits them to play diverse roles in the cell. The differences between the three types of skeletal filaments rely on their building blocks: the protein monomers. The organization of the monomers determines the width of the filaments but obey the same principles concerning their length. Polymerization and de-polymerization of the monomers allows these filaments to vary their length and be highly dynamic. Thick filaments also known as microtubules (MTs) are 24 nm in width and arise in most cells from the centrosome, a Microtubule Organizing Center (MTOC). The building blocks of microtubules are tubulin monomers which exist in alpha and beta form. Microtubules have a wide range of functions but are mostly known to be involved for maintaining cell shape and vesicle transport (Margolis and Wilson, 1981). Intermediate filaments exist in a variety of form as the building blocks that compose them are multiple. Intermediate filaments are on average 10 nm in diameter and serve many functions mostly involved in cell or nuclear shape, cell adhesion and cell organization (Geiger, 1987) but the extent of their role in nuclear movement remains relatively unexplored. Microfilaments, also known as actin filaments, are composed of actin monomers and form 7 nm thick filaments. They are crucial for cell shape and migration (Carlier, 1990). An entire chapter will be dedicated to actin later. Microtubules and actin filaments are the main cytoskeletal entity studied when exploring nuclear movement.

I.4 The Plasma Membrane (PM)

The plasma membrane plays the role of the interface between the inside of the cell and its environment. It is therefore the area where external signals are received, some of which were shown to influence nuclear movement. The serum factor lysophosphatidic acid (LPA) acts on a cell surface G-protein-coupled receptor to activate Cdc42 to initiate cell migration and therefore nuclear movement (Gomes et al., 2005) (Palazzo et al., 2001). As well as playing a signaling role, the plasma membrane is an anchor for the cytoskeleton linked to the nuclear envelop. As such, the plasma membrane is also important as a base on which the cytoskeleton can exert a force on the nucleus as will be seen in certain types of nuclear movements.

I.5 Types of nuclear movement

Nuclear movements across cell types and organisms are quite diverse, hinting to the probability of a variety of underlying mechanisms driving these movements (Figure 3). The various players involved in nuclear movement provide a rich toolbox for the cell to exploit. This section will review the different types of nuclear movement described excluding those observed during cell division which are beyond the scope of this thesis.

When MTs are recruited to influence nuclear dynamics, the nucleus migrates parallel to the microtubules. MT-dependent nuclear movement can be divided into motor-driven and non-motor-driven movements. Motor-driven movements are characterized by motor proteins such as kinesins and dyneins that exert a driving force by linking the nucleus to the MTs and walking along the MT. The nucleus is thus treated similarly to a vesicle (Starr and Fridolfsson, 2010). These types of movements are mostly observed in the developmental stages of a wide range of organisms (Mosley-Bishop et al., 1999) (Tsai et al., 2010) (McKenney et al., 2010). MT-dependent movement may also occur without motor proteins. Such movements were observed before cellular division in yeasts, drosophila oocytes, c.elegan embryos or mammalian cells (Gönczy et al., 1999; Levy and Holzbaur, 2008; Tran et al., 2001; Zhao et al., 2012). The mechanism of this movement relies on the attachment of the MT to the plasma membrane on one end and the nucleus on the other. Polymerization and depolymerization of MTs then exert either a pushing or pulling force on the nucleus (Adames and Cooper, 2000).

Intermediate filaments (IF) were also observed to drive nuclear movement. As stated previously, cytoplasmic IF-dependent nuclear movement has been poorly investigated. It was however demonstrated that the meshwork of IFs in the cytoplasm was essential for nuclear movement in migrating cells. Recent work showed a more direct interaction between the IF subtype vimentin and the nuclear envelope (through Nesprin 3) to move the nucleus in 3D migrating cells. The nucleus in this type of movement is used as a piston to create differential pressures at different areas of the cell and enabling lobopodial movement (Petrie et al., 2014).

Actin-dependent nuclear movements are observed in migrating cells during which the nucleus migrates to the rear of the cell. Localization of the nucleus from a central to a rear-end position was shown to be an active process mediated by actin filaments that run perpendicular to the movement of the nucleus (Desai et al., 2009)' (Gomes et al., 2005). These actin cables are bound to the LINC complex (nesprin 2 and SUN2) and can be visualized on the dorsal side of the nucleus. The Nesprin 2 and SUN2 complex are termed transmembrane actin-associated nuclear (TAN) lines. The exact mechanism of how these perpendicular lines drive nuclear movement remains elusive (Borrego-Pinto et al., 2012; Folker et al., 2011). Another type of actin-dependent movement can be observed in drosophila nurse cells where the nucleus migrates from the center of the cell to its side. Actin cables grow from the plasma membrane and make contact with the nuclear membrane. Steady polymerization of these actin cables pushes the nucleus to the side (Huelsmann et al., 2013a). This is distinct to other actin-related movements that usually exert force by actomyosin contraction. For example, it was shown that neurons migrating in confined spaces push the nucleus towards the leading edge. This push forward is believed to be mediated by an actomyosin net behind the nucleus that contracts and projects the nucleus towards the leading edge (Friedl et al., 2011; Solecki et al., 2009). It has also recently been found that actin can play an indirect role in nuclear movement. In mice oocytes, which lack centrosomes, active diffusion creates a pressure gradient which retains the nucleus in the center of the cell (Almonacid et al., 2015a).

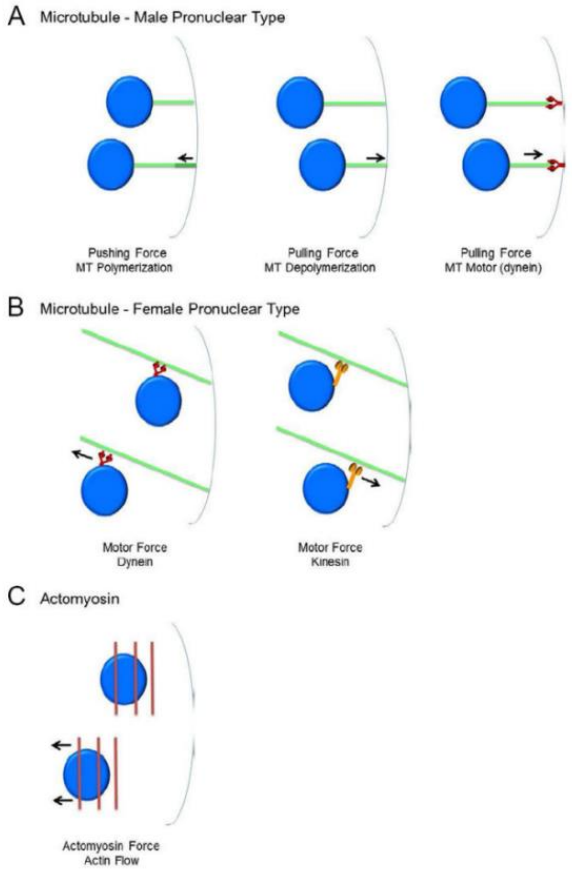

Figure 3. Illustration of nuclear movements driven by different mechanisms and cytoskeletal entities.
Adapted from (Gundersen and Worman, 2013)

I.6 Nuclear Movement in Skeletal Muscle

The mature myofiber (muscle cell) results from the fusion of numerous myoblasts. It is reported that on average between 100 to 150 nuclei can be found in a myofiber originating from that many myoblasts (Lei et al., 2009). In a mature myofiber, these nuclei are positioned at the periphery. Nuclei are equally spaced out along the length of the fiber except below the neuromuscular junction in which aggregates of 4 – 7 nuclei can be found (Grady et al., 2005). It was also reported that nuclei get anchored along the vasculature irrigating the myofiber (Ralston et al., 2006). Nuclei pursue a long voyage during muscle differentiation before being anchored at the membrane. Many nuclear movements can be observed during muscle differentiation each with their own underlying mechanisms (Figure 4).

Centration

When a myoblast fuses with an existing myotube, its nucleus migrates to the center of the myotube to join the other nuclei already present. This process was shown to be MT-dependent and driven by the dynein motor protein (Cadot et al., 2012a). During the initial myofiber differentiation stage, Par6 is recruited to the nuclear envelope (NE) and activated by Cdc42 to regulate dynein-dependent MT polarization. The proposed mechanism is a pulling of the MTs emanating from the migrating nuclei by the dynein motor anchored at the nuclear envelope of the nuclei cohort at the center.

Spreading

After myoblast fusion, nuclei align on the same plane in the growing myotube. Nuclei then disperse parallel to the elongating myotube. This longitudinal movement along the fiber is accompanied by rotation of nuclei. Two mechanisms were proposed to explain nuclear movement: (1) the translocation of the nuclei longitudinally and (2) the rotation of the nuclei. The first mechanism (translocation of the nuclei) was found to be dependent on microtubules, Kinesin Kif5b and the Microtubule Associated Protein Map7 (Metzger et al., 2012a). In this model, the microtubules stemming from nuclei overlap to create a network of anti-parallel microtubules. The kif5b/Map7 complexes exert a pushing force by walking towards the (+) ends inducing spreading of nuclei. The second movement (rotation of nuclei) was shown to involve the LINC complex, kif5b and to a lesser extent dynein. The proposed model is that kif5b and dynein at the NE walk on a network of similarly polarized MTs. Kif5b complexes walk towards the (+) end and dynein the (-) end resulting in rotation of the nucleus and net movement in a specific direction (Wilson and Holzbaur, 2015a). Evidence for dispersion movement in both these models shows the involvement of MTs, the LINC complex and motor proteins.

Dispersion

After dispersion, nuclei migrate to the periphery of the myofibers. How this process occurs is the focus of this thesis as very little is known about this mechanism. However, many muscle disorders as well as muscle regeneration display centrally located nuclei. Hence, understanding how nuclei migrate to the periphery of myofibers is a central question in muscle biology.

Anchoring

Nuclei are anchored at the periphery of myofibers just below the plasma membrane. This positioning at the periphery is not a random process as nuclei are evenly spread out across the fiber (Bruusgaard et al., 2003). It was shown that vascular contact with the myofiber could be a nuclei attractant whereas desmin, an IF, works as a repellent between nuclei (Ralston et al., 2006). Mis-localization of nuclei at the periphery was observed when the LINC complex is disrupted (when SUN and nesprin proteins are impaired) (Elhanany-Tamir et al., 2012a; Lei et al., 2009; Zhang et al., 2010, 2007). Anchoring of nuclei under the muscular junction (NMJ) operates through a different mechanism since many nuclei are aggregated. Nuclear anchoring below the NMJ appears to be strongly linked to the high concentration of acetyl-choline receptors (AchR) in that area. Musk (muscle-specific receptor tyrosine kinase) and Lrp4 (Low-Density Lipoprotein Receptor-Related Protein 4) are two receptors that form a complex sensitive to agrin. Activation of these receptors recruits AchRs (Kim et al., 2008). Musk patterning is similar to that of nesprins in these myonuclei (Apel et al., 2000). The link between AchR concentration and nuclei aggregation remains weak and mostly unexplored.

Nuclear movement in muscle is diverse. Most players involved in nuclear movement in other cell types are at play in muscle which makes it a great model to study nuclear positioning. The transitions between the different movements have largely been unexplored as we are only beginning to dissect the underlying mechanisms driving these movements. Movement of the nuclei from a central position to the periphery will be the central theme of this thesis.

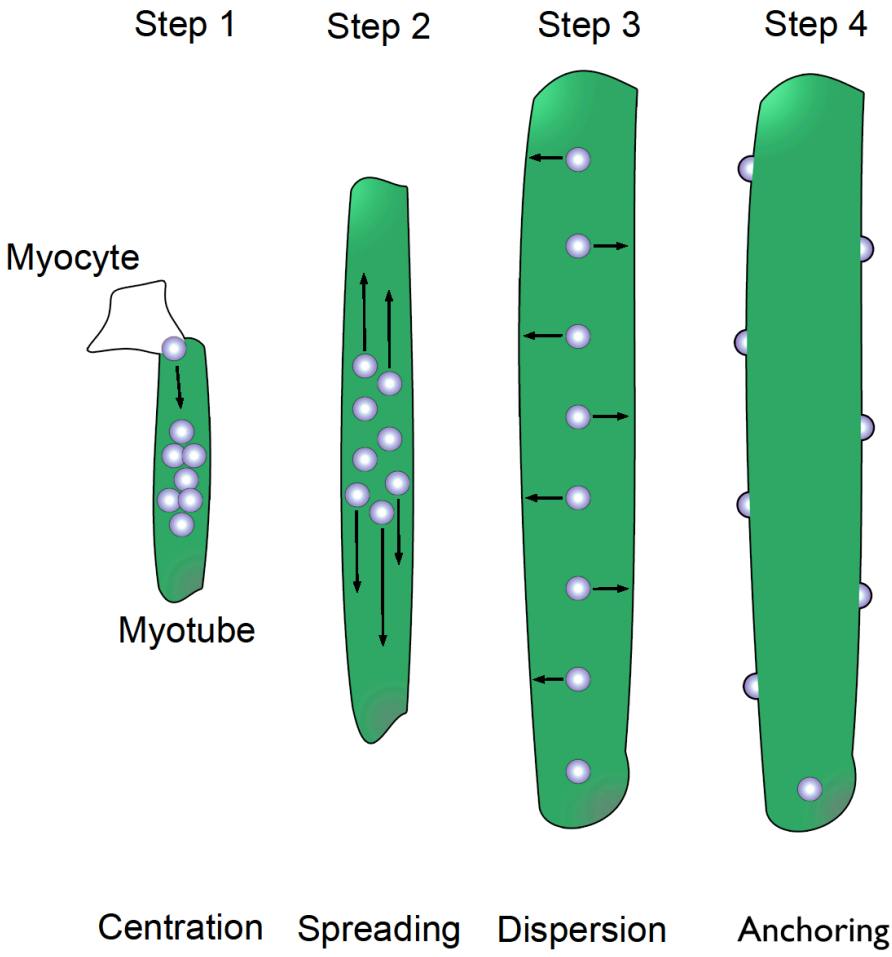

Figure 4. Illustration depicting the sequential movements of nuclei during skeletal muscle development.

II. Skeletal Muscle Physiology

II.1 Muscle structure

Skeletal muscle is the organ responsible for voluntary movement. Essential in our everyday life, the muscle cell is constructed to be efficient and reliable which stems primarily from its unique structure. The muscle is built similarly to a Russian doll with cylindrical structures encapsulated one into the other. The smallest unit is the sarcomere, which is the base of the contraction. Sarcomeres are stacked one after the other and bundled to form myofibrils. The sarcomere is composed of actin and myosin filaments organized in parallel. Actin filaments (thin filaments) and myosin (thick filaments) overlap and are linked by myosin heads which are the motors of muscle contractility. Lines and bands have been assigned to different compartments of the sarcomere. Sarcomeres are encapsulated into a tubular structure termed myofibrils. Like

the parallel alignment of sarcomeres that compose the muscle, myofibrils are cylindrical and aligned parallel to each other. Myofibrils are encapsulated by the muscle cell (aka myofiber or myocyte). The muscle cells are themselves aligned in parallel and span most of muscle length. Muscle cells are grouped in fascicles, themselves bundled into the perimysium, connective tissue surrounding the muscle.

II.2 The Myofiber

The myofiber (the muscle cell) is, as stated previously, the outcome of the fusion of many myoblasts. Its length spans most of the muscle. The space in myofibers is occupied mostly by myofibrils (Vander, 2011). The other components of the cell are jammed in between the sarcomere-composed myofibrils. Of note, mitochondria are heavily present in muscle as sarcomeric contraction is metabolically demanding. Skeletal muscles also possess an organelle named the sarcoplasmic reticulum (SR). In contrast to the endoplasmic reticulum (ER) which is involved in protein modification and transport, the main role of the SR is to store calcium and release it for muscle contraction. Calcium is the trigger of muscle contraction as it initiates a conformational change in the proteins associated with actin filaments of the sarcomere. This results in the exposure of myosin head binding sites on actin, which induces contraction. The nucleus is, as stated previously, localized at the periphery of the cell. The proposed hypothesis for its localization is that an organelle as large as the nucleus in the cytoplasm would deviate the parallel alignment of myofibrils. Growing evidence shows that central localization of the nucleus directly impairs muscle function (Metzger et al., 2012b).

II.3 Desmin

Desmin is one of the 73 intermediate filament proteins (Eriksson et al., 2009) and is expressed in cardiac and skeletal muscle (Hnia et al., 2014). Desmin is a type III intermediate filament protein of 53 kDa and is composed of a central α-helical rod domain flanked by non-helical domains (Goldman et al., 2012). Desmin surrounds the z-lines of myofibrils thereby linking them to one another. In adult skeletal muscle desmin is the main intermediate filament present (Capetanaki et al., 2007). However at the myoblast stage, the main type III intermediate filament is vimentin. It is during muscle development that desmin integrates pre-existing vimentin filaments to form longitudinal strands. This organization shifts into a transversal organization at the z-line

later on in myofiber maturation (Barbet et al., 1991). The transversal organization of desmin is important for crosslinking of myofibrils. Desmin plays further structural role in muscle such as for the sarcolemma (Rybakova et al., 2000), mitochondria (Hnia and Laporte, 2011), the sarcoplasmic reticulum (Amoasii et al., 2013) and nuclear positioning (Staszewska et al., 2015). It is therefore not surprising that mutations in the *DES* gene encoding for desmin leads to sever structural defects. Desmin is linked to most organelles through a cytoskeleton linker called plectin. Different isoforms of plectin exist and allow the binding of desmin to different organelles (Figure 5)(Winter and Wiche, 2013).

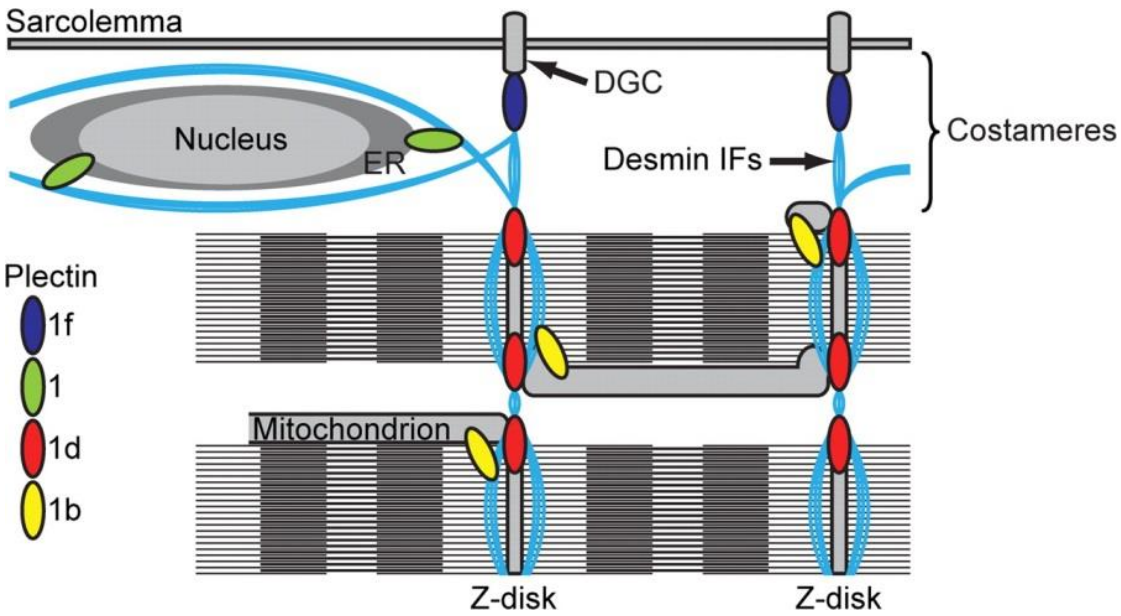

Figure 5. Illustration showing desmin and plectin isoform organization in skeletal muscle cells.
Adapted from (Konieczny et al., 2008).

II.4 Triads

Triads are a specialized compartment in the muscle responsible for excitation-contraction coupling (E-C coupling). The triad is composed of a T-tubule surrounded on both side by the SR, together, this forms a membrane structure localized on each side of the z-line (Al-Qusairi and Laporte, 2011a). T-tubules are invaginations of the plasma membrane and form a network spanning the entire depth of the muscle. Only a specific portion of the SR is associated with triads and is called the terminal cisternae. The role of triads is to convey and transduce the electrical depolarization of the membrane for the release of calcium from the SR. This membrane system that infiltrates the entire depth of the muscle is important for a uniform and synchronized contraction. The pairing of T-tubules and the SR results in a succession of membranes (10 nm between SR and T-tubules). Channels in the T-tubules and the terminal cisternae (SR) bridge theses membrane compartments. The voltage-dependent calcium channel (CACNA1S), also known as the dihydropyridine receptor (DHPR), is embedded in the T-tubule membrane whereas the ryanodine receptor (RyR1) is in the SR membrane. Both channels are linked and are at the center of the E-C coupling mechanism. DHPR an Ryr1 can be seen by electron microscopy (EM) as characteristic "feets" (Figure 6)(Rebbeck et al., 2014).

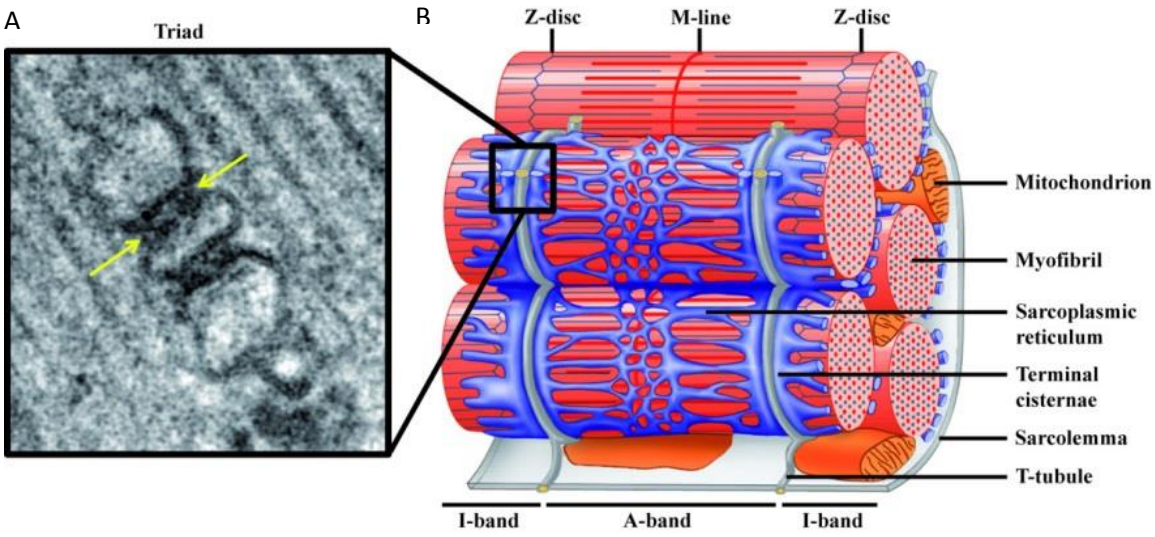

Figure 6. A. Electron microscopy image of triads. Yellow arrows represent the RyR "feet". B. Illustration of the localization of triads relative to sarcomeres.
Adapted from (Al-Qusairi and Laporte, 2011).

The DHPR is a voltage-gated channel of 5 subunits of which the α_1 is the most studied and most important (Bannister, 2007; Dirksen, 2002). The α_{1s} is a canonical voltage-gated ion channel with four membrane inserted repeats, each containing six trans-membrane helices. Helices 5 and 6 of each membrane repeats line the inside of the channel. Helices 4 are positively charged and are the potential sensors across the membrane. The four membrane repeats are linked by cytoplasmic loops. Loop I-II possesses a binding site for the other essential subunit of DHPR: the β subunit (Rousset et al., 2005). The loop linking repeat II and III allows for the DHPR to fold in a tetrad and for binding to RyR1. Many chimera studies playing with this loop were performed to investigate the importance of this segment (Beam and Bannister, 2010; Cui et al., 2009; Grabner et al., 1999; Nakai et al., 1998). Both loop III-IV and the C-terminal tail of α_{1s} also bind RyR1 and mutations in these segments impair E-C coupling (Tang et al., 2002; Weiss et al., 2004). Across from the T-tubule membrane is the SR membrane in which is embedded the RyR1, a calcium homotetramer. Knock out mice of the RyR1 die prenatally of respiratory failure (Galeotti et al., 2008). RyR1 bound to DHPR become activated by conformational change of the DHPR. However, the ratio of RyR1 to DHPR is 4:1 in triad which puts forward the idea that RyR1 can become activated without being bound to DHPR, either by surrounding RyR1 conformational changes or directly by Ca^{2+} (Renganathan et al., 1997). The RyR homotetramer was found to be 2.2 MDa. About $4/5^{th}$ of the protein is the cytosolic N-terminus which binds DHPR and many other regulators. The C-terminus contains the transmembrane domain and the selectivity pore (Amador et al., 2013). RyR1 is not highly selective for cations and undergoes a wide spread conformational change between its open and closed state (Ludtke et al., 2005). Chimeric studies in RyR1 were not as straight forward as in DHPR and although the SPRY2 domain of the RyR1 is the most probable candidate for DHPR binding, further experimentation is required (Casarotto et al., 2006; Cui et al., 2009; Kimura et al., 2007).

Many other proteins are found at the triad. The tight succession of membranes requires many scaffolding proteins to form and maintain triads. These include amphiphysin 2 (BIN1), dynamin 2 (DNM2), triadin, junctin, dysferlin or junctophilin. Other proteins are more involved in membrane trafficking like caveolin 3, myotubularin or a group of proteins called mitsugumins (Al-Qusairi and Laporte, 2011a).

Triad formation and maturation was mostly studied in mice and was found to occur over several weeks starting before birth and ending about 3 weeks after birth (Flucher, 1992; Takekura et al., 2001). T-tubules originate at around E15 first as small invagination of the plasma membrane. The network of tubules develops during E16 and E17 and is mostly longitudinally organized (parallel to the myofibers). The SR appears to be present before T-tubules and RyR1 feet can be seen sparsely and longitudinally at day E15. By E17 and E18. RyR1 stainings reveal transversal organization of the SR on both side of the z-line. SR development appears to parallel myofibrillogenesis. DHPR/RyR1 couplings, also referred to as calcium release units (CRUs), are not required for SR-T-tubule contact but a burst in CRUs was observed with T-tubule biogenesis. CRUs are therefore more present at the surface of the myotube at E15 and slowly become more apparent as the T-tubule network grows. At E17, a concentration of CRUs are observed at the A–I junction before they adopt a transversal orientation later in development. Maturation of triads is not a straight forward process, generation of dyads (only one SR per T-tubule), oblique T-tubules, absence of CRUs is often observed during development. To summarize the sequence of events: T-tubules begin to form longitudinally thus triggering SR/T-tubule junctions. CRUs become integrated rapidly at these junctions, first randomly and then longitudinally at the A-I interface. As T-tubules biogenesis pursues transversally to match terminal cisternae organization, CRUs follow the trend to become transversally organized.

III. Muscle Disorders

III.1 Centronuclear Myopathies (CNMs)

CNMs are genetically inherited disorders characterized by an accumulation of nuclei at the center of the fiber instead of at the periphery (Figure 7). These centrally located nuclei are not the result of degenerative/regenerative myofibers which exhibit centrally located nuclei in contrast to many degenerative myopathies. The severity of the phenotype in patients varies greatly from hypotonia in newborns to late onset muscle weakness in adults (Jungbluth et al., 2008). Besides the abnormal nuclear positioning phenotype, triads are deformed leading to E-C coupling impairments. Three types of CNMs were discovered based on the genes mutated. The most severe CNM is the recessive X-linked myotubular myopathy (XLMTM) caused by mutations in the *MTM1* gene. Mutations in the *DNM2* gene results in an autosomal form of CNM whereas mutations in *BIN1* lead to the autosomal-recessive form of CNM. Sporadic occurrences of CNMs have already been reported without any of these genes being mutated. The existence of additional causative genes must therefore be in play like mutations in the *RYR1* gene (Jungbluth et al., 2008). The three genes mutated in CNMs code for proteins found at triads and are involved in membrane trafficking (Jungbluth et al., 2008; Romero and Bitoun, 2011).

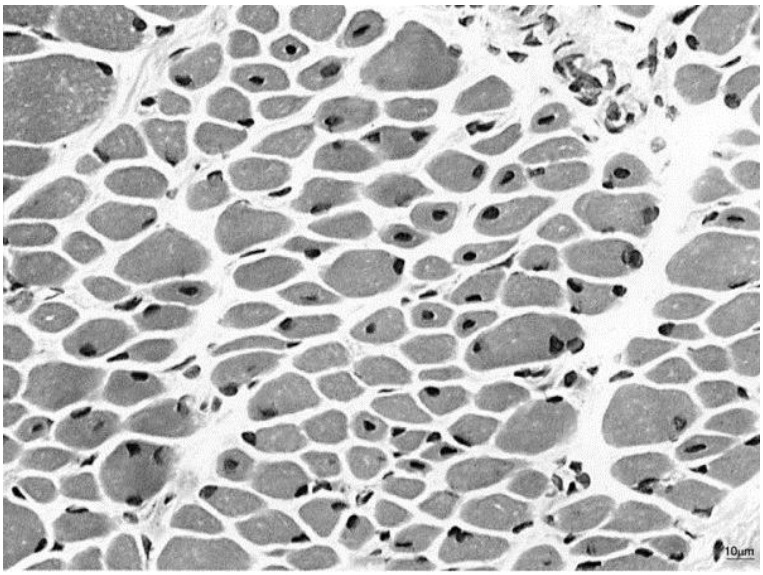

Figure 7. Light-microscopy image from cross-sectional cut of CNM patient exhibiting an accumulation of centrally located nuclei.
Adapted from (Jungbluth et al., 2008).

Amphiphysin 2 also termed bridging integrator-1 (BIN1) possesses a BAR domain and an amphipathic helix at its N-terminus. The positively charged BAR domain binds to the membrane to sense the curvature whereas the amphipathic helix inserts itself in it (Frost et al., 2009; Peter et al., 2004). The muscle isoform of BIN1 possesses a phosphoinositide (PI) binding motif which may be responsible to target BIN1 at T-tubules (Butler et al., 1997; Nicot et al., 2007a). A Myc-binding-domain (MBD) is also present in BIN1 and was found to inhibit c-Myc probably to slow proliferation (Sakamuro et al., 1996). The C-terminus of BIN1 contains a Src homology 3 (SH3) domain. The SH3 domain allows BIN1 to bind proline-rich motifs that may be found in proteins like dynamin 2 (DNM2) or Neuronal Wiskott–Aldrich Syndrome protein (N-WASP) (Owen et al., 1998; Yu et al., 1994). BIN1 has many cellular functions including membrane trafficking and remodeling, cytoskeletal dynamics, DNA repair, cell cycle and apoptosis (Toussaint et al., 2010). Bin1-related CNMs vary greatly in severity. Onset is usually not observed at birth but becomes evident for motor milestones later in development and includes muscular atrophy, diffuse weakness, facial dysplasia, ptosis, and varying degrees of ophthalmoplegia are usually present. Different mutations were found in *BIN1* which resulted in the CNM phenotype (Claeys et al., 2010; Nicot et al., 2007a). Mutations in the BAR domain or mis-splicing of the *BIN1* mRNA to skip the PI motif resulted in impaired tubulation capacities (Böhm et al., 2013). A mutation leading to the truncation of the SH3 domain has also been reported and leads to impaired intramolecular and DNM2 binding (Nicot et al., 2007a). Misregulated alternative splicing of *BIN1* were also found to cause myotonic dystrophy (DM) which share many clinical and histopathological features with bin1-related CNM. The genetic cause of DM was found to be mis-splicing of the mRNA to exclude the muscle-specific exon11 coding for the PI motif (Fugier et al., 2011a).

Dynamin 2 is a 98 kDa protein with a catalytic GTPase domain at its N-terminus. DNM2 is capable of self-assembly through a middle domain (MD) and is capable of interacting with membrane phosphatidylinositols at the membrane due to a pleckstrin homology domain (PH). DNM2 possesses a GTPase effector domain (GED) to regulate its GTPase activity and several SH3 motifs at its C-terminus which allows DNM2 to bind other proteins (Briñas et al., 2013). Dynamins are capable of self-

assembly resulting in tetrameric complexes with greater GTPase activity. This is essential for many cellular processes including membrane trafficking and remodeling (essential for clathrin-mediated and clathrin-independent endocytosis (Gold et al., 1999; Warnock et al., 1997)) and vesicular transport between the endosomal system and the Golgi apparatus (van Dam and Stoorvogel, 2002; Jones et al., 1998). DNM2 was reported to bind directly to actin or microtubules to promote faster dynamics (Herskovits et al., 1993; Mooren et al., 2009; Okamoto et al., 2001). Of note, DNM2 was shown to be part of a complex with cortactin and the Arp2/3 complex to promote actin branching during lamelopodial movement (Krueger et al., 2003). Focal adhesion disassembly was reported to be DNM2–mediated thereby influencing the cytoskeletal structure of the cell (Briñas et al., 2013). Finally, DNM2 was reported to play a role in apoptosis through its GTPase activity (Soulet et al., 2006). Mutations to DNM2 was linked to a rare form of Charcot–Marie-Tooth peripheral neuropathy (CMT) (Bitoun et al., 2008; Fabrizi et al., 2007) and autosomal dominant CNM (Bitoun et al., 2009; Echaniz-Laguna et al., 2007). *DNM2*-related CNM is slowly progressive and similarly to *BIN1*-related CNM, the severities vary greatly amongst affected patients but most common feature are delayed motor milestones, facial and generalized muscle weakness, ptosis, and ophthalmoplegia (Fischer et al., 2006). The mutations causing CNM were found in the MD thereby usually promoting DNM2 self-assembly, or the PH domain which is essential to recruit DNM2 to the membrane or the GED domain responsible for GTPase activity. Overall, mutations in DNM2 are linked with a loss of control of GTPase activity which is enhanced regardless of DNM2 self-assembly (Durieux et al., 2010).

Myotubularin 1 (MTM1) is 1 of the 14 proteins part of the myotubularin family. Myotubularins have both protein-protein and protein-lipid binding domains (Hnia et al., 2012). MTM1 is mostly known for its dephosphorylation of phospho-inositides (PIs) thus promoting their turnover (Blondeau et al., 2000; Taylor et al., 2000). PIs are signaling hubs for membrane trafficking and endocytosis. MTM1 binds PIs through its PH-GRAM (Pleckstrin homology-glucosyltransferases, rab-like GTPase activators and myotubularins) domain at its N-terminus (Choudhury et al., 2006; Tsujita et al., 2004). It can localize to the membrane thanks to a Rac-induced recruitment (RID) domain that targets it to the membrane (Laporte et al., 2002). MTM1 also possesses two protein-protein binding domain: SID (SETinteractingdomain) and PDZ (Previtali et al., 2003).

MTM1 is regulated by homo- or hetero-dimerization which done at its C-terminus through a coiled-coil (CC) domain (Berger et al., 2006). Finally, MTM1 exerts its desphosphorylating capacity with a PTP/DSP catalytic domain that contains the PTP signature $C(X)_5R$ necessary for enzymatic activity (Lecompte et al., 2008). The incidence of XLMTM is 2/100 000 male births in France. XLMTM is the most severe form of CNM as muscle weakness, external ophthalmoplegia and respiratory failure are present at birth (Jungbluth et al., 2008). When miscarriage does not occur, newborns often have development defects (Osborne et al., 1983; Teeuw et al., 1993). Mutations found to cause XLMTM include deletions/insertions, nonsense, missense and splice mutations. Most of these mutations occur between exon 8 and 12 coding for the catalytic PTP region of the MTM1 protein (Jungbluth et al., 2008).

III.2 Laminopathies

Laminopathies, which arise from mutations in the *LMNA* gene, can be subdivided into 4 distinct groups dependent on the tissue affected: striated muscles, adipose tissue, nervous system or systemic (accelerated aging syndrome). We will focus here on laminopathies with a muscle phenotype. The first mutation in *LMNA* was discovered in Emery–Dreifuss muscular dystrophy patients (EDMD) (Bonne et al., 1999). Two other skeletal muscle disorders followed, namely limb-girdle muscular dystrophy (LGMD-1B) (Muchir et al., 2000) and a congenital form of muscular dystrophy (L-CMD) (Quijano-Roy et al., 2008). These diseases are characterized by muscle wasting leading to muscle weakness and are accompanied by heart problems. Knock out mice models and derived cell lines have helped our understanding of lamin A/C function as discussed previously, but knock in models, recapitulating patient mutations have given a greater insight into the pathophysiology of lamin A-related muscle disorders (Azibani et al., 2014a). For example, the *Lmna*$^{H222P/H222P}$ mice were generated to reproduce the EDMD phenotype and many pathways such as the Smad/TGFβ, the mitogen activated protein kinases (MAPK) pathways or the Akt-mammalian target of Rapamycin (mTOR) were shown to be pathogenically activated (Arimura et al., 2005) (Muchir et al., 2007) (Choi et al., 2012). Other KI mouse models like the KI-*Lmna*$^{\Delta K32}$ mice for L-CMD have showed that these mutations lead to the mislocalization of lamin A/C from the NE to the cytoplasm (Bertrand et al., 2012). Greater understanding of the mechanisms underlying these diseases is expected to arise

with the reprogramming of cells from laminopathy patients into skeletal or cardiac muscle cells.

III.3 Desminopathies

Mutations in the *DES* gene coding for the desmin protein lead to desminopathies. As desmin is principally expressed in muscle, affected individuals develop myopathies or cardiomyopathies. The disease onset ranges from childhood to late adulthood to which there is currently no available treatment (Clemen et al., 2013a). Desminopathies are characterized by desmin-positive aggregates and degeneration of the myofibrillar machinery (Vajsar et al., 1993). The omnipresence of desmin in the architecture of muscle makes this disease a complex and multilevel issue directly affecting formation and maintenance of myofibrils but also mitochondrial function (Vernengo et al., 2010), central nuclear positioning (although believed to be due to degeneration/regeneration of myofibers)(Claeys et al., 2009) and cell signaling. Although mutations span the entire *DES* gene, skeletal muscle associated desminopathies are predominant in exon 6, which codes for the C-terminal half of the coil 2 domain. Mutations higher up in the gene are cardiac-related desminopathies. In vitro studies reproducing the coil 2 mutations of the *DES* gene demonstrated a strong impairment in the capacity for desmin to polymerize, ranging from irregular filament width and length to complete disturbance of pre-existing WT desmin networks (Bär et al., 2006). The impairment of desmin assembly does explain many of the phenotypes observed in desminopathies including its mislocalization into aggregates and organelle scaffolding issues.

IV. Molecular Pathways involved in Arp2/3 dynamics

IV.1.1 Nucleation Promoting factors (NPFs)

The field of nucleation promoting factors (NPFs) was made possible from the investigation of a disease named Wiskott–Aldrich syndrome (WAS), an X-linked recessive disorder. Symptoms are immunodeficiency, thrombocytopenia and eczema. The mutated gene was found to be solely expressed in hematopoietic cells and was

termed *WAS*. The hematopoietic cells of patients afflicted with WAS are very smooth at the surface guiding researchers to investigate WAS as a cytoskeleton regulator (Aldrich et al., 1954; Ochs and Notarangelo, 2005; Thrasher, 2002). Neuronal Wiskott–Aldrich syndrome (N-WASP) was later discovered in neurons as an interactor with growth-factor receptor-bound protein 2 (Grb2) (Miki et al., 1996). N-WASP is however not only expressed in neurons but many other cell types including skeletal muscle. N-WASP is involved in actin dynamics. A whole family of NPFs (WASP, N-WASP, WAVEs and JMY) was subsequently found with each member possessing subtle differences in their structures, allowing for fine tune cytoskeletal arrangements (Rottner et al., 2010).

IV.1.2 WASP and N-WASP

WASP and N-WASP are characterized by their C terminus, which is constituted of 3 domains: a verprolin-homology domain (V; also known as WASP-homology-2 domain (WH2)), a cofilin-homology domain (also known as central domain (C)) and anacidic domain (A). These three domains form the VCA region. The V domain binds monomeric actin G-actin whereas the CA domain binds the Arp2/3 complex, an actin nucleator (Pollard and Borisy, 2003; Takenawa and Miki, 2001). The VCA region is sufficient for Arp2/3 binding. Other domains of the protein control activation regulation of the protein. The N-terminus of WASP and N-WASP is a WH1 domain also known as the Ena-VASP-homology-1 (EVH1 domain), which allows WASP interacting proteins to bind (Volkman et al., 2002). These include WASP-interaction proteins (WIPs), corticosteroids and regional expression-16 (CR16) (Ho et al., 2001; Ramesh et al., 1997; Volkman et al., 2002). WIP binding stabilizes N-WASP in vitro and is thought to repress N-WASP activity (Martinez-Quiles et al., 2001) despite their role in recruiting N-WASP at actin dynamic hot spots (Ho et al., 2004). Mutations in the WH1 domain of WASPs are common in patients suffering from WAS (Ochs and Notarangelo, 2005). A basic region located after WH1 domain also regulates WASP proteins. This region was found to bind phosphoinositides (PIs) to induce N-WASP activation (Ho et al., 2004; Rohatgi et al., 2000). To complement PI-induced activation, WASP and N-WASP possess a CDC42/Rac-interactive binding domain (CRIB) or more commonly known as the GTPase-binding Domain (GBD) which, as its name indicates, is capable of binding small Rho GTPases (Hall, 1998; Miki et al., 1998). Finally, N-WASP and WASP have a proline rich domain capable of binding SH3 proteins (Prehoda et al., 2000). These

include Nck, Grb2, Dip, Spin90 or Amphiphysin 2, all have the capacity to activate N-WASP (Carlier et al., 2000; Rohatgi et al., 2000). N-WASP is in an auto-inhibited state under normal conditions. The protein is folded on itself as this confirmation is mediated by the basic domain, the CRIB domain and the proline-rich regions of the protein (Kim et al., 2000). The multitudes of proteins capable of binding or phosphorylating these regions play an integral part in the regulation of WASP and N-WASP.

IV.1.3 WAVE family and other NPFs

The WAVE family consists of WAVE1, WAVE2 and WAVE3 (Eden et al., 2002; Gautreau et al., 2004; Suetsugu et al., 2006). Like WASP and N-WASP, the WAVE family has a VCA region but only one V region instead of two like their WASP counterparts. They also possess basic and proline-rich regions. The differences between WASPs and WAVEs also lie at the N-terminus in which WAVE have a WAVE-homology domain (WHD) capable of binding other partners to WASPs (Gautreau et al., 2004; Leng et al., 2005). WAVEs lack the CRIB domain meaning that they are not directly regulated by small GTPases (Takenawa and Suetsugu, 2007). Activation of WAVEs is thus elicited through different pathways than WASPs. For a long time, WASPs and WAVEs were the only known NPFs but recent work has revealed a new class of NPFs which include WASH, WHAMM and JMY. WASH, WHAMM and JMY all have a VCA region but the amounts of V regions vary. WASH has a single V domain (like WAVEs), WHAMM possesses two (like WASPs) and JMY contains three (Rottner et al., 2010). At the N-terminus, WASH has a WASH-homology-domain (WAHD1) and tubulin binding region (TBR). Its binding partners are thus different to WASPs and WAVEs. WASH was found to be involved in endosome membrane assembly and vesicle trafficking at the trans-Golgi (Derivery et al., 2009; Duleh and Welch, 2010; Gomez and Billadeau, 2009) . WHAMM and JMY also have different domains at their N-terminus. WHAMM has a WHAMM membrane-interaction-domain (WMD) that targets it to the cis-Golgi where it is involved in membrane trafficking (Campellone et al., 2008). JMY can bind to the transcriptional regulator p300/CBP which augments the p53 response and is the only NPF that can nucleate actin independently of arp2/3 thanks to its three WH2 domains and a short actin linker

domain (L) (Shikama et al., 1999). JMY's function is less clear than the other NPFs but has been linked with cell motility and nuclear actin (Coutts et al., 2009).

The rich array of NPFs demonstrates the complexity of actin dynamics in the cell. The different partners and the different localization of NPFs allows for specific regulations of their activities in unique areas of the cell. Overall the plurality of NPFs helps to fine tune cytoskeletal rearrangements in the cell.

IV.1.4 N-WASP activation

In its normal state, N-WASP's GBD domain binds part of the VCA domain thereby preventing Arp2/3 to be recruited. Auto-inhibited N-WASP is still capable of binding G-actin. The GBD region thus binds the CA portion of the VCA region. In vitro, the auto-inhibitory confirmation of N-WASP can be released when Cdc42 binds to the GBD, by phophoinositides at the basic region or by SH3 containing proteins (Nck, Grb2 or BIN1). However, in vivo, the WIP/N-WASP complex, which keeps N-WASP inactivated, overrules activation by Cdc42, SH3 containing proteins or PIs.

N-WASP was found to play a role in a multitude of cellular processes. N-WASP is closely associated with the membrane through its proline-rich repeats and therefore drives many of the cytoskeletal rearrangements in membrane trafficking and remodeling. It was found to be involved in endocytosis, vesicle trafficking, cellular motility, focal adhesion assembly and filopodium, podosome and invapodium formation.

IV.2 The Arp2/3 complex

Arp2/3 is a 7 subunit complex involved in actin dynamics. Following nucleation of an actin mother filament, Arp2/3 generates a daughter filament stemming from the mother filament at a 70^{o} angle from this latter. Arp2/3 is therefore involved in branching actin networks (Campellone and Welch, 2010).

First purification of the Arp2/3 complex revealed it was composed of 7 polypeptides (Figure 8) (Machesky et al., 1994). Arp2 and Arp3, two of the

polypeptides discovered, are actin related and gave the name to the protein. The most drastic conformational changes for the complex to become active are mediated by Arp2 and Arp3 which enables these subunits to interact with the pointed end of the mother filament. The structure of Arp2 and Arp3 is so similar to actin that they form the first two subunits of the daughter filament (Rouiller et al., 2008). The remaining five subunits were named in order of their molecular weight but are now referred to as Actin related protein complex-1 (Arpc1), Arpc2, Arpc3, Arpc4 and Arpc5. Arpc1 exists in two isoforms: Arpc1A and Arpc1B. The Arpc1 subunit is a WD-repeat protein which participates in the assembly of the complex and is a seven-bladed-propeller protein (Goley and Welch, 2006). Arpc2 forms with Arpc4 the core of the complex with other proteins organized around them. The Arpc2/Arpc4 heterodimer is the main site of interaction with the mother filament while anchoring Arp3, the first subunit of the daughter filament (Gournier et al., 2001a; Machesky and Insall, 1998; Zhao et al., 2001). Arpc3 and Arpc5 are primarily α-helical and are the most peripheral of the subunits (Goley and Welch, 2006). Arpc3 was found to be essential for NPF binding and stabilizes the link between Arp3 and the mother filament thereby stabilizing the complex in a closed state (Xu et al., 2012). Arpc5 exists in two isoforms: Arpc5 and Arpc5L. The α-helices of Arpc5 stabilize Arp2 to become the second subunit of the daughter filament. The arp2/3 complex is in an inactivated state under basal condition and undergoes a conformational change to bind and branch actin (Rouiller et al., 2008). The specifics of the conformation it adopts in its activated state remains unclear but certain principles were mapped. All seven subunits of the complex are in contact with the mother filament.

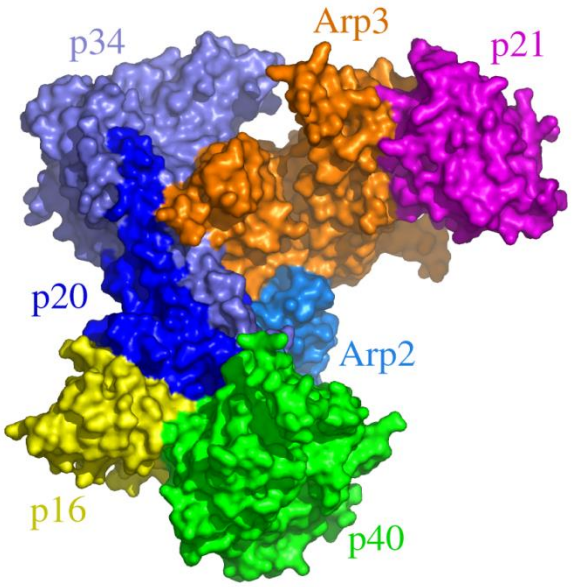

Figure 8. 3-D reconstruction of the 7 subunits of the Arp2/3 complex.
Adapted from (Robinson et al., 2001).

The crystal structure of bovine Arp2/3 complex was determined to be an assembly of seven proteins that initiates actin polymerization in eukaryotic cells, at 2.0 angstrom resolution. Actin-related protein 2 (Arp2) and Arp3 are folded like actin, with distinctive surface features. Subunits ARPC2 p34 and ARPC4 p20 in the core of the complex associate through long carboxyl-terminal alpha helices and have similarly folded amino-terminal alpha/beta domains. ARPC1 p40 is a seven-blade beta propeller with an insertion that may associate with the side of an actin filament. ARPC3 p21 and ARPC5 p16 are globular alpha-helical subunits. We predict that WASp/Scar proteins activate Arp2/3 complex by bringing Arp2 into proximity with Arp3 for nucleation of a branch on the side of a preexisting actin filament.

Regulation of the Arp2/3 complex is mediated by NPFs, and ATP binding and hydrolysis (Figure 9). The conformational change of Arp2/3 requires the binding of ATP to both Arp2 and Arp3 in order to activate the complex (Dayel et al., 2001; Le Clainche et al., 2001). Point mutations in either of the two proteins severely reduced the complex's activity (Goley et al., 2004; Martin et al., 2005). A synergistic effect between NPFs and ATP binding was observed as binding of NPFs to Arp2/3 increases ATP binding affinity and vice versa (Dayel et al., 2001; Le Clainche et al., 2001). The hydrolysis of ATP also plays a role in Arp2/3 regulation but its precise role remains

controversial, as it is associated to both actin nucleation and branching disassembly. Only Arp2-mediated ATP hydrolysis was observed to be influential but this data was generated in vitro leaving the door open to the necessity for a co-factor to be present in Arp3-mediated hydrolysis. It is believed that hydrolysis of ATP weakens the contact between actin and Arp subunits leading to branching disassembly (Dayel and Mullins, 2004; Le Clainche et al., 2003; Martin et al., 2006). As discussed previously, the Arp2/3 complex is also regulated by NPFs. Two classes of NPFs exist and the discrepancy lies in the mechanism by which they activate Arp2/3 (Goley and Welch, 2006). Class I NPFs will be the subject of focus here as they include both WASPs and WAVEs. The VCA region (WH2 repeats, central domain C and acidic domain A) of NPFs is enough to trigger Arp2/3 to branch actin. The CA region binds Arp2/3; more precisely to subunits Arp2, Arp3, Arpc1 and Arpc3 (Kreishman-Deitrick et al., 2005; Weaver et al., 2002; Zalevsky et al., 2001a). The WH2 repeats bind G-actin and bring the actin monomer close to the Arp2 and Arp3 subunits. This newly formed trimer is the building block from which to construct the daughter filament. The central region C induces the conformational change of the Arp2/3 complex which is required for binding to the mother filament (Panchal et al., 2003; Zalevsky et al., 2001b). FRET and Cryo-EM experiments demonstrated that the C region brings the Arp2 and Arp3 subunits closer together. The variability of the C region found in the different NPFs modulate the proximity to which Arp2 and Arp3 are brought together, thereby regulating differently the complex's activity (Goley et al., 2004; Rodal et al., 2005). ATP and NPFs are therefore the two main regulators of the Arp2/3 complex. The rich array of NPFs allows

for variability in activation state of the complex and ATP binding and hydrolysis provide temporal adaptability. Another dimension to which the Arp2/3 complex may be regulated is the number of NPFs present per complex. Conflicting models exist whether one or two NPFs are required to activate Arp2/3. The two NPF model stipulates that NPFs act competitively or synergistically to activate the complex. It is also reported that different combination of NPFs may act on the same Arp2/3 complex which would permit the cell to fine-tune actin branching to an even greater extent (Campellone and Welch, 2010). Once branching occurs, NPFs leave the complex to activate other Arp2/3 complexes (Egile et al., 2005).

It is worth noting that Arpin, a protein with an acidic domain was shown to compete with NPFs for binding to Arp2/3 and inhibits the activity of the complex (Dang et al., 2013). The inhibitory function of this competitive inhibitor is particularly important under specific areas of lamellopodia and was therefore stipulated to be an inhibitory steering protein for migration. Another inhibitor of the Arp2/3 complex is Ck666, which is a compound that stabilizes the inactive confirmation of the complex by preventing Arp2 and Arp3 reorientation (Hetrick et al., 2013).

Actin branching and debranching serves many cellular functions. Deleting subunits of the Arp2/3 is lethal in S. cerevisiae, S. pombe, D. melanogaster, C. elegans and mammals. Only in plants is Arp2/3 not essential for survival (Goley and Welch, 2006). The most known and studied role of Arp2/3 is its involvement in cell migration. Actin-based motility relies on actin dynamics at the plasma membrane to form

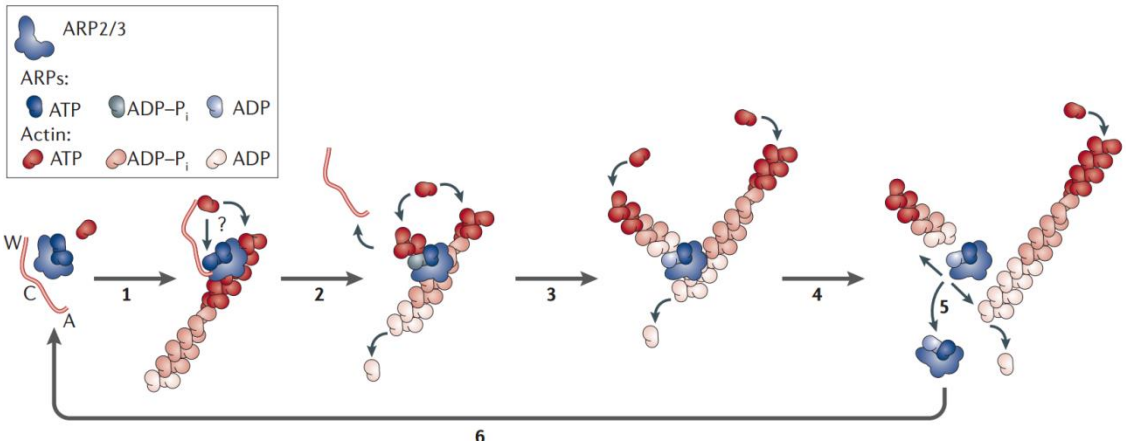

Figure 9. Illustration showing Arp2/3-mediated actin branching through ATP hydrolysis.
Adapted from (Goley and Welch, 2006).

lamellopodia, pseudopodia and filapodia which are cell protrusion that drive the cell forward (Pollard and Borisy, 2003). Arp2/3 was found present just below the leading edge of lamellopodia and pseudopodia but not filapodia (Machesky et al., 1997; Welch et al., 1997). In lamellopodia, actin Y branches can be observed by Cryo-EM thus comforting the notion of Arp2/3's involvement in lamellopodia (Mullins et al., 1998; Svitkina and Borisy, 1999). Inhibiting Arp2/3 by siRNA inhibits lamellopodia (Rogers et al., 2003; Steffen et al., 2006) movement whereas constitutively activated Airpin hampers cell migration and direction (Dang et al., 2013). WAVEs are the main NPFs to drive Arp2/3 activation at the leading edge during lamellopodial movement (Nozumi et al., 2003; Stovold et al., 2005). Focal adhesion proteins and small GTPases like Rac1 were found to be involved in WAVE-Arp2/3 activation pointing towards the possibility that Arp2/3 branching of actin is mediated by extracellular contacts arising from other cells or extracellular matrix (DeMali et al., 2002; Kovacs et al., 2002).

Arp2/3 is involved in other membrane related processes such as cargo transportation. Disrupting the activity of Arp2/3 was shown to impair endocytosis in mammals and yeast (Benesch et al., 2005; Schaerer-Brodbeck and Riezman, 2000). The precise role of Arp2/3 in clathrin-mediated endocytosis remains ambiguous. It may be involved in membrane invagination, pinching off of the vesicle or driving it away (Kaksonen et al., 2006). Different models exist to explain actin branching at endocytic sites including circular constriction at the neck of the vesicle, branching towards the membrane or away from it. In contrast to lamellopodial movement in which WAVEs are the main NPFs involved, N-WASP is the major NPF driving endocytosis (Merrifield et al., 2004, 2005). Arp2/3 has also been associated with anterograde and retrograde vesicle transport from the Golgi. This is an N-WASP and Cdc42 driven process (Stamnes, 2002). Arp2/3 is also activated by WASH, a class I NPF to branch actin around endosome for vesicle fission. Arp2/3 is also instrumental in phagocytosis, vesicle fusion and formation of adhesions and junctions (Rotty et al., 2012).

Much of the work dissecting Arp2/3 conformational changes and dynamics were able thanks to intracellular pathogens that highjack or mimic the WASP-Arp2/3 apparatus of the cell to move around in the cytoplasm. These intracellular pathogens such as listeria and shigella use actin dynamics and branching as propellers to navigate in the cell, the trail of actin that can be seen at the rear of the pathogens are called comets (Lambrechts et al., 2008; Pizarro-Cerdá and Cossart, 2006). Their capacity to recruit NPFs, Arp2/3 and actin make them a great model to study the complex. The

variability in speed at which these pathogens move in the cell or the length of the comets enables investigators to explore parameters like the kinetics of the actin branching or the stability of the branches. Listeria possesses an ActA protein that sticks out of the pathogen membrane and is composed of a polyproline region (PLP) that mimic focal adhesion proteins Zixin and Vinculin, and capable of recruiting Ena-VASP complexes (Auerbuch et al., 2003; Niebuhr et al., 1997). ActA also has a type of VCA domain thereby being able to bind monomeric actin and Arp2/3 thereby looking very similar to constitutively activated NPFs (Welch et al., 1998). Ena-VASP proteins localize at actin stress fibers and mediate their dynamics by inhibiting single actin filaments grow through capping of their barbed ends. Although Ena-VASP recruitment is not essential for listeria navigation, the presence of these proteins significantly increases the speed of the pathogen (Auerbuch et al., 2003; Loisel et al., 1999). Ena-VASP was shown to recruit profilin which favors actin monomers. The availability of these actin monomers is fuel for the comet tails, thus demonstrating that Arp2/3's branching kinetics may be increased with a greater pool of G-actin in its surroundings (Ferron et al., 2007). α-actinin was shown to stabilize filamentous actin (F-actin) by crosslinking the comet tails and therefore increasing the efficiency of the pathogen movement. α-actinin is known to bind vinculin (Loisel et al., 1999) and is therefore associated with FAs.

Three of the seven subunits of the Arp2/3 complex exist in two isoforms. As such, the Arpc1 and Arpc5 subunit are each encoded by two different genes with 67% identity, namely Arpc5 exists in the Arpc5 or Arpc5L isoform and Arpc1 in the Arpc1A or Aprc1B isoform. Using the vaccina model, it was shown that based on the isoform constituting the Arp2/3 complex, different actin dynamics occurred. An Arp2/3 complex composed with Arpc5L and Arpc1B lead to a longer actin tail in motile vaccina viruses in contrast to Arpc5 and Arpc1A-containing Arp2/3 complexes. This was demonstrated to be due to slower disassembly kinetics. The subunits composing the Arp2/3 complex are therefore important for the assembly and disassembly kinetics of actin branching (Abella et al., 2016a).

The Arp2/3 complex plays a central role in a variety of cellular processes. It's involvement in endocytosis, cell migration, membrane trafficking and phagocytosis makes it a pivotal complex in many specialized cell types. Understanding the exact mechanisms of its regulation and of how it branches actin will bring useful insight in the

fields of immunology, hematology, cancer metastasis and cell biology. The full extent of Arp2/3's influence in cells remains to be discovered.

IV.3 Actin

The building block of microfilaments is actin. This 42 kDa monomer polymerizes in a double helix to form a microfilament of 6 nm in width, the thinnest of the cytoskeleton filaments. Actin exists in two forms, globular actin (G-Actin), the free monomer, and filamentous actin (F-Actin). Actin participates in many important cellular processes, including cell motility, cell division and cytokinesis, vesicle and organelle movement, cell signaling, muscle contraction, and the establishment and maintenance of cell junctions and cell shape (Vander, 2011).

The actin monomer is a polarized molecule that possesses an ATP-binding cleft and protein binding sites. In most cases, G-actin is bound to ATP and F-actin to ADP as the catalytic activity is increased $40x10^3$ times when actin is in a filament. Actin filaments grow only from one end with new monomers being added to what is referred to as the (+) end or "barbed" end whereas the (-) end or "pointed" end is recognizable for having its ATP-binding cleft exposed (Carlier, 1990). Actin binding proteins (ABPs) regulate filament dynamics like polymerization, stability, organization in bundles or networks, fragmentation and destruction. For example, Profilin and thymosin β4 impede polymerization by sequestering actin monomers and favoring ATP bound actin states respectively. Other proteins like gelsolin and cofilin regulate actin cable lengths by cutting them which leads to more active ends from which polymerization can be initiated. Capz, another ABP binds the (+) end of the actin filaments and stabilizes the structure. Troponin performs the same function as Capz but binds to the (-) end (Shekhar et al., 2016). Finally, some proteins are involved in creating filament networks that are more complex than linear cables like Arp2/3 discussed previously (Machesky et al., 1994).

Actin exists in 6 isoforms from 6 different genes sharing at least 93% sequence identity (Perrin and Ervasti, 2010). They were discovered based on different isoelectric points. α-actin is the most negatively charged/acidic, followed by β-actin while γ-actin is the most positively charged. α-actin exists in 3 different isoforms: α-skeletal, α-cardiac, and α-smooth actin for skeletal, cardiac, and smooth muscles, respectively. γ-actin exists as γ-smooth and γ-cytoplasmic actin (Kee et al., 2009; Simiczyjew et al., 2013). β-cytoplasmic and γ-cytoplasmic actin are the most similar actin isoforms as they

differ at only 4 out of the 375 amino acids near the N-terminus. The differences in amino acids are conservative between β-cytoplasmic and γ-cytoplasmic actin (Perrin and Ervasti, 2010). The actin isoform sequences are conserved from birds to mammals suggesting that each isoform plays its own important biological role. Both β-cytoplasmic and γ-cytoplasmic actins are involved in cell shape and migration but their specific roles are contested among groups (Bunnell and Ervasti, 2011). In most cell types, β-actin is the main isoform of actin. However, in skeletal muscle this ratio is inversed with some groups finding no β-actin expression at all (Gokhin and Fowler, 2011a). The general view is that β-actin is present at the cell edge to drive cell migration whereas γ-actin has a more structural role (Dugina et al., 2009). In vitro studies demonstrated that both β-cytoplasmic and γ-cytoplasmic actins polymerize, depolymerize or become nucleated at similar rates except in high calcium environment. It was also shown that the two actin isoforms may co-polymerize when calcium is sequestered (Bergeron et al., 2010a). In vivo, β-cytoplasmic actin knock out in mice is lethal (Shawlot et al., 1998) whereas γ-cytoplasmic actin knock out mouse models survive despite developing several problems (Belyantseva et al., 2009).

Actin isoforms in skeletal muscle

Knock out of each of the four actin muscle isoforms in mice leads to different phenotypes suggesting a unique function for each isoform (Perrin and Ervasti, 2010). However, overexpression of another isoform rescues the muscle actin knock out phenotypes (Nowak et al., 2009). It therefore appears that actin isoforms can substitute for one another but that they are regulated and utilized specifically by the cell. This rescue is not seen between non-muscle (β-cytoplasmic and γ-cytoplasmic) and muscle (α-skeletal, α-cardiac, α-smooth and γ-smooth) actins (Jaeger et al., 2009). Non-muscle and muscle actins thus seem to have the most distinct functions although γ-actin was found to be capable of incorporating into thin filaments of the sarcomere. β-cytoplasmic and γ-cytoplasmic actins are believed to have overlapping functions similarly to the muscle actins. However, in muscle, γ-actin is localized at the sarcolemma, the costamere and adjacent to the z-disks (Kee et al., 2004). The localization of β-actin is undetermined. Localization of actin isoforms was done in fully mature muscle. In contrast to other cell types in which β-actin is the predominant isoform of actin, in skeletal muscle, γ-actin is the main actin isoform. Conditional knock out studies of γ-cyto actin mice skeletal muscle revealed that γ-actin is not essential for muscle

development but mice develop a progressive centro-nuclear myopathy with time. Conditional knock out of β-actin in skeletal muscle lead to a quadriceps myopathy (QM) linked to dystrophin misregulation. Central nuclei are also observed in these mice (Prins et al., 2011; Sonnemann et al., 2006a).

Results

1. **N-WASP is required for Amphiphysin-2/BIN1-dependent nuclear positioning and triad organization in skeletal muscle and is involved in the pathophysiology of centronuclear myopathy.**
   Falcone, S.*, Roman, W.*, Hnia, K., Gache, V., Didier, N., Lainé, J., Auradé, F., Marty, I., Nishino, I., Charlet-Berguerand, N., Gomes ER.
   EMBO Mol. Med. *6*, 1455–1475.
   doi: http://dx.doi.org/10.15252/emmm.201404436

N-WASP is required for Amphiphysin-2/BIN1 dependent nuclear positioning and triad organization in skeletal muscle and is involved in the pathophysiology of centronuclear myopathy

Sestina Falcone[1),2),8),10)], William Roman[1),8),10)], Karim Hnia[3)], Vincent Gache[1)2)], Nathalie Didier[1),8)], Jeanne Lainné[2),8)], Frederic Aurade[1),8)], Isabelle Marty[5)], Ichizo Nishino[6)], Nicolas CharletBerguerand[3)],Norma Romero[4)8)], Giovanna Marazzi[1)], David Sassoon[1)], Jocelyn Laporte[3)], Edgar R. Gomes[1)2)7)8)9)]

[1)] Myology Group, UMR S 787 INSERM, Université Pierre et Marie Curie Paris 6, Paris 75634, France

[2)] Institut de Myologie, Groupe Hospitalier Pitié-Salpêtrière, Paris 75013, France

[3)] IGBMC-CNRS UMR 7104 INSERM U964 Illkirch, France

[4)] Morphology Unit, Myology Institut, Pitié Salpêtrière Hospital Paris, France

[5)] INSERM U836, Grenoble Institut des Neurosciences, Equipe Muscle et Pathologies, Grenoble 38042, France

[6)] National Center of Neurology and Psychiatry, Tokyo, Japan

[7)] Instituto de Medicina Molecular, Faculdade de Medicina da Universidade de Lisboa, Lisboa, Portugal

[8)] Current address: Sorbonne Universités UPMC - INSERM UMRS 974, CNRS FRE 3617, Myology Research Center, Paris, France

[9)] Corresponding author: edgar.gomes@upmc.fr

[10)] These authors contributed equally to this work

Running title: N-Wasp drives nuclear positioning and triad formation in skeletal muscle.

Keywords: Centronuclear Myopathy, nuclear movement, triad formation, cytoskeleton

Abstract: Mutations in amphiphysin-2/BIN1, dynamin 2 and myotubularin are associated with centronuclear myopathy (CNM), a muscle disorder characterized by myofibers with atypical central nuclear positioning and abnormal triads. Mis-splicing of amphiphysin-2/BIN1 is also associated with myotonic dystrophy that shares histopathological hallmarks with CNM. How amphiphysin-2 orchestrates nuclear positioning and triad organization and how CNM-associated mutations lead to muscle dysfunction remains elusive. We find that N-WASP interacts with amphiphysin-2 in myofibers and that this interaction and N-WASP distribution are disrupted by amphiphysin-2 CNM mutations. We establish that N-WASP functions downstream of amphiphysin-2 to drive peripheral nuclear positioning and triad organization during

myofiber formation. Peripheral nuclear positioning requires microtubule/Map7/kif5b-dependent distribution of nuclei along the myofiber and is driven by actin and nesprins. In adult myofibers, N-WASP and amphiphysin-2 are only involved in the maintenance of triad organization but not in the maintenance of peripheral nuclear positioning. Importantly, we confirmed that N-WASP distribution is disrupted in CNM and myotonic dystrophy patients. Our results support a role for N-WASP in amphiphysin-2-dependent nuclear positioning and triad organization and in CNM and myotonic dystrophy pathophysiology.

Introduction

Centronuclear myopathy (CNM) is a rare neuromuscular disease associated with skeletal muscle weakness and hypotonia (Nicot et al., 2007; Pierson et al., 2005). CNM muscle fibers from patients and mouse models have centrally positioned nuclei and exhibit defects in T-tubules, triads and excitation-contraction coupling (Dowling et al., 2009; Al-Qusairi et al., 2009; Toussaint et al., 2011). Unlike many myopathies, centrally positioned nuclei in CNMs are not linked to excessive degeneration-regeneration processes. Several forms of CNM have been described in humans including the X-linked form (XLCNM, OMIM#310400), which exhibits the most severe phenotype and affects newborns, due to mutations in myotubularin (*MTM1*), a phosphoinositide phosphatase (Laporte et al., 1996), the autosomal dominant form (ADCNM, OMIM#160150) due to mutations in dynamin 2 (*DNM2*), a large GTPase (Bitoun et al., 2005), and an autosomal recessive form (ARCNM, OMIM#255200) due to mutations in *AMPH2/BIN1* (Nicot et al., 2007).

During skeletal muscle development, nuclei move towards the center of the myotube after myoblast fusion and spread along the center of the myotube prior to positioning at the periphery of the myofiber (Cadot et al., 2012; Metzger et al., 2012)Nuclear spreading along the myotube is mediated by microtubules, Map7 and Kif5b microtubule binding proteins and is independent of nesprin proteins (Metzger et al 2012). Nesprins are nuclear envelope proteins that tether the nucleus to the actin cytoskeleton (Zhang et al., 2007) Myofibers lacking nesprins exhibit peripheral nuclear positioning defects but it is unknown at which stage of skeletal muscle development nesprins are involved in nuclear positioning. Furthermore, how CNM mutated genes are involved in nuclear positioning is also unknown.

Amphiphysin-2 (amph2), encoded by AMPH2/BIN1, is involved in T-tubule

biogenesis and a skeletal muscle specific isoform of amph2 expressing exon 11 is localized to the T-tubules (Butler et al., 1997; Lee et al., 2002; Toussaint et al., 2011). T-tubules are invaginations of the plasma membrane (sarcolemma) that become associated and transversally paired with a specific region of the sarcoplasmic reticulum (SR), the junctional SR/terminal cisternae. The structure formed between one T-tubule and two junctional SR compartments is named triad (Flucher et al., 1991). Triads couple the excitation of the sarcolemma and T-tubules with the release of calcium from the SR leading to muscle contraction, a process named excitation-contraction (EC) coupling. Multiple proteins are specifically localized in these structures, but the molecular mechanisms involved in triad organization are still poorly understood (Al-Qusairi and Laporte, 2011).

Alternative splicing of amph2 has been recently found in skeletal muscle biopsies from patients with myotonic dystrophy. CNM and myotonic dystrophy share some histopathological features such as centrally positioned nuclei and defects in T-tubules and triads (Fugier et al., 2011), suggesting a common unknown mechanism involving a role for amph2 on nuclear positioning and triad function in both CNM and myotonic dystrophy.

Amph2 has an N-terminal BAR domain responsible for membrane binding and curvature, and a C-terminal SH3 domain implicated in protein-protein interaction. These domains are mutated in ARCNM patients (Nicot et al., 2007; Prokic et al., 2014). SH3 domains interact and regulate multiple protein machineries, in particular different actin nucleation promoting factors involved in membrane remodeling (Suetsugu and Gautreau, 2012). N-WASP is an actin nucleation promoting factor that activates the Arp2/3 complex, an actin nucleator (Rohatgi et al., 1999). In skeletal muscle, N-WASP was recently found to be involved in myoblast fusion, nebulin-dependent actin nucleation during myofibrillogenesis, and IGF-1 dependent muscle hypertrophy (Gruenbaum-Cohen et al., 2012; Takano et al., 2010). However, a role for N-WASP in nuclear positioning and triad organization is unknown. Amphiphysin-1, a member of the amphiphysin family expressed primarily in the brain, regulates actin dynamics and membrane remodeling during endocytosis through activation of N-WASP (Yamada et al., 2009). Furthermore, a cardiac muscle-specific amph2 isoform interacts with N-WASP in vitro (Hong et al., 2014). We therefore explored the potential involvement of N-WASP downstream of amph2, a homolog of amphyphysin-1, in nuclear positioning and triad organization during skeletal myofiber maturation and its role in the

pathophysiology of centronuclear myopathy and myotonic dystrophy.

Results

In vitro maturation of myofibers with peripheral nuclei and organized triads

During myofiber maturation, a complex network of signaling and cytoskeletal proteins operate to organize cellular structures such as contractile myofibrils and triads that allow EC coupling. In parallel, nuclei move from the center of the myofiber to the periphery (Flucher et al., 1991; Franzini-Armstrong, 1986; Metzger et al., 2012; Starr and Fridolfsson, 2010). Multiple myogenic cell lines along with primary myoblasts will readily differentiate into myotubes in culture (Blau et al., 1985; Davis et al., 1987). Thus far, it has proven difficult to generate mature myofibers *in vitro* with T-tubules transversally paired with SR in striated transversal triads and peripheral nuclei (Cooper et al., 2004; Cusimano et al., 2009; Flucher et al., 1991). We therefore developed an *in vitro* system in which we used primary myoblasts isolated from WT or histone 2B-GFP (H2B-GFP) P5 mouse pups to generate mature myofibers (Hadjantonakis and Papaioannou, 2004). The H2BGFP allowed us to visualize nuclei positioning by time-lapse microscopy (Figure 1A). Primary myoblasts were differentiated into myotubes and treated with agrin. Myotubes were then covered with a matrigel layer, as described in the methods section and Figure S1A. We observed the maturation of these myotubes treated with agrin by dual color phase-contrast/epi-fluorescence multi-positioning time-lapse microscopy over a period of 10 days (Figure 1A, suppl movie1). Myotubes elongated and their nuclei migrated and rotated throughout the length of the myotube during differentiation. Nuclear movements decreased during differentiation and nuclei became positioned at the periphery of the myofiber between day 5 and day 10 (Figure 1A). We also observed migration of mononucleated cells, sometimes touching the myofibers, although we never observed fusion between mononucleated cells and differentiating myofibers after agrin addition. After 10 days, we noted increased myofiber detachment and death.

To quantify the percentage of peripheral nuclei observed during myofiber maturation, cell cultures from WT and H2B-GFP mice were fixed 5 and 10 days after agrin addition, and immunostained for dihydropyridine receptor (DHPR) and triadin. DHPR, a voltage-gated channel is found at the T-tubules. Triadin, an adaptor protein, is

found at the junctional SR compartment (Flucher et al., 1991; Marty et al., 2000). DHPR and triadin are not expressed in mononucleated myoblasts (Marty et al., 2000; Zheng et al., 2002) which allowed us to distinguish between peripheral nuclei in myofibers from nuclei in mononucleated cells attached to the myofibers (Figure S1B). Five days after agrin addition, about 20% of nuclei where observed at the periphery in either WT or H2B-GFP myofibers (Figure 1B). DHPR and triadin were found throughout the cytoplasm in clusters (Figure 1C). Ten days after the addition of agrin, 70% of nuclei were positioned at the periphery of the myofiber (Figure 1B, D). Remarkably, we observed that DHPR and triadin were organized in a striated pattern of triads (Figure 1D). Hence, the percentage of fibers with organized triads was also measured 5 and 10 days after agrin addition. We scored 20% of myofibers with organized triads 5 days after agrin addition and up to 80% of myofibers with transversal triads 10 days after agrin addition (Figure 1E). Electron microscopy (EM) confirmed the organization of triads transversally with one t-tubule coupled with two terminal cisternae of the SR and ryanodine receptor (RyR) feet (Figure 1F, G). Finally, we analyzed myofibrillogenesis during myofiber maturation and found that myofibrils (visualized by co-staining with α-actinin and F-actin) were already formed 5 days after agrin addition (Figure S1C). Therefore, our *in vitro* conditions were sufficient to generate mature myofibers with peripheral nuclei as well as T-tubules and SR organized in striated transversal triads.

Amph2, dynamin 2 and myotubularin are involved in the peripheral positioning of nuclei and triad organization

Amph2 is involved in the formation of T-tubules and is localized to transversal triads in adult myofibers (Butler et al., 1997; Lee et al., 2002). We investigated the localization of amph2 in *in vitro* myofibers 10 days after agrin addition. We observed that amph2 was organized in tubular structures both longitudinally and transversally throughout myofibers (Figure 2A,B). These structures co-localized with RyR1, found at the junctional SR (Zalk et al., 2007) and caveolin-3, found at the T-tubules and sarcolemma (Parton et al., 1997). Thus, amph2 also localizes to the organized striated triads in newly differentiated myofibers.

To determine a role for amph2 in nuclear positioning and transversal triad organization during myofiber differentiation, we transfected myoblasts with *Amph2*

exon 3 siRNA, *Amph2* exon 11 siRNA or *GAPDH siRNA* (as control) (Figure 2C-D, Figure S2A, Figure S4A). *Amph2* exon 3 is expressed in all amph2 isoforms whereas *Amph2* exon 11 is specifically expressed in skeletal muscle isoforms (Nicot et al., 2007). Upon transfection, myoblasts were differentiated into myotubes and agrin was added 24 hours after (Figure S1A). Ten days after agrin addition, the number of nuclei per myofiber (fusion index) was similar in all experimental conditions (Figure S2P). The levels of amph2 expression were strongly reduced in both *Amph2* exon 3 and exon 11 siRNA when compared to *GAPDH* siRNA (Figure S2A-C, S4A). We found that nuclear positioning at the myofiber periphery, formation of transversal triads and myofiber thickness were significantly inhibited in either *Amph2* exon3 or exon11 siRNAs when compared to non-transfected or *GAPDH* siRNA transfected myofibers (Figure 2C,D,G,H,I; Figure S4A-C). Reducing the expression of dynamin 2 and myotubularin, encoded by genes mutated in CNM, also leads to a decrease in peripheral nuclei, myofibers with organized triads and myofiber thickness (Figure S2D-O).

To study if amph2 was involved in the regulation of myofibrillogenesis, we examined the morphology of myofibrils and found no differences between *Amph2* siRNA myofibers and *GAPDH* siRNA myofibers (Figure 2E,F). We also evaluated the microtubule cytoskeleton in *Amph2* siRNA myofibers, since microtubules are involved in nuclear positioning (Metzger et al., 2012). We did not observe any changes in the morphology of microtubules and in the expression of β-tubulin on *Amph2* siRNA myofibers when compared with *GAPDH* siRNA (Figure S1D-G).

Alterations in triad structure and organization have been related to defects in intracellular calcium homeostasis after membrane depolarization (Powell et al., 1996). A role for amph2 in calcium homeostasis has been described in isolated muscle fibers after *Amph2* shRNA electroporation *in vivo* (Tjondrokoesoemo et al., 2011). To determine if amph2 is also involved in calcium homeostasis during myofiber formation we measured cytoplasmic calcium concentration in myofibers 10 days after agrin addition, using a fluorescent Fluo-4 direct calcium sensor (Taneike et al., 2011). We observed a reduction of cytoplasmic calcium influx after KCl-induced membrane depolarization or caffeine-induced calcium release from the sarcoplasmic reticulum in *Amph2* siRNA myofibers, when compared to *GAPDH* siRNA (Figure S3A-C). These results suggest that amph2 is involved in calcium homeostasis during myofiber formation,

Finally, we tested the role of *AMPH2* mutations (associated with ARCNM) in

nuclear positioning and triad organization. We transfected myotubes with cDNA encoding GFP-tagged amph2 mutated in the BAR domain (Amph2 R154Q) and in the SH3 domain (Amph2 K575X) (Toussaint et al., 2011). We found that expression of either R154Q or K575X amph2 mutants inhibited nuclear positioning at the periphery of myofibers and disrupted the organization of DHPR (Figure S3D-G). We also observed a decrease in the thickness of the myofibers transfected with amph2 R154Q or amph2 K575X when compared to the GFP transfected controls (Figure S3H). Overall, these results reveal that amph2, dynamin 2 and myotubularin regulate nuclear peripheral positioning and triad organization during myofiber formation and that these functions are also disrupted by mutations in amph2 associated with ARCNM.

N-WASP associates with amph2 in myofibers and is involved in nuclear localization and triad organization.

N-WASP interacts and regulates amphiphysin orthologs in *D. melanogaster* and *S. cerevisiae,* and amphiphysin-1 in mammalian brain (Madania et al., 1999; Salazar et al., 2003; Yamada et al., 2009; Zelhof and Hardy, 2004). Thus, we hypothesized that N-WASP could interact with amph2 in skeletal muscle and play a role in myofiber maturation and amph2-dependent ARCNM phenotype. We found that N-WASP co-immunoprecipitated with endogenous amph2 from extracts of mouse primary mature myofibers and C2C12 myotubes (Figure 3A, B,). Conversely, amph2 co-immunoprecipitated with endogenous N-WASP from extracts of primary mature myofibers (Figure 3C). To identify the amph2 domain involved in the interaction with N-WASP, we expressed GFP-tagged full length human amph2, SH3 or BAR domains of amph2 in C2C12 myoblasts (Figure 3D). We observed that GFP antibodies co-immunoprecipitated endogenous NWASP together with amph2 SH3 domain or full length amph2 (Figure 3F). We observed a very weak signal in BAR domain amph2 after co-immunoprecipitation, probably due to dimerization amph2 via the BAR domain (Friesen et al., 2006; Lee et al., 2002). In addition, we purified human GST-tagged full length, SH3 or BAR domains of amph2, and found that the SH3 domain and the full length amph2 pulled down N-WASP from muscle homogenates or from *in vitro* transcribed/translated GFP-N-WASP (Figure 3H). These results demonstrate that the SH3 domain of amph2 associates with N-WASP in skeletal muscle and that likely this interaction is direct.

We next tested whether the *AMPH2* mutations found in ARCNM patients could disrupt the interaction of amph2 with N-WASP. We expressed human GFP-tagged amph2 with BAR domain mutations (D151N and R154Q) or SH3 domain mutations (Q573X and K575X) in C2C12 cells (Figure3E). We observed that amph2 with BAR domain mutations co-immunoprecipitated with the same amount of N-WASP as full length amph2 (Figure 3G). In contrast, amph2 SH3 mutation Q573X and amph2-K575X did not co-immunoprecipitate with endogenous N-WASP. In addition, we expressed and purified GST-tagged amph2 SH3 domain with the same Q573X and K575X mutations and found that these proteins did not pull down N-WASP from muscle homogenates or from *in vitro* transcribed/translated GFP-N-WASP, except for SH3-K575X that pulled down a residual amount of *in vitro* transcribed/translated GFP-N-WASP (Figure 3H).

Finally, we tested the role of N-WASP on peripheral positioning of nuclei and triad organization during myofiber differentiation. We efficiently reduced the levels of N-WASP in myotubes using siRNA without observing any changes in fusion index when compared with *GAPDH* siRNA (Figure S2P, Figure S3I-J). We observed a reduction of peripheral nuclear positioning, triad organization and myofiber thickness in *N-WASP* siRNA myofibers (Figure 4A,B,EG). Myofibrils morphology was not affected when compared to *GAPDH* siRNA myofibers (Figure 4C,D). Altogether, these results suggest a role for N-WASP in peripheral nuclei positioning and triad organization, probably mediated by N-WASP interaction with amph2. Moreover, the disruption of amph2 and N-WASP interaction by SH3 domain mutations found in ARCNM suggests that alteration of N-WASP function participates in the etiology of the disease.

N-WASP functions downstream of amph2 to regulate nuclear localization and triad organization

Our results demonstrating a physical interaction between amph2 and N-WASP in myofibers, and the similar phenotypes observed when N-WASP or amph2 are depleted in myofibers suggest that N-WASP functions together with amph2 to regulate peripheral nuclear localization and triad organization. N-WASP activity is modulated by the switch from an auto-inhibited configuration to an activated state by different mechanisms; among them is the binding of SH3 domains to the polypro region of N-WASP. Once activated, the C-terminal VCA domain of N-WASP interacts with the Arp2/3 complex, leading to actin polymerization (Padrick and Rosen, 2010; Prehoda et al., 2000). To determine if N-WASP functions downstream of amph2, we expressed full length N-WASP or the constitutively active VCA domain of N-WASP in *amph2 or GAPDH* siRNA myotubes. After 10 days of differentiation in the presence of agrin, we found that expression of the VCA domain of N-WASP in *Amph2* exon 3 or exon 11 siRNA myofibers restored peripheral localization of nuclei, triad organization as well as myofiber thickness to the same level as the *GAPDH* siRNA (Figure 5A,B,EG, Figure S4A-C). Expression of full length N-WASP or GFP in *Amph2* siRNA myofibers was not able to restore any of these phenotypes suggesting that amph2 is required to activate N-WASP. Furthermore, the expression of either GFP, full length N-WASP or VCA domain in *GAPDH* siRNA myofibers did not interfere with peripheral localization of nuclei, triad organization or myofiber thickness (Figure 5A, E-G; Figure S4B-C). To rule out that the rescue effect we observed upon GFP-VCA expression in *Amph2* siRNA myofibers was not due to an indirect role of N-WASP on gene expression (Wu et al., 2006), we tagged the VCA domain with TdTomato (TdT-VCA), a 60Kd fluorescent protein, to prevent the accumulation of the VCA domain in the nucleus (Figure S4D). We found that expression of TdT-VCA in *Amph2* siRNA myofibers also restored peripheral localization of nuclei and triad organization (Figure S4E,F). Furthermore, we observed that amph2 was not detectable by western blot or immunofluorescence analysis in myofibers transfected with GFP-VCA and *Amph2* exon 3 or exon 11 siRNA (Figure 5C,D, Figure S4A). Therefore, expression of VCA does not induce expression of amph2 in *Amph2* siRNA myofibers. Finally, we also tested if N-WASP could function downstream of myotubularin and dynamin 2. We expressed GFP-VCA in myofibers depleted for myotubularin or dynamin 2. We found that GFP-VCA expression rescued peripheral nuclear positioning and triad organization in *dynamin 2*

siRNA myofibers, but not *myotubularin* siRNA myofibers (Figure S2M,N).

Overall these results indicate that N-WASP functions downstream of amph2 and dynamin 2 to regulate peripheral nuclear localization and triad organization formation during myofiber maturation.

Nuclear localization and triad organization are regulated by independent pathways

Our results suggest that nuclear positioning at the periphery of the myofiber is dependent on N-WASP. We next decided to investigate how N-WASP controls peripheral nuclear positioning. We previously showed that the spreading of nuclei along the myofibers is dependent on a conserved mechanism involving Map7, a microtubule binding protein, and Kif5b, a kinesin, and microtubules (Metzger et al., 2012). Thus, since spreading of nuclei along the myofibers precedes peripheral nuclear positioning (Figure 1A), we therefore explored the involvement of Map7/Kif5b/microtubule pathway on nuclear positioning at the periphery of myofibers and triad organization. We measured peripheral nuclear position and triad organization in myofibers depleted for Map7 and Kif5b using siRNA. We observed that nuclei in *Map7* and *Kif5b* siRNA myofibers were not spread along the myofibers as we previously described (Figure 6B,C) (Metzger et al., 2012; Wang et al., 2013). We also found that peripheral nuclear positioning and myofiber thickness were reduced in *Map7* and *Kif5b* siRNA myofibers. Remarkably, triad organization was not impaired (Figure 6 A-F).

At day 5 after agrin addition, nuclei in the myofibers are already spread along the myofiber, but are not yet positioned at the periphery of the myofiber (Figure 1A-C, Supp Movie 1). Thus, the inhibition of peripheral nuclear positioning could be due to an impairment of the spreading of nuclei along the myofiber or due to the direct involvement of the Map7/Kif5b/microtubule pathway on peripheral nuclear positioning. To distinguish between these two hypothesis, we treated myofibers at day 5 after agrin addition with low dose of nocodazole (75 nM), which alters microtubule dynamics required for microtubule-dependent nuclear movement (Cadot et al., 2012) and allow us to test if microtubule are directly involved in peripheral nuclear positioning. We found that inhibition of microtubule dynamics after day 5 of agrin addition did not prevent peripheral nuclear positioning (Figure 6H,J). We also did not observe any alterations in triad organization or myofiber thickness (Figure 6K,L). Overall, these results suggest that peripheral nuclear positioning is not dependent on microtubules but requires

Map7/Kif5b/microtubule dependent spreading of nuclei along the myofiber prior to nuclear positioning at the periphery of the fiber. Furthermore, triad organization is not dependent on nuclear positioning.

Our results suggest that nuclear positioning at the periphery of the myofiber is dependent on N-WASP, an actin regulator (Figure 4). Nesprins are a class of KASH-domain nuclear envelope proteins that bind to actin and are involved in the position of the nucleus in matured myofibers (Grady et al., 2005). We previously showed that the spreading of nuclei along myofibers is independent of nesprins, therefore nesprins are probably involved in nuclear positioning events that occur after nuclei spreading in the myofibers (Metzger et al., 2012). To test this hypothesis, we expressed in myoblasts a dominant-negative KASH construct (SR-KASH) that removes KASH proteins from the nuclear envelope and disrupts the connection between the nucleus and the actin cytoskeleton (Grady et al., 2005). We also expressed a control KASH construct lacking the c-terminal region required for nuclear envelope anchoring (KASHΔL) (Luxton et al., 2010). We observed that expression of SR-KASH inhibited peripheral nuclear position ten days after agrin addition, without any effect on triad organization when compared with control KASHΔL (figure 6MP). In addition, expression of SR-KASH induced a minor, although significant, decrease of myofiber thickness, when compared with KASHΔL (Figure 6Q). These results suggest that nesprins are involved in peripheral nuclear positioning but not in triad organization. Finally, to determine if actin is also involved in peripheral nuclear positioning, we treated myofibers at day 5 after agrin addition with latrunculin B to impair actin dynamics. We observed that peripheral nuclear positioning, triad organization and fiber thickness were reduced 10 days after agrin addition (figure 6 I-L), suggesting that actin is involved in peripheral nuclear positioning and triad organization. Overall our results demonstrate that peripheral nuclear positioning is dependent on the correct spreading of nuclei along the myofiber driven by Map7/Kif5b/microtubules pathway, on nesprins and on actin. Furthermore, we show that triad organization is not dependent on the position of the nucleus at the periphery of the myofiber.

N-WASP and amph2 are involved in the maintenance of triad organization in skeletal muscle

Amph2 is localized specifically at striated triads whereas N-WASP is mainly

found at the Z-line and also in discrete patches between Z-lines in longitudinal sections of mature muscle fibers (Butler et al., 1997; Razzaq et al., 2001; Takano et al., 2010) (Figure S5B). Since striated triads are found primarily between Z-lines (Flucher, 1992) (Figure S5D), we hypothesized that the discrete patches of N-WASP observed between Z-lines could localize to the triads. We determined the localization of N-WASP in adult mouse isolated fibers and observed that the discrete patches of NWASP co-localized with amph2 and DHPR (Figure 7A, Figure S5C). In transversal sections of adult mouse and human muscle fibers, we observed strong co-localization between N-WASP and DHPR (Figure S5A, Figure 8), suggesting that N-WASP is also found at the triads in mature muscle fibers. Finally, we analyzed human muscle biopsies by differential centrifugation (Gokhin and Fowler, 2011) and found that N-WASP was present in the same cellular membrane fractions as amph2 and DHPR (Figure S8A). To determine when N-WASP is recruited to the triads, we analyzed the localization of N-WASP during myofiber formation *in vitro*. We found that 10 days after agrin addition, N-WASP starts to accumulate at the newly formed striated triads (Figure S5E).

Overall these results strongly suggest that a pool of N-WASP is also localized to the triads in newly formed and matured myofibers.

We next determined whether the localization of N-WASP in adult muscle fibers was dependent on amph2. We electroporated *Amph2* or *GAPDH* siRNA together with a plasmid encoding the fluorescent protein TdT, in adult mouse muscle. We collected whole muscle or isolated single muscle fibers expressing TdT 10 days after electroporation (Figure S6A) and immunostained for amph2 and N-WASP either in muscle sections or in isolated fibers. The distribution of amph2 and N-WASP was not affected in *GAPDH* siRNA muscle sections (Figure 7B, C) or isolated fibers (Figure S6B) compared to non-transfected controls. Importantly, N-WASP distribution was disrupted in *Amph2* depleted myofibers (Figure 7D and S7B) and myofibril morphology was not altered, as previously reported (Figure S7A) (Toussaint et al., 2011).

We next determined the involvement of N-WASP in the distribution of amph2. We collected whole muscle and isolated fibers from muscles electroporated with *N-WASP* siRNA and observed that amph2 distribution was disrupted (Figure 7E and S6B). No changes in myofibril morphology were detected in *N-WASP* siRNA myofibers, when compared to *GAPDH* siRNA myofibers, as previously reported (FigureS7A) (Takano et al., 2010). Interestingly, nuclei remained at the periphery of the myofibers depleted for

amph2 and N-WASP, suggesting that these proteins are not involved in anchoring the nuclei at the periphery of muscle fibers in adult skeletal muscle at least up to 10 days after electroporation (data not shown). Finally, we tested the role of amph*2* ARCNM mutations on the distribution of N-WASP in adult muscle. We electroporated GFP-tagged amph2 with a BAR domain (D151N) or a SH3 domain (K575X) mutations into adult muscle and isolated single muscle fibers positive for GFP expression (Figure S6C). We found that both mutations disrupted the localization of N-WASP (Figure S6D). Overall, these results suggest that amph2 is involved in the distribution of N-WASP in muscle. Conversely, N-WASP is also involved in the distribution of amph2 in muscle.

Our results show that amph2 and N-WASP are involved in the organization of triads during myofiber maturation (Figure 2, 4). Thus we next determined the involvement of amph2 and NWASP in the maintenance of organized triads in adult muscle. We electroporated amph*2*, *N-WASP* or *GAPDH* siRNA into adult mouse muscle and analyzed the distribution of DHPR and RyR1 in longitudinal muscle sections. Knockdown of *Amph2* or *N-WASP* in muscle fibers lead to disruption of DHPR distribution (Figure 7F,G). RyR1 distribution was also disrupted in *N-WASP* siRNA fibers but less disrupted in *Amph2* siRNA fibers (Figure 7H,I). We also analyzed isolated single muscle fibers from muscle transfected with *Amph2* or *N-WASP* siRNA and observed a strong alteration of triad organization (Figure 7J). These results suggest a role for amph2 and N-WASP on the maintenance organized triads in adult muscle fibers.

N-WASP distribution and expression is altered in centronuclear myopathy and myotonic dystrophy

Since our results support a role for N-WASP in amph2-associated ARCNM, we analyzed the localization of N-WASP in a muscle biopsy from an ARCNM patient carrying *Amph2* mutation (R154Q), and compared it to a healthy muscle biopsy. In transversal sections of healthy muscle biopsy, N-WASP was found in a reticulated structure that co-localized with DHPR and amph2 (Figure 8A,B). However, N-WASP organization in ARCNM muscle biopsy was severely disrupted, with a significant accumulation around the centrally located nuclei (Figure 8A,B). DHPR and amph2 distribution was also severely impaired, as previously described (Figure 8A,B) (Toussaint et al., 2011). Analysis of the same muscle biopsies by differential

centrifugation confirmed the changes in the distribution of N-WASP, amph2, DHPR and Cav3, but not α-actinin (Figure S8 A,B). We also determined the localization of N-WASP, amph2 and DHPR in muscle biopsies from ADCNM and XLCNM patients carrying DNM2 mutation (E368K) and *MTM1* mutation (R421InsFIG) respectively (Figure S8 C-F). In ADCNM patients, N-WASP, amph2 and DHPR exhibited a more diffused distribution, with accumulation around the centrally located nuclei similar to what was observed for ARCNM patients. On the other hand, the changes in distribution of N-WASP, amph2 and DHPR between XLCNM and healthy patient biopsies were milder.

The changes in organization of N-WASP could be caused by alterations of N-WASP expression in muscle. We measured mRNA levels of *N-WASP*, *DHPR*, *Amph2*, *DNM2* and *MTM1* in different CNM muscle biopsies and did not find any changes when compared with healthy biopsies (Figure S9A), except for *MTM1* in XLCNM, as previously described ((Vasli et al., 2012). Next we measured protein levels in the same CNM muscle biopsies and found that N-WASP protein levels were decreased in ARCNM and ADCNM, but not in XLCNM (Figure S9B,C). Therefore, mutations in AMPH2 and DNM2, but not MTM1, can result in a reduction of the stability of N-WASP protein.

Amph2 is mis-spliced in myotonic dystrophy of type 1 (DM1), a muscular dystrophy with histopathological features such as centrally located nuclei without signs of regeneration, muscle fiber atrophy and T-tubules alterations, also observed in CNM (Fugier et al., 2011). Therefore we analyzed the distribution of N-WASP and amph2 in transversal section of biopsies from patients with DM1. We found that N-WASP and amph2 distribution was disrupted, when compared with a healthy biopsy (Figure 8C). We also measured the levels of mRNA and did not detect a decrease of *N-WASP*, *AMPH2*, *DHPR*, *DNM2* and *MTM1* mRNA in DM1 patient muscle samples (figure S9 A). These results suggest that N-WASP might also be implicated in DM1 pathology.

Discussion

In this work we identified a role for N-WASP downstream of amph2 regulating the organization of triads and the position of the nucleus at the periphery of myofibers. Furthermore, we showed that nuclear positioning at the periphery of myofibers is dependent on nesprins, actin and requires prior distribution of nuclei along the myofibers, driven by microtubules, Map7 and Kif5b. In addition, triad organization occurs independently of nuclear positioning at the periphery of myofibers (Figure 8D,E). Finally we provide evidence for the disruption of N-WASP function suggesting an impairment of the identified molecular mechanism on these muscle disorders.

An *in vitro* system suitable to study molecular mechanisms of myofiber maturation and muscle disorders

Previous reports described the formation of differentiated myofibers *in vitro*. Flucher et al. (Flucher et al., 1994) described the organization of T-tubules in longitudinal orientation in mouse myotubes, although transversal organization was occasionally observed and peripheral localization of nuclei was not assessed. Cusimano et al. (Cusimano et al., 2009) observed the formation of aligned striated triads, but the peripheral localization of nuclei was not reported. Cooper et al. (Cooper et al., 2004) reported peripheral positioning of nuclei in mouse myofibers, although triad organization was not studied. In this manuscript we report a novel *in vitro* system to differentiate mouse myoblasts into mature myofibers with clearly observable striated transversal triads, myofibrils and peripheral nuclei (Figure 1). The ultrastructure of triads and myofibrils of the *in vitro* myofibers were more developed than myofibers from neonatal mouse muscle since most of the triads were already transversally organized and we rarely observed diads (Ito et al., 2001; Takekura et al., 2001).

We used this system to identify the role of amph2 and N-WASP on triad organization and peripheral nuclear positioning, to identify the mechanism that drives peripheral nuclear positioning and to describe that triad organization occurs independently of peripheral nuclear positioning. We also showed that mutations in amph2 associated with ARCNM disrupt the function of amph2 and N-WASP on nuclear positioning and triad organization. This system can be used to study molecular mechanisms that occur during myofiber formation from initial fusion events to later

stages of the establishment of functional transversal triads. Furthermore, this system provides a platform to screen for potential drugs that will prevent myofiber defects associated with CNM and other muscle disorders. in centronuclear myopathies and myotonic dystrophies, probably downstream of amph2,

Involvement of amph2 and N-WASP in triad organization

The mechanisms of triad organization and maintenance are poorly understood. Formation and maintenance of membrane deformation of the T-tubules could be mediated by the actin cytoskeleton which provides the required scaffold to stabilize membrane shape (Suetsugu and Gautreau, 2012). amph2, a BAR domain containing protein, is involved in T-tubule biogenesis and accumulates to T-tubules (Butler et al., 1997; Lee et al., 2002; Toussaint et al., 2011). Our data suggest that the SH3 domain of amph2 forms a complex with N-WASP that is important for triad organization (Figure 3,4). Amph2 is probably involved in the localization of N-WASP to triads since Amph2 BAR domain mutations perturb the distribution of N-WASP without disrupting the interaction between amph2 and N-WASP (Figure 3G, S6D, 8). In addition, the distribution of NWASP in DM1 patient samples is also disturbed probably due to mislocalization of alternatively spliced amph2 (Figure 8C)(Fugier et al., 2011). We also provide evidence for a role of N-WASP downstream of amph2 regulating triad organization since we found that expression of constitutively active N-WASP restored triad organization in amph2-depleted myofibers (Figure 5 and S4).

We propose a model in which amph2 recruits N-WASP to the vicinity of T-tubules allowing NWASP to regulate the actin cytoskeleton required for structural stability and organization of triads. The actin cytoskeleton that regulates the organization and maintenance of triads is unknown; however, gamma-actin is a good candidate. Gamma-actin accumulates in the vicinity of the triads (Kee et al., 2004, 2009) and co-fractions with SR proteins after differential centrifugation (Gokhin and Fowler, 2011). In addition, skeletal muscles of gamma-actin knockout mice progressively accumulate centrally located nuclei without any signs of regeneration (damaged sarcolemma, inflammation and fibrosis), which is similar to what can be observed in CNM (Sonnemann et al., 2006; Biancalana et al., 2003; Al-Qusairi et al., 2009). In our model, N-WASP might regulate this pool of gamma-actin via the Arp2/3 complex or/and nebulin (Prehoda et al., 2000; Takano et al., 2010). Furthermore, tropomyosin Tm5NM1 was described to accumulate specifically at the triads and Tm5NM1 knockout mice

show defects in triad organization and EC-coupling (Vlahovich et al., 2009). Tropomyosins are involved in actin filaments stabilization, therefore, we speculate that an equilibrium between actin dynamics regulated by N-WASP and actin stabilization regulated by tropomyosin might be involved in triad organization and maintenance, similar to what is observed in lamellipodium-based cell motility (Bugyi et al., 2010). N-WASP was recently found to regulate the polymerization of alpha-actin at the Z-lines of myofibrils (Takano et al., 2010). N-WASP is not required for the formation of myofibrils, however is involved in myofibril maturation and myofiber growth (Takano et al., 2010) (figure 4C,D,G). Therefore, we speculate that N-WASP could regulate two independent pools of actin (alpha- and gamma-) in two different myofiber structures (Z-lines and triads). A similar mechanism is probably present in cardiac muscle where an amph2-specific isoform is involved in t-tubule morphology (Hong et al., 2014). Future experiments in cardiac muscle should provide evidence for an interaction between amph2 and N-WASP and a role for NWASP on t-tubule morphology.

Molecular mechanism of nuclear positioning during myofiber formation

Nuclei are positioned at the periphery during myofiber differentiation, a process which is highly regulated (Bruusgaard et al., 2003; Starr and Fridolfsson, 2010). We can deduce that peripheral nuclear positioning during myofiber maturation is not simply the consequence of unspecific peripheral pushing forces due to sarcomere formation because; 1) sarcomeres are formed prior to peripheral nuclear positioning and 2) we do not observe any defects on sarcomere morphology when peripheral nuclear positioning is inhibited (Figures 2,4,6). Several mechanisms dependent on actin-binding proteins of the nuclear envelope (nesprins) and microtubules influence nuclear positioning during skeletal muscle differentiation (Metzger et al., 2012; Zhang et al., 2007). In this work we establish that peripheral nuclear position requires two separate steps. First, nuclei must spread along the myofiber by a microtubule/Map7/Kif5b-dependent mechanism (Metzger et al., 2012). Second, nuclear movement to the periphery is dependent on amph2, N-WASP, actin and nesprins (Figure 8D,E). Therefore, a switch from a microtubule-driven to an actin-driven nuclear positioning mechanism probably occurs during skeletal muscle differentiation. Finally, our results suggest that amph2, N-WASP and actin are involved in both formation of triads and peripheral nuclear positioning. However microtubules, Map7, Kif5 and nesprins are mainly involved in peripheral nuclear positioning with no identifiable role on the formation of triads.

Amph2 and N-WASP involvement in muscle diseases

Centronuclear myopathies are characterized by centrally located nuclei and defects in T-tubules, triads and excitation-contraction coupling (Dowling et al., 2009; Al-Qusairi et al., 2009; Toussaint et al., 2011). Our results strongly suggest that mutations in AMPH2 and DNM2, but not MTM1 prevent N-WASP from accumulating at triads (Figure 8). A common molecular mechanism may thus link amph2 and dynamin 2 with N-WASP, as previously proposed (Cowling et al., 2012). N-WASP function in CNM is probably impaired by disruption of N-WASP targeting to the membranes of T-tubules due to mutations in AMPH2 hampering either the association of N-WASP to amph2 or the association of the N-WASP-Amph2 complex to membranes. How mutations in DNM2 lead to disruption of amph2 and N-WASP localization and function is currently unknown.

AMPH2 mRNA splicing is misregulated in skeletal muscle of myotonic dystrophy patients leading to the expression of amph2 lacking the phosphoinositide-binding (PI) domain encoded by exon 11 which is involved in the targeting of AMPH2 to triads (Fugier et al., 2011; Lee et al., 2002). Amph2 splicing misregulation is associated with the disorganization of triads observed in myotonic dystrophy skeletal muscles. Interestingly, our data suggest that N-WASP is also involved in DM1 pathology since we observed a disruption of the localization of N-WASP on DM1 muscle, as previously reported for amph2 (Figure 8C) (Fugier et al., 2011). Therefore, misregulation of N-WASP function might also underlie the impairment of muscle function in myotonic dystrophy.

Finally, we showed that expression of active N-WASP (VCA domain) can revert the defects on nuclear positioning and triad organization caused by downregulation of amph2 or dynamin-2 (Figure 5 and S4). Therefore, activation of N-WASP in skeletal muscle might improve muscle function in patients with centronuclear myopathy, myotonic dystrophy and other multiple muscle disorders characterized by defects in nuclear positioning and triad organization (Cowling et al., 2012).

Material and Methods

Antibodies

The following antibodies were used: mouse anti DHPR (IF) 1:500 from Chemicon. Rabbit anti triadin (TRISK95) (IF)1:500 is described in (Marty et al., 2000); mouse anti amph2 clone 99D (Upstate) (IF) 1:200; (WB) 1:1000 ; (IP) 2ug, and rabbit anti amph2 2406 (WB)1:1000 is described in (Toussaint et al., 2011); rabbit anti N-WASP from EMC (IF) 1:200 and (WB)1:1000 for and mouse anti N-WASP from Sigma (IF) 1:200; (WB) 1:1000; (IP) 10ug; mouse anti RyR from Sigma (IF)1:200; mouse anti GAPDH (WB)1:5000 (IF) 1:500 from Ambion; mouse anti beta-Tubulin (WB) 1:1000 from Sigma; mouse anti actinin EA53 from Sigma (IF) 1:800; rabbit anti calnexin from Abcam (WB) 1:2000. Anti-tubulin (IF) 1:50 (from rat monoclonal anti-α-tubulin (YL1/2)-producing hybridoma cell line, ATCC)

Plasmids and siRNA GFP-tagged human amph2-K573X, amph2-K575X, amph2-D151N and amph2-R154Q were described (Nicot et al., 2007), GFP tagged N-WASP FL or VCA (Lommel et al 2001) were a gift from Theresia Stradal ; pTdT-VCA has been generated by NheI-BsrGI replacement of GFP in pEGFP-N-WASP.VCA described above with tandem-dimer-Tomato (TdT) sequence. pCITO vector was derived from pCig (Megason and McMahon, 2002) by subcloning TdT in place of nlsGFP. pcDNA GFP was a gift from Alexis Gautreau. RFP-KASHΔL and RFP-SR-KASH were previously described (Luxton et al., 2010). The following siRNAs were purchased from Life Technologies; Amph2 exon3 siRNA(GGAUCUUCGGACCUAUCUGtt); N-WASP siRNAs (#1: GGCUAAUCCACUCUGAGUAtt and #2 : GGCUAUUUUUUAGCAAAGAtt); GAPDH siRNA (cat # AM4624); DNM2 siRNA (GCGAAUUGAAGGCUCGGGAtt), MTM1 siRNA (CGCAUAUCAAACUCAGAAtt), Amph2 exon11 siRNA (CGGCUGCGCAGAAAGAAGAtt), kif5b siRNA (TAGACCGGATAAAGGAAGCAG) and Map7 siRNA (CAGAUUAGAUGUCACCAAUTT).

Western blotting

Cells were lysed in PBS + 1%SDS and passed through a Qiashredder column (Qiagen) to disrupt DNA. For human muscle, protein extracts were obtained from 200-300 sections from each biopsie and lysed in RIPA buffer.

Protein concentration was measured with a BCA kit according to manufacturer instructions (Pierce). Equal amount of sample were boiled in 30ul sample buffer and were loaded on 4-12% pre-cast Bis-Tris gel (Invitrogen) and transferred into nitrocellulose membrane using the iBlot apparatus (Invitrogen). Membranes were blocked with blocking buffer (5% Non Fat Dry Milk, 0.1% Tween in TBS). Primary antibodies were incubated overnight in blocking buffer at 4°C. After three washes with TBS-Tween 0.1%, membranes were incubated with HRP-conjugated secondary antibodies (1 hour at room temperature). Proteins were visualized using ECL reagent (Pierce).

PCR After lysis with RIPA buffer the sample were divided in 2 parts, one were precipitated with acidic phenol/chloroform (pH 4.5) for RNA extraction and the other were used for differential centrifugation followed by western blot as described before. cDNAs were synthesised from 2 to 5 μg of total RNA using Superscript II reverse of cDNAs was performed on Light-Cycler 480 and Light-Cycler 24 instruments (Roche) using 58°C as melting temperature. Primers used were: After lysis with RIPA buffer the sample were divided in 2 parts, one were precipitated with acidic phenol/chloroform (pH 4.5) for RNA extraction and the other were used for differential centrifugation followed by western blot as described before. cDNAs were synthesised from 2 to 5 μg of total RNA using Superscript II reverse transcriptase (Invitrogen) and random hexamers. Quantitative PCR amplification of cDNAs was performed on Light-Cycler 480 and Light-Cycler 24 instruments (Roche) using 58°C as melting temperature. Primers used were: DHPRa1S (CACNA1S) (F- DHPRa1S (F-GCTACTTTGGAGACCCCTGGAA, R-CAGAAGGAGTGCGAACCCTCCT), N-Wasp (WASL) (F CAGAGGCACAACTTAAAGACAGAG, R-CTCCTTCCAGGCCAAGTGTAG), MTM1 (F-TGGAAGAATACAGGAGGC, R-TGGAATTCGATTTCGGGAC) BIN1 (F-TCTCCAGAAGCTGGGGAAG, R-TGACTTGATGTCGGGGAACT), DNM2 (F¬GAGTTTGACGAGAAGGACTTA, R-GATTAGCTCCTGGATAACCAG) and 18S (F¬CGCCGCTAGAGGTGAAATTC, R-TTGGCAAATGCTTTCGCTC).

Immunoprecipitation

For immunoprecipitation of endogenous N-WASP or amph2 anti-N-WASP mAb or antiAmph2 mAb were cross-linked to magnetic Dynabeads protein G (Invitrogen) using BS3 linker (Fisher Scientific) following manufacturer instructions. Cells were lysed in RIPA buffer, centrifuged at 5000rpm for 5min, and cell lysates were pre-cleared with dynabeads for 30 min at 4°C. Supernatants were incubated with the antibody-coupled Dynabeads for 60 min at 4°C, washed with RIPA buffer and dynabeads were boiled in 20 ul of sample buffer and analyzed by western blot. For immunoprecipitation of GFP-tagged proteins, a GFP-Trap system (Chromotek) was used following manufacturer instructions. After thorough washing with the lysis buffer, bound proteins were eluted in sample buffer boiled and analysed by western blot.

For immunoprecipitation in muscle, fresh mouse tibialis anterior muscles (8 weeks old) were dissected and homogenized with a dounce homogenizer in ice-cold co-IP buffer (50 mM Tris-Cl, pH 7.5; 100 mM NaCl; 5 mM EDTA; 5 mM EGTA; 1 mM DTT; 0.5% Triton X-100; and 2 mM PMSF) supplemented with 0.05% (w/v) SDS. Lysates were centrifuged at 14.000 xg at 4°C and precleared with 50 µl of G-sepharose beads (GE Healthcare) and subsequently incubated with antibodies of interest for 12–24 hours at 4°C. Protein G-sepharose beads (50 ml) were then added for 4 hours at 4°C to capture the immune complexes. Beads were washed 4 times with Co-IP buffer and 1 times with high stringency co-IP buffer (with 300 mM NaCl). For all experiments, two negative controls consisted of a sample lacking the primary antibody (Beads) and a sample incubated with IgG antibody (IGBMC, Illkirch, France). Resulting immune-bound complexes were eluted in Laemmli buffer and submitted to SDS-PAGE and Western blot analysis.

GST-Pull down and *in vitro* transcription/translation

cDNA corresponding to full length, BAR+PI, BAR (aa 1-255) and SH3 (aa 380-454) sequences of BIN1, (isoform 8, 454 aa) and to full length sequence of MTM1 were cloned into pENTR1A Gateway entry vector (Invitrogen) and recombined into pDEST15 (N-ter GST fusion) destination vectors. Mutations were introduced in pENTR1A-BIN1 full-length vector using primer-directed PCR mutagenesis. All the constructs were verified by Sanger sequencing. GST fusion proteins were expressed in the *E. coli* strain BL21-Rosetta 2 (Novagen). Recombinat proteins were extracted from

bacterial pellets by adding extraction buffer (50mM Tris-HCl (pH8.0), 100mM NaCl, 5mM EDTA, 1mM EDTA) supplemented with 1mg/ml lysosyme, a cocktail of protease inhibitors (Complete EDTA free, Roche) and 1mM PMSF. After 30 min incubation on ice, detergents were added (0.01 % N-laurylsarcosine and 0,5% Triton-X100) and lysates were incubated O/N at 4°C to obtain high solubilization. Then, lysates were centrifuged at 16.000xg for 30min. GST fusion proteins were purified by incubation with glutathione sepharose 4B beads (GE Healthcare) overnight followed by extensive washing with extraction buffer plus 0,5% Triton-X100.

The purified GST-fusion proteins coupled to glutathione beads were then incubated overnight with N-wasp translated in vitro (TNT Coupled Reticulocyte Lysate Systems, Promega) according to the manufacturer's protocol. Briefly, pEGFP-N-wasp plasmid was incubated with Methionine and TNT T7 quick master mix for 2 h at 30°C. the homogenates was diluted with extraction buffer 50mM Tris-HCl (pH8.0), 100mM NaCl, 5mM EDTA, 1mM EDTA) supplemented with a cocktail of protease inhibitors (Complete EDTA free, Roche) and 1mM PMSF. After washing beads several times with extraction buffer, bound proteins were analyzed by western blot.

Muscle homogenate differential centrifugation

Differential centrifugation of muscle from control and ARCNM biopsies homogenates have been used to obtain different fractions. The homogenate was centrifuged at 1,500 g for 5 min at 4°C, producing a low-speed pellet rich in myofibrils (1500xg pellet). After washing the low-speed pellet four times in rigor buffer, the low-speed supernatant was centrifuged at 15,000 g for 15 min at 4°C, producing a medium-speed pellet rich in organelles, membranes, and other extrasarcomeric structures (15,000xg pellet). The resulting medium-speed supernatant was then centrifuged at 150,000 g for 15 min at 4°C, producing a high-speed pellet rich in microsomes and macromolecular complexes (150,000xg pellet) and a high-speed supernatant containing cytosol.

Cell Culture, Reagents and TA muscle fiber isolation

All procedures using animals were approved by the Institutional ethics committee and followed the guidelines of the National Research Council Guide for the care and use of laboratory animals. Primary myoblasts from WT or H2B-GFP (The Jackson

Laboratories, STOCK Tg(HIST1H2BB/EGFP)1Pa/J) newborn mice were prepared using a protocol adapted from (De Palma et al., 2010). After hind limb muscles isolation, muscles were minced and digested for 1.5 hours in PBS containing 0.5 mg/ml collagenase –Sigma - and 3.5 mg/ml dispase – Gibco. Cell suspension was filtered through a 40 um cell strainer and pre-plated in DMED-10%FBS (Gibco), to discard the majority of fibroblasts and contaminating cells, for 3 hours. Non adherent-myogenic cells were collected and plated in IMDM (Gibco)- 20% FBS- 1% Chick Embryo Extract (MP Biomedical) onto1:100 Matrigel Reduced Factor (BD) in IMDM coated fluorodishes. Differentiation was triggered by medium switch in IMDM + 2% horse serum and 24 hours later a thick layer of matrigel (1:3 in IMDM) was added. Myotubes were treated with 80μg/mL of agrin and the medium was changed every 2 days (see scheme in figS1).

Latrunculin B (EMD Millipore) and Nocodazole (Sigma) were used at 10 μM and 75 nM respectively starting at day 1 or day 5 after agrin addition (see scheme in Figure S1A). Medium was changed every two days supplemented with the drugs.

C2C12 cell line were cultured as described (De Palma et al., 2010) in DMEM + 10% FBS (Gibco).

TA single fibers were isolated as described (Rosenblatt et al., 1995). TA muscle was explanted from 8-12 weeks old CD1 mice, and then digested in DMEM containing 0.2% tipe I collagenase (Sigma) for 2 hours at 37°C. Mechanical dissociation of fibers was performed using a thin pasteur pipette and followed under a transilluminating-fluorescent stereomicroscope.

Immunofluorescence and immunohistochemistry

The same protocol for either in vitro myofibers or isolated muscle fibers was used. Briefly: fluorodishes or fibers were fixed in 4% paraformaldehyde for 10 min, permeabilized with tritonx100 (0.5% in PBS) and aspecific sites were blocked with BSA 1% and Goat serum 10% for 30 min. Primary antibodies were added O.N at 4°C in saponin 0.1% and BSA1% in PBS. Fluorodishes or fibers were washes three times and then incubated with secondary antibodies together with DAPI for 60 minutes.

Peripheral nuclei quantification

Myofibers were stained for DHPR1 and DAPI and images in Z-stacks with 0.5 μm interval were acquired with a Leica SPE confocal microscope with a 63x 1.3 NA Apo objective. Nuclei extruding the myofiber periphery and positively stained for DHPR were scored as peripheral. A minimum of 150 nuclei per condition were counted in at least 3 individual experiments.

Triad quantification

Myofibers were stained for DHPR1, Triadin and DAPI and images in Z-stacks with 0.5 μm interval were acquired with a Leica SPE confocal microscope with a 63x 1.3 NA Apo objective. Myofibers having more than 50% of triads organized, where DHPR and Triadin were transversally overlapping were scored as positive. A minimum of 150 myofibers per condition were counted in at least 3 individual experiments

Fiber thickness quantification

For fiber thickness quantification, myofibers stained for caveolin3 to visualize plasma membrane, were observed with a Leica SPE confocal microscope with a 40x 1.3 NA Apo objective. Average of three measurements per myofiber was performed on 100 myofibers analyzed per each condition in at least 3 individual experiments.

Human biopsies

All patients or their families have agreed and signed the consent for human sample use according to French and Japanese legislation. Biopsies used for protein homogenates to perform western blot and immunoprecitation experiments were obtained from two different healthy donors (46 and 27 years old) as control. Both XLCNM patients were 1 month old with MTM1 c(455-49)445-4)del and MTM1-R421insFIG, respectively. ADCNM patients were 16 (E368K mutation) and 3 (R456W mutation) years old, respectively. For ARCNM patients, we used K575X and D151N mutated patient biopsies, previously described (Toussaint et al., 2011). All biopsies were frozen in liquid nitrogen cooled isopentane (SIGMA) and kept in -80 degree until use. A Biopsy from 35year-old DM1 patient (described in (Fugier et al., 2011)) was also used. Age-matched healthy donor biopsies were used as control for each myopathy.

Cryosectioning and immunofluorescence microscopy.

For cryosectioning, the TA muscles were isolated from mice and frozen in isopentane precooled with liquid nitrogen. Cryosections (10 μm thick) were fixed in PFA 4% for 30 min. Permeabilization was performed in cooled methanol and aspecific sites were blocked in BSA 5%. For human biopsies, sections were prepared as described in (Fugier et al., 2011; Toussaint et al., 2011). Sections were then incubated with primary antibodies O.N in PBS containing 4% BSA, rinsed and incubated with fluorescent secondary antibodies and DAPI 1hour RT.

Microscopy

Live imaging was performed using an incubator to maintain cultures at 37°C and 5% CO2 (Okolab) and × 20 0.3 NA PL Fluo dry objective. Epi-fluorescence images were acquired using a Nikon Ti microscope equipped with a CoolSNAP HQ2 camera (Roper Scientific), an XY-motorized stage (Nikon), driven by Metamorph (Molecular Devices). Multipositioning images were stitched with Metamorph (Molecular Devices). Confocal images were acquired using Leica SPE confocal microscope with a × 63 1.3 NA Apo objective. Electron microscopy was performed on cultured myofibers 10 days after agrin addition. Myofibers were fixed with 2% glutaraldehyde, 2% paraformaldehyde in 0.1 M phosphate buffer (pH 7.4), and post-fixed with 2% OsO4 in 0.1 M phosphate buffer for 30' at 4°C. Myofibers were then dehydrated at 4°C in graded acetone including a 1% uranyl acetate in 70° acetone staining step, before Epon resin embedding. Thin (70 nm) sections were stained with uranyl acetate and lead citrate, observed using a Philips CM120 electron microscope (Philips Electronics NV) and photographed with a digital SIS Morada camera.

Transfection and electroporation

Cells were transfected with siRNA (20nM) using RNAiMAX, cDNA using Lipofectamine-LTX Plus reagent or both using Lipofectamine 2000 following manufacturer instructions (Invitrogen). For primary myoblasts, they were transfected 6 hours prior differentiation, to let protein silencing or overexpression effective since the

beginning of differentiation (see scheme in fig S1).

For in vivo muscle transfection using electroporation, siRNAs were electroporated together with p-CITO-tdTomato (derived from pCig by substituting nlsGFP with tdTomato cDNA) as fluorescent reporter of transfection. 20 μg of each plasmid DNA or 40 μg of siRNA were dissolved in 40 μl of PBS and injected into the TA muscle of mice with a 27-gauge needle centered between a pair of needle electrodes (Nepa Gene). Immediately after the plasmid injection, six pulses of 60ms duration at a voltage of 200V/cm, were administered with a square pulse electroporator system CUY21SC (Nepa Gene). Muscles were retrieved 10 days after electroporation to either cryosectioning or muscle fiber isolation.

Calcium assay

Calcium assay was performed on fully differentiated myofibers at day 10 after agrin addition. Fluo-4 was prepared according to manufacturer instructions (Life Technologies ref# F10471). The myofibers were bathed in the fluo-4 solution at 37°C for 30 minutes and were then incubated at RT for another 30 minutes. The myofibers were subsequently imaged using an argon laser with peak wavelength at 488nm, on an Epi-fluorescence Nikon Ti microscope driven by Metamorph (Molecular Devices) with image acquisition every 6 seconds. Caffeine (50 mM) or KCl (50 mM) were added after 100 seconds. Average of fluorescente intensity of Fluo-4 was performed on 30 myofibers analyzed per each condition in at least 3 individual experiments.

Statistics

Statistical analysis was performed with Prism (version 5.0 of GraphPad Software Inc.). Pair wise comparisons were made with Student's *t*-test. In peripheral nuclei positioning analysis and in fiber thickness analysis in myofibers, Student's *t*-tests were performed between GAPDH siRNA and experimental condition. For biochemical experiments using human samples, statistical analysis was performed using the Mann-Whitney U test or the unpaired Student's test and multiple statistical comparisons between samples were performed by one-way analysis of variance followed by a Bonferroni's t-test posthoc correction to obtain a better evaluation of the variability between samples from the same group and samples from each compared group and statistical significance was set at $*P < 0.05$. The prism program (version 5.0, GraphPad

software Inc.) was used. The distribution of data points is expressed as mean ± SE from three independent experiments

Acknowledgements:

We thank Linda Manere for her assistance in biopsies treatment for IF, Sonia Alonso-Martin for her assistance in isolation and IF of single muscle fiber, and Stephane Vassilopoulos and Marc Bitoun for discussions. We thank the Gomes and Laporte lab for discussions. This work was supported by Muscular Dystrophy Association (MDA), INSERM Avenir programme and Agence Nationale de la Recherche (ANR) grants to E.R.G.

Author contributions:

S.F, W.R. K.H and V.G. conceived, designed and performed experiments. N.D. performed in vivo electroporation experiments. I.M., N.C-B, I.N. and N.R. provided reagents. G.M., D.S. and J.L. conceived and designed experiments. The manuscript was written by S.F. and E.R.G. with assistance from other authors. Request for materials or reprints should be addressed to E.R.G.

References:

Biancalana, V., Caron, O., Gallati, S., Baas, F., Kress, W., Novelli, G., D'Apice, M.R., Lagier-Tourenne, C., Buj-Bello, A., Romero, N.B., et al. (2003). Characterisation of mutations in 77 patients with X-linked myotubular myopathy, including a family with a very mild phenotype. Hum. Genet. *112*, 135–142.

Bitoun, M., Maugenre, S., Jeannet, P.-Y., Lacène, E., Ferrer, X., Laforêt, P., Martin, J.-J., Laporte, J., Lochmüller, H., Beggs, A.H., et al. (2005). Mutations in dynamin 2 cause dominant centronuclear myopathy. Nat. Genet. *37*, 1207–1209.

Blau, H.M., Pavlath, G.K., Hardeman, E.C., Chiu, C.P., Silberstein, L., Webster, S.G., Miller, S.C., and Webster, C. (1985). Plasticity of the differentiated state. Science *230*, 758–766.

Bruusgaard, J.C., Liestøl, K., Ekmark, M., Kollstad, K., and Gundersen, K. (2003). Number and spatial distribution of nuclei in the muscle fibres of normal mice studied in vivo. J Physiol *551*, 467–478.

Bugyi, B., Didry, D., and Carlier, M.-F. (2010). How tropomyosin regulates lamellipodial actin-based motility: a combined biochemical and reconstituted motility approach. EMBO J. *29*, 14–26.

Butler, M.H., David, C., Ochoa, G.C., Freyberg, Z., Daniell, L., Grabs, D., Cremona, O., and De Camilli, P. (1997). Amphiphysin II (SH3P9; BIN1), a member of the amphiphysin/Rvs family, is concentrated in the cortical cytomatrix of axon initial segments and nodes of ranvier in brain and around T tubules in skeletal muscle. J. Cell Biol. *137*, 1355–1367.

Cadot, B., Gache, V., Vasyutina, E., Falcone, S., Birchmeier, C., and Gomes, E.R. (2012). Nuclear movement during myotube formation is microtubule and dynein dependent and is regulated by Cdc42, Par6 and Par3. EMBO Rep. *13*, 741–749.

Cooper, S.T., Maxwell, A.L., Kizana, E., Ghoddusi, M., Hardeman, E.C., Alexander, I.E., Allen, D.G., and North, K.N. (2004). C2C12 co-culture on a fibroblast substratum enables sustained survival of contractile, highly differentiated myotubes with peripheral nuclei and adult fast myosin expression. Cell Motil. Cytoskeleton *58*, 200–211.

Cowling, B.S., Toussaint, A., Muller, J., and Laporte, J. (2012). Defective Membrane Remodeling in Neuromuscular Diseases: Insights from Animal Models. PLoS Genet *8*.

Cusimano, V., Pampinella, F., Giacomello, E., and Sorrentino, V. (2009). Assembly and dynamics of proteins of the longitudinal and junctional sarcoplasmic reticulum in skeletal muscle cells. Proc. Natl. Acad. Sci.
U.S.A. *106*, 4695–4700.

Davis, R.L., Weintraub, H., and Lassar, A.B. (1987). Expression of a single transfected cDNA converts fibroblasts to myoblasts. Cell *51*, 987–1000.

Dorchies, O.M., Laporte, J., Wagner, S., Hindelang, C., Warter, J.M., Mandel, J.L., and Poindron, P. (2001). Normal innervation and differentiation of X-linked myotubular myopathy muscle cells in a nerve-muscle coculture system. Neuromuscul. Disord. *11*, 736–746.

Dowling, J.J., Vreede, A.P., Low, S.E., Gibbs, E.M., Kuwada, J.Y., Bonnemann, C.G., and Feldman, E.L. (2009). Loss of myotubularin function results in T-tubule disorganization in zebrafish and human myotubular myopathy. PLoS Genet. *5*, e1000372.

Flucher, B.E. (1992). Structural analysis of muscle development: transverse tubules, sarcoplasmic reticulum, and the triad. Dev. Biol. *154*, 245–260.

Flucher, B.E., Phillips, J.L., and Powell, J.A. (1991). Dihydropyridine receptor alpha subunits in normal and dysgenic muscle in vitro: expression of alpha 1 is required for proper targeting and distribution of alpha 2. The Journal of Cell Biology *115*, 1345–1356.

Flucher, B.E., Andrews, S.B., and Daniels, M.P. (1994). Molecular organization of transverse tubule/sarcoplasmic reticulum junctions during development of excitation-contraction coupling in skeletal muscle. Mol. Biol. Cell *5*, 1105–1118.

Franzini-Armstrong, C. (1986). The sarcoplasmic reticulum and the transverse tubules. In Myology, (A. Engel and BO. Banker), pp. 125–153.

Friesen, H., Humphries, C., Ho, Y., Schub, O., Colwill, K., and Andrews, B. (2006). Characterization of the Yeast Amphiphysins Rvs161p and Rvs167p Reveals Roles for the Rvs Heterodimer In Vivo. Mol. Biol. Cell *17*, 1306–1321.

Fugier, C., Klein, A.F., Hammer, C., Vassilopoulos, S., Ivarsson, Y., Toussaint, A., Tosch, V., Vignaud, A., Ferry, A., Messaddeq, N., et al. (2011). Misregulated alternative splicing of BIN1 is associated with T tubule alterations and muscle weakness in myotonic dystrophy. Nat. Med. *17*, 720–725.

Gokhin, D.S., and Fowler, V.M. (2011). Cytoplasmic gamma-actin and tropomodulin isoforms link to the sarcoplasmic reticulum in skeletal muscle fibers. J. Cell Biol. *194*, 105–120.

Grady, R.M., Starr, D.A., Ackerman, G.L., Sanes, J.R., and Han, M. (2005). Syne proteins anchor muscle nuclei at the neuromuscular junction. Proc. Natl. Acad. Sci. U.S.A. *102*, 4359–4364.

Gruenbaum-Cohen, Y., Harel, I., Umansky, K.-B., Tzahor, E., Snapper, S.B., Shilo, B.-Z., and Schejter, E.D. (2012). The actin regulator N-WASp is required for muscle-cell fusion in mice. Proc. Natl. Acad. Sci. U.S.A. *109*, 11211–11216.

Hadjantonakis, A.-K., and Papaioannou, V.E. (2004). Dynamic in vivo imaging and cell tracking using a histone fluorescent protein fusion in mice. BMC Biotechnol. *4*, 33.

Hong, T., Yang, H., Zhang, S.-S., Cho, H.C., Kalashnikova, M., Sun, B., Zhang, H., Bhargava, A., Grabe, M., Olgin, J., et al. (2014). Cardiac BIN1 folds T-tubule membrane, controlling ion flux and limiting arrhythmia. Nat. Med. *20*, 624–632.

Ito, K., Komazaki, S., Sasamoto, K., Yoshida, M., Nishi, M., Kitamura, K., and Takeshima, H. (2001). Deficiency of triad junction and contraction in mutant skeletal muscle lacking junctophilin type 1. J. Cell Biol. *154*, 1059–1067.

Kee, A.J., Schevzov, G., Nair-Shalliker, V., Robinson, C.S., Vrhovski, B., Ghoddusi, M., Qiu, M.R., Lin, J.J.C., Weinberger, R., Gunning, P.W., et al. (2004). Sorting of a nonmuscle tropomyosin to a novel cytoskeletal compartment in skeletal muscle results in muscular dystrophy. J. Cell Biol. *166*, 685–696.

Kee, A.J., Gunning, P.W., and Hardeman, E.C. (2009). Diverse roles of the actin cytoskeleton in striated muscle. J. Muscle Res. Cell. Motil. *30*, 187–197.

Kojima, C., Hashimoto, A., Yabuta, I., Hirose, M., Hashimoto, S., Kanaho, Y., Sumimoto, H., Ikegami, T., and Sabe, H. (2004). Regulation of Bin1 SH3 domain binding by phosphoinositides. EMBO J. *23*, 4413–4422.

Kossmann, C.E., and Fawcett, D.W. (1961). The Sarcoplasmic Reticulum of Skeletal and Cardiac Muscle. Circulation *24*, 336–348.

Laporte, J., Hu, L.J., Kretz, C., Mandel, J.L., Kioschis, P., Coy, J.F., Klauck, S.M., Poustka, A., and Dahl, N. (1996). A gene mutated in X-linked myotubular myopathy defines a new putative tyrosine phosphatase family conserved in yeast. Nat. Genet. *13*, 175–182.

Lee, E., Marcucci, M., Daniell, L., Pypaert, M., Weisz, O.A., Ochoa, G.-C., Farsad, K., Wenk, M.R., and De Camilli, P. (2002). Amphiphysin 2 (Bin1) and T-tubule biogenesis in muscle. Science *297*, 1193–1196.

Luxton, G.W.G., Gomes, E.R., Folker, E.S., Vintinner, E., and Gundersen, G.G. (2010). Linear arrays of nuclear envelope proteins harness retrograde actin flow for nuclear movement. Science *329*, 956–959.

Madania, A., Dumoulin, P., Grava, S., Kitamoto, H., Schärer-Brodbeck, C., Soulard, A., Moreau, V., and Winsor, B. (1999). The Saccharomyces cerevisiae homologue of human Wiskott-Aldrich syndrome protein Las17p interacts with the Arp2/3 complex. Mol. Biol. Cell *10*, 3521–3538.

Marty, I., Thevenon, D., Scotto, C., Groh, S., Sainnier, S., Robert, M., Grunwald, D., and Villaz, M. (2000). Cloning and characterization of a new isoform of skeletal muscle triadin. J. Biol. Chem. *275*, 8206–8212.

Megason, S.G., and McMahon, A.P. (2002). A mitogen gradient of dorsal midline Wnts organizes growth in the CNS. Development *129*, 2087–2098.

Metzger, T., Gache, V., Xu, M., Cadot, B., Folker, E.S., Richardson, B.E., Gomes, E.R., and Baylies, M.K. (2012). MAP and kinesin-dependent nuclear positioning is

required for skeletal muscle function. Nature *484*, 120–124.

Nicot, A.-S., Toussaint, A., Tosch, V., Kretz, C., Wallgren-Pettersson, C., Iwarsson, E., Kingston, H., Garnier, J.-M., Biancalana, V., Oldfors, A., et al. (2007). Mutations in amphiphysin 2 (BIN1) disrupt interaction with dynamin 2 and cause autosomal recessive centronuclear myopathy. Nat. Genet. *39*, 1134–1139.

Padrick, S.B., and Rosen, M.K. (2010). Physical mechanisms of signal integration by WASP family proteins. Annu. Rev. Biochem. *79*, 707–735.

De Palma, C., Falcone, S., Pisoni, S., Cipolat, S., Panzeri, C., Pambianco, S., Pisconti, A., Allevi, R., Bassi, M.T., Cossu, G., et al. (2010). Nitric oxide inhibition of Drp1-mediated mitochondrial fission is critical for myogenic differentiation. Cell Death Differ. *17*, 1684–1696.

Parton, R.G., Way, M., Zorzi, N., and Stang, E. (1997). Caveolin-3 associates with developing T-tubules during muscle differentiation. J. Cell Biol. *136*, 137–154.

Pierson, C.R., Tomczak, K., Agrawal, P., Moghadaszadeh, B., and Beggs, A.H. (2005). X-linked myotubular and centronuclear myopathies. J. Neuropathol. Exp. Neurol. *64*, 555–564.

Powell, J.A., Petherbridge, L., and Flucher, B.E. (1996). Formation of triads without the dihydropyridine receptor alpha subunits in cell lines from dysgenic skeletal muscle. J. Cell Biol. *134*, 375–387.

Prehoda, K.E., Scott, J.A., Mullins, R.D., and Lim, W.A. (2000). Integration of multiple signals through cooperative regulation of the N-WASP-Arp2/3 complex. Science *290*, 801–806.

Prokic, I., Cowling, B.S., and Laporte, J. (2014). Amphiphysin 2 (BIN1) in physiology and diseases. J. Mol. Med. *92*, 453–463.

Al-Qusairi, L., and Laporte, J. (2011). T-tubule biogenesis and triad formation in skeletal muscle and implication in human diseases. Skelet Muscle *1*, 26.

Al-Qusairi, L., Weiss, N., Toussaint, A., Berbey, C., Messaddeq, N., Kretz, C., Sanoudou, D., Beggs, A.H., Allard, B., Mandel, J.-L., et al. (2009). T-tubule

disorganization and defective excitation-contraction coupling in muscle fibers lacking myotubularin lipid phosphatase. Proc. Natl. Acad. Sci. U.S.A. *106*, 18763–18768.

Razzaq, A., Robinson, I.M., McMahon, H.T., Skepper, J.N., Su, Y., Zelhof, A.C., Jackson, A.P., Gay, N.J., and O'Kane, C.J. (2001). Amphiphysin is necessary for organization of the excitation-contraction coupling machinery of muscles, but not for synaptic vesicle endocytosis in Drosophila. Genes Dev. *15*, 2967–2979.

Rohatgi, R., Ma, L., Miki, H., Lopez, M., Kirchhausen, T., Takenawa, T., and Kirschner, M.W. (1999). The interaction between N-WASP and the Arp2/3 complex links Cdc42-dependent signals to actin assembly. Cell *97*, 221–231.

Rosenblatt, J.D., Lunt, A.I., Parry, D.J., and Partridge, T.A. (1995). Culturing satellite cells from living single muscle fiber explants. In Vitro Cell. Dev. Biol. Anim. *31*, 773–779.

Royer, B., Hnia, K., Gavriilidis, C., Tronchère, H., Tosch, V., and Laporte, J. (2013). The myotubularinamphiphysin 2 complex in membrane tubulation and centronuclear myopathies. EMBO Rep. *14*, 907–915.

Salazar, M.A., Kwiatkowski, A.V., Pellegrini, L., Cestra, G., Butler, M.H., Rossman, K.L., Serna, D.M., Sondek, J., Gertler, F.B., and Camilli, P.D. (2003). Tuba, a Novel Protein Containing Bin/Amphiphysin/Rvs and Dbl Homology Domains, Links Dynamin to Regulation of the Actin Cytoskeleton. J. Biol. Chem. *278*, 49031–49043.

Sonnemann, K.J., Fitzsimons, D.P., Patel, J.R., Liu, Y., Schneider, M.F., Moss, R.L., and Ervasti, J.M. (2006). Cytoplasmic gamma-actin is not required for skeletal muscle development but its absence leads to a progressive myopathy. Dev. Cell *11*, 387–397.

Starr, D.A., and Fridolfsson, H.N. (2010). Interactions between nuclei and the cytoskeleton are mediated by SUN-KASH nuclear-envelope bridges. Annu. Rev. Cell Dev. Biol. *26*, 421–444.

Suetsugu, S., and Gautreau, A. (2012). Synergistic BAR-NPF interactions in actin-driven membrane remodeling. Trends Cell Biol. *22*, 141–150.

Takano, K., Watanabe-Takano, H., Suetsugu, S., Kurita, S., Tsujita, K., Kimura, S.,

Karatsu, T., Takenawa, T., and Endo, T. (2010). Nebulin and N-WASP cooperate to cause IGF-1-induced sarcomeric actin filament formation. Science *330*, 1536–1540.

Takekura, H., Flucher, B.E., and Franzini-Armstrong, C. (2001). Sequential docking, molecular differentiation, and positioning of T-Tubule/SR junctions in developing mouse skeletal muscle. Dev. Biol. *239*, 204–214.

Taneike, M., Mizote, I., Morita, T., Watanabe, T., Hikoso, S., Yamaguchi, O., Takeda, T., Oka, T., Tamai, T., Oyabu, J., et al. (2011). Calpain Protects the Heart from Hemodynamic Stress. J. Biol. Chem. *286*, 32170– 32177.

Tjondrokoesoemo, A., Park, K.H., Ferrante, C., Komazaki, S., Lesniak, S., Brotto, M., Ko, J.-K., Zhou, J., Weisleder, N., and Ma, J. (2011). Disrupted membrane structure and intracellular Ca^{2+} signaling in adult skeletal muscle with acute knockdown of Bin1. PLoS ONE *6*, e25740.

Toussaint, A., Cowling, B.S., Hnia, K., Mohr, M., Oldfors, A., Schwab, Y., Yis, U., Maisonobe, T., Stojkovic, T., Wallgren-Pettersson, C., et al. (2011). Defects in amphiphysin 2 (BIN1) and triads in several forms of centronuclear myopathies. Acta Neuropathol. *121*, 253–266.

Vasli, N., Laugel, V., Bohm, J., Lannes, B., Biancalana, V., and Laporte, J. (2012). Myotubular myopathy caused by multiple abnormal splicing variants in the MTM1 RNA in a patient with a mild phenotype. Eur J Hum Genet *20*, 701–704.

Vlahovich, N., Kee, A.J., Van der Poel, C., Kettle, E., Hernandez-Deviez, D., Lucas, C., Lynch, G.S., Parton, R.G., Gunning, P.W., and Hardeman, E.C. (2009). Cytoskeletal tropomyosin Tm5NM1 is required for normal excitation-contraction coupling in skeletal muscle. Mol. Biol. Cell *20*, 400–409.

Wang, Z., Cui, J., Wong, W.M., Li, X., Xue, W., Lin, R., Wang, J., Wang, P., Tanner, J.A., Cheah, K.S.E., et al. (2013). Kif5b controls the localization of myofibril components for their assembly and linkage to the myotendinous junctions. Development *140*, 617–626.

Wu, X., Yoo, Y., Okuhama, N.N., Tucker, P.W., Liu, G., and Guan, J.-L. (2006). Regulation of RNApolymerase-II-dependent transcription by N-WASP and its

nuclear-binding partners. Nat. Cell Biol. *8*, 756–
763.

Yamada, H., Padilla-Parra, S., Park, S.-J., Itoh, T., Chaineau, M., Monaldi, I., Cremona, O., Benfenati, F., De Camilli, P., Coppey-Moisan, M., et al. (2009). Dynamic interaction of amphiphysin with N-WASP regulates actin assembly. J. Biol. Chem. *284*, 34244–34256.

Zalk, R., Lehnart, S.E., and Marks, A.R. (2007). Modulation of the ryanodine receptor and intracellular calcium. Annu. Rev. Biochem. *76*, 367–385.

Zelhof, A.C., and Hardy, R.W. (2004). WASp is required for the correct temporal morphogenesis of rhabdomere microvilli. J. Cell Biol. *164*, 417–426.

Zhang, X., Xu, R., Zhu, B., Yang, X., Ding, X., Duan, S., Xu, T., Zhuang, Y., and Han, M. (2007). Syne-1 and Syne-2 play crucial roles in myonuclear anchorage and motor neuron innervation. Development *134*, 901–
908.

Zheng, Z., Wang, Z.-M., and Delbono, O. (2002). Charge movement and transcription regulation of L-type calcium channel alpha(1S) in skeletal muscle cells. J. Physiol. (Lond.) *540*, 397–409.

Figure legends:

Figure 1: Peripheral localization of nuclei and organization of tranversal T-tubules paired with Sarcoplasmic Reticulum (SR) in *in vitro* myofibers

A) Images from a representative time-lapse dual color phase contrast movie of H2B-GFP myotubes (supp movie 1), recorded from day 1 (after agrin addition) until day 10, showing nuclear positioning to the periphery during myofiber maturation. Arrowhead indicates an example of a nucleus going to the periphery. Bar, 15 um.

B) Quantification of peripheral nuclei in H2B-GFP and WT myofibers, treated or untreated with agrin and differentiated for 5 or 10 days. n = 3 Error bars, s.e.m. Unpaired t-test: ***p < 0.001, **p < 0.01, *p < 0.05 (untreated vs. treated condition).

C) Representative immunofluorescence images of WT myofibers treated with agrin for 5 days immunostained for DHPR (red), a T-tubule marker, triadin (green), a junctional SR marker and DAPI (blue). On the right is a 2X magnifications of rectangles. Bar, 15 μm.

D) Representative immunofluorescence images of WT myofibers treated with agrin for 10 days immunostained for DHPR (red), triadin (green) and DAPI (blue). On the right is a 2X magnifications of rectangles. Bar, 15 μm.

E) Quantification of transversal triads in WT myofibers treated or untreated with agrin and differentiated for 5 days or 10 days. Error bars, s.e.m. n = 3 Unpaired t-test: ***p < 0.001, **p < 0.01, *p < 0.05 (untreated vs. treated condition).

F) Representative electron microscopy image of WT primary myofibers, transfected with *GAPDH* siRNA and treated with agrin for 10 days. Bar 1um

G) Magnification of the rectangle in F. Arrows indicate triads located between myofibrils at the level of A-I border. Bar 500nm. Inset: high magnification of the right lower triad. Arrowheads indicate the RyR feet. Bar 100 nm. SR : sarcoplasmic reticulum

Figure 2: Amph2 is required for triad formation and peripheral localization of nuclei in *in vitro* myofibers

A) Representative immunofluorescence images of WT primary myofibers treated with agrin for 10 days and immunostained for Amph2 (red), RyR (green) and DAPI (blue). Bar, 15 μm

B) Representative immunofluorescence images of WT primary myofibers treated with agrin for 10 days and immunostained for Amph2 (red), Cav3 (green) and DAPI (blue). Bar, 15 μm

C) Representative immunofluorescence images of WT primary myofibers transfected with *GAPDH* siRNA, treated with agrin for 10 days and immunostained for DHPR (red), triadin (green) and DAPI (blue). On the right 2X magnifications of rectangles. Bar, 15 μm .

D) Representative immunofluorescence images of WT primary myofibers transfected with *Amph2* siRNA, treated with agrin for 10 days and immunostained for DHPR (red), triadin (green) and DAPI (blue). On the right 2X magnifications of rectangles. Bars, 15 μm.

E) Representative immunofluorescence images of WT primary myofibers transfected with *GAPDH* siRNA, treated with agrin for 10 days and immunostained for α-actinin (red), F-Actin (green). Bar, 15 μm.

F) Representative immunofluorescence images of WT primary myofibers transfected with *Amph2* siRNA, treated with agrin for 10 days and immunostained for α-actinin (red), F-Actin (green). Bar, 15 μm.

G) Quantification of peripheral nuclei in myofibers transfected with *GAPDH*, *Amph2* siRNA or *Amph2 ex11* siRNA, and treated with agrin for 10 days. Error bars, s.e.m. n = 3 Unpaired t-test: ***p < 0.001, **p < 0.01, *p < 0.05 (*GAPDH* siRNA vs. *Amph2* siRNA condition)

H) Quantification of transversal triads in myofibers transfected with *GAPDH*, *Amph2* siRNA or *Amph2 Ex11* siRNA, and treated with agrin for 10 days. Error bars, s.e.m. n = 3 Unpaired t-test: ***p < 0.001, **p < 0.01, *p < 0.05 (*GAPDH*

siRNA vs. *Amph2* siRNA condition)

I) Quantification of myofiber thickness in *GAPDH* siRNA, *Amph2* siRNA or *Amph2 Ex11* siRNA, and treated with agrin for 10 days. Error bars, s.e.m. n = 3 Unpaired t-test: *** $p < 0.001$, **$p < 0.01$, *$p < 0.05$ (*GAPDH* siRNA vs. *Amph2* siRNA condition)

Figure 3: Amph2 interacts with N-WASP and the interaction is disrupted by CNM-associated AMPH2 mutations.

A) Western blot with N-WASP and Amph2 antibodies of endogenous Amph2 immunoprecipitation in primary myofibers, treated with agrin for 10 days.

B) Western blot with N-WASP and Amph2 antibodies of endogenous Amph2 immunoprecipitation in mouse muscle or C2C12 myotubes.

C) Western blot with N-WASP and Amph2 antibodies of endogenous N-WASP immunoprecipitation in primary myofibers.

D) Diagrams of the Amph2 constructs used in F. All constructs are N-terminal tagged with GFP. Numbers are amino acid position.

E) Diagrams of the Amph2–full length CNM mutants used in G. Point mutation position is highlighted by a star. All constructs are N-terminal tagged with GFP.

F-G) Western blot with N-WASP and GFP antibodies of GFP immunoprecipitation in C2C12 cells expressing the indicated constructs.

H) GST pull down of N-WASP using the indicated GST tagged Amph2 proteins from muscle homogenates (top) or in vitro transcribed/translated GFP-N-WASP (middle). Coomassie blue staining of loaded gel is showed in the bottom.

Figure 4: N-WASP is required for peripheral localization of nuclei and triad organization during myofiber formation.

A) Representative immunofluorescence images of WT primary myofibers transfected with *GAPDH* siRNA, treated with agrin for 10 days and immunostained for DHPR

(red), triadin (green) and DAPI (blue). Bar, 15 μm.

B) Representative immunofluorescence images of WT primary myofibers transfected with *NWASP* siRNA, treated with agrin for 10 days and immunostained for DHPR (red), triadin (green) and DAPI (blue). Bars, 15 μm.

C) Representative immunofluorescence images of WT primary myofibers transfected with *GAPDH* siRNA, treated with agrin for 10 days and immunostained for α-actinin (red) and F- Actin (green). Bar, 15 μm.

D) Representative immunofluorescence images of WT primary myofibers transfected with *NWASP* siRNA, treated with agrin for 10 days and immunostained for α-actinin (red) and F-Actin (green). Bar, 15 μm.

E) Quantification of peripheral nuclei in myofibers transfected with *GAPDH* or *N-WASP* siRNA and treated with agrin for 10 days. Error bars, s.e.m. n = 3 Unpaired t-test: ***p < 0.001, **p < 0.01, *p < 0.05.

F) Quantification of transversal triads in myofibers transfected with *GAPDH* or *N-WASP* siRNA and treated with agrin for 10 days. Error bars, s.e.m. n = 3 Unpaired t-test: ***p < 0.001, **p < 0.01, *p < 0.05

G) Quantification of myofiber thickness in myofibers transfected with *GAPDH* or *N-WASP* siRNA and treated with agrin for 10 days. Error bars, s.e.m. n = 3 Unpaired t-test: ***p < 0.001, **p < 0.01, *p < 0.05.

Figure 5: N-WASP involvement downstream of Amph2

A) Representative immunofluorescence images of myofibers transfected with *GAPDH* siRNA and GFP (top), GFP-N-WASP full length (N-WASP FL, middle) or GFP-VCA (VCA, bottom), treated with agrin for 10 days and stained for DHPR (red) and DAPI (blue). Bar, 15 μm.

B) Representative immunofluorescence images of myofibers transfected with *Amph2* siRNA and GFP (top), GFP-N-WASP (middle) or GFP-VCA (bottom), treated with agrin for 10 days and stained for DHPR (red) and DAPI (blue). Bar, 15 μm.

C) Representative immunofluorescence images of myofibers transfected with GFP-VCA and *GAPDH* siRNA (top) or *Amph2* siRNA (bottom), and stained for Amph2 (red) and DAPI (blue). Bar, 15 μm.

D) Western blot with Amph2 and β-tubulin antibodies of myofibers transfected with *Amph2* siRNA or *Amph2* siRNA and GFP-VCA.

E) Quantification of peripheral nuclei in myofibers transfected with *GAPDH* (light blue) or *Amph2* (blue) siRNA and with GFP, GFP-N-WASP-FL or GFP-VCA, and treated with agrin for 10 days. Error bars, s.e.m. n = 3 Unpaired t-test: ***p < 0.001, **p < 0.01, *p < 0.05 (GFP vs GFP-NWASP-FL or GFP-VCA).

F) Quantification of transversal triads in myofibers transfected with *GAPDH* (pink) or *Amph2* (red) siRNA and with GFP, GFP-N-WASP-FL or GFP-VCA, and treated with agrin for 10 days. Error bars, s.e.m. n = 3 Unpaired t-test: ***p < 0.001, **p < 0.01, *p < 0.05 (GFP vs GFP-N-WASPFL or GFP-VCA).

G) Quantification of myofiber thickness in myofibers transfected with *GAPDH* (light green) or *Amph2* (green) siRNA and with GFP and GFP-VCA, and treated with agrin for 10 days. Error bars, s.e.m. n = 3 Unpaired t-test: ***p < 0.001, **p < 0.01, *p < 0.05 (GFP vs GFP-VCA conditions).

Figure 6: Role of microtubules and actin in nuclear positioning and triad organization during myofiber maturation

A-C) Representative immunofluorescence images of WT primary myofibers transfected with *GAPDH* siRNA (A) *Map7* siRNA (B) or K*if5b* siRNA (C), treated with agrin for 10 days and subsequently immunostained for DHPR (red), triadin (green) and DAPI (blue). Bar, 15 μm .

D) Quantification of peripheral nuclei in myofibers transfected with *GAPDH, Map7* or *Kif5b* siRNA. Error bars, s.e.m. Unpaired t-test: n = 3 ***p < 0.001, **p < 0.01, *p < 0.05

E) Quantification of transversal triads in myofibers transfected with *GAPDH, Map7* or *Kif5b* siRNA. Error bars, s.e.m. n = 3 Unpaired t-test: ***p < 0.001, **p < 0.01, *p <

0.05

H) Quantification of myofiber thickness in myofibers transfected with *GAPDH, Map7* or *Kif5b* siRNA. Error bars, s.e.m. n = 3 Unpaired t-test: ***p < 0.001, **p < 0.01, *p < 0.05

I) –I) Representative immunofluorescence images of WT primary myofibers untreated (G) or treated with 75 nM of Nocodazol (H) or 10 μM of Latrunculin B (I) at day 5 after agrin treatment, and immunostained at day 10 for DHPR (red), triadin (green) and DAPI (blue). Bar, 15 μm

J) Quantification of peripheral nuclei in myofibers untreated or treated with nocodazole and latrunculin B as described in G-I. Error bars, s.e.m. n = 3 Unpaired t-test: ***p < 0.001, **p < 0.01, *p < 0.05

K) Quantification of transversal triads in myofibers untreated or treated with nocodazole and latrunculin B as described in G-I. Error bars, s.e.m. n = 3 Unpaired t-test: ***p < 0.001, **p < 0.01, *p < 0.05

L) Quantification of myofiber thickness in myofibers untreated or treated with nocodazole and latrunculin B as described in G-I. Error bars, s.e.m. n = 3 Unpaired t-test: ***p < 0.001, **p < 0.01, *p < 0.05

M) –N) Representative immunofluorescence images of WT primary myofibers transfected with RFP-KASH ΔL (M) and RFP-SR-KASH (N), 10 days after agrin addition immunostained for triadin (green) and DAPI (blue). Bar, 15 μm.

O) Quantification of peripheral nuclei in myofibers transfected with RFP-KASH ΔL or RFP-SRKASH as described in M-N. Error bars, s.e.m. n = 3 Unpaired t-test: ***p < 0.001, **p < 0.01, *p

0.05

0.05

P) Quantification of transversal triads in myofibers transfected with RFP-KASH ΔL or RFP-SRKASH as described in M-N. Error bars, s.e.m. n = 3 Unpaired t-test: ***p <

0.001, **p < 0.01, *p

Q) Quantification of myofibers thickness in myofibers transfected with RFP-KASH ΔL or RFP-SRKASH as described in M-N. Error bars, s.e.m. n = 3 Unpaired t-test: ***p < 0.001, **p < 0.01, *p
< 0.05

Figure 7: N-WASP and Amph2 localization in adult muscle and its role on the maintenance
of triad organization

A) Left panel: representative immunofluorescence images of isolated WT mouse muscle fibers immunostained for Amph2 (red) or N-WASP (green); Right panel: line-scan of indicated region in the left panels showing average intensity of N-WASP (green) and Amph2 (red), respectively. Bar, 1 μm.

B) Representative immunofluorescence images of longitudinal sections of WT mouse muscle electroporated with *GAPDH* siRNA and immunostained after 10 days for GAPDH (red) and Amph2 (green). A star indicates a myofiber depleted for GAPDH. Bar, 50 μm.

C) Representative immunofluorescence images of longitudinal sections of WT mouse muscle electroporated with *GAPDH* siRNA and immunostained after 10 days for GAPDH (red) and NWASP (green). A star indicates a myofiber depleted for GAPDH. Bar, 50 μm.

D) Representative immunofluorescence images of longitudinal sections of WT mouse muscle electroporated with *Amph2* siRNA and immunostained after 10 days for Amph2 (red), N-WASP (green). A star indicates a myofiber depleted for Amph2. Bar, 50 μm.

E) Representative immunofluorescence images of longitudinal sections of WT mouse muscle electroporated with *N-WASP* siRNA and immunostained after 10 days for N-WASP (red), and Amph2 (green). A star indicates a myofiber depleted for N-WASP. Bar, 50 μm.

F) Representative immunofluorescence images of longitudinal sections of WT mouse muscle electroporated with *Amph2* siRNA and immunostained after 10 days for Amph2 (red), DHPR (green). A star indicates a myofiber depleted for Amph2. Bar, 50 μm.

G) Representative immunofluorescence images of longitudinal sections of WT mouse muscle electroporated with *N-WASP* siRNA and immunostained after 10 days for, N-WASP (red) and DHPR (green). A star indicates a myofiber depleted for N-WASP. Bar, 50 μm.

H) Representative immunofluorescence images of longitudinal sections of WT mouse muscle electroporated with *Amph2* siRNA and immunostained after 10 days for Amph2 (red) and RyR (green). A star indicates a myofiber depleted for Amph2. Bar, 50 μm.

I) Representative immunofluorescence images of longitudinal sections of WT mouse muscle electroporated with *N-WASP* siRNA and immunostained after 10 days for N-WASP (red), and RyR (green). A star indicates a myofiber depleted for N-WASP. Bar, 50 μm.

J) Left panels: representative immunofluorescence images of isolated mouse muscle fibers, immunostained for triadin (red) and DHPR (green) in *GAPDH* siRNA, *Amph2* siRNA and *NWASP* siRNA electroporated fibers, respectively. Right panel: line-scan of indicated regions in the left panel showing average intensity of N-WASP staining (green) compared to Amph2 (red), respectively. Bar, 1 μm.

Figure 8: N-WASP and Amph2 localization in muscle from healthy and ARCNM patients

A) Representative immunofluorescence images of transversal sections of human muscle from healthy donor (top) or ARCNM patient carrying AMPH2 R154Q mutation, immunostained for DHPR (red), N-WASP (green) and DAPI (blue). Bars, 15 μm.

B) Representative immunofluorescence images of transversal sections of human

muscle from healthy donor (top) or ARCNM patient carrying AMPH2 R154Q mutation, immunostained for Amph2 (red), N-WASP (green) and DAPI (blue). Bars, 15 μm.

C) Representative immunofluorescence images of transversal sections of human muscle from healthy donor (top) or DM1 patient, immunostained for Amph2 (red), N-WASP (green) and DAPI (blue). Bars, 15 μm

D) Schematic representation of the pathways that regulate triad organization and peripheral nuclear position downstream of Amph2 and N-Wasp.

E) Model for peripheral nuclear positioning during myofiber formation. After fusion of myoblast, nuclei (red) of myotubes cluster in the center of the myotube before nuclear spreading. After nuclei spread along the myotube, they become peripheral located at the myofiber periphery.

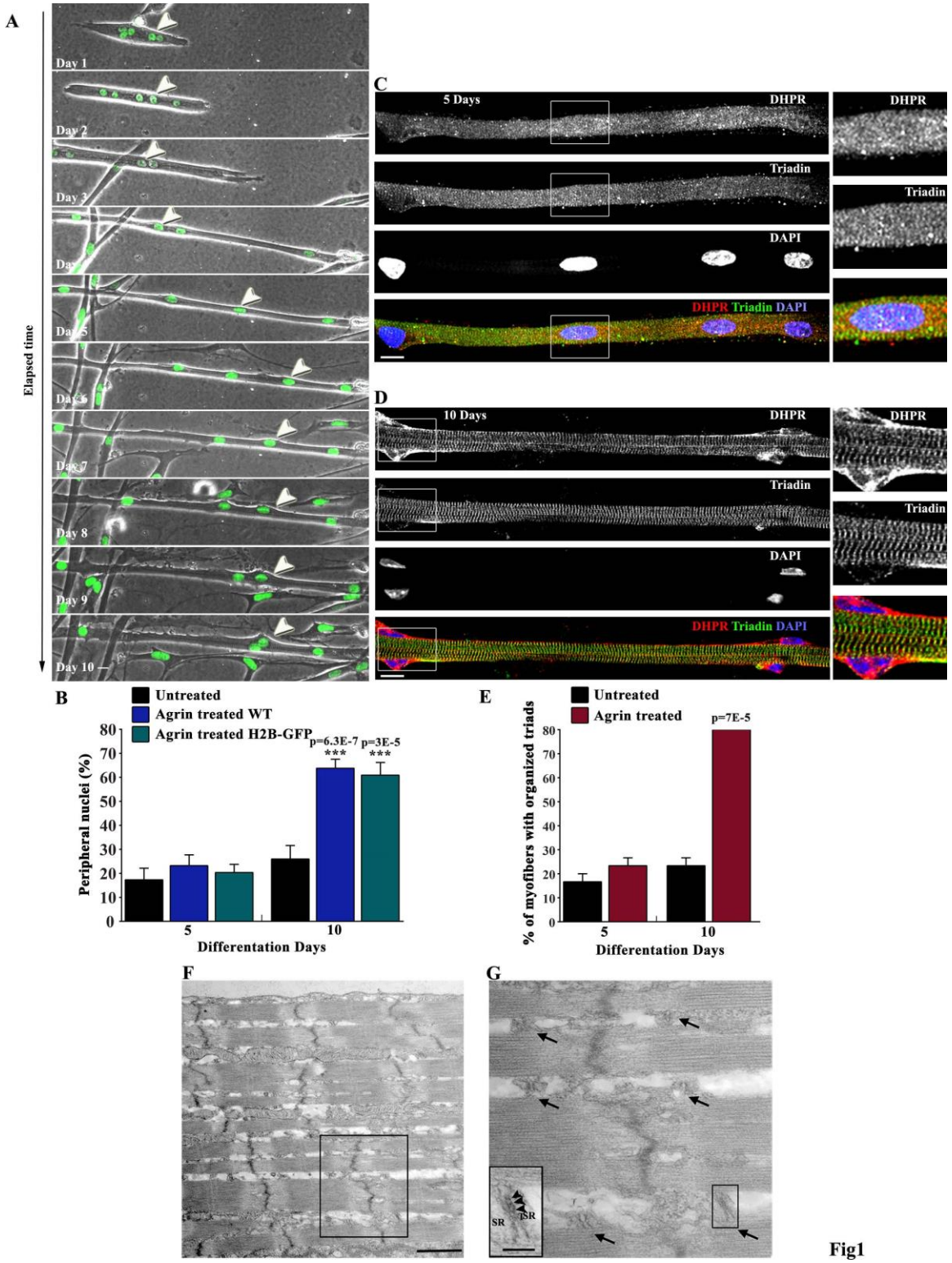
A
Day 1
Day 2
Day 3
Day 4
Day 5
Day 6
Day 7
Day 8
Day 9
Day 10
Elapsed time
C
5 Days
DHPR
Triadin
DAPI
DHPR Triadin DAPI
D
10 Days
DHPR
Triadin
DAPI
DHPR Triadin DAPI
B
Untreated
Agrin treated WT
Agrin treated H2B-GFP
p=6.3E-7
p=3E-5
***
***
Peripheral nuclei (%)
Differentation Days
E
Untreated
Agrin treated
p=7E-5
% of myofibers with organized triads
Differentation Days
F
G
SR
tSR

Fig1

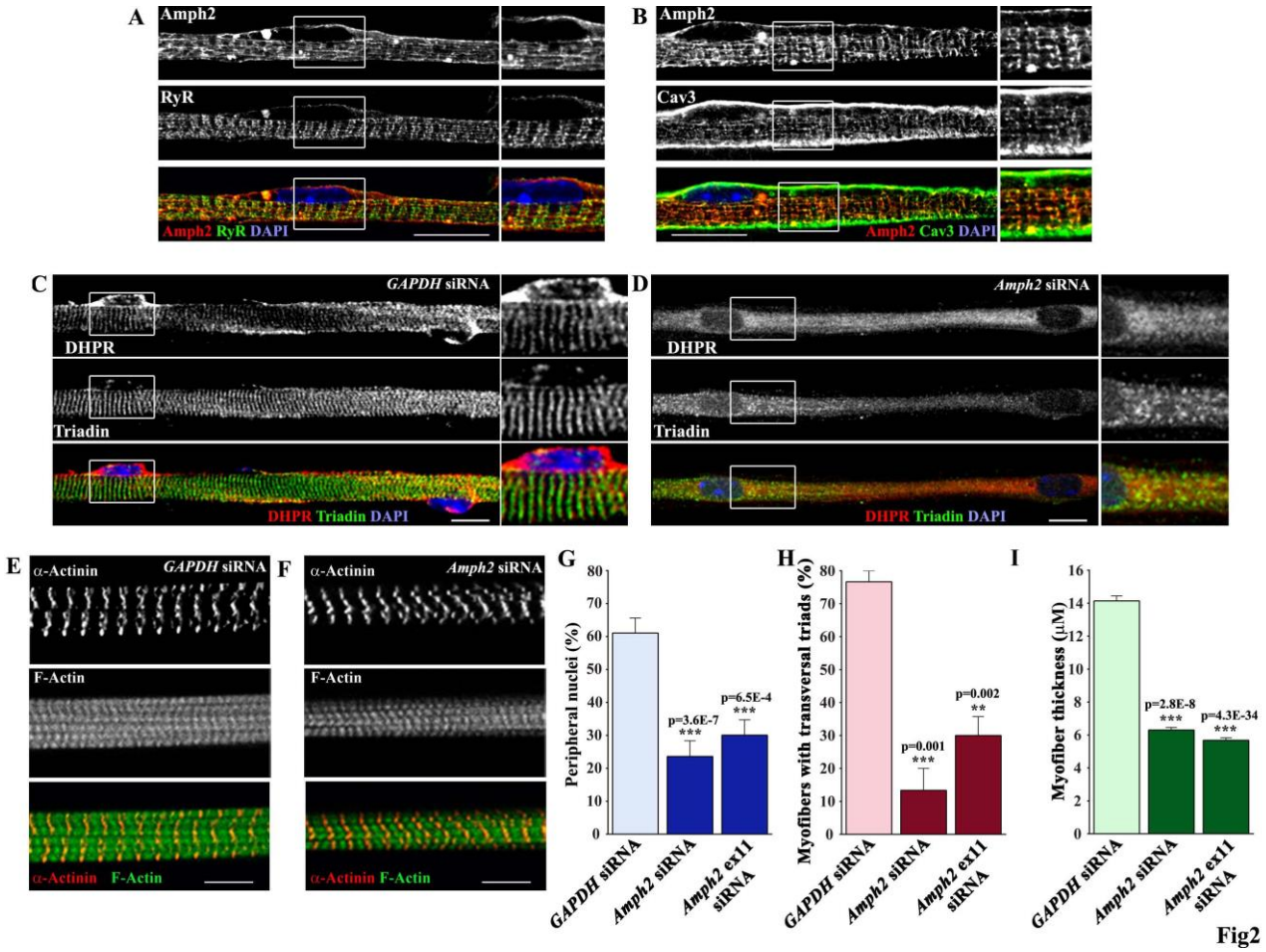
A
Amph2
RyR
Amph2 RyR DAPI
B
Amph2
Cav3
Amph2 Cav3 DAPI
C
GAPDH siRNA
DHPR
Triadin
DHPR Triadin DAPI
D
Amph2 siRNA
DHPR
Triadin
DHPR Triadin DAPI
E
α-Actinin
GAPDH siRNA
F-Actin
α-Actinin F-Actin
F
α-Actinin
Amph2 siRNA
F-Actin
α-Actinin F-Actin
G
Peripheral nuclei (%)
p=3.6E-7
***
p=6.5E-4
***
GAPDH siRNA
Amph2 siRNA
Amph2 ex11 siRNA
H
Myofibers with transversal triads (%)
p=0.001
***
p=0.002
**
GAPDH siRNA
Amph2 siRNA
Amph2 ex11 siRNA
I
Myofiber thickness (μM)
p=2.8E-8
***
p=4.3E-34
***
GAPDH siRNA
Amph2 siRNA
Amph2 ex11 siRNA

Fig2

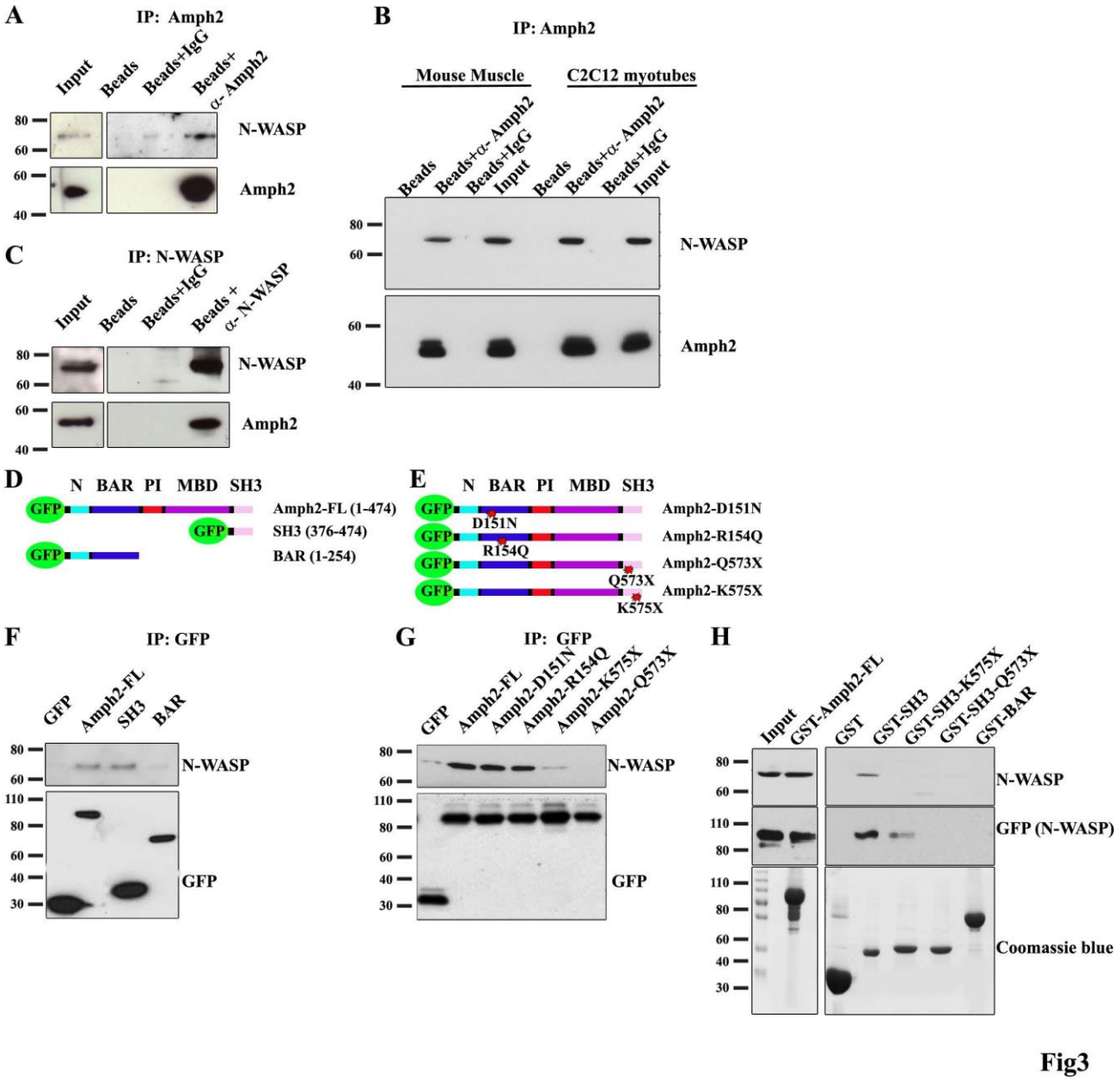
A
IP: Amph2
Input
Beads
Beads+IgG
Beads+ α- Amph2
80
60
60
40
N-WASP
Amph2
B
IP: Amph2
Mouse Muscle
C2C12 myotubes
Beads
Beads+α- Amph2
Beads+IgG
Input
Beads
Beads+α- Amph2
Beads+IgG
Input
80
60
60
40
N-WASP
Amph2
C
IP: N-WASP
Input
Beads
Beads+IgG
Beads + α- N-WASP
80
60
60
40
N-WASP
Amph2
D
N BAR PI MBD SH3
GFP
Amph2-FL (1-474)
GFP
SH3 (376-474)
GFP
BAR (1-254)
E
N BAR PI MBD SH3
GFP
D151N
Amph2-D151N
GFP
R154Q
Amph2-R154Q
GFP
Amph2-Q573X
Q573X
GFP
K575X
Amph2-K575X
F
IP: GFP
GFP
Amph2-FL
SH3
BAR
80
60
110
80
60
40
30
N-WASP
GFP
G
IP: GFP
GFP
Amph2-FL
Amph2-D151N
Amph2-R154Q
Amph2-K575X
Amph2-Q573X
80
60
110
80
60
40
30
N-WASP
GFP
H
Input
GST-Amph2-FL
GST
GST-SH3
GST-SH3-K575X
GST-SH3-Q573X
GST-BAR
80
60
110
80
110
80
60
40
30
N-WASP
GFP (N-WASP)
Coomassie blue

Fig3

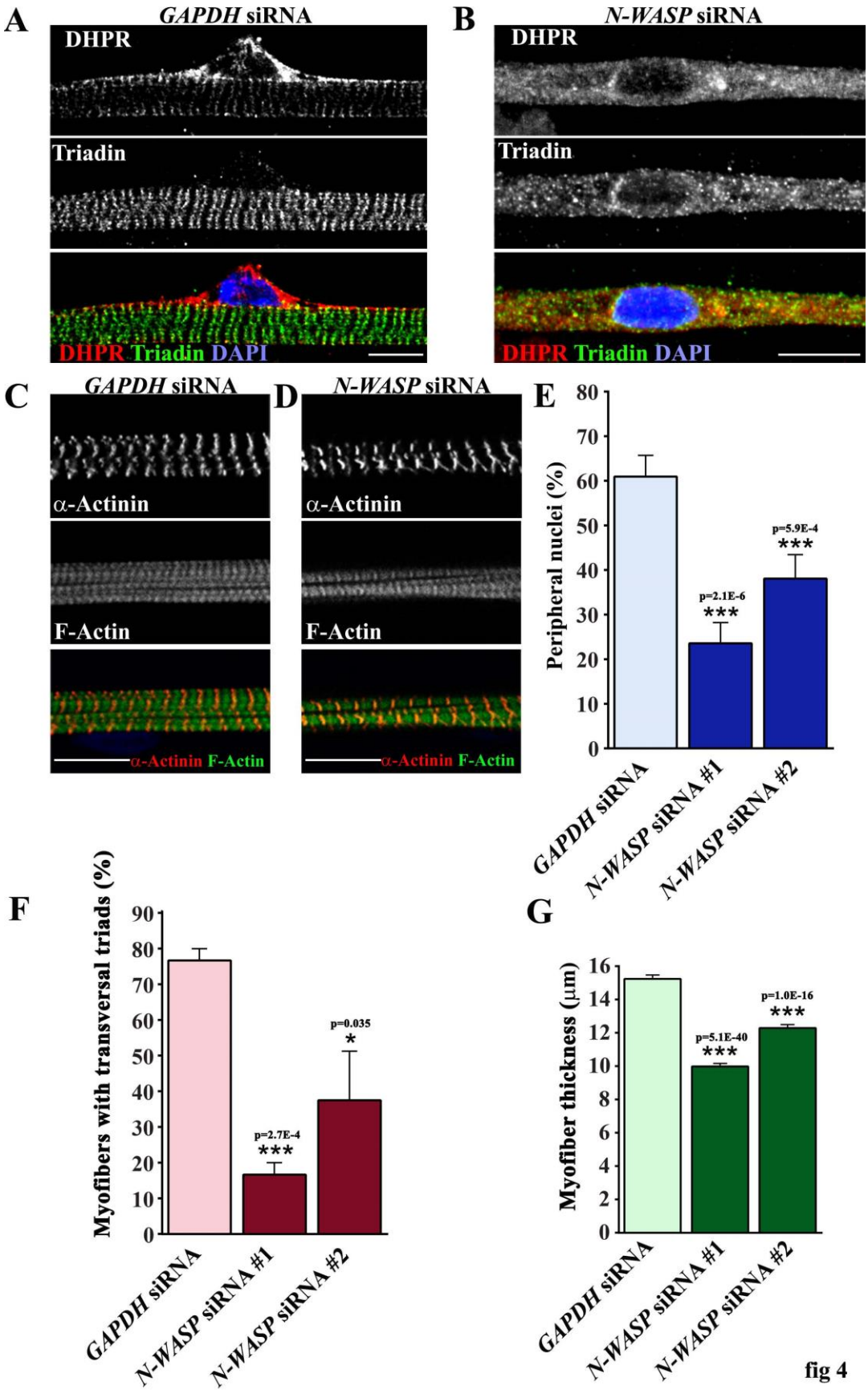
A
GAPDH siRNA
DHPR
Triadin
DHPR Triadin DAPI
B
N-WASP siRNA
DHPR
Triadin
DHPR Triadin DAPI
C
GAPDH siRNA
α-Actinin
F-Actin
α-Actinin F-Actin
D
N-WASP siRNA
α-Actinin
F-Actin
α-Actinin F-Actin
E
Peripheral nuclei (%)
p=2.1E-6
***
p=5.9E-4
***
GAPDH siRNA
N-WASP siRNA #1
N-WASP siRNA #2
F
Myofibers with transversal triads (%)
p=2.7E-4
***
p=0.035
*
GAPDH siRNA
N-WASP siRNA #1
N-WASP siRNA #2
G
Myofiber thickness (μm)
p=5.1E-40
***
p=1.0E-16
***
GAPDH siRNA
N-WASP siRNA #1
N-WASP siRNA #2

fig 4

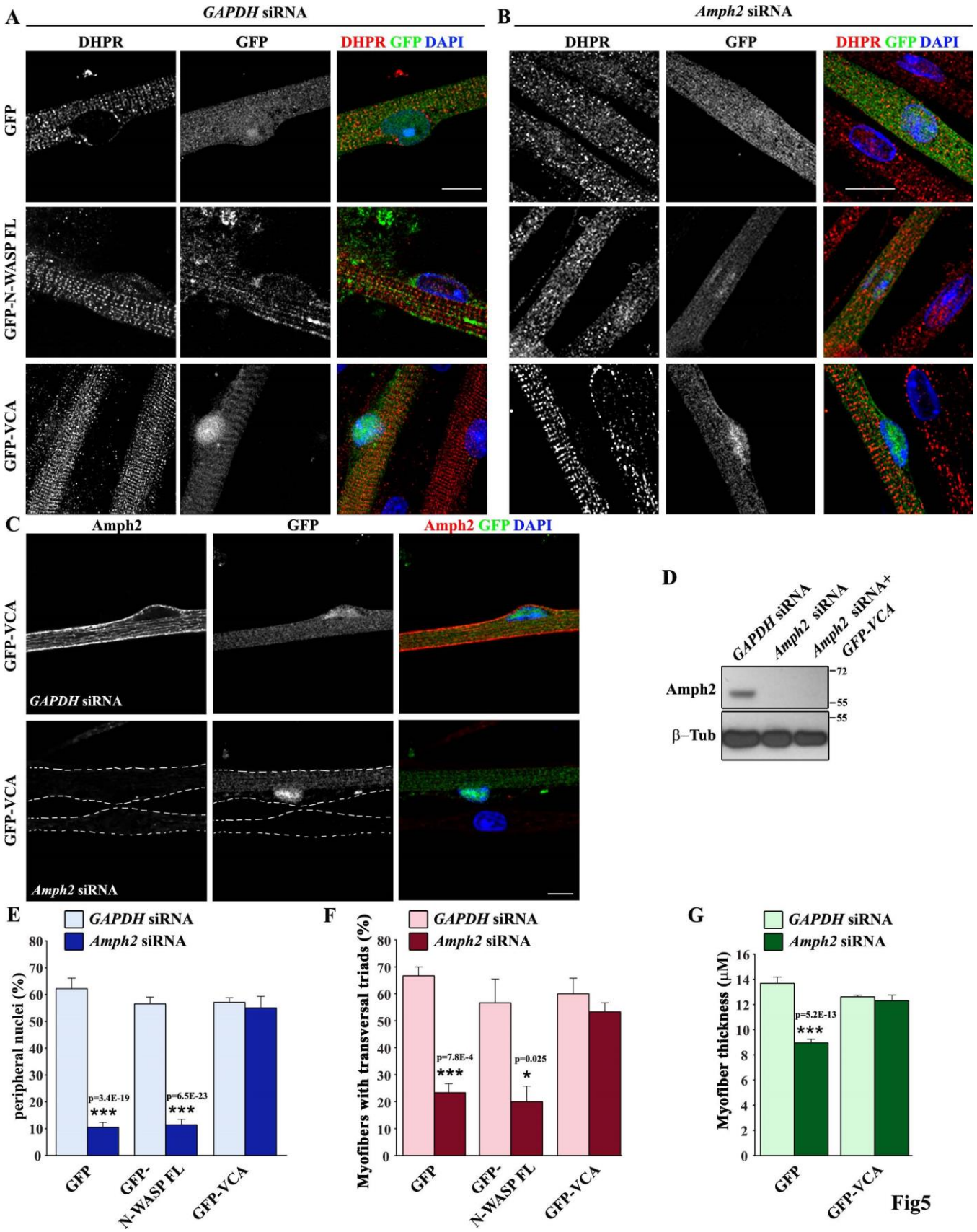
A
GAPDH siRNA
B
Amph2 siRNA
DHPR
GFP
DHPR GFP DAPI
GFP
GFP-N-WASP FL
GFP-VCA
C
Amph2
GFP
Amph2 GFP DAPI
GAPDH siRNA
Amph2 siRNA
D
GAPDH siRNA
Amph2 siRNA
Amph2 siRNA+ GFP-VCA
Amph2
β–Tub
72
55
55
E
peripheral nuclei (%)
p=3.4E-19
***
p=6.5E-23
***
F
Myofibers with transversal triads (%)
p=7.8E-4
***
p=0.025
*
G
Myofiber thickness (μM)
p=5.2E-13
***
GFP
GFP-N-WASP FL
GFP-VCA

Fig5

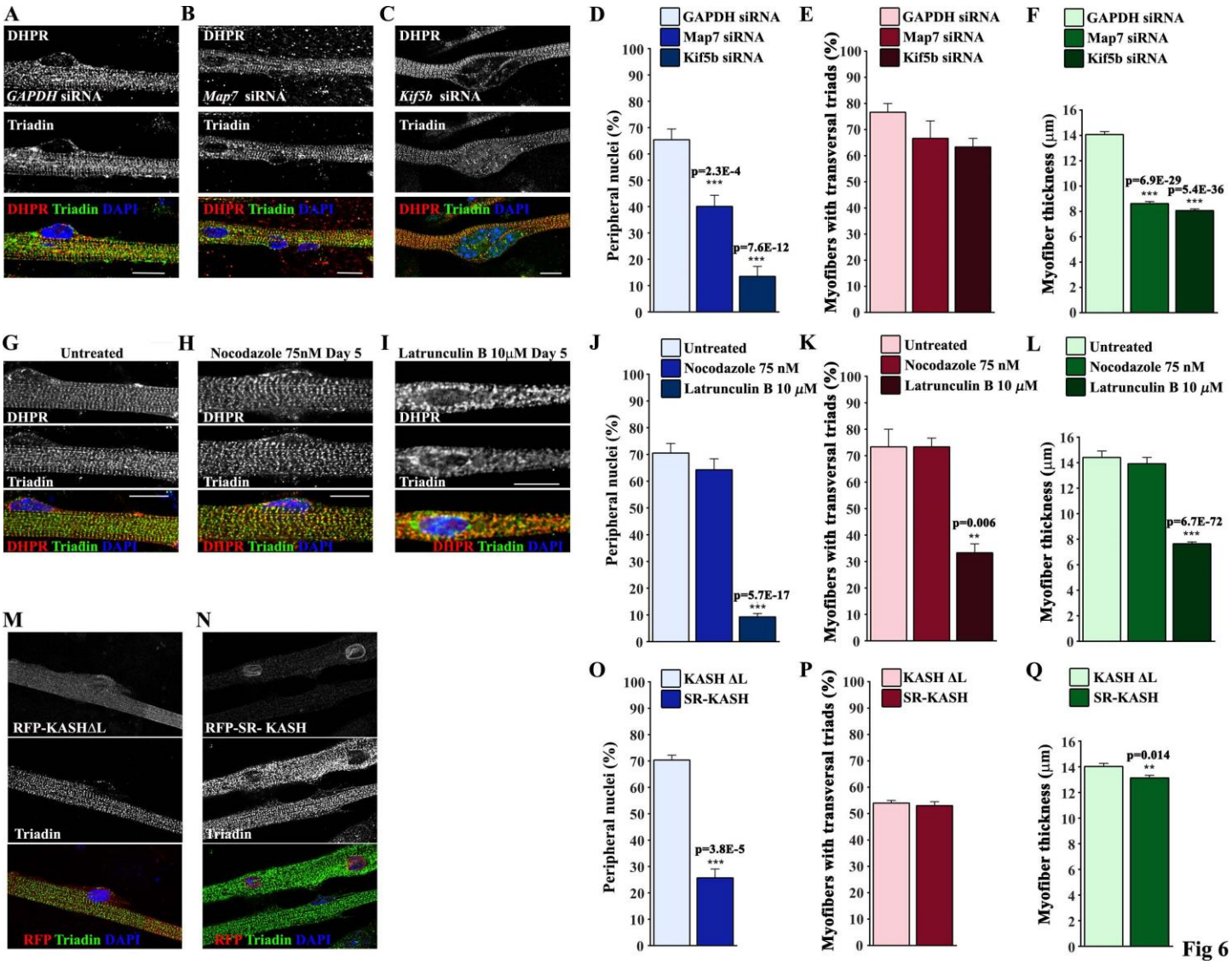
A
B
C
DHPR
GAPDH siRNA
Map7 siRNA
Kif5b siRNA
Triadin
DHPR Triadin DAPI
D
E
F
GAPDH siRNA
Map7 siRNA
Kif5b siRNA
Peripheral nuclei (%)
Myofibers with transversal triads (%)
Myofiber thickness (μm)
p=2.3E-4
p=7.6E-12
p=6.9E-29
p=5.4E-36
G
H
I
Untreated
Nocodazole 75nM Day 5
Latrunculin B 10μM Day 5
J
K
L
Untreated
Nocodazole 75 nM
Latrunculin B 10 μM
p=5.7E-17
p=0.006
p=6.7E-72
M
N
RFP-KASHΔL
RFP-SR- KASH
RFP Triadin DAPI
O
P
Q
KASH ΔL
SR-KASH
p=3.8E-5
p=0.014

Fig 6

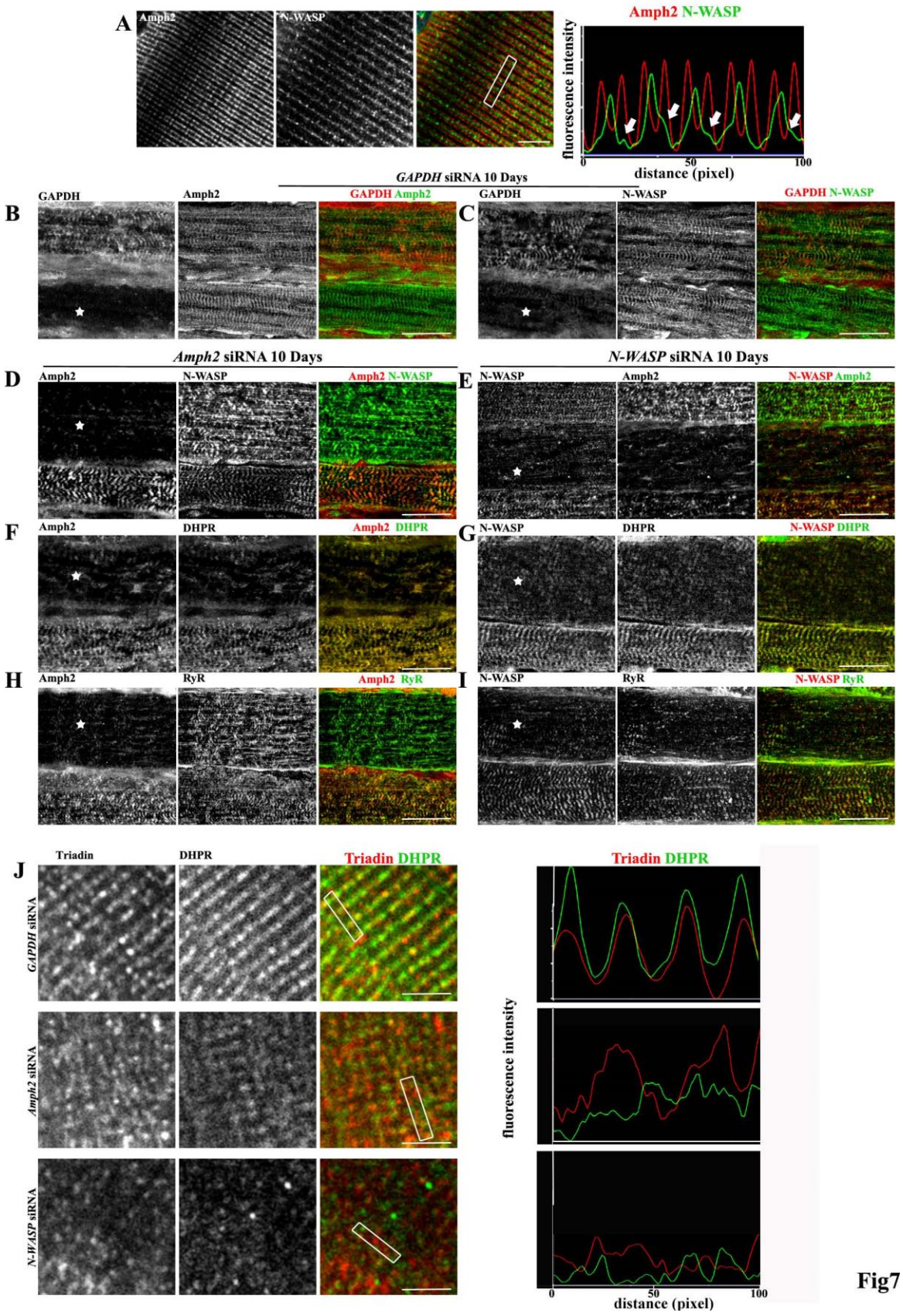
A
Amph2
N-WASP
Amph2 N-WASP
fluorescence intensity
0
50
100
distance (pixel)
GAPDH siRNA 10 Days
B
GAPDH
Amph2
GAPDH Amph2
C
GAPDH
N-WASP
GAPDH N-WASP
Amph2 siRNA 10 Days
D
Amph2
N-WASP
Amph2 N-WASP
N-WASP siRNA 10 Days
E
N-WASP
Amph2
N-WASP Amph2
F
Amph2
DHPR
Amph2 DHPR
G
N-WASP
DHPR
N-WASP DHPR
H
Amph2
RyR
Amph2 RyR
I
N-WASP
RyR
N-WASP RyR
J
Triadin
DHPR
Triadin DHPR
GAPDH siRNA
Amph2 siRNA
N-WASP siRNA
Triadin DHPR
fluorescence intensity
0
50
100
distance (pixel)

Fig7

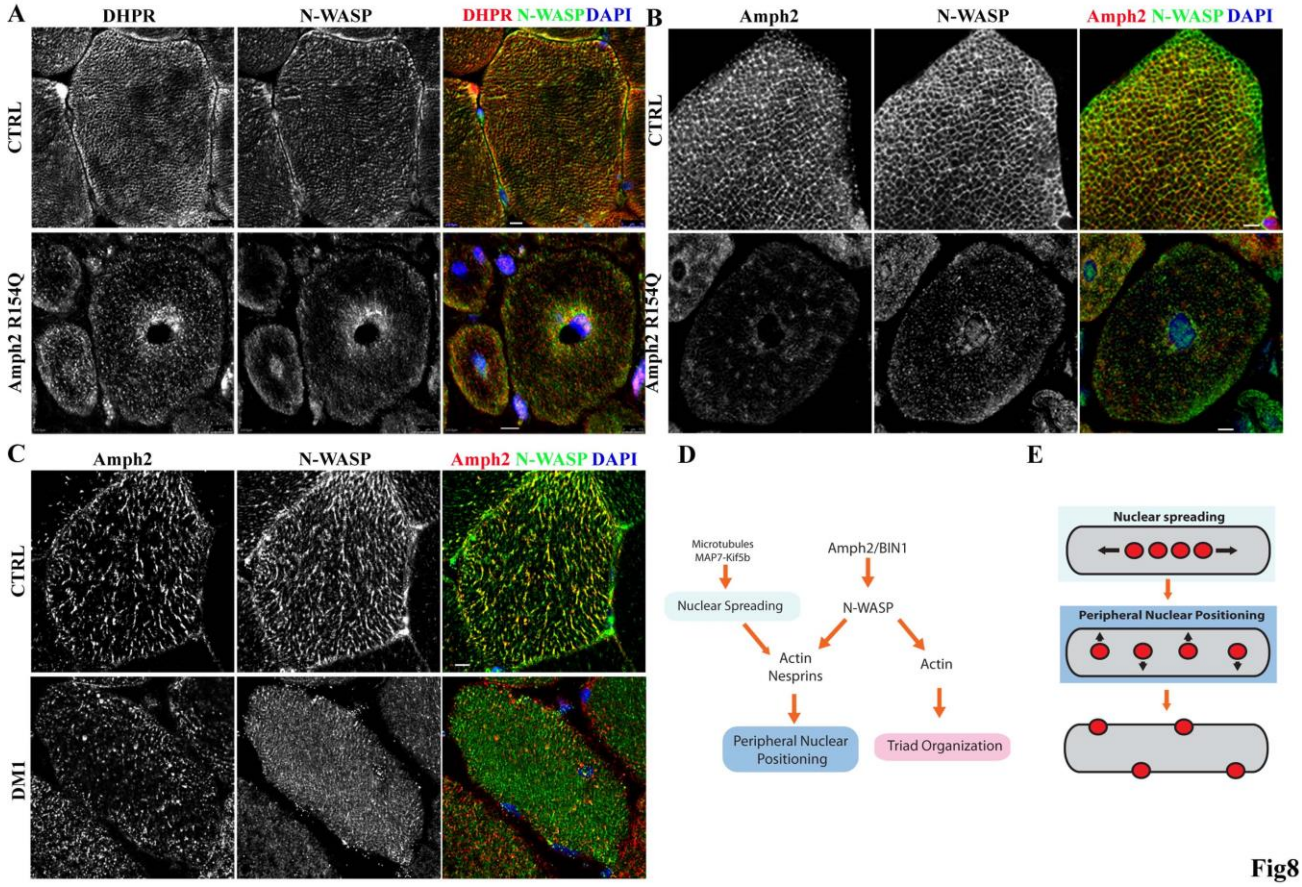
A
DHPR
N-WASP
DHPR N-WASP DAPI
CTRL
Amph2 R154Q
B
Amph2
N-WASP
Amph2 N-WASP DAPI
CTRL
Amph2 R154Q
C
Amph2
N-WASP
Amph2 N-WASP DAPI
CTRL
DM1
D
Microtubules
MAP7-Kif5b
Amph2/BIN1
Nuclear Spreading
N-WASP
Actin
Nesprins
Actin
Peripheral Nuclear Positioning
Triad Organization
E
Nuclear spreading
Peripheral Nuclear Positioning

Fig8

Supplementary legends:

Figure S1: *In vitro* myofiber maturation

A) Schematic representation of *in vitro* model protocol, showing the timeline for plasmid and siRNA transfection, differentiation and matrigel embedding and treatments.

B) Representative immunofluorescence image of H2B-GFP primary myofibers treated with agrin for 10 days and immunostained for F-actin (red), DHPR (green) and DAPI (Blue). Arrows indicate mononucleated myoblasts and arrowheads indicate peripheral nuclei in myofibers. Bar, 15 μm.

C) Representative immunofluorescence image of WT primary myofiber trated with agrin for 5 days and immunostained for α-Actinin (red) and F-Actin (green). Bar, 15 μm. D) Representative immunofluorescence image of WT primary myofiber, transfected with *GAPDH* siRNA, treated with agrin for 10 days and immunostained for β-tubulin (red), and DAPI (Blue). Bar, 15 μm.

E) Representative immunofluorescence image of WT primary myofiber, transfected with *Amph2* siRNA, treated with agrin for 10 days and immunostained for β-Tubulin (red), and DAPI (Blue). Bar, 15 μm.

F) Western Blot with Calnexin2 (Clx2) and β-Tubulin antibodies of myofibers untransfected or transfected with *GAPDH* siRNA or, *Amph2* siRNA or *N-WASP* siRNA and treated with agrin for 10 days.

G) Histograms of relative expression of β-Tubulin showed in F. Error bars, s.e.m.

Figure S2: Amph2, dynamin-2 and myotubularin depletion in cultured primary myofibers and fusion index.

A) Western Blot with GAPDH, Amph2 and β-Tubulin antibodies of myofibers untransfected or transfected with *GAPDH* siRNA or *Amph2*-siRNA and treated with agrin for 10 days.

B-C) Histograms of relative expression of GAPDH (B) or Amph2 (C) in myofibers untransfected or transfected with and *GAPDH* siRNA or *Amph2* siRNA. Error bars, s.e.m. ***$p < 0.001$, **$p < 0.01$, *$p < 0.05$.

D) Western Blot with GAPDH, DNM2 and β-Tubulin antibodies of myofibers untransfected or transfected with *GAPDH* siRNA or *Dnm2*-siRNA and treated with agrin for 10 days.

E -F) Histograms of relative expression of GAPDH (E) or Dnm2 (F) in myofibers untransfected or transfected with and *GAPDH* siRNA or *Dnm2* siRNA. Error bars,

s.e.m. ***p < 0.001, **p < 0.01, *p < 0.05.

G) Western Blot with GAPDH, Mtm1 and β-Tubulin antibodies of myofibers untransfected or transfected with *GAPDH* siRNA or *Mtm1* siRNA and treated with agrin for 10 days.

H-I) Histograms of relative expression of GAPDH (H) or Mtm1 (I) in myofibers untransfected or transfected with and *GAPDH* siRNA or *Mtm1* siRNA. Error bars, s.e.m. ***p < 0.001, **p < 0.01, *p < 0.05.

J) Representative immunofluorescence images of WT primary myofibers transfected with *GAPDH* siRNA, treated with agrin for 10 days, immunostained for DHPR (red), triadin
(green) and DAPI (blue).. Bar, 15 μm .

K) Representative immunofluorescence images of WT primary myofibers transfected with *Dnm2* siRNA, treated with agrin for 10 days, immunostained for DHPR (red), triadin
(green) and DAPI (blue). Bars, 15 μm.

L) Representative immunofluorescence images of WT primary myofibers transfected with *Mtm1* siRNA, treated with agrin for 10 days, immunostained for DHPR (red), triadin
(green) and DAPI (blue). Bars, 15 μm.

M) Quantification of peripheral nuclei of myofibers transfected with *GAPDH* siRNA, *Mtm1* siRNA or *Dnm2* siRNA and GFP (light blue) or GFP-VCA (blue), and treated with agrin for 10 days. Error bars, s.e.m. ***p < 0.001, **p < 0.01, *p < 0.05 (*GAPDH* siRNA vs *Mtm1* or *Dnm2* siRNA).

N) Quantification of the percentage of transversal triads in myofibers transfected with *GAPDH* siRNA, *Mtm1* siRNA or *Dnm2* siRNA and with GFP(pink fill) or GFP-VCA (red fill) and treated with agrin for 10 days Error bars, s.e.m. ***p < 0.001, **p < 0.01, *p < 0.05 (*GAPDH* siRNA vs *Mtm1* or *Dnm2* siRNA).

O) Quantification of myofiber thickness in myofibers transfected with *GAPDH* siRNA, *Mtm1* siRNA or *Dnm2* siRNA and treated with agrin for 10 days. Error bars, s.e.m. ***p < 0.001,

**p < 0.01, *p < 0.05 (*GAPDH* siRNA vs *Mtm1* or *Dnm2* siRNA). P) Histogram of the average number of nuclei/myotubes (fusion index) in myofibers untransfected or transfected with *GAPDH* siRNA, *Mtm1* siRNA or *Dnm2* siRNA and treated with agrin for 10 days . Error bars, s.e.m. p>0.5.

Figure S3: Calcium responses in *Amph2*-depleted myofibers. Effects of *N-WASP* depletion and Amph2 mutations in cultured primary myofibers

A-B) Time course of Fluo-4 fluorescence intensity (F/F0) in steady state and after KCl (A) or Caffeine (B) stimulation of WT primary myofibers transfected with *GAPDH* siRNA (blue line) or *Amph2* siRNA (red line), treated with agrin for 10 days.

C) Images from a representative time-lapse calcium imaging of Fluo-4 fluorescence in steady state (0 and 60 sec) and after Caffeine stimulation (arrow) of WT primary myofibers transfected with *GAPDH* siRNA (top) or *Amph2* siRNA (bottom), treated with agrin for 10 days.

D-E) Representative immunofluorescence images of WT primary myofibers expressing GFP-Amph2 R154Q (D) or GFP-Amph2 K575X (E), treated with agrin for 10 days and immunostained for DHPR (red), triadin (green) and DAPI (blue). Bars, 15 μm.

F) Quantification of peripheral nuclei in myofibers expressing GFP, GFP-Amph2 R154Q or GFP-Amph2 K575X and treated with agrin for 10 days. Error bars, s.e.m. ***p < 0.001, **p < 0.01, *p < 0.05 (GFP vs GFP-Amph2 R154Q or GFP-Amph2 K575X condition).

G) Quantification of transversal triads in myofibers expressing GFP, GFP-Amph2 R154Q or GFP-Amph2 K575X and treated with agrin for 10 days. Error bars, s.e.m. ***p < 0.001, **p < 0.01, *p < 0.05 (GFP vs GFP-Amph2 R154Q or GFP-Amph2 K575X condition).

H) Quantification of myofiber thickness in myofibers expressing GFP or Amph2 GFP R154Q or Amph2 GFP K575X myofibers and treated with agrin for 10 days. Error bars,
s.e.m. ***p < 0.001, **p < 0.01, *p < 0.05 (GFP vs GFP-Amph2 R154Q or GFP-Amph2 K575X condition).

I) Western blot with N-WASP and β-Tubulin antibodies of myofibers transfected with *GAPDH*-siRNA and *N-WASP* siRNA and treated with agrin for 10 days.

J) Histogram of the relative expression of N-WASP in myofibers transfected with *GAPDH* siRNA and *N-WASP* siRNA and treated with agrin for 10 days. Error bars, s.e.m. ***p <
0.001.

Fig S4: Specific role of Amph2 in CNM phenotype and rescue by constitutively active NWASP

A) Western blot with Amph2, GFP and β-Tubulin antibodies of myofibers transfected with *GAPDH* siRNA, *Amph2* ex11 siRNA or *Amph2* ex11 siRNA and VCA-GFP, treated with agrin for 10 days .

B) Quantification of peripheral nuclei in myofibers transfected with *GAPDH* siRNA (light blue fill) or *Amph2* ex11 siRNA (blue), GFP or GFP-VCA, and treated with agrin for 10 days. Error bars, s.e.m. ***p < 0.001, **p < 0.01, *p

< 0.05 (*GAPDH* siRNA vs *Amph2 ex11* siRNA).

C) Quantification of transversal triads in myofibers transfected with *GAPDH* siRNA (light blue fill) or *Amph2* ex11 siRNA (blue), GFP or GFP-VCA, and treated with agrin for 10 days. Error bars, s.e.m. ***p < 0.001, **p < 0.01, *p < 0.05 (*GAPDH* siRNA vs *Amph2 ex11* siRNA).

D) Representative immunofluorescence images of myofibers transfected with *Amph2* ex3 siRNA and TdT (top) or TdT-VCA (bottom), treated with agrin for 10 days and stained for DHPR (red) and DAPI (blue).

E) Quantification of peripheral nuclei in myofibers transfected with *GAPDH* siRNA or *Amph2* siRNA, TdT or TdT-VCA, treated with agrin for 10 days. Error bars, s.e.m. ***p
< 0.001 (*GAPDH* siRNA vs *Amph2* siRNA).

F) Quantification of the percentage of transversal triads in myofibers transfected with *GAPDH* siRNA or *Amph2* siRNA, TdT or TdT-VCA, treated with agrin for 10 days. Error bars, s.e.m. **p < 0.01 (*GAPDH* siRNA vs *Amph2* siRNA).

Figure S5: Amph2 and N-WASP localization in mouse muscle

A) Representative immunofluorescence images of a transversal section of mouse muscle immunostained for DHPR (red) and N-WASP (green). Bar, 10 μm.

B) Left panels: representative immunofluorescence images of isolated mouse muscle fibers, immunostained for α-actinin (red) and N-WASP (green). Right panel: line-scan of indicated regions in the left panels showing average intensity of N-WASP (green) and αactinin (red). Bar, 1 μm.

C) Left panels: representative immunofluorescence images of an isolated mouse muscle fibers, immunostained for DHPR (red) and N-WASP (green). Right panel: line-scan of indicated regions in the left panels showing average intensity of N-WASP (green) and DHPR (red) stainings, respectively. Bar, 1 μm.

D) Left panels: representative immunofluorescence images of an isolated mouse muscle fiber, immunostained for α-actinin (red) and Amph2 (green). Right panel: line-scan analysis of indicated regions in the left panel showing average intensity of Amph2 staining (green) and α-actinin (red) respectively. Bar, 1 μm.

E) Left panel: Representative immunofluorescence images of WT primary myofibers treated with agrin for 10 days and immunostained for DHPR (red), N-WASP (green) and DAPI (blue). Bar, 15 μm; Right panel: line-scan of indicated region in the left panel showing average intensity of N-WASP (green) and DHPR (red), respectively. Bar, 1 μm.

Figure S6: *in vivo* siRNA and plasmid DNA electroporation and fiber isolation

A) Representative images of isolated muscle fibers 10 days after electroporation of siRNA and TdT, showing negative (not expressing TdT) and positive (expressing TdT) myofibers . Left panel: TdT fluorescence. Right panel: Brightfield. Bar, 100 μm.

B) Representative immunofluorescence images of an isolated mouse muscle fibers, electroporated with *GAPDH* siRNA, *Amph2* siRNA or *N-WASP* siRNA, and immunostained for Amph2 (red) and N-WASP (green). Bar, 1 μm.

C) Representative image of isolated muscle fibers 10 days after electroporation of GFP-tagged vectors, showing negative (not expressing GFP) and positive (expressing GFP) myofibers . Left panel: GFP fluorescence. Right panel: Brightfield. Bar, 100 μm.

D) Representative immunofluorescence images of an isolated mouse muscle fibers, electroporated with GFP, GFP-Amph2-R154Q and GFP-Amph2-K573X, and immunostained for N-WASP. Bars, 1 μm.

Figure S7: α-actinin and F-actin organization in myofibers

A) Representative immunofluorescence images of an isolated mouse muscle fiber electroporated with *GAPDH* siRNA, *Amph*2 siRNA and *N-WASP* siRNA, immunostained for α-actinin (red) and F-Actin (green). Bars, 1 μm.

B) Representative immunofluorescence images of isolated mouse muscle fiber electroporated with CTRL GFP, GFP-AMPH2 R154Q and GFP-AMPH2K573X, respectively, and immunostained for α-actinin (red) and F-Actin (green). Bars, 1 μm.

Figure S8: N-WASP and Amph2 localization in muscle from healthy, XLCNM and ADCNM patients

A) Western blot analysis of control and ARCNM human biopsies homogenates after differential centrifugation, with N-WASP, Amph2, DHPR, Caveolin-3 (cav3) and α-Actinin antibodies.

B) Histogram with the quantification of (A), corresponding to the distribution (relative percentage of total protein) of N-WASP, Amph2, DHPR, cav3 and α-Actinin in different cellular fractions (1500g -myofibrils, 15000g -Organelle membranes and extrasarcomeric structures, 150000g -microsomes and macrocomplexes and cytosol). Error bars, s.e.m

C) Representative immunofluorescence images of transversal sections of human muscle from healthy donor (top) and ADCNM patient carrying DNM2 Q368K mutation (bottom), immunostained for DHPR (red), N-WASP (green) and DAPI (blue). Bars, 15 μm.

D) Representative immunofluorescence images of transversal sections of human muscle from healthy donor (CTRL, top) or XLCNM patient carrying R421insFIG mutation (bottom), immunostained for DHPR (red), N-WASP (green) and DAPI (blue). Bars, 15 μm.

E) Representative immunofluorescence images of transversal sections of human muscle from healthy donor (CTRL, top) or ADCNM patient carrying DNM2

Q368K mutation (bottom), immunostained for Amph2 (red), N-WASP (green) and DAPI (blue). Bars, 15
μm.

F) Representative immunofluorescence images of transversal sections of human muscle from healthy donor (CTRL, top) or XLCNM patient carrying R421insFIG (bottom), immunostained for Amph2 (red), N-WASP (green) and DAPI (blue). Bars, 15 μm.

Fig S9: mRNA and protein expression in muscle from healthy, XLCNM, ARCNM, ADCNM and DM1 patients

A) Relative mRNA expression of N-WASP, DHPR, Amph2, DNM2 and MTM1 in muscle biopsies from healthy (CTRL), XLCNM, ARCNM, ADCNM and DM1 patients assessed by real time PCR.

B) Western blot with Amph2, N-WASP, DHPR, DNM2, MTM1 and α-Actinin antibodies in CTRL, XLCNM, ADCNM, ARCNM from healthy or patient muscle biopsies carrying the indicated mutations. Levels may differ depending on patients.

C) Histograms of the relative protein expression of Amph2, N-WASP, DHPR, DNM2, MTM1 and DNM2 in CTRL, XLCNM, ADCNM, ARCNM from healthy or patient muscle biopsies showed in (B). Error bars, s.e.m. ***$p < 0.001$, **$p < 0.01$, *$p < 0.05$ (patient versus ctrl conditions).

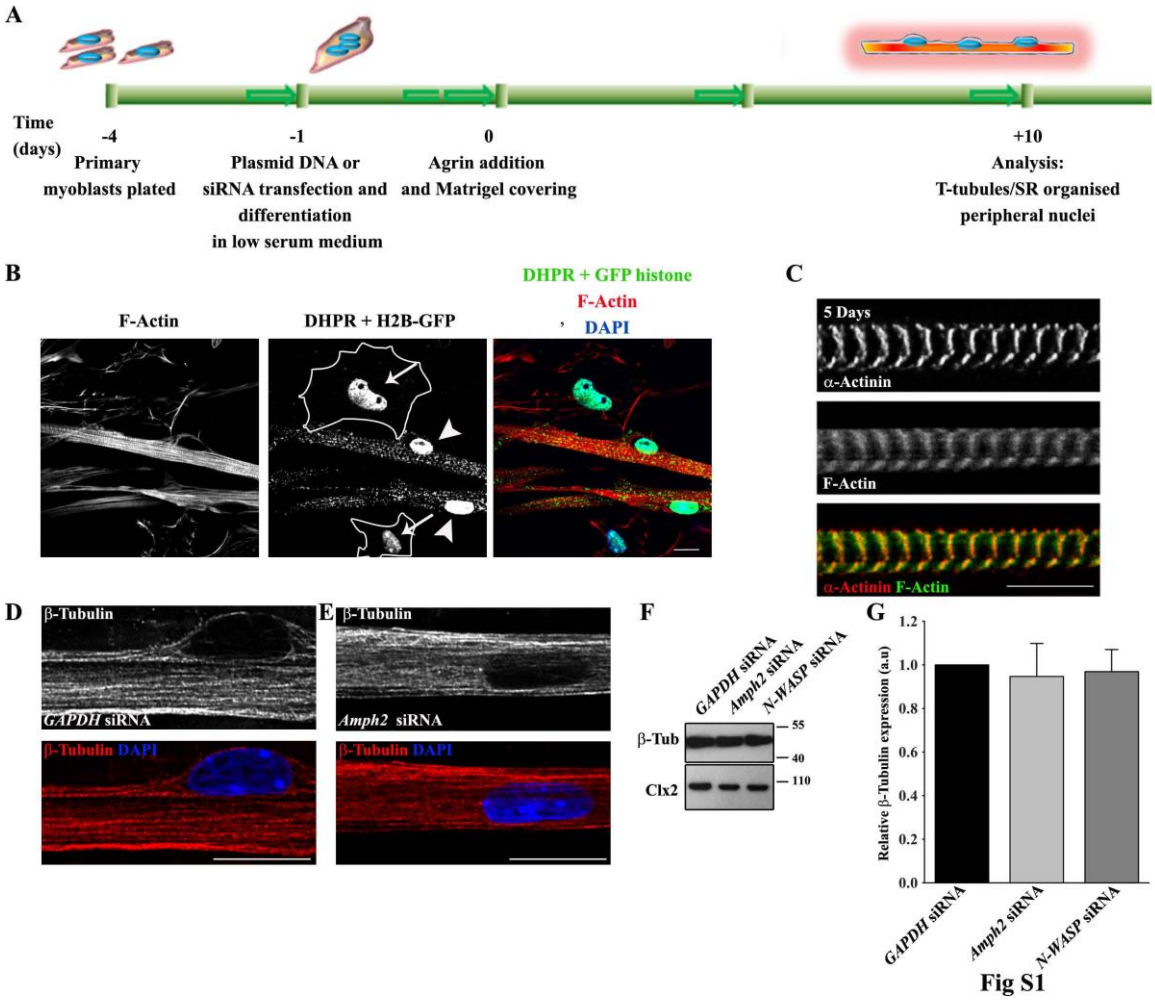
A
Time (days)
-4
Primary myoblasts plated
-1
Plasmid DNA or siRNA transfection and differentiation in low serum medium
0
Agrin addition and Matrigel covering
+10
Analysis: T-tubules/SR organised peripheral nuclei
B
F-Actin
DHPR + H2B-GFP
DHPR + GFP histone
F-Actin
DAPI
C
5 Days
α-Actinin
F-Actin
α-Actinin F-Actin
D
β-Tubulin
GAPDH siRNA
β-Tubulin DAPI
E
β-Tubulin
Amph2 siRNA
β-Tubulin DAPI
F
GAPDH siRNA
Amph2 siRNA
N-WASP siRNA
β-Tub
Clx2
55
40
110
G
Relative β-Tubulin expression (a.u)
1.2
1.0
0.8
0.6
0.4
0.2
0.0
GAPDH siRNA
Amph2 siRNA
N-WASP siRNA

Fig S1

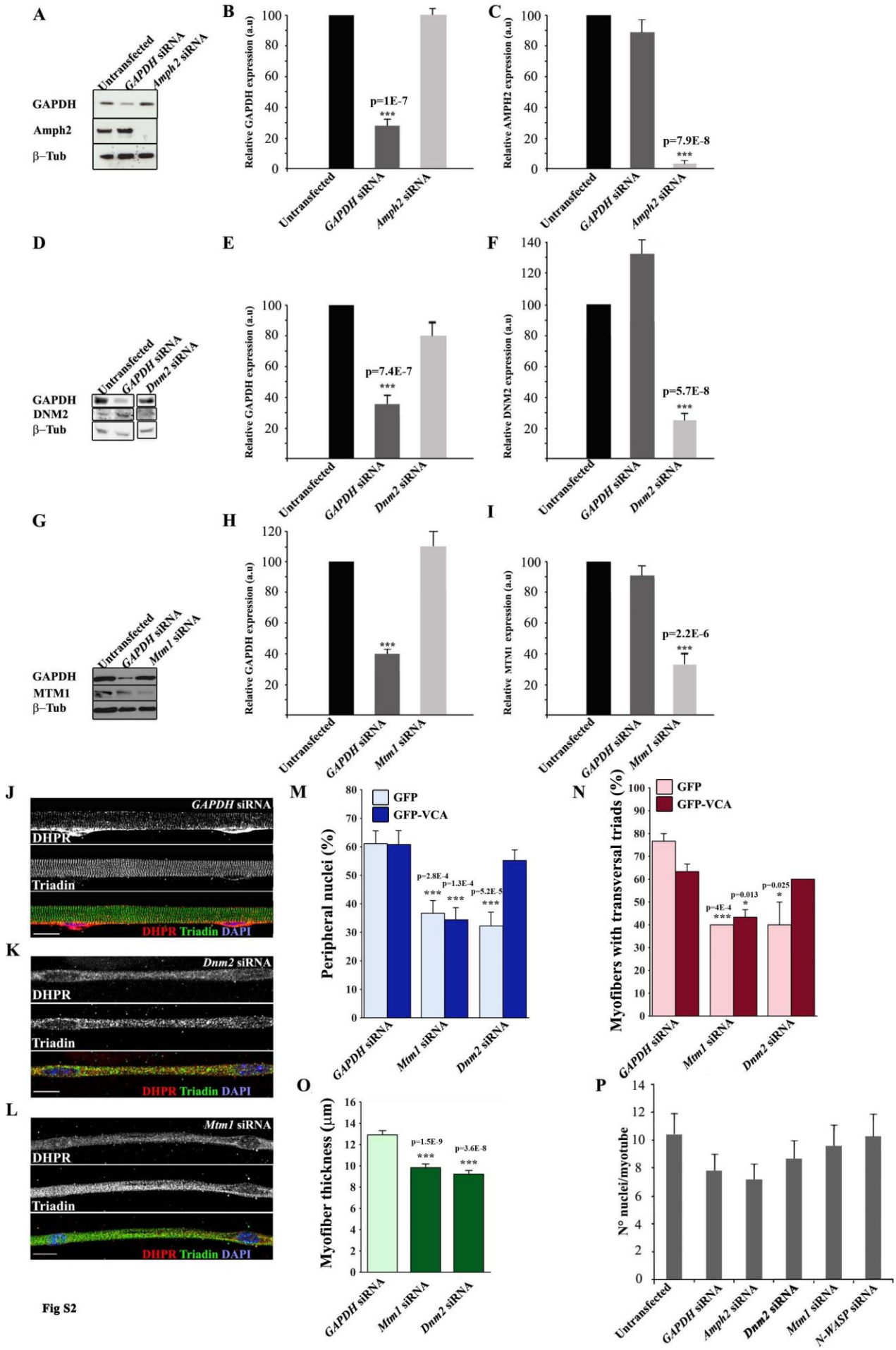
A
Untransfected
GAPDH siRNA
Amph2 siRNA
GAPDH
Amph2
β–Tub
B
Relative GAPDH expression (a.u)
p=1E-7
***
C
Relative AMPH2 expression (a.u)
p=7.9E-8
***
D
Untransfected
GAPDH siRNA
Dnm2 siRNA
GAPDH
DNM2
β–Tub
E
Relative GAPDH expression (a.u)
p=7.4E-7
***
F
Relative DNM2 expression (a.u)
p=5.7E-8
***
G
Untransfected
GAPDH siRNA
Mtm1 siRNA
GAPDH
MTM1
β–Tub
H
Relative GAPDH expression (a.u)
***
I
Relative MTM1 expression (a.u)
p=2.2E-6
***
J
GAPDH siRNA
DHPR
Triadin
DHPR Triadin DAPI
K
Dnm2 siRNA
DHPR
Triadin
DHPR Triadin DAPI
L
Mtm1 siRNA
DHPR
Triadin
DHPR Triadin DAPI
M
GFP
GFP-VCA
Peripheral nuclei (%)
p=2.8E-4
p=1.3E-4
p=5.2E-5
N
GFP
GFP-VCA
Myofibers with transversal triads (%)
p=4E-4
p=0.013
p=0.025
O
Myofiber thickness (µm)
p=1.5E-9
p=3.6E-8
P
N° nuclei/myotube
Untransfected
GAPDH siRNA
Amph2 siRNA
Dnm2 siRNA
Mtm1 siRNA
N-WASP siRNA

Fig S2

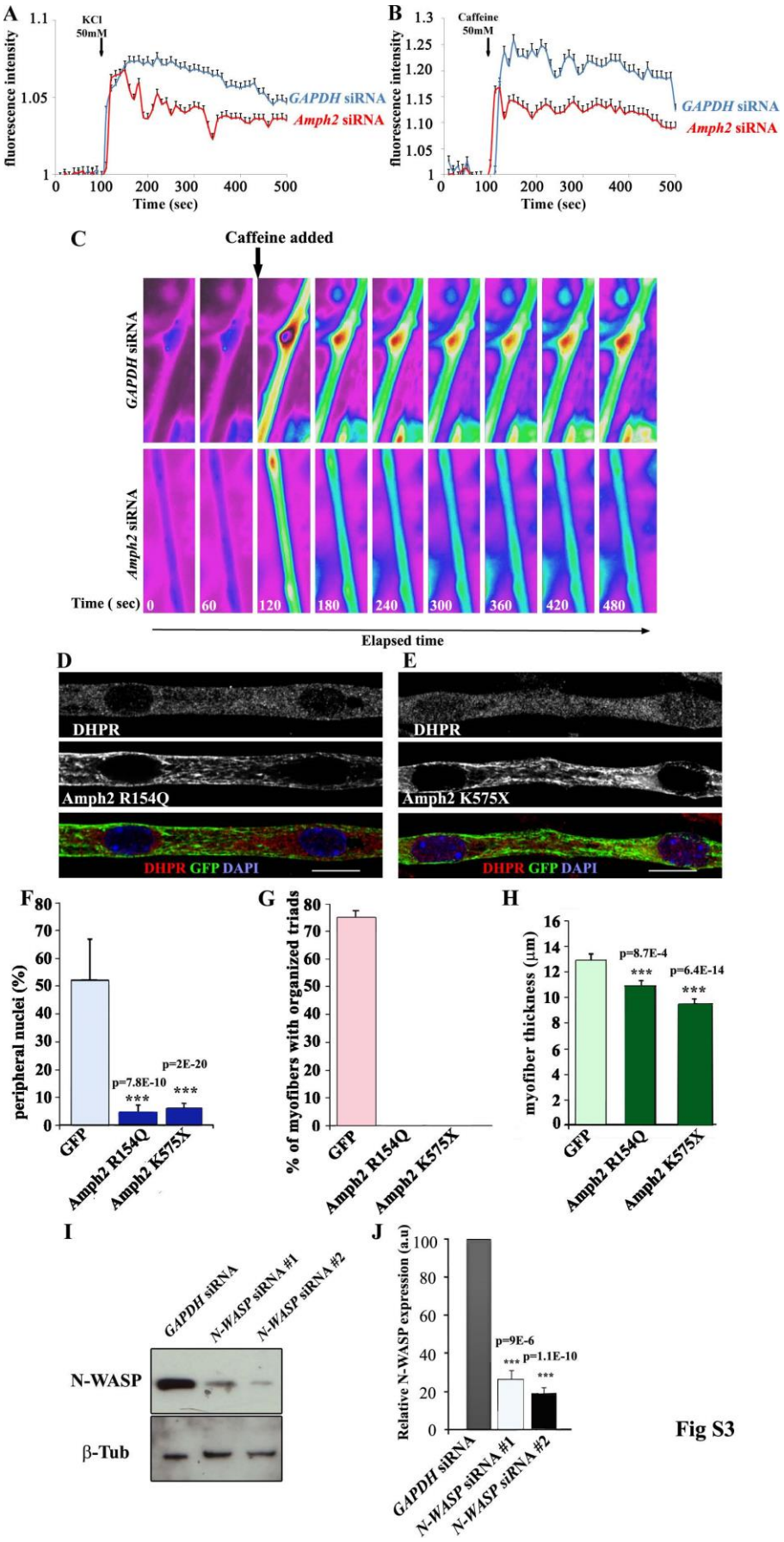
A
KCl
50mM
fluorescence intensity
GAPDH siRNA
Amph2 siRNA
Time (sec)
B
Caffeine
50mM
fluorescence intensity
GAPDH siRNA
Amph2 siRNA
Time (sec)
C
Caffeine added
GAPDH siRNA
Amph2 siRNA
Time (sec)
0
60
120
180
240
300
360
420
480
Elapsed time
D
DHPR
Amph2 R154Q
DHPR GFP DAPI
E
DHPR
Amph2 K575X
DHPR GFP DAPI
F
peripheral nuclei (%)
p=7.8E-10
***
p=2E-20
***
GFP
Amph2 R154Q
Amph2 K575X
G
% of myofibers with organized triads
GFP
Amph2 R154Q
Amph2 K575X
H
myofiber thickness (µm)
p=8.7E-4
***
p=6.4E-14
***
GFP
Amph2 R154Q
Amph2 K575X
I
GAPDH siRNA
N-WASP siRNA #1
N-WASP siRNA #2
N-WASP
β-Tub
J
Relative N-WASP expression (a.u)
p=9E-6
***
p=1.1E-10
***
GAPDH siRNA
N-WASP siRNA #1
N-WASP siRNA #2

Fig S3

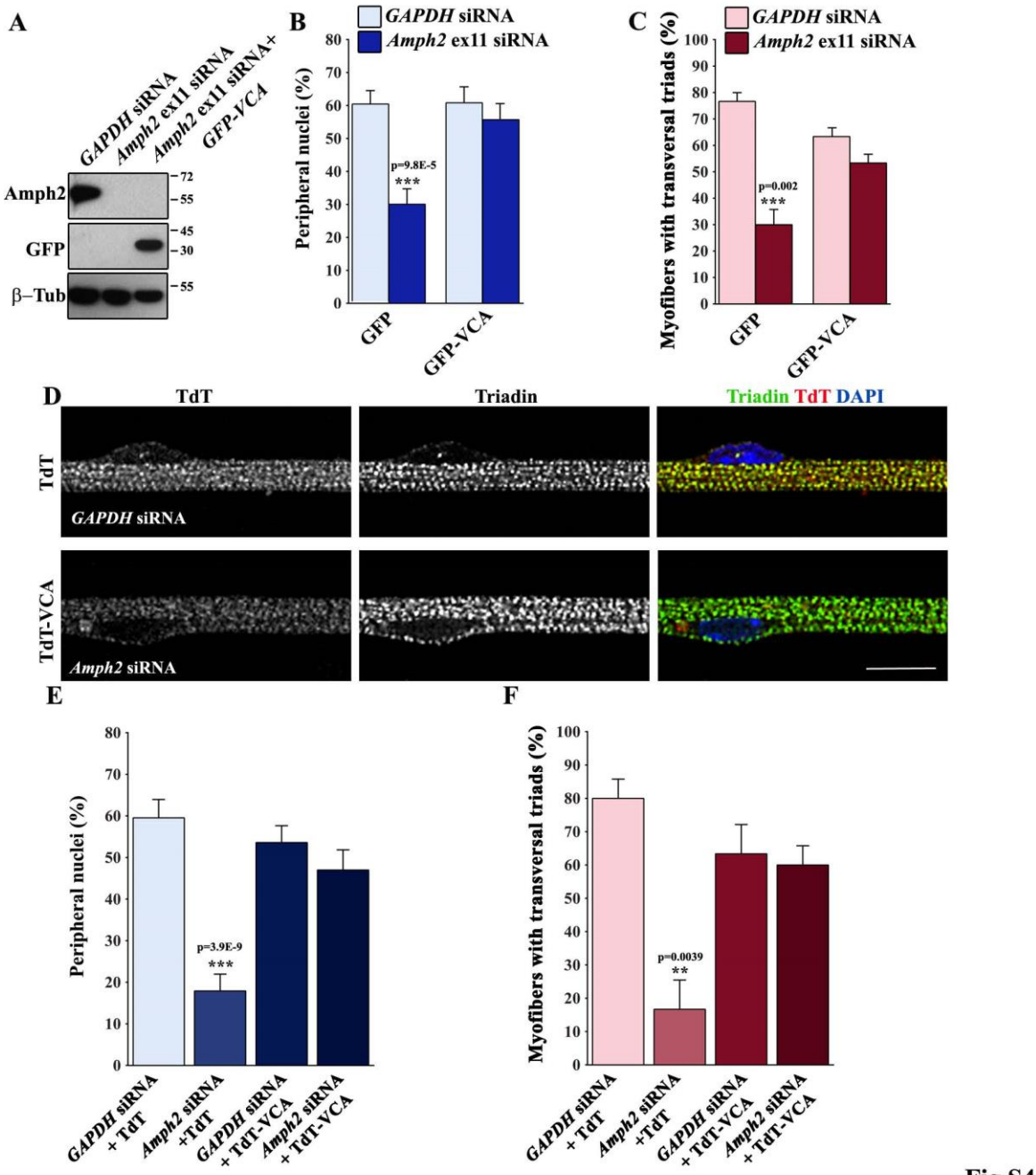
A
GAPDH siRNA
Amph2 ex11 siRNA
Amph2 ex11 siRNA+
GFP-VCA
Amph2
GFP
β–Tub
72
55
45
30
55
B
GAPDH siRNA
Amph2 ex11 siRNA
Peripheral nuclei (%)
p=9.8E-5
***
GFP
GFP-VCA
C
GAPDH siRNA
Amph2 ex11 siRNA
Myofibers with transversal triads (%)
p=0.002
***
GFP
GFP-VCA
D
TdT
Triadin
Triadin TdT DAPI
TdT
GAPDH siRNA
TdT-VCA
Amph2 siRNA
E
Peripheral nuclei (%)
p=3.9E-9
***
GAPDH siRNA + TdT
Amph2 siRNA +TdT
GAPDH siRNA + TdT-VCA
Amph2 siRNA + TdT-VCA
F
Myofibers with transversal triads (%)
p=0.0039
**
GAPDH siRNA + TdT
Amph2 siRNA +TdT
GAPDH siRNA + TdT-VCA
Amph2 siRNA + TdT-VCA

Fig S4

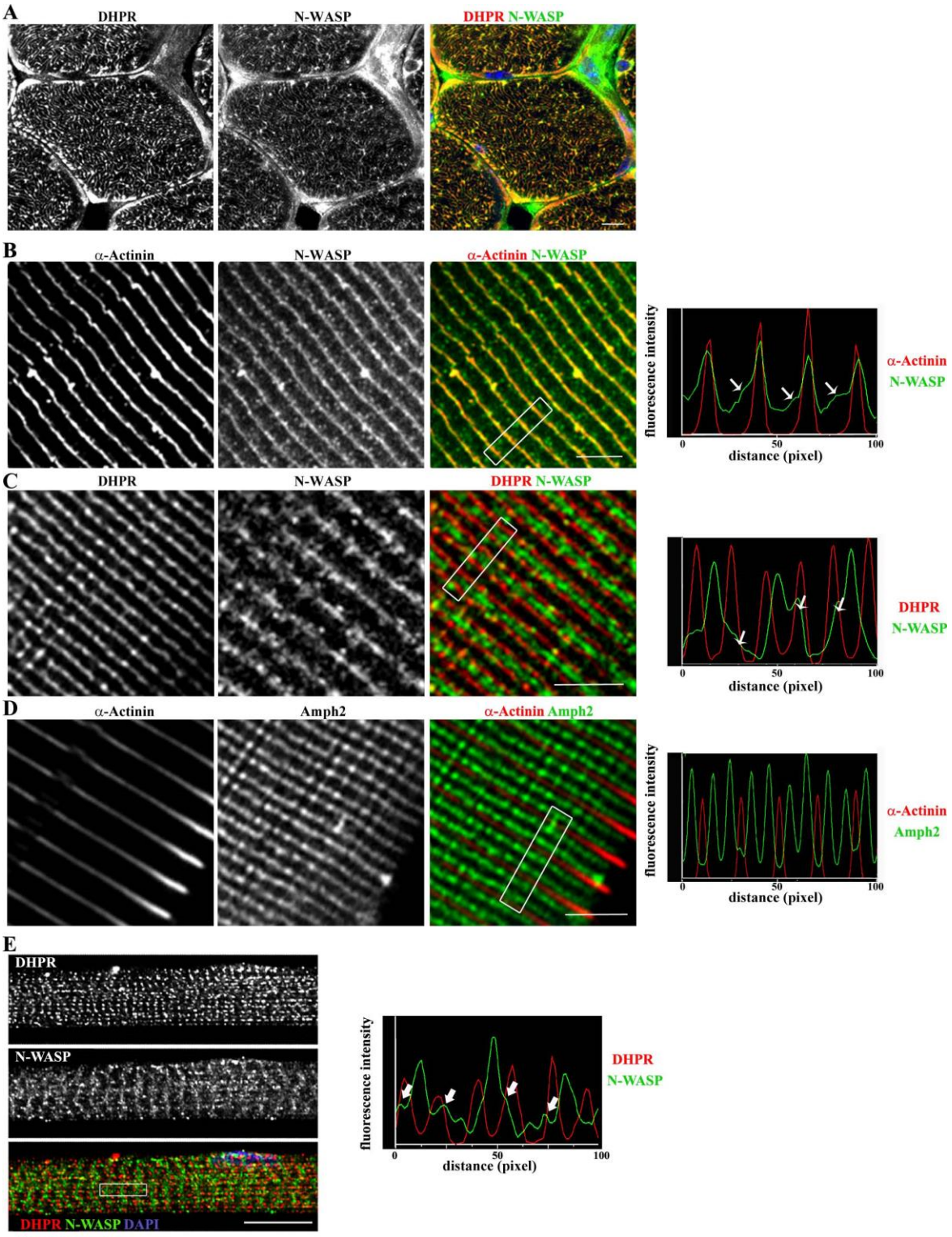
A
DHPR
N-WASP
DHPR N-WASP
B
α-Actinin
N-WASP
α-Actinin N-WASP
fluorescence intensity
α-Actinin
N-WASP
0
50
100
distance (pixel)
C
DHPR
N-WASP
DHPR N-WASP
DHPR
N-WASP
0
50
100
distance (pixel)
D
α-Actinin
Amph2
α-Actinin Amph2
fluorescence intensity
α-Actinin
Amph2
0
50
100
distance (pixel)
E
DHPR
N-WASP
DHPR N-WASP DAPI
fluorescence intensity
DHPR
N-WASP
0
50
100
distance (pixel)

Fig S5

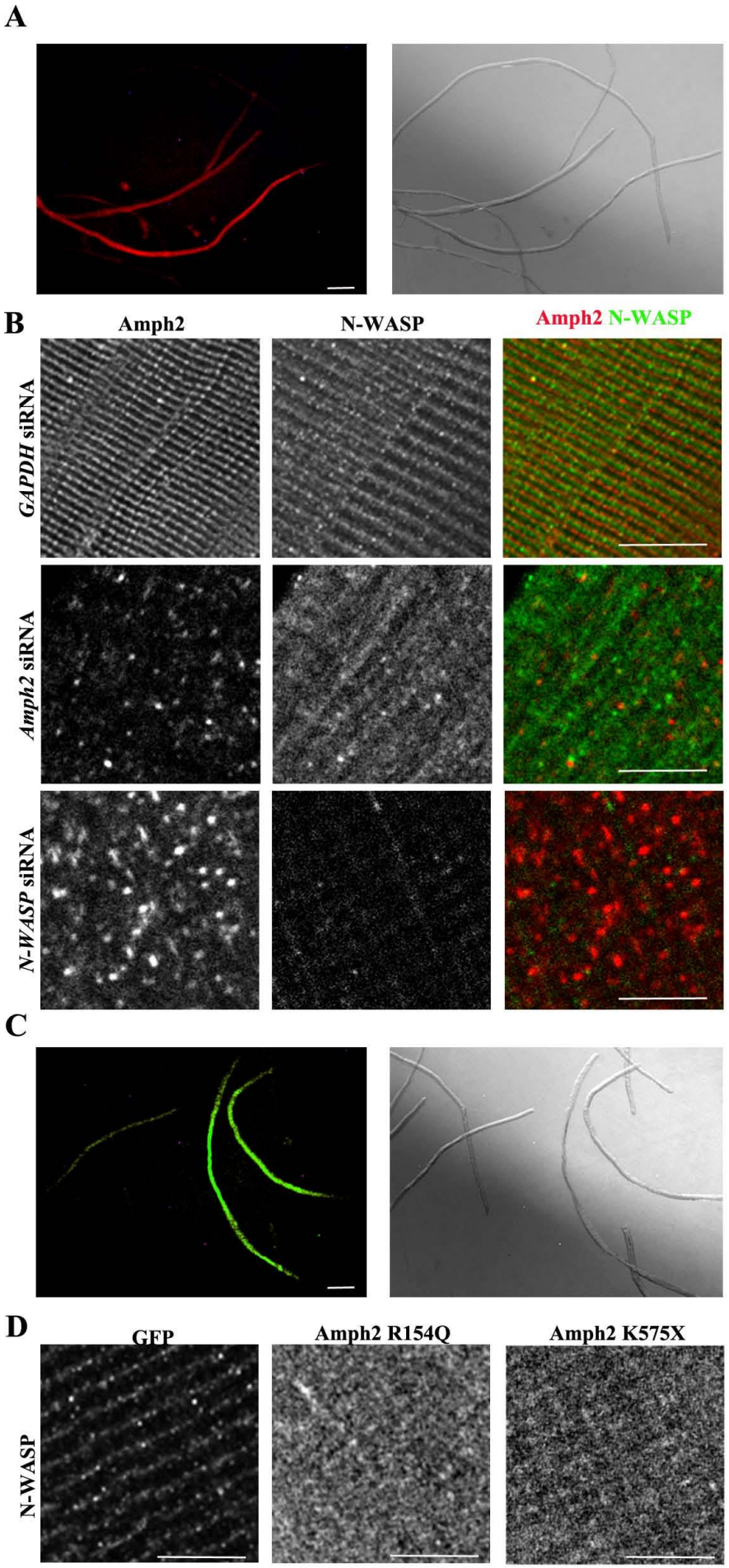
A
B
Amph2
N-WASP
Amph2 N-WASP
GAPDH siRNA
Amph2 siRNA
N-WASP siRNA
C
D
GFP
Amph2 R154Q
Amph2 K575X
N-WASP

fig S6

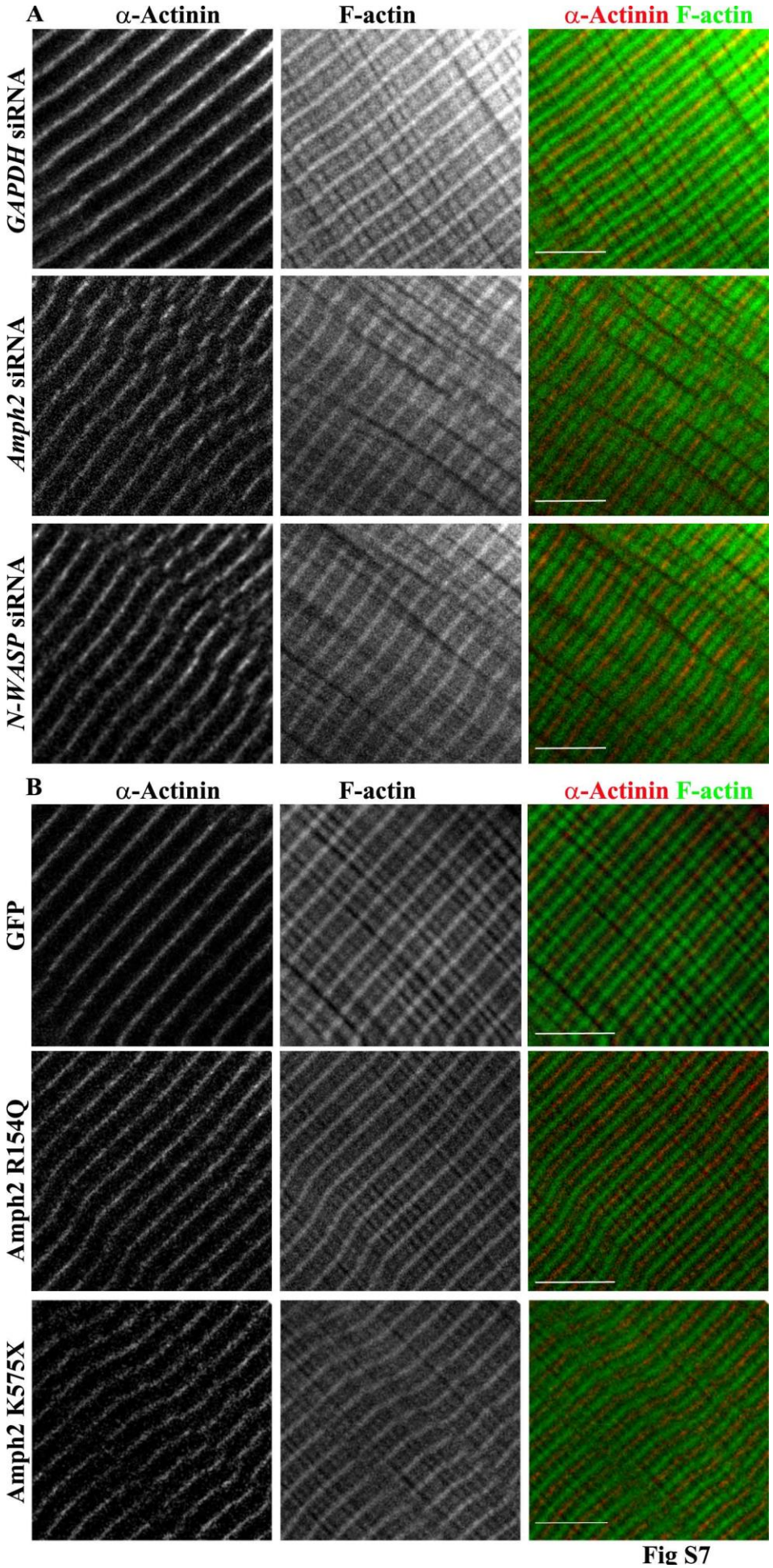
A
α-Actinin
F-actin
α-Actinin F-actin
GAPDH siRNA
Amph2 siRNA
N-WASP siRNA
B
α-Actinin
F-actin
α-Actinin F-actin
GFP
Amph2 R154Q
Amph2 K575X

Fig S7

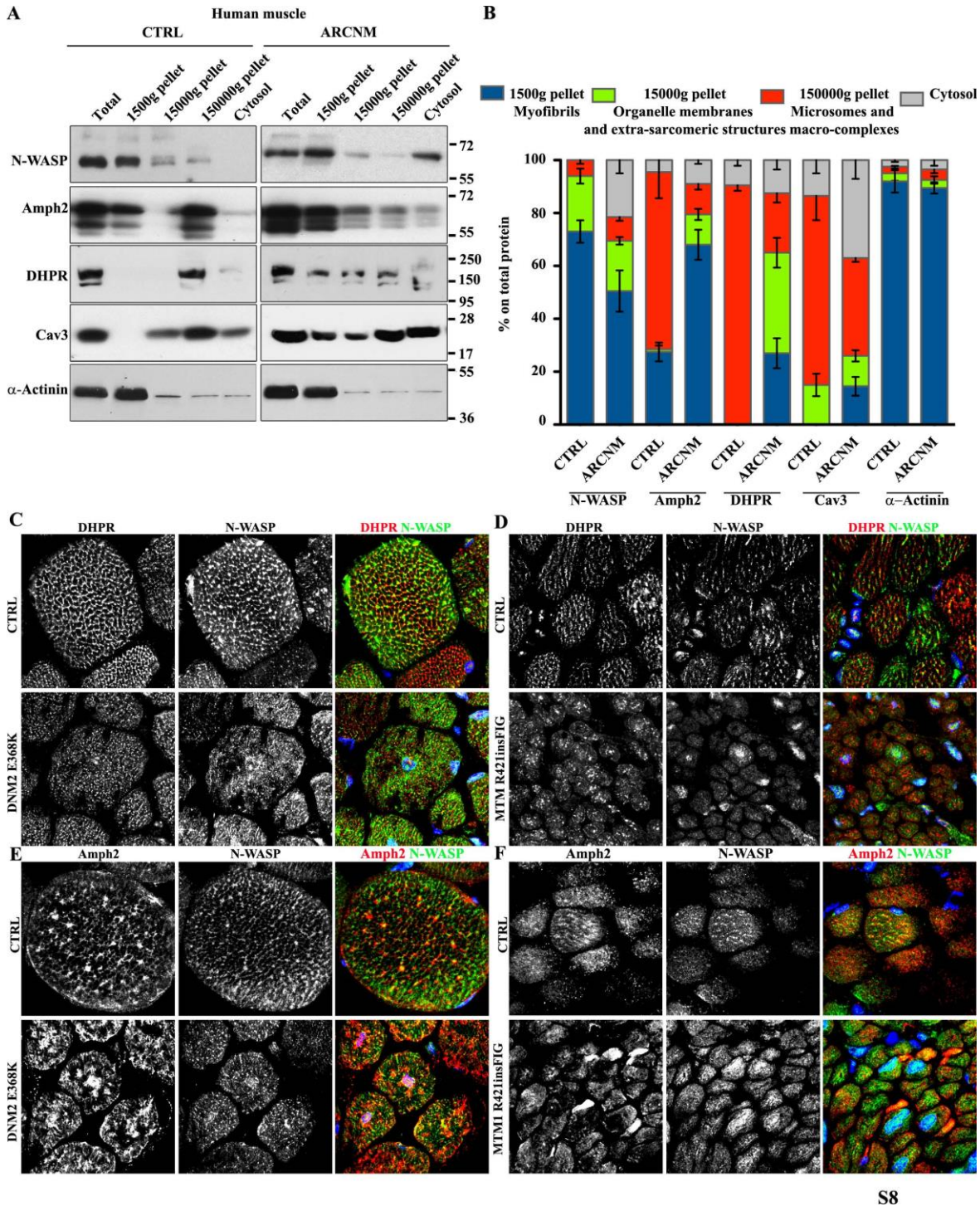
A
Human muscle
CTRL
ARCNM
Total
1500g pellet
15000g pellet
150000g pellet
Cytosol
N-WASP
Amph2
DHPR
Cav3
α-Actinin
72
55
72
55
250
150
95
28
17
55
36
B
1500g pellet
Myofibrils
15000g pellet
Organelle membranes
150000g pellet
Microsomes and
and extra-sarcomeric structures macro-complexes
Cytosol
% on total protein
100
80
60
40
20
0
CTRL
ARCNM
N-WASP
Amph2
DHPR
Cav3
α–Actinin
C
DHPR
N-WASP
DHPR N-WASP
CTRL
DNM2 E368K
D
MTM R421insFIG
E
Amph2
Amph2 N-WASP
F
MTM1 R421insFIG

S8

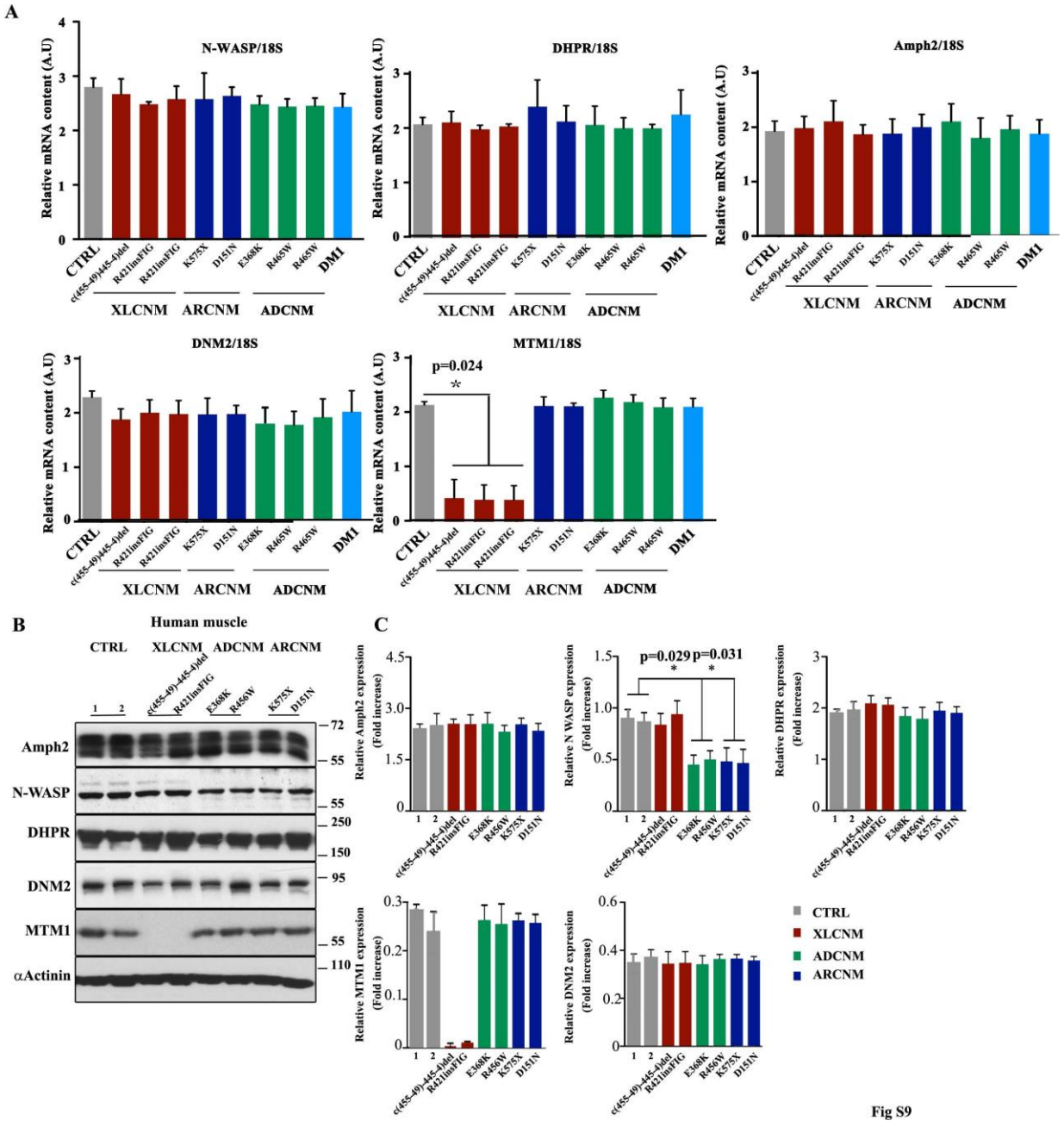
A
N-WASP/18S
DHPR/18S
Amph2/18S
DNM2/18S
MTM1/18S
Relative mRNA content (A.U)
p=0.024
*
CTRL
c(455-49)445-4del
R421insFIG
K575X
D151N
E368K
R465W
DM1
XLCNM
ARCNM
ADCNM
B
Human muscle
CTRL
XLCNM
ADCNM
ARCNM
Amph2
N-WASP
DHPR
DNM2
MTM1
αActinin
72
55
250
150
95
110
C
Relative Amph2 expression (Fold increase)
Relative N WASP expression (Fold increase)
p=0.029 p=0.031
Relative DHPR expression (Fold increase)
Relative MTM1 expression (Fold increase)
Relative DNM2 expression (Fold increase)
CTRL
XLCNM
ADCNM
ARCNM

Fig S9

2. A mechanism to position nuclei at the periphery of skeletal muscle.

Roman W., Voituriez R., Matrins J., Abella J., Cadot B., Way M., Gomes ER. Submitted April 2016

Title:

A mechanism to position nuclei at the periphery of skeletal muscle cells

Authors:
William Roman[1,2], ,Raphael Voituriez[3,4], Joao Martins[2], Jasmine Abella[5], Bruno Cadot[1], Michael Way[5] and Edgar R. Gomes* [1,2]

Affiliations:
[1]Sorbonne Universités, UPMC Univ Paris 06, INSERM UMRS974, CNRS FRE3617, Center for Research in Myology, GH Pitié-Salpêtrière, 47 Boulevard de l'hôpital, 75013 Paris, France; Centre de Référence de Pathologie Neuromusculaire Paris-Est, Institut de Myologie, GHU La Pitié-Salpêtrière, Assistance Publique-Hôpitaux de Paris, Paris, France.
[2]Instituto de Medicina Molecular, Faculdade de Medicina, Universidade de Lisboa, Avenida Professor Egas Moniz, 1649-028, Lisboa, Portugal
[3]Laboratoire de Physique Théorique de la Matière Condensée; CNRS UMR 7600; Université Pierre et Marie Curie, Paris , France.
[4]Laboratoire Jean Perrin; CNRS FRE 3231, Université Pierre et Marie Curie ; Paris, France.
[5]Cellular Signalling and Cytoskeletal Function, The Francis Crick Institute, 44 Lincoln's Inn Fields, London, WC2A 3LY, UK

* corresponding author:
Edgar R. Gomes
Instituto de Medicina Molecular
Faculdade de Medicina da Universidade de Lisboa
Av. Professor Egas Moniz
1649-028 Lisboa
Portugal
Phone: +351 217999515
edgargomes@medicina.ulisboa.pt

Summary

Nuclear movements are important for multiple cellular functions and are driven by polarized forces generated by motor proteins and cytoskeleton. During skeletal myofiber formation or regeneration, nuclei move from the center to the periphery of the myofiber for proper muscle function. Furthermore, centrally located nuclei are found in different muscle disorders. Using theoretical and experimental approaches, we demonstrate that nuclear movement to the periphery of myofibers is mediated by centripetal forces around the nucleus in combination with local changes of nuclear stiffness. The centripetal forces are generated by myofibril contraction, cross-linking and zipping around the nucleus. Local changes of nuclear stiffness are achieved by asymmetric distribution of lamin A/C. Finally, we found that an Arp2/3 complex containing Arpc5L together with γ-actin organizes desmin to cross-link and zip myofibrils for nuclear movement. Our work reveals that centripetal forces exerted by myofibrils squeeze the nucleus to the periphery of myofibers.

Introduction

Nuclear positioning within cells is important for multiple cellular activities during development, immune response, tissue homeostasis and regeneration (Gundersen and Worman, 2013b). Furthermore, nuclear positioning defects result in multiple human disorders such as lissencephaly, deafness, and multiple muscle disorders (Horn et al., 2013; Starr and Fridolfsson, 2010). The mechanisms of nuclear positioning involve different cytoskeletal networks of microtubules, actin and intermediate filaments, together with associated motor proteins (Gundersen and Worman, 2013b). In most cases, the nucleus is connected to the cytoskeleton by nuclear envelope proteins or by the nuclear pore complex (Bolhy et al., 2011; Crisp, 2006; Splinter et al., 2010; Starr and Han, 2002). Additionally, nuclear movement can also be driven by microtubules or actin growing towards the nucleus, as well as by active diffusion (Almonacid et al., 2015b; Huelsmann et al., 2013b; Zhao et al., 2012). All these nuclear movements are driven by forces polarized towards the direction of movement.

The most versatile example of nuclear positioning occurs during skeletal muscle differentiation. Muscle fibers (myofibers) are multinucleated cells that are formed by the fusion of mononucleated muscle precursor cells (myoblasts). After fusion, the

myoblast's nucleus moves towards the center of the myotube (Cadot et al., 2012b). The nuclei then spread along the length of the myotube, followed by their movement towards the periphery (Cadot et al., 2015a; Metzger et al., 2012c). Finally, a couple of nuclei cluster under the neuromuscular junction and at the myo-tendinous junction (Merlie and Sanes, 1985).

We recently showed that nuclear positioning within myofibers is required for proper muscle function (Metzger et al., 2012c). In addition, several monogenic muscle disorders exhibit centrally located nuclei including centronuclear myopathies, myotonic dystrophy, desminopathies and muscle laminopathies (Goldfarb and Dalakas, 2009; Romero, 2010; Sonnemann et al., 2006b). Furthermore, centrally located nuclei are also routinely identified in regenerative muscle thus suggesting that nuclear positioning is important for muscle maintenance and regeneration.

The architecture of skeletal muscle is designed for its contractile purpose. Sarcomeres, the contractile unit, are connected to one another longitudinally by the z-line and form bundles named myofibrils that span the entire length of the myofiber (Clark et al., 2002). These myofibril bundles are cross-linked by desmin networks which are intermediate filaments connected at the z-line. Myofibrils are surrounded by transversal triads, specialized junctions between t-tubules and sarcoplasmic reticulum. These structures are responsible for excitation-contraction (EC) coupling, allowing the transduction of electric membrane potentials into muscle contractions (Al-Qusairi and Laporte, 2011b). During development, myofibrils are formed during gestation and surround the centrally located nuclei. The positioning of the nuclei at the periphery only occurs near birth. Transversal triads are only formed at a later stage in the first postnatal weeks (Flucher et al., 1993).

Recent work identified different mechanisms for nuclear movement during skeletal muscle differentiation (Cadot et al., 2012b; Elhanany-Tamir et al., 2012b; Folker et al., 2013; Metzger et al., 2012c; Wilson and Holzbaur, 2015b, 2015b). However these studies did not address nuclear movements that occur later during development such as nuclear movement to the periphery. We recently found that BIN1/amphiphysin-2 (mutated in centronuclear myopathies) interacts with N-WASP and both are required for actin-dependent peripheral nuclear movement and transversal triad formation (Falcone et al., 2014). These results suggest a role for actin, that is nucleated by the Arp 2/3 complex, in nuclear movement to the periphery.

Here we explore the mechanism of nuclear movement to the periphery of myofibers. We found that nuclei are moved to the periphery of myofibers by an unexpected mechanism involving the cross-linking and contraction of myofibrils. Myofibrils induce growing centripetal forces on centrally located nuclei. These centripetal forces eventually squeeze and extrude the nuclei to the cell periphery. The direction of nuclear movement relies on a local asymmetry of nuclear stiffness promoting nuclear blebbing to the periphery. We demonstrate that Arp2/3 complexes containing Arpc5L together with γ-actin organize desmin at the z-line to mediate the cross-linking of myofibrils that act as closing zippers on both sides of the nucleus.

Results

Nuclei are squeezed by myofibrils when moving towards the myofiber periphery

To identify the mechanism of nuclear movement to the periphery of muscle cells, we used an *in vitro* differentiated myofiber system that uniquely recapitulates the embryonic and neonatal development of muscle fibers (Falcone et al., 2014; Flucher et al., 1993). After 3 days, myofibers with myofibrils exhibit centrally located nuclei and no transversal triads. Between days 4-6, nuclei move to the periphery followed by transversal triads organization at day 7 (Fig. 1A).

We performed dual-color 3D time-lapse spinning disk microscopy of these differentiated *in vitro* myofibers labeled for myofibrils (YFP-α-actinin) and nuclei (H2B-iRFP) between day 4.5 and 5.5. Before movement to the periphery, centrally located nuclei are surrounded by myofibril bundles when moving longitudinally along the myofiber (Fig. S1A) (Supplementary movie S1). The movement of the nucleus to the periphery begins with the emergence of an elongated nuclear wrinkle through a narrow gap in between myofibrils (Fig. 1B). With time the wrinkle increases into a bleb and the nucleus undergoes a dramatic deformation. This results in the nucleus being expelled from the middle of the myofibril bundles to the myofiber periphery (Supplementary movie S2). Nuclear movement to the periphery occurs over a period of

2h25min +/- 41 min, with an average speed of 4.2 μm/h, which is the slowest nuclear movement event ever described (Cadot et al., 2015a). The deformation of nuclei reaching the periphery of myofibers was also observed in either isolated myofibers or whole muscles from newborn mice (P0)(Fig. 1D,E).

Desmin cross-links myofibrils for nuclear movement to the myofiber periphery

Quantification of 3D nuclear shape revealed that the sphericity and volume of the nucleus decrease prior to nuclear emergence. This is followed by the re-establishment of sphericity and volume as the nucleus starts to emerge at the periphery (Fig. 2A,B). These changes in nuclear morphology suggest increasing forces applied to the nucleus before the initiation of nuclear movement.

When we analyzed the middle plane of the myofiber, we observed an area next to the nucleus depleted of myofibrils (Fig. 1C). We quantified this area depleted of myofibrils over time at the onset of nuclear movement and found that this area decreases prior to nuclear movement as though myofibrils zip together towards the nucleus (Fig. 2C). Desmin is an intermediate filament known to cross-link myofibrils by forming a network running through the z-line of myofibrils (Clemen et al., 2013b). We therefore explored the role of desmin in nuclear movement to the periphery. We found that depletion of desmin by siRNA-mediated knock down impairs nuclear movement to the periphery (Fig. 2D-F). Furthermore, we observed that the desmin network is already organized at z-lines before nuclear movement but only in sections of the myofibers away from centrally located nuclei (Fig 2G). In contrast, desmin is disorganized near the centrally located nuclei in both the area devoid of myofibrils and the myofibrils bordering that area (Fig. 2G). To determine the dynamics of the desmin network during nuclear movement, we visualized EmGFP-desmin by time-lapse epi-fluorescence microscopy during nuclear movement to the periphery. Over time, we observed the organization of desmin in striations towards the nucleus, similar to the myofibril zipping mechanism that we witnessed prior to nuclear migration to the periphery (Fig. 1C,2H). These data suggest that myofibril cross-linking and zipping by desmin leads to the squeezing of the nucleus to the cell periphery.

A theoretical model predicts the role of myofiber contraction, cross-linking and nuclear stiffness for nuclear movement to the periphery

To further understand how myofibril cross-linking drive nuclear movement to the periphery, we developed a theoretical model using known biophysical parameters of myofiber components. Before peripheral movement, the nucleus (of radius $R_0 \approx 6$ μm) is assumed to be a linear elastomer wrapped by a bundle of $N \approx 30$ myofibrils (Goldspink, 1970) and centered along the symmetry axis of the bundle. Each myofibril is modeled as an active spring, whose relaxed tension ($T \approx 1$ to 10 nN) is induced by myofibrils at the measured sarcomere length of 2.7 μm (Fig. 3A) (Yoshikawa et al., 1999). Myofibril cross-linking (L) induces a centripetal force Fn on the nucleus of elastic modulus E towards the myofiber axis of the order of $Fn \approx 4TR_0/L$ for each myofibril (Fig. 3B). Upon the increase of this force mediated by myofibril cross-linking, the nucleus is squeezed and elongates along the myofiber axis inducing a decrease in nuclear sphericity and volume. We measured an average distance $L \approx 30$ μm between cross-linking points in opposite sides of the nuclei in the onset of peripheral nuclear movement (Fig. 3C). Denoting g the effective stiffness of the nucleus (assumed viscous at the time scale of the experiments), the amplitude of nuclear deformation can be estimated as $DR \approx 4NTR_0/(gL) \approx 0.1$ to 1 μm. This results in the formation of wrinkles between squeezing myofibrils, as was experimentally confirmed (Fig. S1B)(Supplementary movie S3). As soon as the height h of one of these wrinkles is of the order of its width $2\pi R/N$, the wrinkle is destabilized and forms a bleb into which all the nucleus content flows, so that the nucleus finally leaks out of the myofibril bundle (Fig. 3D). The threshold of this instability is given by $ER_0 \approx 4T/L$ or $1 \approx 4T/LR_0E$. Given the above orders of magnitude this threshold is not reached with cross-linking alone (Fig.3E). In order to reach the instability threshold, other parameters such as myofibril tension T must vary. It is reported that myofibril tension increases 25 folds during contraction (Colomo et al., 1997). When we use this value ($T = 250$nN) in our theoretical model, the instability threshold is still not reached for L values we measured. This suggests that the elastic modulus parameter E must also decrease to reach instability (Fig. 3E). However, such global decrease of the elastic modulus of the nucleus will enforce large deformations needing an adaptation of the analysis. The nucleus will adopt a cylindrical shape, squeezed between almost undeformed myofibrils. The instability will therefore only be reached for $g < 4NTr_f^3/(R_0^3L)$, where r_f is the typical radius of the myofibrils bundle in absence of nucleus. The instability is

not reached with the biophysical parameters of the model. Therefore, the decrease of nuclear stiffness predicted by the theoretical model to be required to reach the instability threshold probably only occurs locally, in between myofibrils when the nuclear blebs are formed, while the overall nucleus stiffness remains constant. Thus, peripheral nuclear movement only occurs within a window of nuclear stiffness for the entire nucleus (Fig. 3F). Overall, this theoretical model predicts that myofiber contraction and changes in nuclear stiffness (globally and locally) play a part in nuclear movement to the periphery.

Nuclear movement requires myofiber contraction and nuclear stiffness

Our theoretical model suggests that myofibril contraction is required for peripheral nuclear movement. Myofibrils contract early on during myofiber development, prior to the movement of the nucleus to the periphery (Falcone et al., 2014). To test the involvement of contraction in nuclear movement, we inhibited myofibril contraction with tetradotoxin and found that peripheral nuclear position is inhibited (Fig. 4A). To further explore if contraction are required for nuclear movement, we expressed a light-sensitive sodium channel (ChR2-GFP) in myofibers to optogenetically manipulate myofibril contraction with light prior to day 4.5 (which corresponds to the beginning of nuclear movements to the periphery) (Fig. S1C) (Supplementary movie S4) (Sakar et al., 2012). We found that ChR2-GFP mediated myofibril contractions at day 3.5 promote the premature movement of nuclei to the periphery of myofibers (Fig. 4B,C) (Supplementary movie S5). Therefore, myofibril contraction is involved in peripheral nuclear positioning as predicted by the theoretical model.

The dramatic deformation of the nucleus, the formation of a bleb during movement to the periphery and the theoretical model suggest a role for nuclear stiffness in nuclear movement. Since lamin A/C is the main determinant of nuclear stiffness, we manipulated the stiffness of myofiber nuclei either by siRNA mediated knockdown of lamin A/C (to decrease stiffness) (Fig. S2A) or by mCherry-lamin A/C overexpression (to increase stiffness). We found that both the loss or over expression of lamin A/C leads to a decrease of peripheral nuclei (Fig. 4D,E). Inv contrast, the downregulation of lamin B did not decrease peripheral nuclei (Fig. S2B,C). We also found that the levels of overexpressed mCherry-lamin A/C were inversely correlated with the velocity of nuclear movement to the periphery (Fig. 4F). This suggests that variations of nuclear

stiffness (decrease or increase) impair nuclear movement as predicted by the theoretical model. Next, to test if local decreases in nuclear stiffness could be associated with bleb formation, we directly visualized lamin A/C during nuclear movement by performing 3D time-lapse spinning disk microscopy on myofibers expressing mCherry-lamin A/C. Initially, mCherry-lamin A/C is symmetrically distributed at the nuclear envelope except for a relative decrease in a nuclear wrinkle. As the nucleus starts to squeeze and bleb, the lamin A/C asymmetry is even more pronounced, suggesting a reduction of nuclear stiffness in the nuclear bleb (Fig. 4G). Endogenous lamin A/C, but not lamin B, is also asymmetrically distributed at the early initiation of bleb formation (Fig. S2D,E) and this asymmetry remains throughout the movement (Fig. S2G,H). Furthermore, a reduction of lamin A/C multimerization, detected with an epitope specific antibody (lamin A/C-C), occurs at the bleb during nuclear movement (Fig. S2F,I)(Ihalainen et al., 2015). We observed this lamin A/C asymmetry in all nuclei blebbing to the periphery (n=30). Therefore, global and local nuclear stiffness regulated by lamin A/C are involved in peripheral nuclear positioning.

Arp5L-containing Arp2/3 complex and γ--actin are required for nuclear movement

We previously showed that amphipysin-2/BIN1, which is mutated in centronuclear myopathies, triggers peripheral nuclear positioning via N-Wasp and actin (Falcone et al., 2014) (Fig. S3A). The Arp2/3 complex is an actin nucleator that is activated by N-Wasp, and therefore a good candidate to mediate this process (Egile et al., 1999; Machesky et al., 1999; Yarar et al., 1999). We found that depletion of Arpc2, essential for Arp2/3 nucleation activity (Gournier et al., 2001b; Korobova and Svitkina, 2008), inhibits peripheral nuclear positioning in 10-day differentiated myofibers, but not myofibril formation (Fig. S3B-D). Furthermore, transversal triad formation, that occurs later on during myofiber differentiation, is also inhibited (Fig. S3B-D). These results were confirmed using CK666 (Nolen et al., 2009), an inhibitor of the Arp2/3 complex (Fig. S3D).

It was recently described that Arp2/3 complexes differ in their actin assembly activity depending on the isoforms of Arpc1 (Arpc1A and Arpc1B) and Arpc5 (Arpc5 and Arpc5L) subunits (Fig. S3E) (Abella et al., 2016b). We therefore tested the role of these Arp2/3 isoforms on nuclear positioning. Depletion of Arpc1A or Arpc1B prevents

both peripheral nuclear positioning and transversal triad formation in 10-day myofibers (Fig. S3F,G). However, depletion of Arpc5L, but not Arpc5, only inhibits nuclear positioning whereas depletion of Arpc5, but not Arpc5L only inhibits transversal triad formation but not nuclear positioning (Fig. 5A,B and Fig. S3H). Therefore Arp2/3 complexes containing Arpc5L or Arpc5 have independent functions during myofiber formation. Given this, we wondered whether γ-actin and β-actin isoforms, nucleated by the Arp2/3 complex, also play independent roles during myofiber assembly (Fig. S4A). By performing siRNA mediated knock down (Fig. S4B), we found that γ-actin, but not β-actin, is required for peripheral nuclear position (Fig. 5C,D). In contrast, β-actin is only involved in transversal triad formation (Fig. 5C,D). We confirmed these results by performing rescue experiments with siRNA-resistant GFP-tagged γ-actin and β-actin (Fig. S4C,D,E).

Next, we tested if Arpc5 and actin isoforms interact differently within myofibers. We found that γ-actin co-immunoprecipitates (co-IP) with GFP-tagged Arpc5L but not Arpc5, whereas β-actin preferentially associates with Arpc5 (Fig. 6A). Conversely, Arpc5L preferentially associates with GFP-γ-actin, when compared with GFP-β-actin, whereas Arpc5 associates with GFP-β-actin, but not GFP-γ-actin (Fig. 6B). In all situations, Arpc2 was also present in the IP providing evidence that these interactions occur via Arp2/3 complexes. Finally, endogenous γ-actin co-immunoprecipitates with endogenous Arpc5L, but not Arpc5 (Fig. 6C). Therefore nuclear position is specifically mediated by an Arpc5L-containing Arp2/3 complex and γ-actin (Fig. S5A).

To understand how Arpc5L-containing Arp2/3 complexes and γ-actin regulate the mechanism of nuclear movement to the periphery, we recorded the movement of nuclei between day 4.5 and 5.5 in myofibers depleted of Arpc5L or γ-actin. In all situations, nuclei move longitudinally along the myofiber with intermittent pausing events, as previously described (Falcone et al., 2014). However, nuclei do not move to the periphery in Arpc5L or γ-actin knocked down myofibers (Fig. S5B-G) (Supplementary movie S6,S7,S8). Although the speeds and displacements of nuclei during longitudinal movement are similar in all cohorts (Fig. S5H), pause durations are shorter in myofibers lacking Arpc5L or γ-actin (Fig. 6D). We found that sphericity and volume of nuclei in scrambled myofibers decrease during pausing events. This decrease is not observed in Arpc5L or γ-actin depleted myofibers (Fig. 6E,F) suggesting that both proteins play a role in increasing the force on nuclei for their movement to the

periphery. As this force on the nucleus is probably mediated by contraction and myofibril cross-linking (required for squeezing the nucleus to the periphery of the myofiber), we tested if contraction was impaired in Arpc5L or γ-actin knockdown myofibers. By optogenetically inducing contraction, we found that Arpc5L or γ-actin knockdown myofibers were still able to contract (Fig. S5J-K). However, optogenetically-induced contractions were not sufficient to induce peripheral nuclear position in 3.5-day myofibers knocked down for Arpc5L or γ-actin (Fig. S5I). Thus, we hypothesized that Arpc5L and γ-actin are involved in myofiber cross-linking. To test this hypothesis, we quantified the area next to the nucleus, devoid of myofibrils, during nuclear pausing. We observed a greater decrease of the area in the scramble knocked down myofibers compared to those lacking Arpc5L and γ-actin (Fig. 6G). This data suggests that Arpc5L-containing Arp2/3 complexes and γ-actin are involved by cross-linking myofibrils. Consistent with this, Arpc5L and γ-actin co-localize in small patches between myofibrils near centrally located nuclei in 5 day myofibers (Fig. 6H), in contrast to Arpc5 and β-actin which are transversally organized (Fig. S6A-B).

Arp5L and γ-actin organize desmin to cross-link myofibrils for nuclear movement

Our data shows that desmin is the myofibril cross-linker required for nuclear movement to the periphery. We therefore tested if Arpc5L and γ-actin are important for desmin organization for cross-linking. Depletion of Arpc5L or γ-actin leads to disorganization of desmin which is no longer found at the z-lines (Fig. 7A). On the other hand, desmin is normally found at the z-line in myofibers knocked down for Arpc5 or β-actin (not involved in nuclear positioning) (Fig. S6C). Therefore, Arpc5L and γ-actin organize desmin at the z-line.

It was previously shown that plectin is a cytoskeletal linker that connects desmin to the z-line (Konieczny et al., 2008a). We therefore depleted plectin from myofibers and indeed observed an inhibition of peripheral nuclear positioning (Fig. 7B-C). Moreover, just before nuclei move to the periphery at day 5, plectin co-localizes with desmin at the z-line (Fig. 7D). Furthermore, desmin organization at the z-line is completely disrupted in the plectin knock down myofibers (Fig. 7D). We next determined if Arpc5L and γ-actin were involved in desmin organization via plectin. In the absence of Arpc5L or γ-actin, plectin organization was not disrupted, suggesting that Arpc5L and γ-actin organize desmin cytoskeleton for cross-linking via plectin (Fig. 7E). Overall, our data shows that an Arpc5L-containing Arp2/3 complex and γ-actin

organize desmin at the z-line through plectin to cross-link myofibrils for nuclear movement.

Discussion

Here we demonstrate that nuclear movement to the periphery of myofiber is driven by myofibril cross-linking, zipping and contraction, and requires a tight regulation of nuclear stiffness by lamin A/C (Fig. 7F). Furthermore we show that an Arpc5L-containing Arp2/3 complex together with γ-actin mediate the cross-linking of myofibrils by desmin for nuclear movement.

Centripetal forces around the nucleus drive nuclear movement

All nuclear movements previously characterized require a polarization of the machinery inducing the force in the direction of nuclear movement (Gundersen and Worman, 2013b). In contrast, the nuclear movement to the periphery of myofibers we have now described does not involve polarized machinery. The forces induced by myofibrils around the nucleus are centripetal and symmetrically distributed around the nucleus. The polarization of the movement stems from the formation of a nuclear bleb which is dependent on local changes of nuclear stiffness. Thus, the direction of nuclear movement depends on intrinsic properties of the nucleus. Future work should address if these local changes are stochastic or locally triggered. The mechanism for nuclear movement we have documented is analogous to bleb-based cell migration (Paluch and Raz, 2013a). Both mechanisms share a local change of surface stiffness that leads to the formation of the bleb important for directionality of the movement of the object.

Distinct Arp2/3 complexes and actin isoforms are involved in nuclear movement and transversal triad organization

We also found that distinct populations of Arp2/3 complexes together with specific actin isoforms have segregated functions in skeletal myofibers. Peripheral nuclear positioning is mediated by Arpc5L-containing Arp2/3 complex and γ-actin whereas transversal triad formation is mediated by Arpc5-containing Arp2/3 complexes and β-actin. Arpc5L and γ-actin organize the desmin network to cross-link myofibrils at the z-line by plectin. Such organization might use similar mechanisms found in migrating cells where actin retrograde flow organizes the vimentin intermediate filament cytoskeleton via plectin (Jiu et al., 2015). Nevertheless, how these distinct Arp2/3 complexes and actin isoforms have such specific functions in cells remains unknown. This specificity can be achieved by compartmentalization of the Arp 2/3 and actin complexes, different nucleation activities of Arpc5 isoforms or by different

polymerization rates of actin isoforms dependent on Ca^{2+} concentration (Abella et al., 2016b; Bergeron et al., 2010b; Gokhin and Fowler, 2011b). The versatility of Arp2/3 populations to perform different actin-related function is a testament to the cells' capacity to fine tune cytoskeletal processes.

Nuclear positioning in muscle disorders

Some of the genes encoding the proteins involved in the described mechanism are mutated in different muscle disorders, most of which exhibit centrally located nuclei. *BIN1*, which encodes for Amphiphysin-2 is mutated in centronuclear myopathies and mis-spliced in myotonic dystrophy (Fugier et al., 2011b; Nicot et al., 2007b). Amphiphysin-2 mutations disrupt N-Wasp localization and activity thereby probably preventing Arp2/3-dependent nucleation of γ-actin for desmin cross-linking (Falcone et al., 2014). Moreover, Emery Dreifuss and Limb-Girdle muscular dystrophies which belong to the group of laminopathy diseases, are caused by mutations in the lamin A/C gene (LMNA) (Azibani et al., 2014b). The *LMNA* mutations associated with muscular dystrophy were found to cause a reduction in nuclear stiffness (Lammerding et al., 2004b). The failure to regulate nuclear stiffness in these diseases is most probably responsible for hindering nuclear movement to the periphery of myofibers. Finally, desminopathies, which result from mutations in *DES* gene that encodes for desmin are another class of muscle diseases exhibiting misplaced nuclei (Clemen et al., 2013b). Desmin mutations are known to lead to defects in myofibril cross-linking. We show here that myofibril cross-linking is necessary for nuclear movement to the periphery thereby providing mechanistic evidence for the centronuclear phenotype found in desminopathies. Overall, our observations on the mechanism of nuclear positioning explains why mutations in apparently diverse proteins leads to a common phenotype of centrally located nuclei in different muscle disorders (Goldfarb and Dalakas, 2009; Romero, 2010; Sonnemann et al., 2006b).

Acknowledgements:

We thank M-H. Verlhac, M. Dias, J. Pinto, G. Gundersen and S. Tapscot for comments on the manuscript. We thank the Gomes Laboratory for discussions. This work was supported by the European Research Council (ERG), EMBO installation (ERG), AIM

France (WR, BC, ERG), Cancer Research UK (MW) and by postdoctoral fellowships from FRQS (Fonds de recherche du Québec - Santé), EMBO and the Canadian Institutes of Health Research (CIHR) to JVGA.

Author Contributions:

W.R. carried out experiments and analyzed data; J.M. performed desmin-related experiments; W.R., B.C. and E.R.G. conceived and designed experiments; J.V.G.A. and M.W. provided Arp2/3-related unpublished tools; W.R., R.V. and B.C. designed and executed the physical model; W.R. and E.G. wrote the manuscript with assistance from other authors; All authors participated in the critical review and revision of the manuscript.

Competing Financial Interests:

The authors declare no competing financial interests

References:

Biancalana, V., Caron, O., Gallati, S., Baas, F., Kress, W., Novelli, G., D'Apice, M.R., Lagier-Tourenne, C., Buj-Bello, A., Romero, N.B., et al. (2003). Characterisation of mutations in 77 patients with X-linked myotubular myopathy, including a family with a very mild phenotype. Hum. Genet. *112*, 135–142.

Bitoun, M., Maugenre, S., Jeannet, P.-Y., Lacène, E., Ferrer, X., Laforêt, P., Martin, J.-J., Laporte, J., Lochmüller, H., Beggs, A.H., et al. (2005). Mutations in dynamin 2 cause dominant centronuclear myopathy. Nat. Genet. *37*, 1207–1209.

Blau, H.M., Pavlath, G.K., Hardeman, E.C., Chiu, C.P., Silberstein, L., Webster, S.G., Miller, S.C., and Webster, C. (1985). Plasticity of the differentiated state. Science *230*, 758–766.

Bruusgaard, J.C., Liestøl, K., Ekmark, M., Kollstad, K., and Gundersen, K. (2003). Number and spatial distribution of nuclei in the muscle fibres of normal mice studied in vivo. J Physiol *551*, 467–478.

Bugyi, B., Didry, D., and Carlier, M.-F. (2010). How tropomyosin regulates lamellipodial actin-based motility: a combined biochemical and reconstituted motility approach. EMBO J. *29*, 14–26.

Butler, M.H., David, C., Ochoa, G.C., Freyberg, Z., Daniell, L., Grabs, D., Cremona, O., and De Camilli, P. (1997). Amphiphysin II (SH3P9; BIN1), a member of the

amphiphysin/Rvs family, is concentrated in the cortical cytomatrix of axon initial segments and nodes of ranvier in brain and around T tubules in skeletal muscle. J. Cell Biol. *137*, 1355–1367.

Cadot, B., Gache, V., Vasyutina, E., Falcone, S., Birchmeier, C., and Gomes, E.R. (2012). Nuclear movement during myotube formation is microtubule and dynein dependent and is regulated by Cdc42, Par6 and Par3. EMBO Rep. *13*, 741–749.

Cooper, S.T., Maxwell, A.L., Kizana, E., Ghoddusi, M., Hardeman, E.C., Alexander, I.E., Allen, D.G., and North, K.N. (2004). C2C12 co-culture on a fibroblast substratum enables sustained survival of contractile, highly differentiated myotubes with peripheral nuclei and adult fast myosin expression. Cell Motil. Cytoskeleton *58*, 200–211.

Cowling, B.S., Toussaint, A., Muller, J., and Laporte, J. (2012). Defective Membrane Remodeling in Neuromuscular Diseases: Insights from Animal Models. PLoS Genet *8*.

Cusimano, V., Pampinella, F., Giacomello, E., and Sorrentino, V. (2009). Assembly and dynamics of proteins of the longitudinal and junctional sarcoplasmic reticulum in skeletal muscle cells. Proc. Natl. Acad. Sci.
U.S.A. *106*, 4695–4700.

Davis, R.L., Weintraub, H., and Lassar, A.B. (1987). Expression of a single transfected cDNA converts fibroblasts to myoblasts. Cell *51*, 987–1000.

Dorchies, O.M., Laporte, J., Wagner, S., Hindelang, C., Warter, J.M., Mandel, J.L., and Poindron, P. (2001). Normal innervation and differentiation of X-linked myotubular myopathy muscle cells in a nerve-muscle coculture system. Neuromuscul. Disord. *11*, 736–746.

Dowling, J.J., Vreede, A.P., Low, S.E., Gibbs, E.M., Kuwada, J.Y., Bonnemann, C.G., and Feldman, E.L. (2009). Loss of myotubularin function results in T-tubule disorganization in zebrafish and human myotubular myopathy. PLoS Genet. *5*, e1000372.

Flucher, B.E. (1992). Structural analysis of muscle development: transverse tubules, sarcoplasmic reticulum, and the triad. Dev. Biol. *154*, 245–260.

Flucher, B.E., Phillips, J.L., and Powell, J.A. (1991). Dihydropyridine receptor alpha subunits in normal and dysgenic muscle in vitro: expression of alpha 1 is required for proper targeting and distribution of alpha 2. The Journal of Cell Biology *115*, 1345–1356.

Flucher, B.E., Andrews, S.B., and Daniels, M.P. (1994). Molecular organization of transverse tubule/sarcoplasmic reticulum junctions during development of excitation-contraction coupling in skeletal muscle. Mol. Biol. Cell *5*, 1105–1118.

Franzini-Armstrong, C. (1986). The sarcoplasmic reticulum and the transverse tubules. In Myology, (A. Engel and BO. Banker), pp. 125–153.

Friesen, H., Humphries, C., Ho, Y., Schub, O., Colwill, K., and Andrews, B. (2006). Characterization of the Yeast Amphiphysins Rvs161p and Rvs167p Reveals Roles for the Rvs Heterodimer In Vivo. Mol. Biol. Cell *17*, 1306–1321.

Fugier, C., Klein, A.F., Hammer, C., Vassilopoulos, S., Ivarsson, Y., Toussaint, A., Tosch, V., Vignaud, A., Ferry, A., Messaddeq, N., et al. (2011). Misregulated alternative splicing of BIN1 is associated with T tubule alterations and muscle weakness in myotonic dystrophy. Nat. Med. *17*, 720–725.

Gokhin, D.S., and Fowler, V.M. (2011). Cytoplasmic gamma-actin and tropomodulin isoforms link to the sarcoplasmic reticulum in skeletal muscle fibers. J. Cell Biol. *194*, 105–120.

Grady, R.M., Starr, D.A., Ackerman, G.L., Sanes, J.R., and Han, M. (2005). Syne proteins anchor muscle nuclei at the neuromuscular junction. Proc. Natl. Acad. Sci. U.S.A. *102*, 4359–4364.

Gruenbaum-Cohen, Y., Harel, I., Umansky, K.-B., Tzahor, E., Snapper, S.B., Shilo, B.-Z., and Schejter, E.D. (2012). The actin regulator N-WASp is required for muscle-cell fusion in mice. Proc. Natl. Acad. Sci. U.S.A. *109*, 11211–11216.

Hadjantonakis, A.-K., and Papaioannou, V.E. (2004). Dynamic in vivo imaging and cell tracking using a histone fluorescent protein fusion in mice. BMC Biotechnol. *4*, 33.

Hong, T., Yang, H., Zhang, S.-S., Cho, H.C., Kalashnikova, M., Sun, B., Zhang, H., Bhargava, A., Grabe, M., Olgin, J., et al. (2014). Cardiac BIN1 folds T-tubule membrane, controlling ion flux and limiting arrhythmia. Nat. Med. *20*, 624–632.

Ito, K., Komazaki, S., Sasamoto, K., Yoshida, M., Nishi, M., Kitamura, K., and Takeshima, H. (2001). Deficiency of triad junction and contraction in mutant skeletal muscle lacking junctophilin type 1. J. Cell Biol. *154*, 1059–1067.

Kee, A.J., Schevzov, G., Nair-Shalliker, V., Robinson, C.S., Vrhovski, B., Ghoddusi, M., Qiu, M.R., Lin, J.J.C., Weinberger, R., Gunning, P.W., et al. (2004). Sorting of a nonmuscle tropomyosin to a novel cytoskeletal compartment in skeletal muscle results in muscular dystrophy. J. Cell Biol. *166*, 685–696.

Kee, A.J., Gunning, P.W., and Hardeman, E.C. (2009). Diverse roles of the actin cytoskeleton in striated muscle. J. Muscle Res. Cell. Motil. *30*, 187–197.

Kojima, C., Hashimoto, A., Yabuta, I., Hirose, M., Hashimoto, S., Kanaho, Y., Sumimoto, H., Ikegami, T., and Sabe, H. (2004). Regulation of Bin1 SH3 domain binding by phosphoinositides. EMBO J. *23*, 4413–4422.

Kossmann, C.E., and Fawcett, D.W. (1961). The Sarcoplasmic Reticulum of Skeletal and Cardiac Muscle. Circulation *24*, 336–348.

Laporte, J., Hu, L.J., Kretz, C., Mandel, J.L., Kioschis, P., Coy, J.F., Klauck, S.M., Poustka, A., and Dahl, N. (1996). A gene mutated in X-linked myotubular myopathy defines a new putative tyrosine phosphatase family conserved in yeast. Nat. Genet. *13*, 175–182.

Lee, E., Marcucci, M., Daniell, L., Pypaert, M., Weisz, O.A., Ochoa, G.-C., Farsad, K., Wenk, M.R., and De Camilli, P. (2002). Amphiphysin 2 (Bin1) and T-tubule biogenesis in muscle. Science *297*, 1193–1196.

Luxton, G.W.G., Gomes, E.R., Folker, E.S., Vintinner, E., and Gundersen, G.G. (2010). Linear arrays of nuclear envelope proteins harness retrograde actin flow for nuclear movement. Science *329*, 956–959.

Madania, A., Dumoulin, P., Grava, S., Kitamoto, H., Schärer-Brodbeck, C., Soulard, A., Moreau, V., and Winsor, B. (1999). The Saccharomyces cerevisiae homologue of human Wiskott-Aldrich syndrome protein Las17p interacts with the Arp2/3 complex. Mol. Biol. Cell *10*, 3521–3538.

Marty, I., Thevenon, D., Scotto, C., Groh, S., Sainnier, S., Robert, M., Grunwald, D., and Villaz, M. (2000). Cloning and characterization of a new isoform of skeletal muscle triadin. J. Biol. Chem. *275*, 8206–8212.

Megason, S.G., and McMahon, A.P. (2002). A mitogen gradient of dorsal midline Wnts organizes growth in the CNS. Development *129*, 2087–2098.

Metzger, T., Gache, V., Xu, M., Cadot, B., Folker, E.S., Richardson, B.E., Gomes, E.R., and Baylies, M.K. (2012). MAP and kinesin-dependent nuclear positioning is required for skeletal muscle function. Nature *484*, 120–124.

Nicot, A.-S., Toussaint, A., Tosch, V., Kretz, C., Wallgren-Pettersson, C., Iwarsson, E., Kingston, H., Garnier, J.-M., Biancalana, V., Oldfors, A., et al. (2007). Mutations in amphiphysin 2 (BIN1) disrupt interaction with dynamin 2 and cause autosomal recessive centronuclear myopathy. Nat. Genet. *39*, 1134–1139.

Padrick, S.B., and Rosen, M.K. (2010). Physical mechanisms of signal integration by WASP family proteins. Annu. Rev. Biochem. *79*, 707–735.

De Palma, C., Falcone, S., Pisoni, S., Cipolat, S., Panzeri, C., Pambianco, S., Pisconti, A., Allevi, R., Bassi, M.T., Cossu, G., et al. (2010). Nitric oxide inhibition of Drp1-mediated mitochondrial fission is critical for myogenic differentiation. Cell Death Differ. *17*, 1684–1696.

Parton, R.G., Way, M., Zorzi, N., and Stang, E. (1997). Caveolin-3 associates with developing T-tubules during muscle differentiation. J. Cell Biol. *136*, 137–154.

Pierson, C.R., Tomczak, K., Agrawal, P., Moghadaszadeh, B., and Beggs, A.H. (2005). X-linked myotubular and centronuclear myopathies. J. Neuropathol. Exp. Neurol. *64*, 555–564.

Powell, J.A., Petherbridge, L., and Flucher, B.E. (1996). Formation of triads without the dihydropyridine receptor alpha subunits in cell lines from dysgenic skeletal muscle. J. Cell Biol. *134*, 375–387.

Prehoda, K.E., Scott, J.A., Mullins, R.D., and Lim, W.A. (2000). Integration of multiple signals through cooperative regulation of the N-WASP-Arp2/3 complex. Science *290*, 801–806.

Prokic, I., Cowling, B.S., and Laporte, J. (2014). Amphiphysin 2 (BIN1) in physiology and diseases. J. Mol. Med. *92*, 453–463.

Al-Qusairi, L., and Laporte, J. (2011). T-tubule biogenesis and triad formation in skeletal muscle and implication in human diseases. Skelet Muscle *1*, 26.

Al-Qusairi, L., Weiss, N., Toussaint, A., Berbey, C., Messaddeq, N., Kretz, C., Sanoudou, D., Beggs, A.H., Allard, B., Mandel, J.-L., et al. (2009). T-tubule disorganization and defective excitation-contraction coupling in muscle fibers lacking myotubularin lipid phosphatase. Proc. Natl. Acad. Sci. U.S.A. *106*, 18763–18768.

Razzaq, A., Robinson, I.M., McMahon, H.T., Skepper, J.N., Su, Y., Zelhof, A.C., Jackson, A.P., Gay, N.J., and O'Kane, C.J. (2001). Amphiphysin is necessary for organization of the excitation-contraction coupling machinery of muscles, but not for synaptic vesicle endocytosis in Drosophila. Genes Dev. *15*, 2967–2979.

Rohatgi, R., Ma, L., Miki, H., Lopez, M., Kirchhausen, T., Takenawa, T., and Kirschner, M.W. (1999). The interaction between N-WASP and the Arp2/3 complex links Cdc42-dependent signals to actin assembly. Cell *97*, 221–231.

Rosenblatt, J.D., Lunt, A.I., Parry, D.J., and Partridge, T.A. (1995). Culturing satellite cells from living single muscle fiber explants. In Vitro Cell. Dev. Biol. Anim. *31*, 773–779.

Royer, B., Hnia, K., Gavriilidis, C., Tronchère, H., Tosch, V., and Laporte, J. (2013). The myotubularinamphiphysin 2 complex in membrane tubulation and centronuclear myopathies. EMBO Rep. *14*, 907–915.

Salazar, M.A., Kwiatkowski, A.V., Pellegrini, L., Cestra, G., Butler, M.H., Rossman, K.L., Serna, D.M., Sondek, J., Gertler, F.B., and Camilli, P.D. (2003). Tuba, a Novel Protein Containing Bin/Amphiphysin/Rvs and Dbl Homology Domains, Links Dynamin to Regulation of the Actin Cytoskeleton. J. Biol. Chem. *278*, 49031–49043.

Sonnemann, K.J., Fitzsimons, D.P., Patel, J.R., Liu, Y., Schneider, M.F., Moss, R.L., and Ervasti, J.M. (2006). Cytoplasmic gamma-actin is not required for skeletal muscle development but its absence leads to a progressive myopathy. Dev. Cell *11*, 387–397.

Starr, D.A., and Fridolfsson, H.N. (2010). Interactions between nuclei and the cytoskeleton are mediated by SUN-KASH nuclear-envelope bridges. Annu. Rev. Cell Dev. Biol. *26*, 421–444.

Suetsugu, S., and Gautreau, A. (2012). Synergistic BAR-NPF interactions in actin-driven membrane remodeling. Trends Cell Biol. *22*, 141–150.

Takano, K., Watanabe-Takano, H., Suetsugu, S., Kurita, S., Tsujita, K., Kimura, S., Karatsu, T., Takenawa, T., and Endo, T. (2010). Nebulin and N-WASP cooperate to cause IGF-1-induced sarcomeric actin filament formation. Science *330*, 1536–1540.

Takekura, H., Flucher, B.E., and Franzini-Armstrong, C. (2001). Sequential docking, molecular differentiation, and positioning of T-Tubule/SR junctions in developing mouse skeletal muscle. Dev. Biol. *239*, 204–214.

Taneike, M., Mizote, I., Morita, T., Watanabe, T., Hikoso, S., Yamaguchi, O., Takeda, T., Oka, T., Tamai, T., Oyabu, J., et al. (2011). Calpain Protects the Heart from Hemodynamic Stress. J. Biol. Chem. *286*, 32170– 32177.

Tjondrokoesoemo, A., Park, K.H., Ferrante, C., Komazaki, S., Lesniak, S., Brotto, M., Ko, J.-K., Zhou, J., Weisleder, N., and Ma, J. (2011). Disrupted membrane structure and intracellular Ca^{2+} signaling in adult skeletal muscle with acute knockdown of Bin1. PLoS ONE *6*, e25740.

Toussaint, A., Cowling, B.S., Hnia, K., Mohr, M., Oldfors, A., Schwab, Y., Yis, U., Maisonobe, T., Stojkovic, T., Wallgren-Pettersson, C., et al. (2011). Defects in amphiphysin 2 (BIN1) and triads in several forms of centronuclear myopathies. Acta Neuropathol. *121*, 253–266.

Vasli, N., Laugel, V., Bohm, J., Lannes, B., Biancalana, V., and Laporte, J. (2012). Myotubular myopathy caused by multiple abnormal splicing variants in the MTM1 RNA in a patient with a mild phenotype. Eur J Hum Genet *20*, 701–704.

Vlahovich, N., Kee, A.J., Van der Poel, C., Kettle, E., Hernandez-Deviez, D., Lucas, C., Lynch, G.S., Parton, R.G., Gunning, P.W., and Hardeman, E.C. (2009). Cytoskeletal tropomyosin Tm5NM1 is required for normal excitation-contraction coupling in skeletal muscle. Mol. Biol. Cell *20*, 400–409.

Wang, Z., Cui, J., Wong, W.M., Li, X., Xue, W., Lin, R., Wang, J., Wang, P., Tanner, J.A., Cheah, K.S.E., et al. (2013). Kif5b controls the localization of myofibril components for their assembly and linkage to the myotendinous junctions. Development *140*, 617–626.

Wu, X., Yoo, Y., Okuhama, N.N., Tucker, P.W., Liu, G., and Guan, J.-L. (2006). Regulation of RNApolymerase-II-dependent transcription by N-WASP and its nuclear-binding partners. Nat. Cell Biol. *8*, 756–
763.

Yamada, H., Padilla-Parra, S., Park, S.-J., Itoh, T., Chaineau, M., Monaldi, I., Cremona, O., Benfenati, F., De Camilli, P., Coppey-Moisan, M., et al. (2009). Dynamic interaction of amphiphysin with N-WASP regulates actin assembly. J. Biol. Chem. *284*, 34244–34256.

Zalk, R., Lehnart, S.E., and Marks, A.R. (2007). Modulation of the ryanodine receptor and intracellular calcium. Annu. Rev. Biochem. *76*, 367–385.

Zelhof, A.C., and Hardy, R.W. (2004). WASp is required for the correct temporal morphogenesis of rhabdomere microvilli. J. Cell Biol. *164*, 417–426.

Zhang, X., Xu, R., Zhu, B., Yang, X., Ding, X., Duan, S., Xu, T., Zhuang, Y., and Han, M. (2007). Syne-1 and Syne-2 play crucial roles in myonuclear anchorage and motor neuron innervation. Development *134*, 901–
908.

Zheng, Z., Wang, Z.-M., and Delbono, O. (2002). Charge movement and transcription regulation of L-type calcium channel alpha(1S) in skeletal muscle cells. J. Physiol. (Lond.) *540*, 397–409.

Figure 1. **Visualizing nuclear movement to the periphery.**

A. Timeline of muscle differentiation in the *in vitro* system used to study peripheral nuclear positioning and transversal triad formation. Nuclei are in red, myofibrils in white (with z-lines in green) and transversal triads as purple lines. Day 3: myofibril formation. Day 5: initiation of peripheral nuclear positioning. Day 7: transversal triad formation.

B. Kymograph from a time-lapse movie of a 5-day myofiber depicting peripheral movement of a nucleus (H2B-iRFP, red) through myofibrils (YFP-α-actinin, green). Left: view from the side, surface three-dimensional rendering. Middle: view from the right side, with transparent myofibrils three-dimensional rendering. Right: view from the top, surface three-dimensional rendering. Scale bar, 10 μm.

C. 2D view of the central plane of a kymograph from a time-lapse movie of a 5-day myofiber depicting peripheral movement of a nucleus (H2B-iRFP, red) through myofibrils (YFP-α-actinin, green). Scale bar, 10 μm.

D. Representative image of a nucleus squeezing to the periphery from an *in vivo* isolated myofiber of a newborn mouse and stained for myofibrils (α-actinin, green) and nucleus (red). Left: 3D rendering. Middle left: 2D orthogonal view, yellow lines represent slices seen in right side panels. Middle right: 2D plane from yellow slice 1. Right: 2D plane from yellow slice 2. Scale bar, 10 μm.

E. Representative image of a nucleus squeezing to the periphery from the clearing of a whole muscle in a newborn mouse and stained for myofibrils (α-actinin, green) and nucleus (red). Left: 3D rendering. Middle left: 2D orthogonal view, yellow lines represent slices seen in right side panels. Middle right: 2D plane from yellow slice 1. Right: 2D plane from yellow slice 2. Scale bar, 10 μm.

Figure 2. **Myofiber cross-linking by desmin drives nuclear movement to the periphery.**

A. Quantification of the sphericity of nuclei during nuclear movement to the periphery in 5-day myofibers. Dashed line corresponds to the emergence of the nucleus at the myofiber periphery (n = 8).

B. Quantification of the volume of nuclei during nuclear movement to the periphery in 5-day myofibers. Dashed line corresponds to the emergence of the nucleus at the myofiber periphery (n = 8).

C. Quantification of the area in between myofibrils around the nucleus (left xy axis and blue line) and the percentage of area of the nucleus at the periphery over time (right xy axis and orange line) in 5-day myofibers. Dashed line corresponds to the emergence of the nucleus to the periphery (n = 8).

D. Representative immunofluorescence image of a 10-day myofiber knocked down for scrambled or desmin and stained for F-actin (phalloidin, magenta), desmin (green) and DAPI (nucleus, blue). Scale bar, 10 μm.
E. Western blot with indicated antibodies from 10-day myofibers knocked down for scrambled or desmin.
F. Quantification of peripheral nuclei positioning and traversal triads in 10-day myofibers knocked down for scrambled or desmin.
G. Representative immunofluorescence image of a 4.5-day myofiber knocked stained for F-actin (phalloidin, magenta), desmin (green) and DAPI (nucleus, blue). Arrow indicates organized desmin whereas arrowhead indicates disorganized desmin. Scale bar, 10 μm.
H. Kymograph from a time-lapse movie of a 5-day myofiber depicting desmin organization (Emerald-desmin, gray) during nuclear (H2B-iRFP, red) movement to the periphery. 00:00 (hh:mm). Arrowhead indicate the transversal organization of desmin. Scale bar, 10 μm.

Figure 3. **Theoretical model of peripheral nuclear movement.**
A-C. Schematic of a nucleus (red) surrounded by myofibrils (white) before (A) and during (B and C) peripheral migration. Longitudinal view (left) and transversal view (right). $R_{0\,=}$ radius of the undeformed nucleus. ΔR = amplitude of radial deformation. F_n = force applied by myofibrils on the nucleus. L = length between the crosslinkers (blue) on each side of the nucleus. h = height of a nuclear wrinkle formed by myofibril pressure.
D. Transversal schematic of a stable nuclear wrinkle (left) and unstable nuclear bleb (right). w = width of a nuclear wrinkle/bleb. h = height of a nuclear wrinkle/bleb. ΔP = difference in hydrostatic pressure between nucleus and wrinkle upon an increase of h.
E. Model prediction of the stability of wrinkles relative to force on the nucleus. The scaled wrinkle size h/w is plotted as a function of crosslinking L based on the function $4T/L*R_0*E$. Above the threshold $h/w \approx 1$, the wrinkle becomes an unstable bleb and the nucleus is moved to the periphery. Blue line represents crosslinking of myofibrils that are relaxed. Green line represents crosslinking of myofibrils that contract. Orange line represents crosslinking of myofibrils using the nuclear elastic modulus value necessary to reach the unstable threshold and initiate nuclear movement to the periphery.
F. Model prediction of the stability of wrinkles relative to global nuclear stiffness. The scaled wrinkle size h/w is plotted as a function of global E.

Figure 4. **Contraction and nuclear stiffness are involved in nuclear movement to the periphery**

A. Quantification of peripheral nuclei positioning in 10-day myofibers treated with the contraction inhibitor tetrodotoxin from day 4.5.
B. Representative images of the first (left) and last (right) frame of a 24-hour time-lapse movie of untransfected as well as ChR2-GFP (green) and H2B-iRFP (red) transfected myofibers. Nuclei from transfected myofibers are emphasized with a red dashed circle and nuclei from untransfected myofibers are emphasized with a yellow dashed circle. 00:00 (hh:mm) corresponds to 3.5-day myofibers. Scale bar, 10 μm.
C. Quantification of nuclei migrating to the periphery from a 24-hour time-lapse movie in 3.5-day moyfibers expressing ChR2-GFP and untransfected myofibers (control).
D. Representative immunofluorescence images of 10-day myofibers knocked down for lamin A/C, scrambled or over-expressing mCherry-lamin A/C (mCh-lamin A/C) and stained for lamin A/C (magenta), F-actin (green) and DAPI (nucleus, blue). Scale bar, 10 μm.
E. Quantification of peripheral nuclei positioning in 10-day myofibers knocked down for lamin A/C or scrambled, or over-expressing H2B-mCherry or mCherry-lamin A/C.
F. Plot correlating velocity of nuclear movement to the periphery with the intensity of the mCherry-lamin A/C signal in time-lapse movies of myofibers expressing mCherry-lamin A/C between 4.5 and 5.5 days. Red line corresponds to the significant linear regression ($p=0.0001$ of $R^2 = 0.5004$).
G. Kymograph from a time-lapse movie of a 5-day myofiber over-expressing low levels of mCherry-lamin A/C during nuclear squeezing. Top: Transversal 2D section of lamin A/C color-coded as a heatmap. White arrowheads indicate asymmetry of lamin A/C. bottom: 3D rendering of mCherry-lamin A/C (heatmap) and myofibrils (α-actinin, green). Scale bar, 10 μm.

Figure 5. **Actin and Arp2/3 isoforms play different roles in myofiber differentiation**.
A. Representative immunofluorescence images of 10-day myofibers knocked down for scrambled, Arpc5L or Arpc5 and stained for triadin (triad marker, magenta), α-actinin (myofibrils/Z-line marker, green) and DAPI (nucleus, blue). Scale bar, 10 μm. 2x Magnifications corresponding to the yellow squares are showed in the right of each image.
B. Quantification of peripheral nuclei positioning (left) and transversal triad formation (right) in 10-day myofibers knocked down for scrambled, Arpc5L or Arpc5.
C. Representative immunofluorescence images of a 10-day myofiber knocked down for scrambled, γ-actin or β-actin and stained for triadin (triad marker, magenta), α-actinin (myofibrils/Z-line marker, green) and DAPI (nucleus, blue). Scale bar, 10 μm. 2x

Magnifications corresponding to the yellow squares are showed in the right of each image.
D. Quantification of peripheral nuclei positioning (left) and transversal triad formation (right) in 10-day myofibers knocked down for scrambled, γ-actin or β-actin.

Figure 6. **Arpc5L and γ-actin crosslink myofibrils**
A. Western blots with indicated antibodies of GFP, GFP-Arpc5L or GFP-Arpc5 immunoprecipitated from 5-day myofibers.
B. Western blots with indicated antibodies of GFP, GFP-γ-actin and GFP-β-actin immunoprecipitated from 5-day myofibers.
C. Western blots with indicated antibodies of IgG control, Arpc5L and Arpc5 immunoprecipitated from 5-day myofibers.
D. Quantification of the duration of longitudinal nuclear pausing from 24-hour time-lapse movies in 4.5-day myofibers knocked down for scrambled, Arpc5L or γ-actin. (scrambled n = 27, γ-actin n = 24, Arpc5L n = 29).
E. Quantification of nuclear sphericity before (movement) and during (pause) pausing events in 4.5-day myofibers knocked down for scrambled, Arpc5L or γ-actin. (n = 10).
F. Quantification of nuclear volume before (movement) and during (pause) pausing events in 4.5-day myofibers knocked down for scrambled, Arpc5L or γ-actin. (n = 10).
G. Quantification of the area in between myofibrils around the nucleus before (movement) and during (pause) pausing events in 4.5-day myofibers knocked down for scrambled, Arpc5L or γ-actin. (n = 10).
H. Representative immunofluorescence images of 5-day myofibers expressing GFP-γ-actin (green) and immunostained for ArpC5L (magenta) in 5-day myofibers (left). Scale bar, 10 μm. 4x Magnifications corresponding to the numbered yellow squares are showed in the right.

Figure 7. **Arp5L and γ-actin organize desmin to cross-link myofibrils for nuclear movement**

A. Representative image of 5-day myofibers knocked down for scramble, Arpc5L or γ-actin and stained for F-actin (phalloidin, magenta), desmin (green) and DAPI (nucleus, blue). Scale bar, 10 μm.
B. Western blot with indicated antibodies from 10-day myofibers knocked down for scrambled or plectin.
C. Quantification of peripheral nuclei positioning in 10-day myofibers knocked down for scrambled or plectin.

D. Representative immunofluorescence image of a 4.5-day myofiber knocked down for scrambled or plectin and stained for plectin (magenta), desmin (green) and DAPI (nucleus, blue). Scale bar, 10 μm.
E. Representative immunofluorescence image of a 4.5-day myofiber knocked down for Arpc5L or γ-actin and stained for plectin (magenta), desmin (green) and DAPI (nucleus, blue). Scale bar, 10 μm.
F. Model of nuclear movement to the periphery. The nucleus (red) is deformed and moved to the periphery of myofiber by crosslinking (blue), zipping and contraction of myofibrils (white).

Figure 1

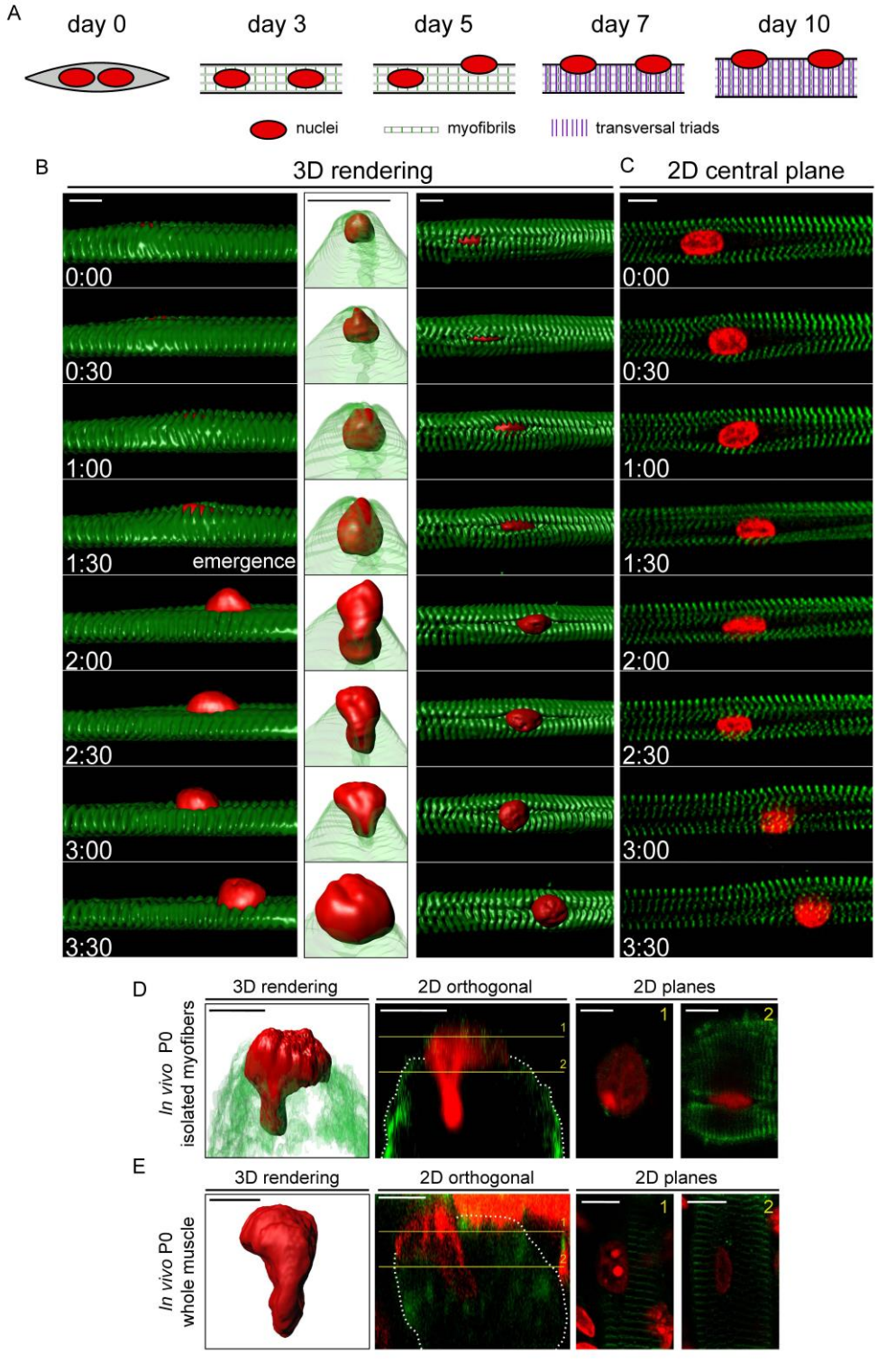
A
day 0
day 3
day 5
day 7
day 10
nuclei
myofibrils
transversal triads
B
3D rendering
C
2D central plane
0:00
0:30
1:00
1:30
emergence
2:00
2:30
3:00
3:30
D
3D rendering
2D orthogonal
2D planes
In vivo P0
isolated myofibers
E
3D rendering
2D orthogonal
2D planes
In vivo P0
whole muscle

Figure 2

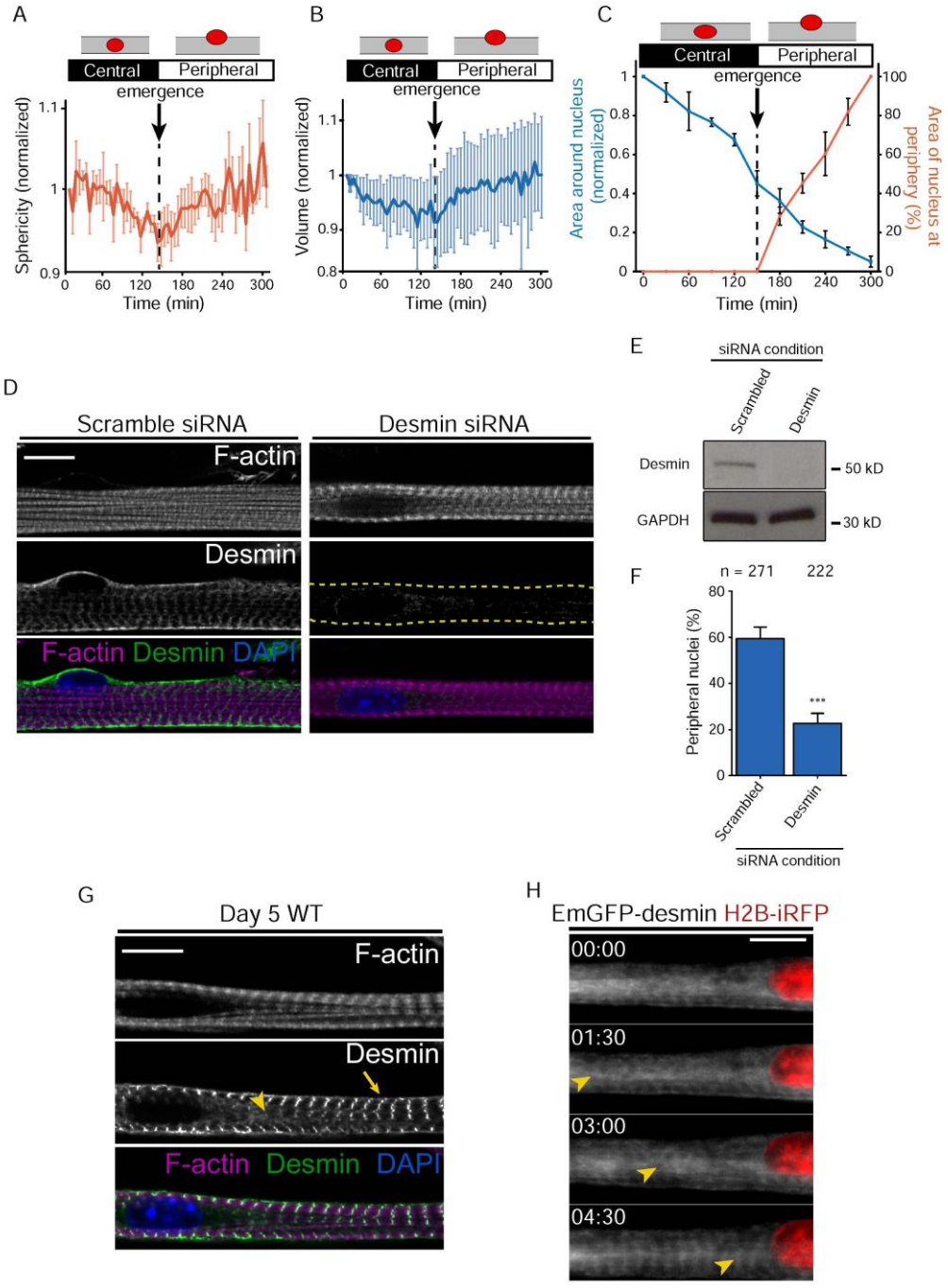
A
Central
Peripheral
emergence
Sphericity (normalized)
Time (min)
B
Central
Peripheral
emergence
Volume (normalized)
Time (min)
C
Central
Peripheral
emergence
Area around nucleus (normalized)
Area of nucleus at periphery (%)
Time (min)
D
Scramble siRNA
Desmin siRNA
F-actin
Desmin
F-actin Desmin DAPI
E
siRNA condition
Scrambled
Desmin
Desmin
GAPDH
50 kD
30 kD
F
n = 271
222
Peripheral nuclei (%)
***
Scrambled
Desmin
siRNA condition
G
Day 5 WT
F-actin
Desmin
F-actin Desmin DAPI
H
EmGFP-desmin H2B-iRFP
00:00
01:30
03:00
04:30

Figure 3

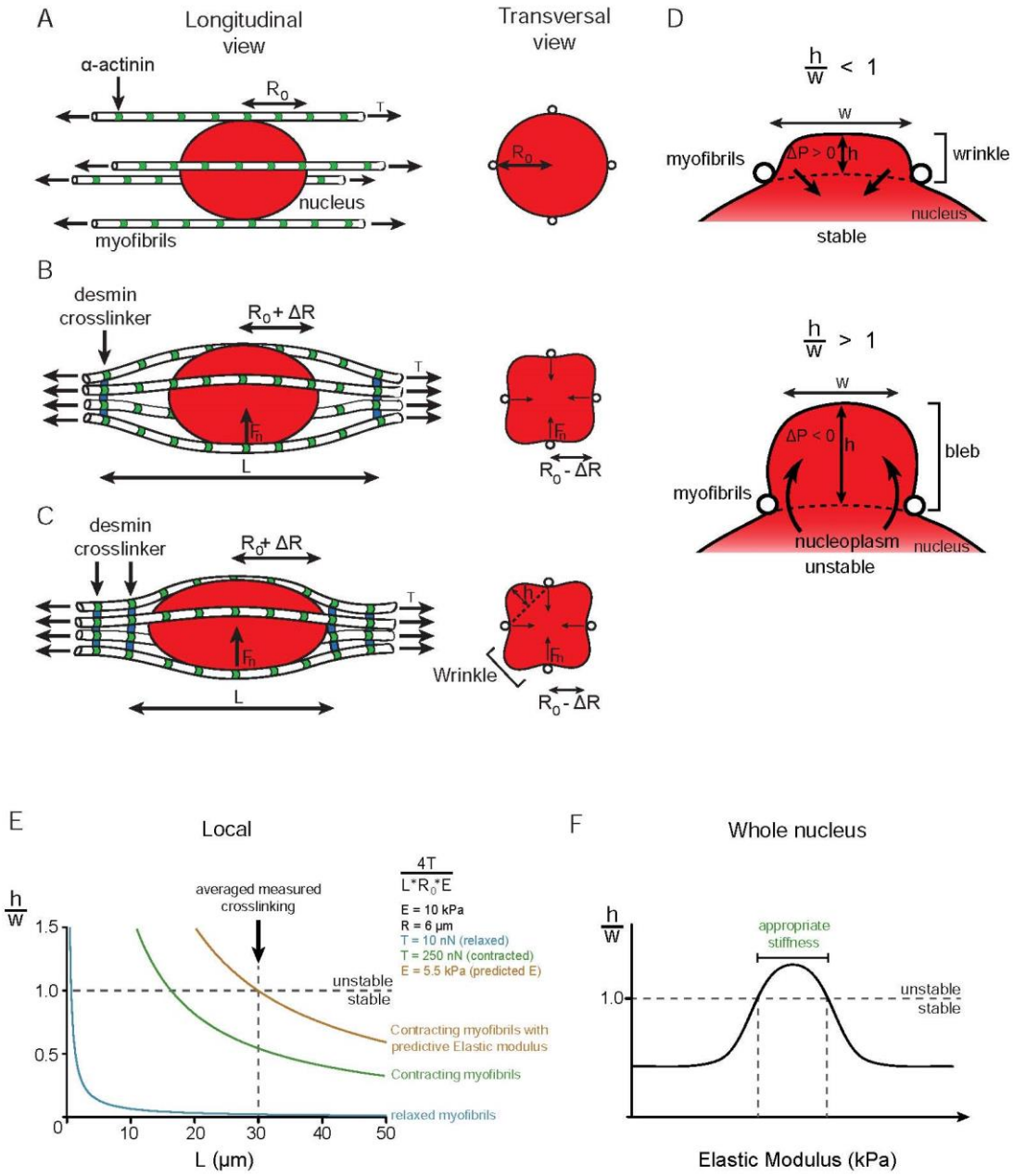
A
Longitudinal view
Transversal view
α-actinin
R_0
T
nucleus
myofibrils
B
desmin crosslinker
$R_0 + \Delta R$
F_n
L
$R_0 - \Delta R$
C
Wrinkle
D
$\frac{h}{w} < 1$
w
ΔP > 0
h
wrinkle
stable
$\frac{h}{w} > 1$
ΔP < 0
bleb
nucleoplasm
unstable
E
Local
$\frac{4T}{L^*R_0^*E}$
E = 10 kPa
R = 6 µm
T = 10 nN (relaxed)
T = 250 nN (contracted)
E = 5.5 kPa (predicted E)
averaged measured crosslinking
unstable
stable
Contracting myofibrils with predictive Elastic modulus
Contracting myofibrils
relaxed myofibrils
L (µm)
F
Whole nucleus
appropriate stiffness
Elastic Modulus (kPa)

Figure 4

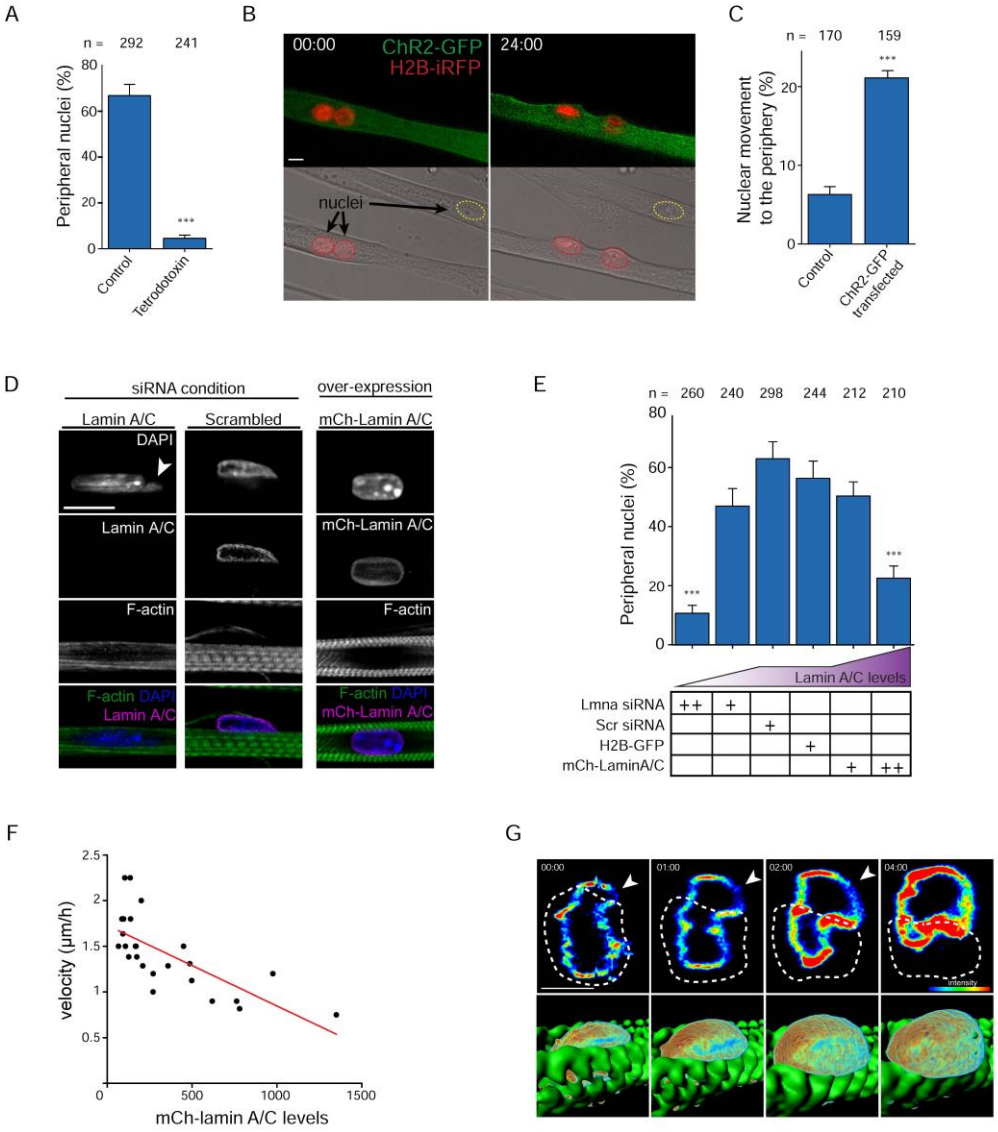
A
n = 292 241
Peripheral nuclei (%)
80
60
40
20
0
***
Control
Tetrodotoxin
B
00:00
ChR2-GFP
H2B-iRFP
24:00
nuclei
C
n = 170 159
Nuclear movement to the periphery (%)
20
10
0
***
Control
ChR2-GFP transfected
D
siRNA condition
over-expression
Lamin A/C
Scrambled
mCh-Lamin A/C
DAPI
Lamin A/C
F-actin
F-actin DAPI
Lamin A/C
mCh-Lamin A/C
E
n = 260 240 298 244 212 210
Peripheral nuclei (%)
80
60
40
20
0
***
***
Lamin A/C levels
Lmna siRNA ++ + + + + ++
Scr siRNA + +
H2B-GFP +
mCh-LaminA/C + ++
F
velocity (µm/h)
2.5
2
1.5
1
0.5
0
500
1000
1500
mCh-lamin A/C levels
G
00:00
01:00
02:00
04:00
intensity

Figure 5

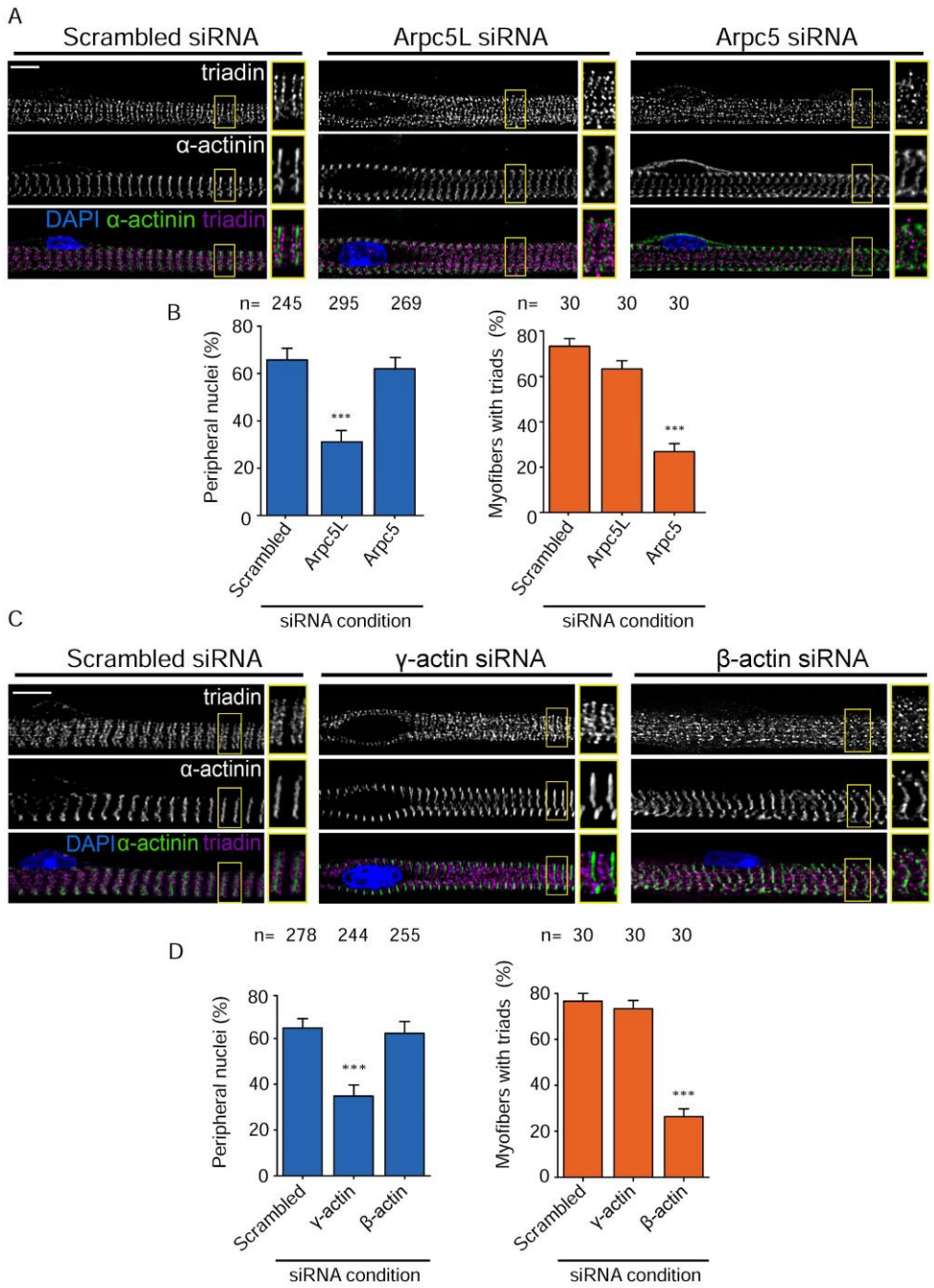
A
Scrambled siRNA
Arpc5L siRNA
Arpc5 siRNA
triadin
α-actinin
DAPI α-actinin triadin
B
n= 245 295 269
Peripheral nuclei (%)
***
Scrambled
Arpc5L
Arpc5
siRNA condition
n= 30 30 30
Myofibers with triads (%)
***
Scrambled
Arpc5L
Arpc5
siRNA condition
C
Scrambled siRNA
γ-actin siRNA
β-actin siRNA
triadin
α-actinin
DAPI α-actinin triadin
D
n= 278 244 255
Peripheral nuclei (%)
***
Scrambled
γ-actin
β-actin
siRNA condition
n= 30 30 30
Myofibers with triads (%)
***
Scrambled
γ-actin
β-actin
siRNA condition

Figure 6

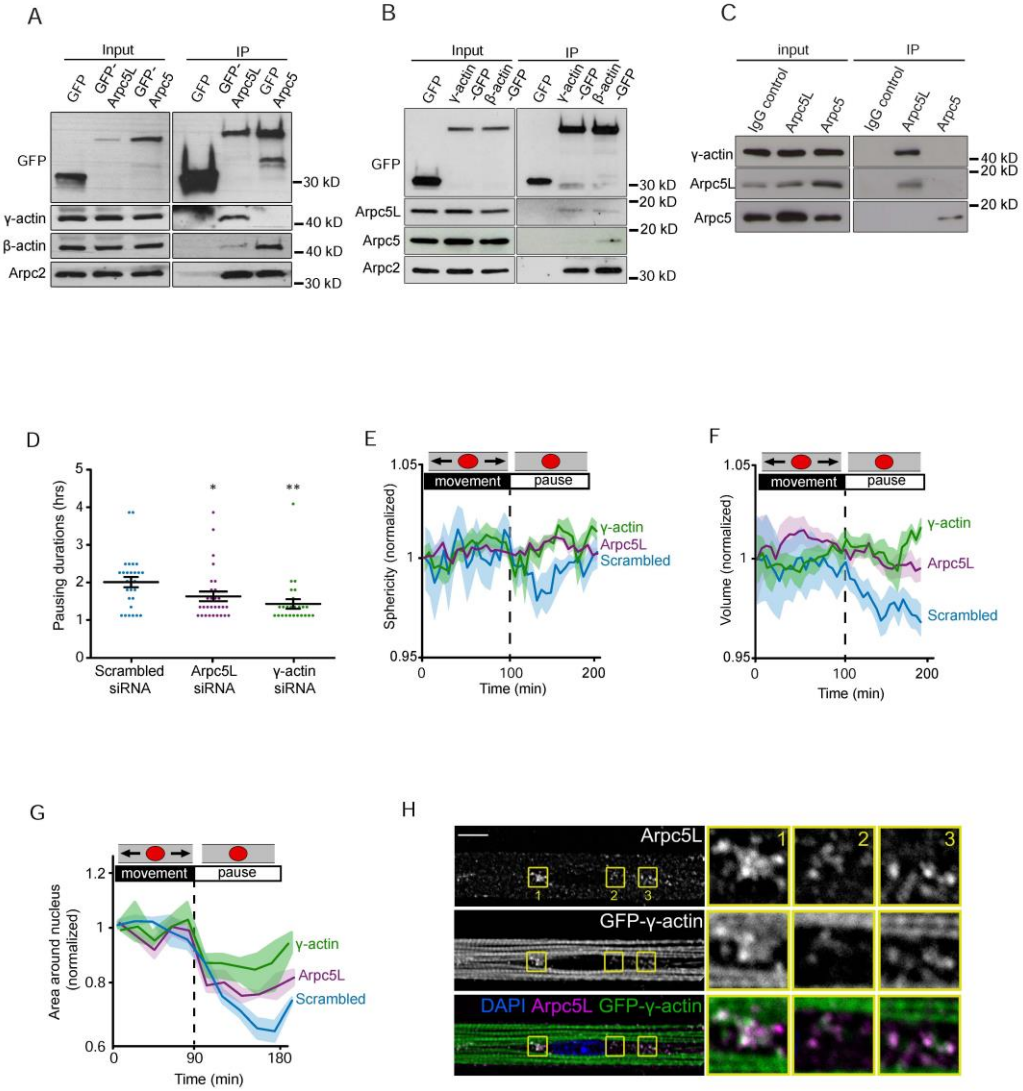
A
Input
IP
GFP
GFP-Arpc5L
GFP-Arpc5
GFP
GFP-Arpc5L
GFP-Arpc5
GFP
γ-actin
β-actin
Arpc2
30 kD
40 kD
40 kD
30 kD
B
Input
IP
GFP
γ-actin-GFP
β-actin-GFP
GFP
γ-actin-GFP
β-actin-GFP
GFP
Arpc5L
Arpc5
Arpc2
30 kD
20 kD
20 kD
30 kD
C
input
IP
IgG control
Arpc5L
Arpc5
IgG control
Arpc5L
Arpc5
γ-actin
Arpc5L
Arpc5
40 kD
20 kD
20 kD
D
Pausing durations (hrs)
Scrambled siRNA
Arpc5L siRNA
γ-actin siRNA
E
movement
pause
Sphericity (normalized)
γ-actin
Arpc5L
Scrambled
Time (min)
F
movement
pause
Volume (normalized)
γ-actin
Arpc5L
Scrambled
Time (min)
G
movement
pause
Area around nucleus (normalized)
γ-actin
Arpc5L
Scrambled
Time (min)
H
Arpc5L
GFP-γ-actin
DAPI Arpc5L GFP-γ-actin
1
2
3

Figure 7

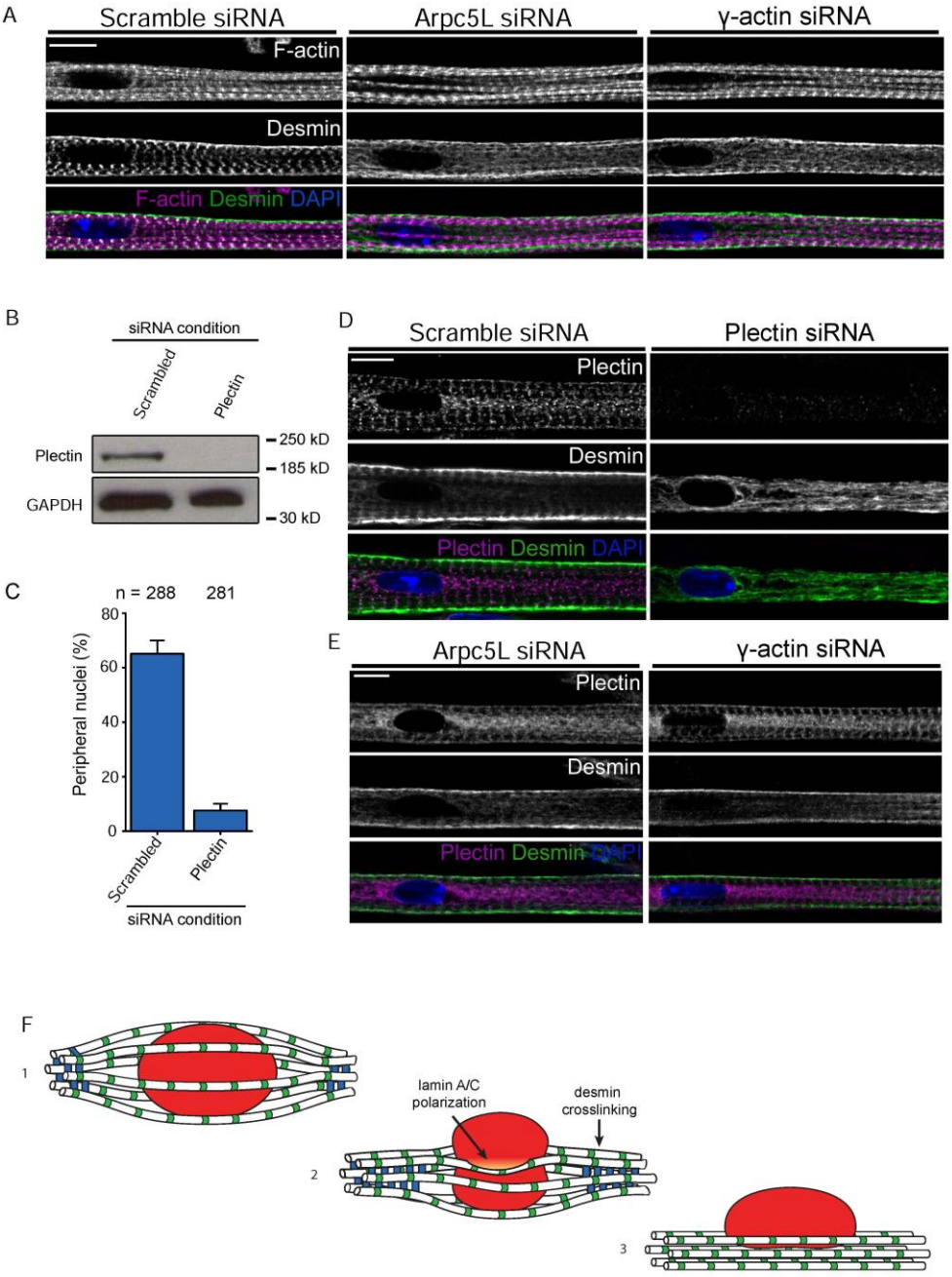
A
Scramble siRNA
Arpc5L siRNA
γ-actin siRNA
F-actin
Desmin
F-actin Desmin DAPI
B
siRNA condition
Scrambled
Plectin
Plectin
GAPDH
250 kD
185 kD
30 kD
C
n = 288
281
Peripheral nuclei (%)
80
60
40
20
0
Scrambled
Plectin
siRNA condition
D
Scramble siRNA
Plectin siRNA
Plectin
Desmin
Plectin Desmin DAPI
E
Arpc5L siRNA
γ-actin siRNA
Plectin
Desmin
Plectin Desmin DAPI
F
1
lamin A/C polarization
desmin crosslinking
2
3

Experimental procedures

Cell Culture, transfections and reagents

All procedures using animals were approved by the Institutional ethics committee and followed the guidelines of the National Research Council Guide for the care and use of laboratory animals. In vitro myofibers were generated using the protocol previously described(Falcone et al., 2014).

Cells were transfected with siRNA (20nM) using RNAiMAX (cat # 15338-100), cDNA 1ug/ul using Lipofectamine-LTX Plus reagent (cat# 13778-150) or both using Lipofectamine 2000 (cat# 11668-019) following manufacturer instructions (Life Technologies, see individual catalogue numbers). For primary myoblasts, cells were transfected 6 hours prior to differentiation in order to promote protein silencing or overexpression effectiveness from the beginning of differentiation.

CK666 (Arp2/3 inhibitor) was obtained from Sigma (cat# SML0006-5MG) and was added to 4.5-day myofibers at a concentration of 50 μM. Tetrodotoxin (contraction inhibitor) was obtained from Sigma (cat# T8024) and was added to 4.5-day myofibers at a concentration of 10 μM.

Plasmids

pcDNA GFP was a gift from Alexis Gautreau. GFP-Arpc5 and GFP-Arpc5L were previously described(Abella et al., in press). The γ-actin mouse cDNA, synthesized from Life Technologies with silent point mutations to make it resistant against siRNA, was cloned into a pDONR221 Gateway entry vector (Life Technologies) and recombined into a pEGFP_C1-GW destination vector and a pRFP-GW destination vector to generate a pEGFP_C1- γ-actin and pRFP-γ-actin plasmids respectively. The β-actin cDNA, synthesized from Life Technologies with silent point mutations to make it resistant against siRNA, was cloned into a pDONR221 Gateway entry vector (Life Technologies) and recombined into a pEGFP-C1-GW destination vector and a pRFP-GW destination vector to generate a pEGFP_C1-β-actin and pRFP-β-actin plasmids respectively. The ChR2-GFP construct was obtained through addgene (Plasmid #20939). YFP-α-actinin plasmid was a gift from Pekka Lappalainen. iRFP-H2B was a gift from Mathieu Coppey. EmGFP-Desmin was obtained through addgene (plasmid #54059).

Antibodies

Antibody epitope	Species	Company	Concentration
γ-actin	Mouse	Courtesy of Dr. Chapponier laboratory	WB 1:1000
β-siRNA	Mouse	Courtesy of Dr. Chapponier laboratory	WB 1:500
α-actinin	Mouse	Sigma (cat #A7732)	IF 1:200
Triadin	Rabbit	Courtesy of Dr. Marty laboratory	IF 1:500
Arpc2	Rabbit	EMD Millipore (cat #07-227)	WB 1:1000
Arpc5	Mouse	Santa Cruz Biotech (cat #sc-166760)	IF 1:100 WB 1:500
Arpc5L	Rabbit	Abcam (cat #ab169763)	IF 1:200 WB 1:500
Arpc1A	Mouse	Thermo Scientific (cat #PA534870)	WB 1:250
Arpc1B	Rabbit	Bethyl Laboratories (cat# A302-780A)	WB: 1:1000
Dhpr	Mouse	EMD Millipore (cat# MAB427)	IF: 1:200
Desmin	Mouse	Dako (cat# Clone D33)	IF: 1:200 WB: 1:1000
Plectin	Rabbit	Sigma (cat# HPA029906)	IF: 1:200 WB: 1:1000
Lamin A/C	Rabbit	Santa Cruz Biotech (cat# sc-20681)	IF: 1:100 WB: 1:1000
Lamin A/C-C	Mouse	Abcam (cat# ab8984)	IF: 1:200
Lamin B1	Rabbit	Abcam (cat# ab16048)	IF: 1:200
Phalloidin	-	Thermo Scientific (cat# A12379)	IF: 1:200

siRNA

Target	Ambion ID	Sequence (sense)	Sequence (anti-sense)
Scrambled	genecust	UUCUCCGAACGUGUCACGUtt	ACGUGACACGUUCGGAGAAtt
γ-actin	s61904	AGAUAAUGUUUGAAACCUUtt	AAGGUUUCAAACAUUAUCUgc
β-actin	s200989	UGACGUUGACAUCCGUAAAtt	UUUACGGAUGUCAACGUCAca
Arpc2	s94587	AAAACAUCCGACUUC	UAAGGAAGUCGGAUGUUU

		CUUAtt	Utg
Arpc1A	s80581	GCCGAUGCUCUUUAACUAtt	UAGUUAAAGAGCAUCGGGCag
Arpc1B	161925	GGGCUGCUUUGCUGAAUGUtt	ACAUUCAGCAAAGCAGCCCtt
Arpc5	s206017	AGAUGAUGCUAUAAGUAtt	UACACUUAUAGCAUCAUCUgg
Arpc5L	s92445	GCGUGGAUAUCGACGAAUUtt	AAUUCGUCGAUAUCCACGCgg
Lamin A/C	S69252	GGCUUGUGGAGAUCGAUAAtt	UUAUCGAUCUCCACAAGCCgc
Lamin B1	S69255	GACUUGGAGUUUCGUAAAAtt	UUUUACGAAACUCCAAGUCct
Desmin	s64942	GAGGAGAUCCGACACCUUAAt	UUAGGUGUCGGAUCUCCUCct
Plectin	S201802	CGAGUACACCUUUGAGGGAtt	UCCCUCAAAGGUGUACUCGgg

Western Blotting

Cells were lysed in PBS + 1%SDS and passed through a Qiashredder column (Qiagen) to disrupt DNA. Protein concentration was measured with a BCA kit according to manufacturer instructions (Pierce). Equal amount of sample were boiled in 30ul sample buffer and were loaded on 4-12% pre-cast Bis-Tris gel (Invitrogen) and transferred into nitrocellulose membrane using the iBlot apparatus (Invitrogen). Membranes were blocked with blocking buffer (5% Non Fat Dry Milk, 0.1% Tween in TBS). Primary antibodies were incubated overnight in blocking buffer at 4°C. After three washes with TBS-Tween 0.1%, membranes were incubated with HRP-conjugated secondary antibodies (1 hour at room temperature). Proteins were visualized using ECL reagent (Pierce).

Immunoprecipitation

For immunoprecipitation of GFP-tagged proteins, a GFP-Trap system (Chromotek cat# gtm-20) was used following manufacturer instructions. After thorough washing with the lysis buffer, bound proteins were eluted in sample buffer boiled and analyzed by western blot.

Immunofluorescence and immunohistochemistry

Fluorodishes were fixed in 4% paraformaldehyde for 10 min, permeabilized with tritonx100 (0.5% in PBS) and aspecific sites were blocked with BSA 1% and Goat serum 10% for 30 min. Primary antibodies were added O.N at 4°C in saponin 0.1% and BSA 1% in PBS. Fluorodishes or fibers were washes three times and then incubated with secondary antibodies together with DAPI for 60 minutes.

Isolation of myofibers

TA single fibers were isolated as described(Falcone et al., 2014). TA muscle was explanted from newborn male or female CD1 mice and then digested in DMEM containing 0.2% typeI collagenase (Sigma) for 2 h at 37°C. Mechanical dissociation of fibers was performed using a thin pasteur pipette and followed under a transilluminating-fluorescent stereomicroscope.

Whole muscle clearing

Legs of newborn mice were isolated and fixed overnight in PFA 4%. Legs were pre-treated overnight with (1% triton, 0.5% tween, 0.25%NP-40, 0.25% Na-deoxycholate, 3% BSA, 0.002% NA-azide, 1% urea in PBS). The following day, legs were incubated in CBB before being incubated with primary antibody for 2 days. After primary antibody incubation, legs were washed several time with PBT and left rotated to wash over night. The following day, legs were incubated with secondary antibody for 2 days and then washed with PBT several times and overnight. DAPI was subsequently added for 3 hours and washed several times before starting the clearing treatment. Clearing began by incubating legs with 25% formamide and 10% PEG for an hour, followed by 50% formamide and 20% PEG for an hour and finishing with 50% formamide and 20% PEG overnight. Legs were then mounted with fluoromount and imaged.

Peripheral nuclei position quantification

Quantification was performed as previously described(Falcone et al., 2014). Briefly, Myofibers were stained for DAPI and traids and images in Z-stacks with 0.5 mm interval were acquired with a Leica SPE confocal microscope with a 63x 1.3 NA Apo objective. Nuclei extruding the myofiber periphery were scored as peripheral.

Transversal triad quantification

Quantification was performed as previously described(Falcone et al., 2014). Briefly, Myofibers were stained for DHPR1, triadin and DAPI and images in Z-stacks with 0.5 mm interval were acquired with a Leica SPE confocal microscope with a 63x 1.3 NA Apo objective. Myofibers having more than 50% of triads organized, where DHPR and Triadin were transversally overlapping,were scored as positive.

Microscopy

Live imaging was performed using an incubator to maintain cultures at 37°C and 5% CO2 (Okolab) and × 20 0.3 NA PL Fluo dry objective. Epi-fluorescence images were acquired using a Nikon Ti microscope equipped with a CoolSNAP HQ2 camera (Roper Scientific), an XY-motorized stage (Nikon), driven by Metamorph (Molecular Devices). Confocal images were acquired using Leica SPE confocal microscope with a 63x 1.3 NA Apo objective or Zeiss LSM 710 with a 63x 1.4 NA Plan-Apochromat objective. 3D-time-lapse spinning disk microscopy was performed using a Zeiss Cell Observer Spinning Disk system equipped with Z-piezo (Prior), Spinning Disk CSU-X1M 5000 (Yokogawa), 488nm 561nm and 638nm excitation laser, an incubator to maintain cultures at 37°C and 5% CO2 (Pekon), EM-CCD camera Evolve 512 (Photometrics) and a 63x 1.4 NA Plan-Apochromat objective.

Area around the nucleus quantification

Images from the middle plane of a z-stack expressing YFP- α-actinin and H2B-iRFP, obtained with spinning disk microscopy were used. One transversal line was drawn at a distance of 30 μm on each side of the nucleus. The dark area on each side of the nucleus between this line, the myofibrils and the nucleus was measured using Fiji. These measurements were performed in time-lapse images. Values were normalized relative to the first time point.

Percentage of nucleus at the periphery

During nuclear movement to the periphery, area of nuclei emerging from the myofiber and total area of the nucleus were assessed. A ratio was obtained and a percentage was calculated over time.

Spherical and volumetric assessment

time-lapse imageswere reconstructed in 3D and over time using the software Imaris© and surface 3-dimensional rendering was performed. Spherical and volumetric values were extracted from the 3D-render of nuclei at each time point. Values were normalized relative to the first time point.

Pausing duration quantifications

Nuclear movement velocity along myofibers was calculated using software ICY. Nuclei were considered pausing when they moved less than 0.0015 μm/s for a minimum time of an hour. The cut-off values of pausing considerations (one hour at less than 0.0015 μm/s) was chosen based on visual correlation between nuclear movement and pausing from live imaging movies.

Model

The nucleus of radius $R_0 \approx 6$ μm (at rest) has a complex rheology. It is often described as a linear elastomer (Young's modulus E ≈ 1 to 10 kPa), whose elastic component is largely due to the lamina envelope. However for large and slow deformations a viscous behavior is expected, as was suggested in other contexts (Racine and Piel). The effective surface tension of the nucleus in skeletal muscle cell can therefore be estimated as $g \approx R_0E$. Before peripheral movement, the nucleus is wrapped by a bundle of N ≈ 30 myofibrils and centered along the symmetry axis of the bundle. We assume that each myofibril can be modeled as an active spring, whose passive tension (T ≈ 1 to 10mN/mm^2) was assessed using 2.7 μm sarcomere length (empirical measurement).

During peripheral migration of the nucleus to the periphery, we assume that myofibrils are crosslinked together through Arpc5L-containing Arp2/3 complexes and γ-actin (with a typical distance between myofibrils of the order of 1 μm) and with a distance L ≈ 30 μm between cross-linking points along the myofiber. This induces a normal force F_n on the nucleus towards the myofiber axis of the order of $F_n \approx 4TR_0/L$ for each myofibril. This force first induces a global deformation of the nucleus, which elongates along the myofiber axis. The deformation can be estimated by balancing the surface energy cost of a deformation of amplitude DR of the nucleus, which is $dE_s \approx g\ DR^2$, and

the work of the total normal force exerted by myofibrils given by $dW \approx NF_nDR$. This yields $DR \approx 4NT/(LE) \approx 0.1$ to 1 μm, which is consistent with observations.

Such conformation of the nucleus squeezed by myofibrils is unstable. Between each myofibril squeezing a wrinkle can form. It can be shown that as soon as the height h of one of these wrinkles is of the order of its width $2\pi R/N$, the wrinkle is destabilized forming a bleb and all the nucleus content flows into the bleb, so that the nucleus is expelled out of the bundle. For $h < 2\pi R/N$, an increase of the wrinkle height h locally increases the curvature leading to an increase in the hydrostatic pressure in the wrinkle which subsequently relaxes. Conversely, for $h > 2\pi R/N$, an increase of h reduces the curvature thereby leading to a decrease in the local hydrostatic pressure in the wrinkle. The nucleoplasm subsequently flows into the wrinkle, which is henceforth destabilized and leads to bleb formation. The threshold of this instability is reached when $gR_0 \approx 4TR_0/L$, or $T > ER_0L/4$. Given the above orders of magnitude, this threshold can indeed be reached, which shows that such mechanism of nucleus off centering can indeed be at work. In particular this mechanism shows that the motion of the nucleus to the periphery is favored by an increased tension of myofibrils and a reduced distance between crosslinkers.

When the surface tension is low (i.e at low level of lamin A/C), the nucleus undergoes large deformations and this analysis needs to be adapted. One finds that a cylindrical shape of the nucleus, squeezed between almost undeformed myofibrils, is stable for $g< 4NTr_f^3/(R_0^3L)$, where r_f is the typical radius of the myofibrils bundle in absence of nucleus. Altogether, this shows that the mechanism of positioning of the nucleus to the periphery is efficient only within a window of values of nucleus rigidity (here modeled effectively as a surface tension), which is controlled by lamin A/C levels.

Optogenetically-induced contraction

Myofibers were transfected with the ChR2-GFP and iRFP-H2B constructs. Upon blue light exposure, the ChR2 channel opens to become permeable to Na^+ ions. This induces a depolymerization of the membrane and a subsequent contraction of the myofiber. To monitor the effect of contraction on peripheral nuclear localization, 3.5-day myofibers were exposed to 100 milliseconds of blue light using a bandpass filter 470/40every 10 minutes for 24 hours. Brighfield and epifluorescent images were acquired every xx min. Number of peripheral nuclear positioned over a period of 24 hours were assessed both in transfected and untransfected myofibers. Peripheral nuclei were scored when more

than a quarter of the total size of nuclei protruded the membrane. A ratio of nuclei having reached the periphery over total nuclei assessed was obtained and a percentage calculated.

Correlative velocity of nuclei and lamin A/C expression

Time-lapse movies of myofibers overexpressing mCherry-lamin A/C were analyzed by quantifying the overall intensity of nuclei expressing the construct and the time required to reach the periphery (20 minutes per frame).

Statistics

Statistical analysis was performed with Prism (version 5.0 of GraphPad Software Inc.). Pair wise comparisons were made with Student's *t*-test. In peripheral nuclei positioning analysis and in fiber thickness analysis in myofibers, Student's *t*-tests were performed between scramble siRNA and experimental condition. For biochemical experiments using human samples, statistical analysis was performed using the Mann-Whitney U test or the unpaired Student's test and multiple statistical comparisons between samples were performed by two-way analysis of variance followed by a Bonferroni's t-test posthoc correction to obtain a better evaluation of the variability between samples from the same group and samples from each compared group and statistical significance was set at $*P < 0.05$. The prism program (version 5.0, GraphPad software Inc.) was used. The distribution of data points is expressed as mean ± SE from three independent experiments.

References:

Abella, J.V.G., Galloni, C., Pernier, J., Barry, D.J., Kjær, S., Carlier, M.-F., and Way, M. (2016). Isoform diversity in the Arp2/3 complex determines actin filament dynamics. Nat. Cell Biol. *18*, 76–86.

Almonacid, M., Ahmed, W.W., Bussonnier, M., Mailly, P., Betz, T., Voituriez, R., Gov, N.S., and Verlhac, M.-H. (2015). Active diffusion positions the nucleus in mouse oocytes. Nat. Cell Biol. *17*, 470–479.

Al-Qusairi, L., and Laporte, J. (2011). T-tubule biogenesis and triad formation in skeletal muscle and implication in human diseases. Skelet. Muscle *1*, 26.

Azibani, F., Muchir, A., Vignier, N., Bonne, G., and Bertrand, A.T. (2014). Striated muscle laminopathies. Semin. Cell Dev. Biol. *29*, 107–115.

Bergeron, S.E., Zhu, M., Thiem, S.M., Friderici, K.H., and Rubenstein, P.A. (2010). Ion-dependent Polymerization Differences between Mammalian - and -Nonmuscle Actin Isoforms. J. Biol. Chem. *285*, 16087–16095.

Bolhy, S., Bouhlel, I., Dultz, E., Nayak, T., Zuccolo, M., Gatti, X., Vallee, R., Ellenberg, J., and Doye, V. (2011). A Nup133-dependent NPC-anchored network tethers centrosomes to the nuclear envelope in prophase. J. Cell Biol. *192*, 855–871.

Cadot, B., Gache, V., Vasyutina, E., Falcone, S., Birchmeier, C., and Gomes, E.R. (2012). Nuclear movement during myotube formation is microtubule and dynein dependent and is regulated by Cdc42, Par6 and Par3. EMBO Rep. *13*, 741–749.

Cadot, B., Gache, V., and Gomes, E.R. (2015). Moving and positioning the nucleus in skeletal muscle – one step at a time. Nucleus *6*, 01–09.

Clark, K.A., McElhinny, A.S., Beckerle, M.C., and Gregorio, C.C. (2002). Striated muscle cytoarchitecture: an intricate web of form and function. Annu. Rev. Cell Dev. Biol. *18*, 637–706.

Clemen, C.S., Herrmann, H., Strelkov, S.V., and Schröder, R. (2013). Desminopathies: pathology and mechanisms. Acta Neuropathol. (Berl.) *125*, 47–75.

Colomo, F., Piroddi, N., Poggesi, C., Te Kronnie, G., and Tesi, C. (1997). Active and passive forces of isolated myofibrils from cardiac and fast skeletal muscle of the frog. J. Physiol. *500*, 535.

Crisp, M. (2006). Coupling of the nucleus and cytoplasm: role of the LINC complex. J. Cell Biol. *172*, 41–53.

Egile, C., Loisel, T.P., Laurent, V., Li, R., Pantaloni, D., Sansonetti, P.J., and Carlier, M.-F. (1999). Activation of the Cdc42 Effector N-Wasp by the Shigella flexneri Icsa Protein Promotes Actin Nucleation by Arp2/3 Complex and Bacterial Actin-Based Motility. J. Cell Biol. *146*, 1319–1332.

Elhanany-Tamir, H., Yu, Y.V., Shnayder, M., Jain, A., Welte, M., and Volk, T. (2012). Organelle positioning in muscles requires cooperation between two KASH proteins and microtubules. J. Cell Biol.

Falcone, S., Roman, W., Hnia, K., Gache, V., Didier, N., Lainé, J., Auradé, F., Marty, I., Nishino, I., Charlet-Berguerand, N., et al. (2014). N-WASP is required for Amphiphysin-2/BIN1-dependent nuclear positioning and triad organization in skeletal muscle and is involved in the pathophysiology of centronuclear myopathy. EMBO Mol. Med. *6*, 1455–1475.

Flucher, B.E., Takekura, H., and Franzini-Armstrong, C. (1993). Development of the Excitation-Contraction Coupling Apparatus in Skeletal Muscle: Association of Sarcoplasmic Reticulum and Transverse Tubules with Myofibrils. Dev. Biol. *160*, 135–147.

Folker, E.S., Schulman, V.K., and Baylies, M.K. (2013). Translocating myonuclei have distinct leading and lagging edges that require Kinesin and Dynein. Development dev.095612.

Fugier, C., Klein, A.F., Hammer, C., Vassilopoulos, S., Ivarsson, Y., Toussaint, A., Tosch, V., Vignaud, A., Ferry, A., Messaddeq, N., et al. (2011). Misregulated alternative splicing of BIN1 is associated with T tubule alterations and muscle weakness in myotonic dystrophy. Nat. Med. *17*, 720–725.

Gokhin, D.S., and Fowler, V.M. (2011). Cytoplasmic γ-actin and tropomodulin isoforms link to the sarcoplasmic reticulum in skeletal muscle fibers. J. Cell Biol.

Goldfarb, L.G., and Dalakas, M.C. (2009). Tragedy in a heartbeat: malfunctioning desmin causes skeletal and cardiac muscle disease. J. Clin. Invest. *119*, 1806–1813.

Goldspink, G. (1970). The Proliferation of Myofibrils During Muscle Fibre Growth. J. Cell Sci. *6*, 593–603.

Gournier, H., Goley, E.D., Niederstrasser, H., Trinh, T., and Welch, M.D. (2001). Reconstitution of Human Arp2/3 Complex Reveals Critical Roles of Individual Subunits in Complex Structure and Activity. Mol. Cell *8*, 1041–1052.

Gundersen, G.G., and Worman, H.J. (2013). Nuclear Positioning. Cell *152*, 1376–1389.

Horn, H.F., Brownstein, Z., Lenz, D.R., Shivatzki, S., Dror, A.A., Dagan-Rosenfeld, O., Friedman, L.M., Roux, K.J., Kozlov, S., Jeang, K.-T., et al. (2013). The LINC complex is essential for hearing. J. Clin. Invest.

Huelsmann, S., Ylänne, J., and Brown, N.H. (2013). Filopodia-like Actin Cables Position Nuclei in Association with Perinuclear Actin in Drosophila Nurse Cells. Dev. Cell *26*, 604–615.

Ihalainen, T.O., Aires, L., Herzog, F.A., Schwartlander, R., Moeller, J., and Vogel, V. (2015). Differential basal-to-apical accessibility of lamin A/C epitopes in the nuclear lamina regulated by changes in cytoskeletal tension. Nat. Mater. *advance online publication*.

Jiu, Y., Lehtimäki, J., Tojkander, S., Cheng, F., Jäälinoja, H., Liu, X., Varjosalo, M., Eriksson, J.E., and Lappalainen, P. (2015). Bidirectional Interplay between Vimentin Intermediate Filaments and Contractile Actin Stress Fibers. Cell Rep. *11*, 1511–1518.

Konieczny, P., Fuchs, P., Reipert, S., Kunz, W.S., Zeöld, A., Fischer, I., Paulin, D., Schröder, R., and Wiche, G. (2008). Myofiber integrity depends on desmin network targeting to Z-disks and costameres via distinct plectin isoforms. J. Cell Biol. *181*, 667–681.

Korobova, F., and Svitkina, T. (2008). Arp2/3 Complex Is Important for Filopodia Formation, Growth Cone Motility, and Neuritogenesis in Neuronal Cells. Mol. Biol. Cell *19*, 1561–1574.

Lammerding, J., Schulze, P.C., Takahashi, T., Kozlov, S., Sullivan, T., Kamm, R.D., Stewart, C.L., and Lee, R.T. (2004). Lamin A/C deficiency causes defective nuclear mechanics and mechanotransduction. J. Clin. Invest. *113*, 370–378.

Machesky, L.M., Mullins, R.D., Higgs, H.N., Kaiser, D.A., Blanchoin, L., May, R.C., Hall, M.E., and Pollard, T.D. (1999). Scar, a WASp-related protein, activates nucleation of actin filaments by the Arp2/3 complex. Proc. Natl. Acad. Sci. *96*, 3739–3744.

Merlie, J.P., and Sanes, J.R. (1985). Concentration of acetylcholine receptor mRNA in synaptic regions of adult muscle fibres. Nature *317*, 66–68.

Metzger, T., Gache, V., Xu, M., Cadot, B., Folker, E.S., Richardson, B.E., Gomes, E.R., and Baylies, M.K. (2012). MAP and kinesin-dependent nuclear positioning is required for skeletal muscle function. Nature *484*, 120–124.

Nicot, A.-S., Toussaint, A., Tosch, V., Kretz, C., Wallgren-Pettersson, C., Iwarsson, E., Kingston, H., Garnier, J.-M., Biancalana, V., Oldfors, A., et al. (2007). Mutations in amphiphysin 2 (BIN1) disrupt interaction with dynamin 2 and cause autosomal recessive centronuclear myopathy. Nat. Genet. *39*, 1134–1139.

Nolen, B.J., Tomasevic, N., Russell, A., Pierce, D.W., Jia, Z., McCormick, C.D., Hartman, J., Sakowicz, R., and Pollard, T.D. (2009). Characterization of two classes of small molecule inhibitors of Arp2/3 complex. Nature *460*, 1031–1034.

Paluch, E.K., and Raz, E. (2013). The role and regulation of blebs in cell migration. Curr. Opin. Cell Biol. *25*, 582–590.

Romero, N.B. (2010). Centronuclear myopathies: A widening concept. Neuromuscul. Disord. *20*, 223–228.

Sakar, M.S., Neal, D., Boudou, T., Borochin, M.A., Li, Y., Weiss, R., Kamm, R.D., Chen, C.S., and Asada, H.H. (2012). Formation and optogenetic control of engineered 3D skeletal muscle bioactuators. Lab. Chip *12*, 4976–4985.

Sonnemann, K.J., Fitzsimons, D.P., Patel, J.R., Liu, Y., Schneider, M.F., Moss, R.L., and Ervasti, J.M. (2006). Cytoplasmic [gamma]-Actin Is Not Required for Skeletal Muscle Development but Its Absence Leads to a Progressive Myopathy. Dev. Cell *11*, 387–397.

Splinter, D., Tanenbaum, M.E., Lindqvist, A., Jaarsma, D., Flotho, A., Yu, K.L., Grigoriev, I., Engelsma, D., Haasdijk, E.D., Keijzer, N., et al. (2010). Bicaudal D2, Dynein, and Kinesin-1 Associate with Nuclear Pore Complexes and Regulate Centrosome and Nuclear Positioning during Mitotic Entry. PLoS Biol *8*, e1000350.

Starr, D.A., and Fridolfsson, H.N. (2010). Interactions Between Nuclei and the Cytoskeleton Are Mediated by SUN-KASH Nuclear-Envelope Bridges. Annu. Rev. Cell Dev. Biol. *26*, 421–444.

Starr, D.A., and Han, M. (2002). Role of ANC-1 in tethering nuclei to the actin cytoskeleton. Science *298*, 406–409.

Wilson, M.H., and Holzbaur, E.L.F. (2015). Nesprins anchor kinesin-1 motors to the nucleus to drive nuclear distribution in muscle cells. Development *142*, 218–228.

Yarar, D., To, W., Abo, A., and Welch, M.D. (1999). The Wiskott–Aldrich syndrome protein directs actin-based motility by stimulating actin nucleation with the Arp2/3 complex. Curr. Biol. *9*, 555–S1.

Yoshikawa, Y., Yasuike, T., Yagi, A., and Yamada, T. (1999). Transverse elasticity of myofibrils of rabbit skeletal muscle studied by atomic force microscopy. Biochem. Biophys. Res. Commun. *256*, 13–19.

Zhao, T., Graham, O.S., Raposo, A., and St. Johnston, D. (2012). Growing Microtubules Push the Oocyte Nucleus to Polarize the Drosophila Dorsal-Ventral Axis. Science.

Figure S1.

A. Kymograph from a time-lapse movie of a 4-day myofiber depicting a centrally located nucleus (H2B-iRFP, red) surrounded by myofibrils bundles (YFP-α-actinin, green) while moving longitudinally within these myofibrils Left: 2D view of the central plane. Middle: transversal view in the middle of the nucleus. Right: surface three-dimensional rendering. Scale bar, 10 μm.

B. Nucleus (H2B-iRFP, red) and myofibrils (YFP-α-actinin, green) from a 4.5-day myofiber without (left) and with (right) pronounced wrinkles due to myofibril tension. Top: longitudinal surface three-dimensional rendering of the nucleus. Middle: 2D transversal view of the nucleus (red) and myofibrils (green). Bottom: 2D transversal view of the nucleus. Arrowheads indicate enhanced wrinkles. Scale bar, 10 μm.

C. Top: Representative epi-fluorescent (left) and bright-field light image (right) of the first frame from time-lapse movie of two 3.5-day myofibers, one transfected with the ChR2-GFP and the other untransfected. Bottom: Kymograph of the region in yellow from the top right panel and showing contraction when blue light is emitted (blue boxes).

Figure S2.

A. Western blot with indicated antibodies from 10-day myofibers knocked down for scrambled or lamin A/C.
B. Representative immunofluorescence images of 10-day myofibers knocked down for scrambled or lamin B and stained for lamin B (magenta), F-actin (phalloidin, green) and DAPI (nucleus, blue). Scale bar, 10 μm.
C. Quantification of peripheral nuclei in 10-day myofibers knocked down for scrambled or lamin B.
D. Orthogonal view of nuclei from 5 day myofibers with bleb initiation, stained with lamin A/C the intensity signal represented as a heat map. White dashed line represents the outline of myofibrils. White arrowheads represent asymmetry nuclear stiffness.
E. Orthogonal view of nuclei from 5 day myofibers with bleb initiation, stained for lamin B1 with the intensity signal represented as a heat map. White dashed line represents the outline of myofibrils.
F. Orthogonal view of nuclei from 5 day myofibers with bleb initiation, stained with lamin A/C-C the intensity signal represented as a heat map. White dashed line represents the outline of myofibrils. White arrowheads represent asymmetry nuclear stiffness.
G. Orthogonal view of nuclei from 5 day myofibers in the middle of nuclear movement to the periphery and stained for lamin A/C with the intensity signal represented as a heat map. White dashed line represents the outline of myofibrils. White arrowheads represent asymmetry nuclear stiffness.
H. Orthogonal view of nuclei from 5 day myofibers in the middle of nuclear movement to the periphery and stained for lamin B1 with the intensity signal represented as a heat map. White dashed line represents the outline of myofibrils.
I. Orthogonal view of nuclei from 5 day myofibers in the middle of nuclear movement to the periphery and stained for lamin A/C-C with the intensity signal represented as a heat map. White dashed line represents the outline of myofibrils. White arrowheads represent asymmetry nuclear stiffness.

Figure S3.
A. Schematic representation of the pathways that regulate peripheral nuclear position and transversal triad formation.
B. Western blot with indicated antibodies from 10-day myofibers knocked down for scrambled or Arpc2.
C. Representative immunofluorescence images of 10-day myofibers knocked down for scrambled or Arpc2 and stained with triadin (triad marker, magenta), α-actinin (myofibrils/Z-line marker, green) and DAPI (nucleus, blue). Scale bar, 10 μm. 2x

Magnifications corresponding to the yellow squares are showed in the right of each image.

D. Quantification of peripheral nuclei positioning (left) and transversal triads (right) in 10-day myofibers knocked down for scrambled or Arpc2, or treated with the Arp2/3 inhibitor CK666.

E. Table enumerating Arp2/3 subunits and their isoforms.

F. Quantification of peripheral nuclei (left) and transversal triads (right) in 10-day myofibers knocked down for scrambled, Arpc1A or Arpc1B.

G. Western blot with indicated antibodies from 10-day myofibers knocked down for scrambled, Arpca1 or Arpc1b.

H. Western blot with indicated antibodies from 10-day myofibers knocked down for scrambled, Arpc5L or Arpc5.

Figure S4.

A. Table enumerating different actin isoforms.

B. Western blot with indicated antibodies from 10-day myofibers knocked down for scrambled, γ-actin or β-actin.

C. Representative immunofluorescence images of 10-day myofibers knocked down for γ-actin or β-actin and transfected with siRNA resistant GFP-γ-actin (green) and GFP-β-actin (green), respectively, and stained for triadin (triad marker, magenta) and DAPI (blue). Scale bar, 10 μm.

D. Quantification of peripheral nuclei positioning and traversal triads in 10-day myofibers expressing either GFP or the siRNA resistant GFP-γ-actin construct and knocked down either with scrambled or γ-actin.

E. Quantification of peripheral nuclei positioning and traversal triads in 10-day myofibers expressing either GFP or the siRNA resistant GFP-β-actin construct and knocked down either with scrambled or β-actin.

Figure S5.

A. Schematic representation of the pathways that regulate peripheral nuclear position and transversal triad formation.

B. First frame from a time-lapse bright-field movie of a 4.5-day myofiber transfected with H2B-iRFP (nucleus, green) and scrambled siRNA with the highlighted regions used for the kymograph in B. Scale bar, 10 μm.

C. Kymographs of the regions indicated in A. to visualize nuclear movement along the myofiber (longitudinal movement, Left and corresponding to red region in A.) and peripheral nuclear movement (Right, and corresponding to yellow region in A.). Note that the yellow region on the right was rotated 90^{o} and aligned with the nucleus over time. 00:00 (hh:mm) corresponds to 4.5-day myofibers.

D. First frame from a time-lapse bright-field movie of a 4.5-day myofiber transfected with H2B-iRFP (nucleus, green) and Arpc5L siRNA with the highlighted regions used for the kymograph in D. Scale bar, 10 μm.

E. Kymographs of the regions indicated in C. to visualize nuclear movement along the myofiber (longitudinal movement, Left and corresponding to red region in C.) and absence of peripheral nuclear movement (Right and corresponding to yellow region in C.). Note that the yellow region on the right was rotated 90^{o} and aligned with the nucleus over time. 00:00 (hh:mm) corresponds to 4.5-day myofibers.

F. First frame from a time-lapse bright-field movie of a 4.5-day myofiber transfected with H2B-iRFP (nucleus, green) and γ-actin siRNA with the highlighted regions used for the kymograph in F. Scale bar, 10 μm.

G. Kymographs of the regions indicated in E. to visualize nuclear movement along the myofiber (longitudinal movement, Left and corresponding to red region in E.) and absence of peripheral nuclear movement (Right and corresponding to yellow region in C.). Note that the yellow region on the right was rotated 90^{o} and aligned with the nucleus over time. 00:00 (hh:mm) corresponds to 4.5-day myofibers.

H. Quantification of the average speeds and displacement of nuclei from live imaging of myofibers from day 4.5 to 5.5 and knock down for scrambled, γ-actin or Arpc5L.

I. Quantification of nuclei migrating to the periphery from a 24-hour time-lapse movie in 3.5-day untransfected myofibers (control) and myofibers expressing ChR2-GFP alone (ChR2) or knocked down for either Arpc5L or γ-actin.

J. left: Representative epi-fluorescent and bright-field light image of the first frame from time-lapse movie of a 3.5-day myofibers transfected with ChR2-GFP and knocked down for Arpc5L. right: Kymograph of the region in yellow from the left panel and showing contraction when blue light is emitted (blue boxes).

K. left: Representative epi-fluorescent and bright-field light image of the first frame from time-lapse movie of a 3.5-day myofibers transfected with ChR2-GFP and knocked down for γ-actin. right: Kymograph of the region in yellow from the left panel and showing contraction when blue light is emitted (blue boxes).

Figure S6.

A. Representative immunofluorescence images of 5-day myofibers expressing GFP-β-actin (green) and immunostained for Arpc5 (magenta). Scale bar, 10 μm.

B. Representative immunofluorescence image of a 5-day myofiber transfected with GFP-β-actin (green) and stained for α-actinin (myofibrils/Z-line marker, magenta). 2x Magnifications corresponding to the yellow squares are showed in the right of each image. Scale bar, 10 μm.

C. Representative immunofluorescence image of a 4.5-day myofiber knocked down for Arpc5 or β-actin and stained for F-actin (phalloidin, magenta), desmin (green) and DAPI (nucleus, blue). Scale bar, 10 μm.

Figure S1

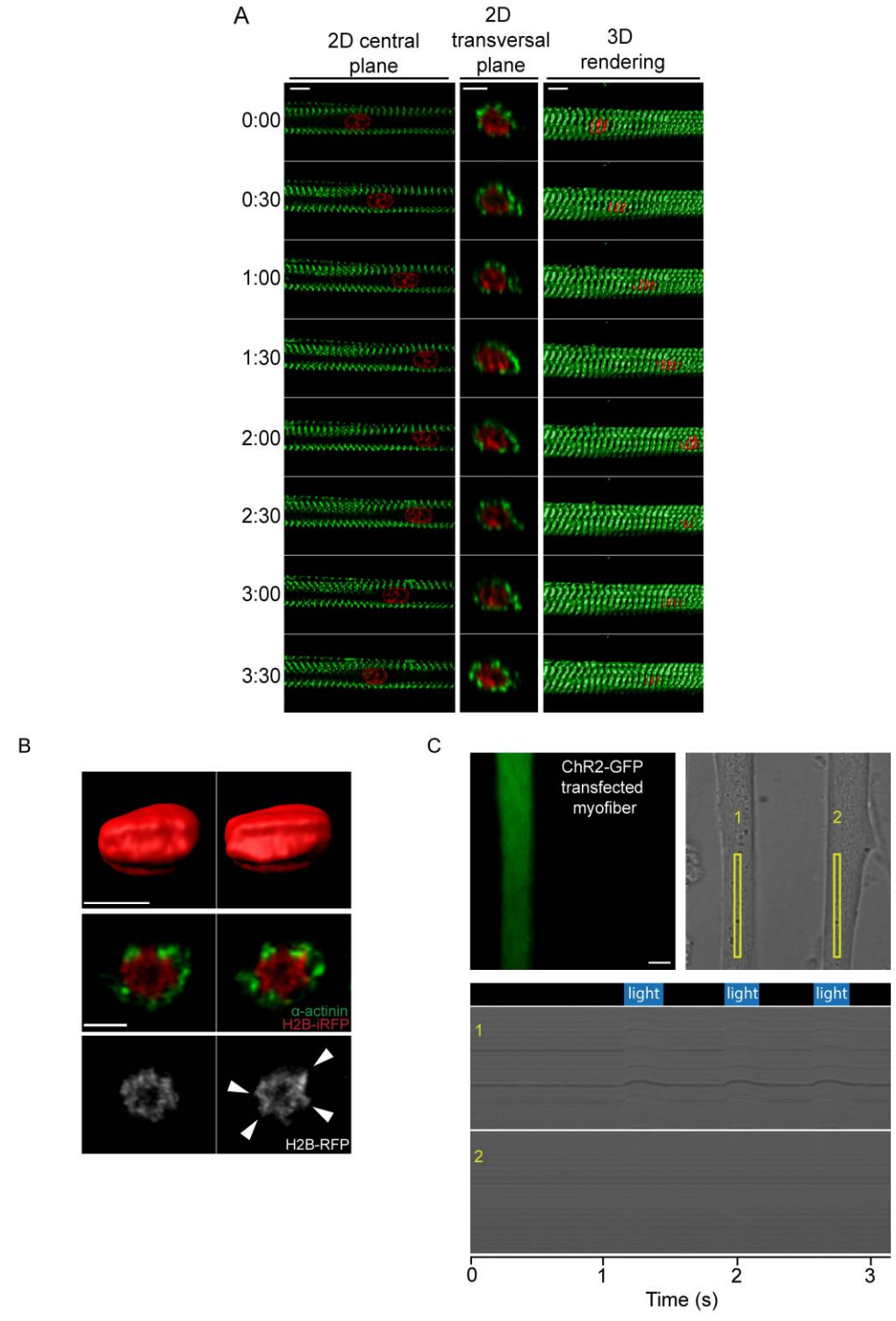
A
2D central plane
2D transversal plane
3D rendering
0:00
0:30
1:00
1:30
2:00
2:30
3:00
3:30
B
α-actinin
H2B-iRFP
H2B-RFP
C
ChR2-GFP transfected myofiber
1
2
light
light
light
1
2
0
1
2
3
Time (s)

Figure S2

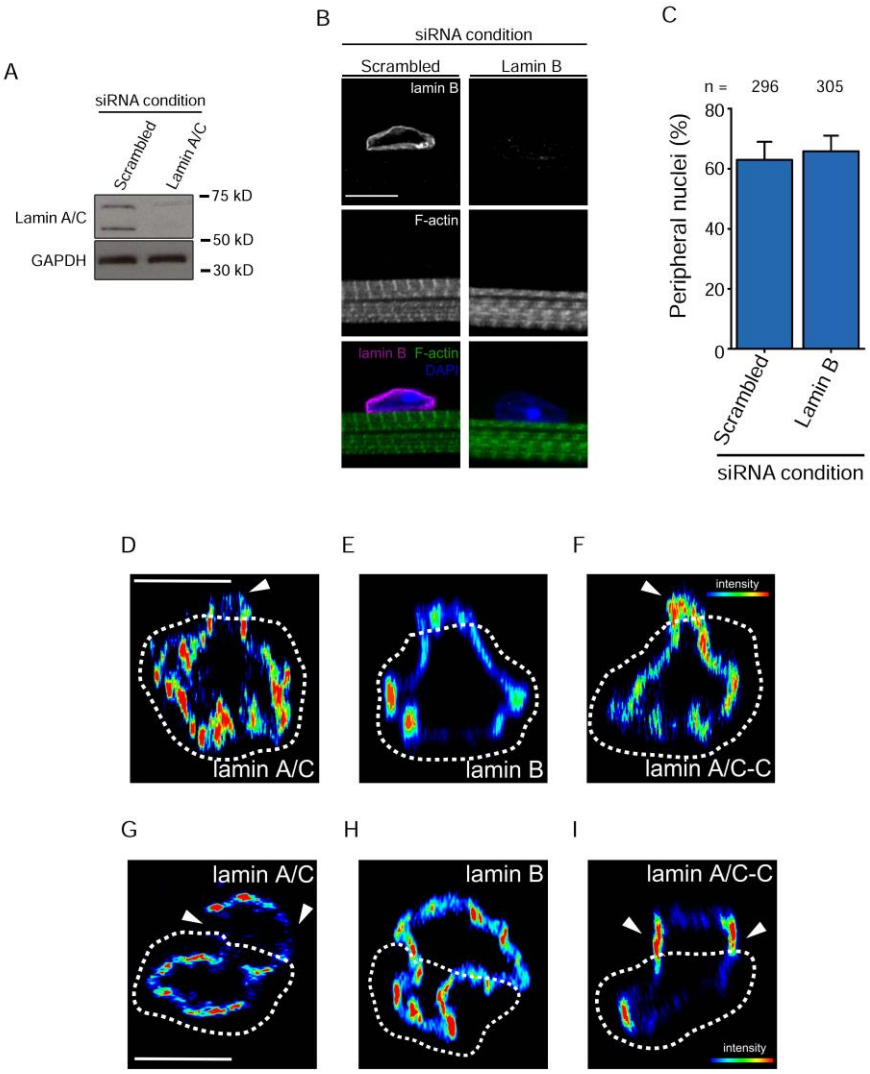
A
siRNA condition
Scrambled
Lamin A/C
Lamin A/C
GAPDH
75 kD
50 kD
30 kD
B
siRNA condition
Scrambled
Lamin B
lamin B
F-actin
lamin B F-actin
DAPI
C
n = 296 305
Peripheral nuclei (%)
80
60
40
20
0
Scrambled
Lamin B
siRNA condition
D
lamin A/C
E
lamin B
F
intensity
lamin A/C-C
G
lamin A/C
H
lamin B
I
lamin A/C-C
intensity

Figure S3

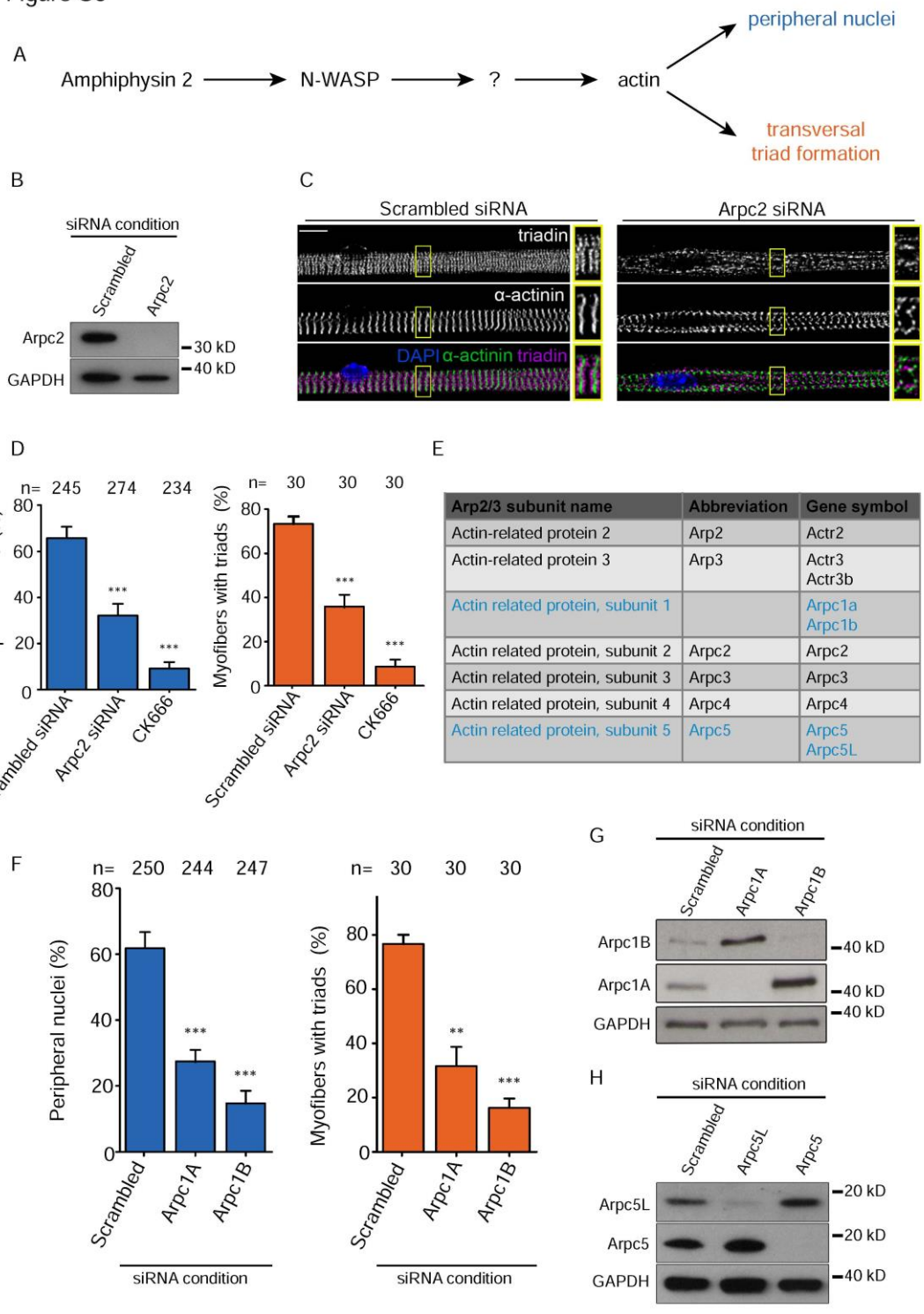

Arp2/3 subunit name	Abbreviation	Gene symbol
Actin-related protein 2	Arp2	Actr2
Actin-related protein 3	Arp3	Actr3 Actr3b
Actin related protein, subunit 1		Arpc1a Arpc1b
Actin related protein, subunit 2	Arpc2	Arpc2
Actin related protein, subunit 3	Arpc3	Arpc3
Actin related protein, subunit 4	Arpc4	Arpc4
Actin related protein, subunit 5	Arpc5	Arpc5 Arpc5L

Figure S4

A

Actin name	Abbreviation	Gene symbol	Expression
Actin alpha 1, skeletal muscle	α-$_{sk}$-actin	Acta1	Skeletal muscle
Actin alpha 2, smooth muscle	α-$_{sm}$-actin	Acta2	Smooth muscle, aorta
Actin alpha, cardiac 1	α-$_{ca}$-actin	Actc1	Heart
Actin beta 1	β-actin	Actb1	Ubiquitous
Actin gamma 1	γ-actin	Actg1	Ubiquitous
Actin gamma 2, smooth muscle	γ-$_{sm}$-actin	Actg2	Smooth muscle

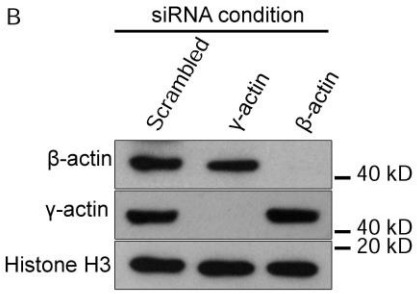

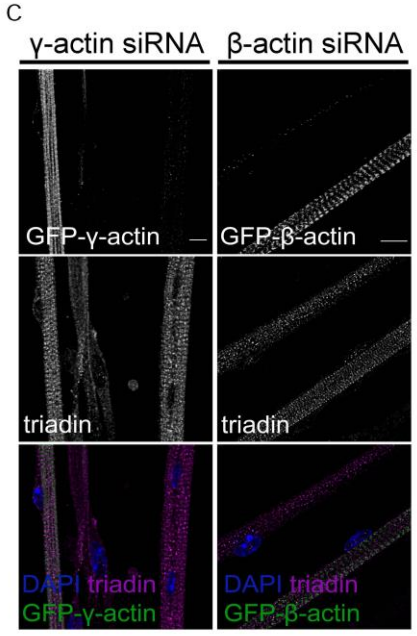

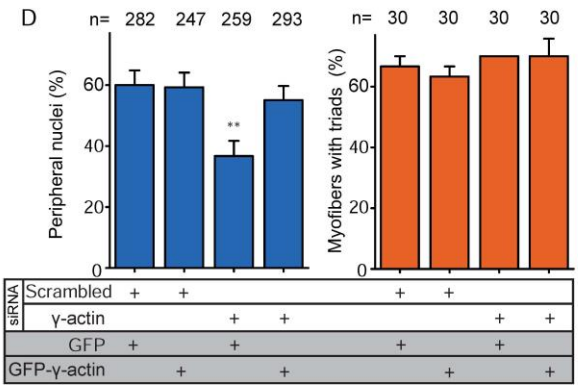

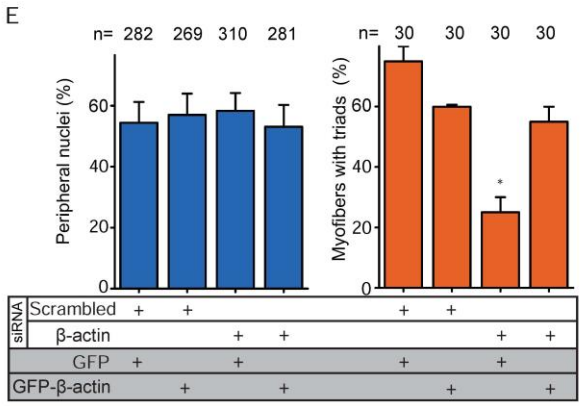

Figure S5

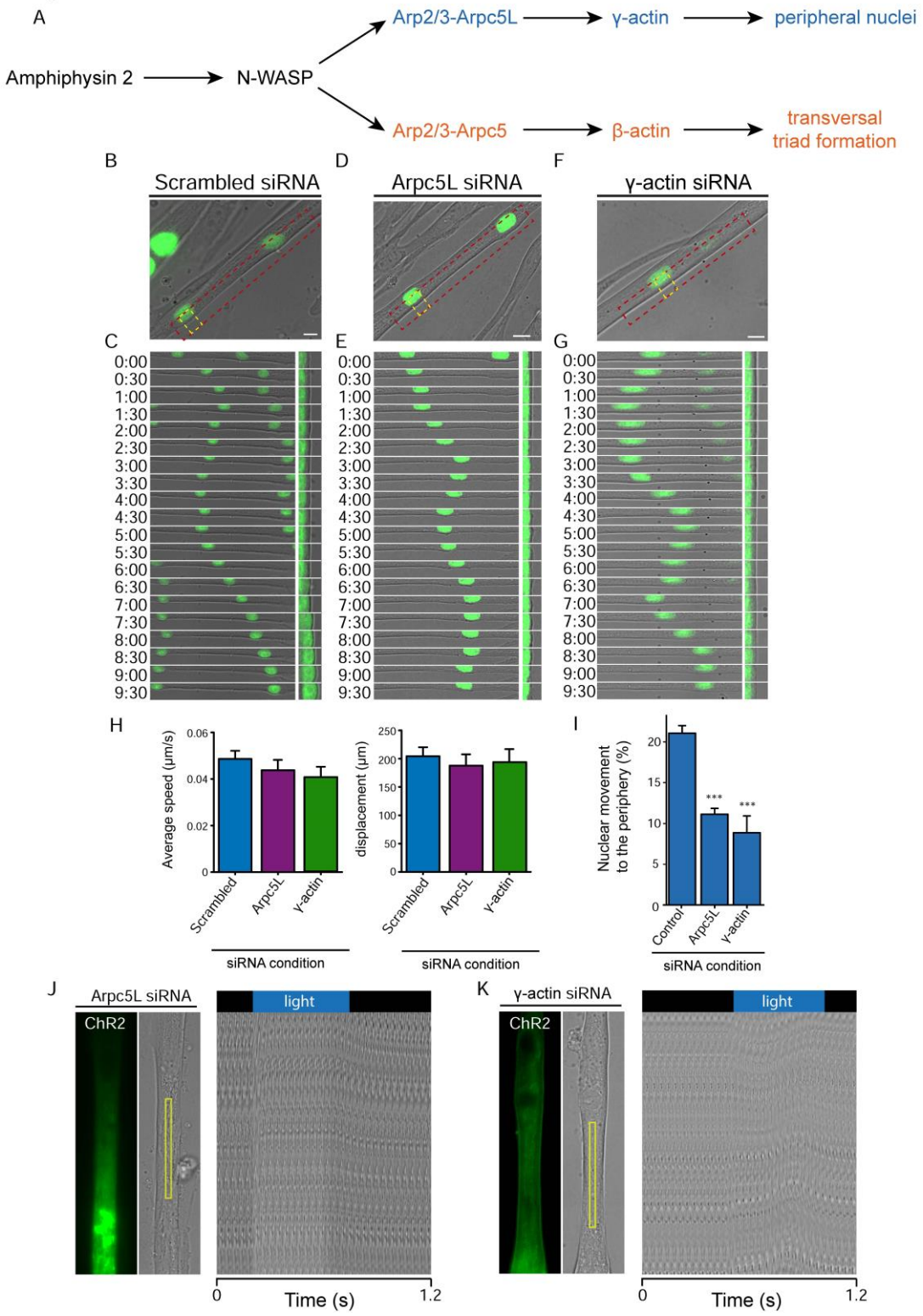
A
Amphiphysin 2
N-WASP
Arp2/3-Arpc5L
γ-actin
peripheral nuclei
Arp2/3-Arpc5
β-actin
transversal triad formation
B
Scrambled siRNA
D
Arpc5L siRNA
F
γ-actin siRNA
C
E
G
0:00
0:30
1:00
1:30
2:00
2:30
3:00
3:30
4:00
4:30
5:00
5:30
6:00
6:30
7:00
7:30
8:00
8:30
9:00
9:30
H
Average speed (μm/s)
displacement (μm)
Scrambled
Arpc5L
γ-actin
siRNA condition
I
Nuclear movement to the periphery (%)
***
Control
J
Arpc5L siRNA
ChR2
light
Time (s)
K
γ-actin siRNA

Figure S6

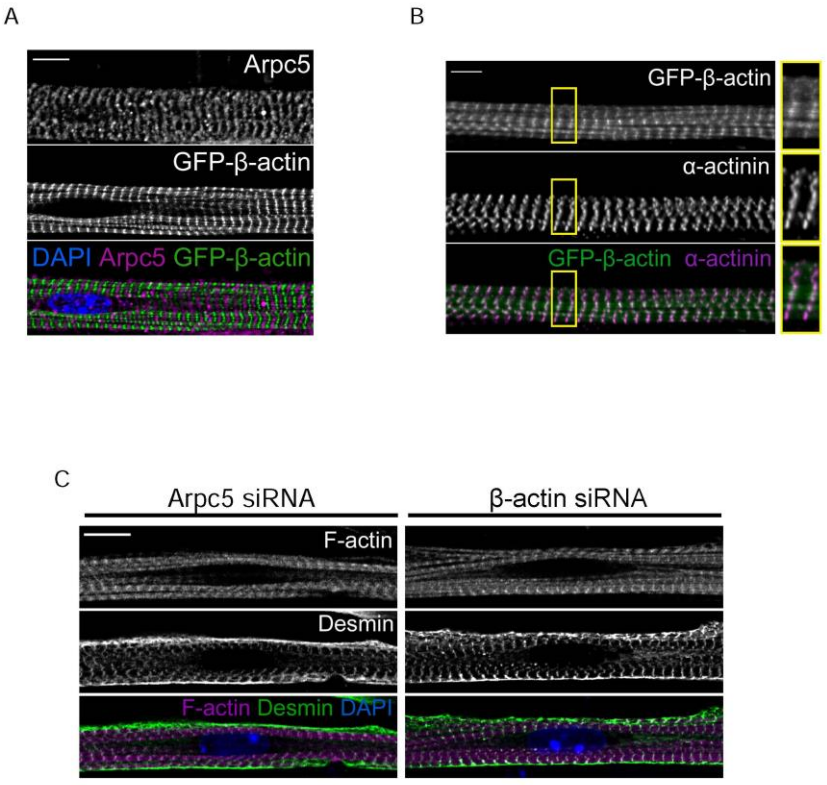
A
Arpc5
GFP-β-actin
DAPI Arpc5 GFP-β-actin
B
GFP-β-actin
α-actinin
GFP-β-actin α-actinin
C
Arpc5 siRNA
β-actin siRNA
F-actin
Desmin
F-actin Desmin DAPI

Discussion

In this thesis we explored the mechanism of nuclear movement to the periphery of skeletal muscle. Positioning of nuclei at the periphery is a hallmark of skeletal muscle and has remained relatively unexplored both functionally and mechanistically. Using an in vitro system that recapitulates the different stages of skeletal muscle development, we observed that nuclei squeeze through a narrow gap in between myofibrils to reach the periphery. Predictive theoretical modeling and experimental data revealed that myofibril crosslinking and contraction are involved in generating a growing force on centrally located nuclei that eventually squeeze to the periphery. Myofibril crosslinking acts as a closing zipper on both sides of the nucleus. This process is regulated by desmin, the muscle intermediate filament known to crosslink myofibrils. Moreover, nuclear movement to the periphery is dependent on nuclear deformability which is mediated by local changes of nuclear stiffness regulated by lamin A/C. Finally, we identified one of the pathway involved in nuclear movement to the periphery and transversal triad formation. We found that Amphiphysin 2 (BIN1) mutated in centronuclear myopathy (CNM) interacts with N-WASP, a protein involved in actin dynamics. N-WASP is mislocalized in CNM patients with *BIN1* mutations and we show in our in vitro system that the accumulation of centrally located nuclei in *BIN1* knock down myofibers can be rescued by expressing a constitutively active N-WASP fragment. The Arp2/3 complex is regulated by N-WASP but the pathway bifurcates at this stage between nuclear movement to the periphery and transversal triad formation. This is mediated by different Arp2/3 populations differing in their subunit composition. Arp2/3 populations composed with the Arpc5L subunit are important for nuclear movement to the periphery whereas Arpc5-containing Arp2/3 complexes are required for transversal triad formation. We also show that actin isoforms preferentially interact with the different Arp2/3 populations. As such, γ-actin preferentially interacts with Arpc5L-containing Arp2/3 complexes and are together involved in nuclear movement. β-actin interacts with Arpc5-containing Arp2/3 complexes to drive transversal triad formation. We show that this Amphiphysin 2 pathway is involved in organizing desmin at the z-line and therefore mediates crosslinking of myofibrils.

I. Nuclear movement

Nuclear positioning plays a central role in many cellular processes such as cell migration, development and division. The mechanisms driving these movements are various and defects are associated with multiple disorders (Gundersen and Worman, 2013a).

I.1 Nuclear movement to the periphery is an actin and intermediate filament-driven process.

γ-actin and desmin are the two main cytoskeleton players identified in nuclear movement to the myofiber periphery. Our data suggests that γ-actin organizes desmin at the z-line via plectin, a cytoskeleton linker. This is the first nuclear movement described that relies on an interplay between two cytoskeletal networks.

Actin's involvement in the process is more indirect than other actin-driven nuclear movements. Previously described actin-driven nuclear movements mostly rely on interaction between actin and the LINC complex (Gundersen and Worman, 2013a) whereas actin is used here as a scaffold to establish the nuclear movement machinery. Hence, this mechanism is unlike others previously described.

In contrast to 2D cell migration, TAN lines are not observed near myonuclei. The speed of the movement is also much slower in myofibers suggesting that the mechanism of rear-end positioning of nuclei during cell migration is different to the one described here. Nuclei in drosophila nurse cells share the peripheral directionality of nuclear migration but this process is mediated by actin polymerization from the plasma membrane to the nucleus (Huelsmann et al., 2013a). Although it is difficult to test if a similar mechanism is at play in nuclear movement to the periphery of myofibers, it seems unlikely that the force generated by actin polymerization is sufficient to squeeze nuclei like was observed in drosophila nurse cells. Nuclear movements in confined migrating cells rely on acto-myosin mechanisms allowing the generateion of force to displace nuclei (Solecki et al., 2009). Blebbistatin thus inhibits these nuclear movements which is also the case in nuclear migrations to the myofiber periphery. It is however most probable that blebbistatin impairs the sarcomeres and thus contraction rather than an acto-myosin mechanism solely devoted to nuclear movement. Actin-dependent nuclear movement in mouse oocyte relies on active diffusion to position nuclei at the center of the cell (Almonacid et al., 2015a). Although the direction of the

movement is inverse (peripheral vs central), this mechanism is also regulated by actin in a very indirect fashion. These two movement are however very different in nature.

Desmin's participation in nuclear movement to the periphery is not surprising. Desmin has previously been reported to be involved in nuclear positioning in skeletal muscle and its localization around the nucleus in mature myofibers suggests it plays a role in nuclear movement (Hnia et al., 2014). However, we show here that desmin's involvement is not as straight forward as expected. Our data shows that desmin becomes organized at z-lines prior to nuclear movement but without accumulation of desmin around the nucleus. This suggests that nuclear movement to the periphery relies on desmin-mediated crosslinking of myofibrils. This is more indirect than originally believed in which most data tended towards a direct interaction between desmin and the nuclear envelope for nuclear movement to the periphery. The accumulation of desmin around the nucleus, which occurs after nuclear movement to the periphery, may be important for anchoring of nuclei at the membrane.

Nuclear movement to the myofiber periphery does not depend on microtubules. Inhibiting microtubule dynamics impairs longitudinal movement of nuclei along the myofiber but we observed no changed in the number of peripheral nuclei after a 5-day nocodazole treatment. Moreover, nuclei appear to be less prone to longitudinal movement before they initiate a peripheral movement. This may be explained by the fact that the space in between myofibrils disappears due to myofibril crosslinking. It would not be surprising that sliding microtubules, responsible for longitudinal nuclear movement, use this space to spread nuclei along the fiber. Crosslinking of myofibrils would therefore rarify these sliding mechanisms thereby limiting microtubule-dependent longitudinal movement.

Although we found that actin and desmin are involved in crosslinking myofibrils to drive nuclear movement to the periphery, another role for cytoskeleton networks and the LINC complex cannot be excluded. Expressing a dominant negative KASH construct (hampering the connection of the LINC complex with the cytoskeleton) blocks nuclear movement to the periphery. By performing live imaging of myofibers expressing this dominant negative KASH construct we observed that nuclei are rounder, roll longitudinally along myofibers more extensively and have a tendency to be more

aggregated. Disabling the LINC complex, which was shown to be involved in nuclear centration and dispersion (Cadot et al., 2012a; Wilson and Holzbaur, 2015a), may impair the chronological resolution to observe its importance in movement to the periphery. The phenotypes observed when expressing the dominant negative construct are complex and should be studied to establish the possible role of the LINC complex in nuclear movement.

I.2 Nuclear movement to the periphery is driven by centripetal forces

The apparel to drive nuclear movement previously described involves polarized machinery composed of the cytoskeleton and motor proteins (Gundersen and Worman, 2013a). Forces are usually exerted on the nucleus through the LINC complex which determines the direction of nuclear movement. This is the case for nuclear movements during cell migration or in microtubule-driven pro-nuclear movements of oocyte. In 2D cell migration, TAN lines at the top of the nucleus give directionality towards the rear end of the cell (Luxton et al., 2010) whereas intermediate filament vimentin cables located at the front of the cell in 3D cell migration pull the nuclei frontward (Petrie et al., 2014). Forces in the pro-nucleus of oocyte are generated by microtubule-associated motor proteins (Tsai et al., 2010). LINC complex independent nuclear movements such as direct microtubule pushing of the nucleus (Tran et al., 2001) or active diffusion of vesicles (Almonacid et al., 2015a) rely on cytoskeleton polarization or gradients. In contrast, the machinery involved in nuclear movement to the periphery of skeletal muscle cells is symmetrical. Centripetal forces are applied to the nucleus by myofibrils surrounding the nucleus. These forces are resisted by nuclear tension at the cost of nuclear deformability. It is at the site of the weakest nuclear stiffness that the myofibrils entrenched in the nuclei will deform most extensively the nucleus thereby creating a nuclear bleb. As such, the direction of movement is dependent on intrinsic properties of the nucleus and more precisely on local changes of nuclear stiffness. This mechanism is analogous to bleb-based cell migration (Paluch and Raz, 2013b). Both mechanisms share a local change of surface stiffness leading to the formation of a bleb which will give directionality to the movement. Future work should address of these local changes are stochastic or locally triggered.

I.3 Nuclear stiffness regulated by lamin A/C is important for nuclear movement to the periphery

Microdevices and 3D collagen matrices have allowed the study of cell migration through tight spaces in controlled environments (Davidson and Lammerding, 2014; Thiam et al., 2016). The limiting step in cells migrating through tight spaces is the capacity for nuclei to squeeze. It was recently shown that the important deformability of nuclei through tight spaces may lead to rupture of the nuclear envelope resulting in leakage of nucleoplasm content in the cytoplasm (Denais et al., 2016). A decrease in nuclear stiffness mediated by lamin A/C is observed at the site of rupture. This work may be of great importance to inhibit migrating metastatic cancer cells through tight spaces. The mechanism of nuclear movement to the periphery of myofibers also involves changes in nuclear stiffness mediated by lamin A/C. However, in contrast to microtubes or microdevices in which the width of tight spaces is controlled, squeezing of the nucleus occurs intracellularly in between myofibrils. We never observed a leakage of the nucleoplasm from the cell which would most likely be detrimental to the cell. It is possible that the regulation of lamin A/C in muscle cell nuclei is adapted to respond to the important forces that are exerted on it by contracting myofibrils. As such, we observed that a narrow range of nuclear stiffness for the whole nucleus is required for nuclear movement. A nucleus that is too stiff may resist external forces however it lacks the flexibility to migrate to the periphery. On the other side of the spectrum, a ductile nucleus will end up being completely deformed by myofibrils (as was observed in lamin A/C knock out nuclei) and adopt a rod-like shape. Locally however, we witnessed a decrease in nuclear stiffness at the site of the nuclear bleb which will give the direction of nuclear movement. This decrease of stiffness provides flexibility to a nucleus that is increasingly under pressure. The mechanisms that regulate this lamin A/C asymmetry should be further studied to understand how the lamin A/C network reorganizes when forces are applied to the nucleus.

I.4 Nesprin involvement in nuclear movement

The role of nesprins in nuclear movement is difficult to assess in skeletal muscle. Final nuclear positioning at the periphery of myofibers is the endpoint of a long journey driven by many mechanisms. Nesprins were shown to be involved in centration and spreading of nuclei (Cadot et al., 2012a; Wilson and Holzbaur, 2015a). As such, nesprin knock down studies impair nuclear movements before the one presently studied.

Furthermore, nesprin isoform redundancy and the size of the protein also contribute in complicating our understanding of nesprins in this movement. We have however begun to explore precise functions. By performing live-imaging in over-expressing KASH dominant negative myofibers, we observed differences in nuclear shape and movement which attests the complexity of nesprins' involvement. Nuclei over-expressing the KASH dominant negative construct appear rounder. This was already observed in nesprin 1 knock down endothelial cells in which nuclei adopt a rounded shape due to loss of cytoskeletal connections with focal adhesions (King et al., 2014). Moreover, during spreading, nuclei appear to roll along the myofiber. This movement was enhanced in KASH dominant negative nuclei. We also observed Nesprin 2 at the z-line of sarcomeres which was previously described (Zhang et al., 2005). Nesprin 2 at z-lines may therefore bind centrally located nuclei to stabilize them during the myofibril zipping process. Establishing the role of other nesprins as well as their splice variants could bring many insights into nuclear positioning in skeletal muscle.

I.5 Nuclear movement as a checkpoint for skeletal muscle development

Nuclear movement to the periphery is an integral part of skeletal muscle development. Although it was shown that nuclear positioning was important for proper muscle function (Metzger et al., 2012a), the reason for peripheral localization of the nucleus is still not fully understood. Is the peripheral localization a purely mechanical optimization of sarcomere alignment or do nuclei at the periphery play a special role in their behavior? The extreme squeezing of the nucleus through myofibrils that we observe during nuclear movement to the periphery does however raise new questions regarding the development of skeletal muscle. Deformation of the nucleus and lamin A/C reorganization may affect chromatin organization and therefore the expression profile of the nucleus. Before nuclear movement to the periphery, the expression profile of nuclei might be tuned to the first stages of muscle development. The nuclear squeezing event could serve to signal the maturity of the muscle cell and trigger a different expression profile more adapted to the later stages of muscle development. The process of nuclear movement to the periphery will therefore act as a developmental checkpoint in muscle growth. We are currently using visual tools to observe chromatin reorganization during nuclear movement to the periphery and we are isolating RNA from nuclei before, during and after peripheral nuclear movement by laser capture microdissection (LCM) to observe expression profiles. As such, the mechanism by how

nuclei reach the periphery would be essential for muscle development. Positioning of nuclei at the periphery may nonetheless be important for proper muscle function to allow the straight alignment of myofibrils and to prevent the pounding of nuclei by contracting myofibrils.

I.6 Post-periphery nuclear movements in skeletal muscle

As stated in the introduction, nuclear movement to the periphery is not the last movement observed in skeletal muscle. Live imaging of our developing myofibers shows that nuclei continue to move longitudinally along the myofibers once they reach the periphery. Using cytoskeleton inhibiting drug, it appears this process is driven by microtubules. This movement is not observed in mature myofibers suggesting that at some point, nuclei become anchored. It was reported that nuclei are not anchored randomly but are well distributed along the myofiber (Bruusgaard et al., 2003). How nuclei reach this final position and become anchored is for the moment unknown. The organized distribution of nuclei does suggest that nuclei must communicate in one way or another. Moreover, a couple of nuclei aggregate under the neuromuscular and myo-tendinous junction (Cadot et al., 2015b). What attracts nuclei to these areas of the myofibers and if these nuclei have a specific function remains unknown. We are currently exploring the microdomain theory, which stipulates that each nucleus takes care of its own area along the myofiber thereby providing nuclear support throughout the length of the cell.

II. Nuclear Positioning in Muscle Disorders

Many muscle diseases exhibit an accumulation of centrally located nuclei (Cadot et al., 2015b). How much this central nuclear phenotype contributes to the pathophysiology of these muscle disorders remains unknown. Regenerative myofibers are also routinely identified as possessing central nuclei (Chargé and Rudnicki, 2004). As such, determining if centrally located nuclei are the result of developmental defects or myofiber degeneration/regeneration has obscured our understanding of the importance of nuclear positioning in skeletal muscle. Mis-localization of nuclei in centronuclear myopathies (CNMs) results from defects in the machinery driving nuclei to the periphery rather than myofiber turnover. Genes mutated in CNM are therefore a solid starting point in our investigation.

II.1 Nuclear positioning and the pathophysiology of centronuclear myopathies

Four genes are mutated in CNMs namely *BIN1*, *DNM2*, *MTM1* and *RYR1* (Böhm et al., 2012; Jungbluth et al., 2008). The first three genes give rise to proteins involved in membrane dynamics whereas *RYR1* yields the ryanodine receptor important for E-C coupling. CNMs display deformed triads and centrally located nuclei not due to regenerative myofibers. Although the triadic phenotype is still not fully established due to our limited understanding of triad genesis, we can make a direct link between the genes mutated in CNM and triads which are membrane networks. In contrast, the nuclear phenotype is not as evident. We show here that Amphiphysin 2 (BIN1) interacts with N-WASP and that N-WASP is mis-localized in patients affected by Bin1-related CNM. BIN1 therefore appears to have an anchoring role allowing the binding of signaling proteins such as N-WASP. The Amphiphysin2/N-WASP complex is required in the pathway leading to triad formation and to crosslink myofibrils for nuclear movement to the periphery. However, BIN1 is a membrane-bound protein which raises the question of how N-WASP is recruited by BIN1 in between myofibrils to crosslink them. Chronologically, transversal triads which span the entire depth of muscle only appear after nuclear movement to the periphery ruling out the involvement of transversal triads in nuclear movement. However, as stated in the introduction, triads (CRUs at this stage) are initially organized longitudinally at the surface of the developing myofibers (Flucher, 1992). Just before birth (which coincides with nuclear movement to the periphery), these CRUs are found deeper in the muscle. These membrane structures house Amphiphysin 2 as well as triadic proteins like the ryanodine receptor. CRUs may therefore be essential to recruit signaling proteins like N-WASP which will allow myofibril crosslinking as well as gathering E-C coupling proteins like Ryr1 involved in myofibril contraction. Defects in constructing these CRUs could occur in BIN1, MTM1 or DNM2-related CNMs. It is also possible that amphiphysin 2 plays a much more direct role; it was recently shown that amphiphysin 2 interacts directly with nesprins, actin and CLIP170, a microtubule binding protein. The absence of amphiphysin 2 leads to mispostioned and misshaped nuclei. However this phenotype is rescued by the introduction of a fused protein composed of KASH and a CLIP170 ortholog capable of binding microtubules(D'Alessandro et al., 2015). This entails that Amphiphsin 2 is primordially important for microtubule dependant nuclear positioning and may pertain to the first step of nuclear movement in skeletal muscle (centration and

spreading). It is still suggested that binding of Amph2 to actin may serve to fine tune the dynamics between the nuclear envelop and the cytoskeleton.

II.2 Desminopathies, plectinopathies and laminopathies

Desminopathies are characterized by misalignment of myofibrils, perturbation of myofibril anchorage to the sarcolemma and loss of nuclear shape and positioning believed to be due to degeneration/regeneration of myofibers. Desmin slowly replaces vimentin during development to become the main intermediate filament network in muscle (Hnia et al., 2014). Our data shows that knocking down desmin in our myofibers leads to important structural impairments including fiber size, nuclear positioning, sarcomeric organization and triad formation. Being such a central protein for muscle architecture, it is difficult to narrow down precise roles for desmin since much of the muscle can be affected by desmin mutations. This is particularly relevant here to distinguish between the abnormal shape of nuclei and the mis-positioning of nuclei observed in desminopathies. A silver lining may lie in the plectin family of proteins which are cytoskeleton linkers that exist in various isoforms (Winter and Wiche, 2013). These isoforms bind desmin at different locations of the muscle thereby providing a compartmental resolution to study the different functions of desmin. Plectin 1 was found to link nuclei with desmin whereas plectin isoform 1f links desmin at the z-lines of myofibrils (myofibril crosslinking). Interestingly, individuals affected by mutations in plectin isoform 1f have an accumulation of centrally located nuclei but nuclear shape is preserved (Gundesli et al., 2010). This is also observed in knock out mouse models (Konieczny et al., 2008b). In contrast, plectin 1 isoform knock out models have peripheral but deformed nuclei (Staszewska et al., 2015). These observations are concordant with our findings that myofibril crosslinking is more important for nuclear movement than by a mechanism relying on the interaction between desmin and the nucleus which appears to be more important for nuclear anchoring and shape. These phenotypic subtleties are a testament to desmin's omnipresence in many events of skeletal muscle development and maintenance. Although beyond the scope of this work, studying plectin isoforms in skeletal muscle will paint a clearer picture of nuclear movements and the roles of desmin in muscle architecture.

The mechanism here described also involves a tight regulation of nuclear stiffness thereby implicating lamin A/C in nuclear movement. Lamin A/C is involved in nuclear protein localization, nuclear integrity, cytoskeletal proteins regulation and mechanotransduction, transcriptional regulation and chromatin remodeling (Burke and Stewart, 2012). As such, many forms of laminopathies exist, some of which are muscle specific, namely Emery-Dreifuss muscular dystrophy and Limb Girdle muscular dystrophy (Azibani et al., 2014a). The prevalent view on both these pathologies relies on the hypothesis that the nucleus fails in acting as a sensor for nuclear architecture. The expression profile of nuclei therefore depends on lamin A to organize chromatin and resist the heavy mechanical stress subjected by muscle contractions. It is difficult to elaborate on the link between nuclear movement to the periphery and specific lamin A mutations, a part from the fact that patients and animal models exhibit centrally located nuclei. Nuclear mechanics have not been assessed in these patients with regards to nuclear stiffness. However, investigating if nuclear squeezing to the periphery reorganizes chromatin architecture would provide strong evidence that regulation of lamin A/C might be necessary for movement and changing the expression profile of nuclei.

II.3 Regeneration

The complexity of skeletal muscle regeneration has confined the study of this process to in vivo studies due to the lack of an adequate in vitro system. It is however accepted that after muscle injury, satellite cells either fuse with existing myofibers and myonuclei are positioned at the center or alternately fuse to one another to form new myofibers exhibiting central nuclei (Chargé and Rudnicki, 2004). Interestingly it is only reported that nuclei in newly formed myofibers eventually migrate to the periphery. Myonuclei integrated into pre-existing myofibers were observed to remain central throughout the study of 6 months (Wada et al., 2008). It must be noted that the animal model used as well as the type and degree of injury induced may give varying results. Nevertheless, the mechanism of nuclear movement to the periphery here described relies on a shift in nucleoplasm pressure between the nuclear bleb and the rest of the nucleus. The number of myofibrils surrounding each nucleus was essential in raising this model which suggests that myofiber thickness is an important parameter in nuclear movement to the periphery. This could explain why injured myofibers become

transiently hypotrophic after injury but also why certain nuclei fail to migrate to the periphery when they integrate pre-existing myofibers that remain thick.

Regeneration is central in the pathophysiology of muscular dystrophies. These disorders are often described as the loss of balance between the degeneration/regeneration capacities of the muscle. Elucidating the role of centrally located nuclei in regenerative myofibers may open new therapeutic avenues to ameliorate the regenerative capacity of diseased skeletal muscle.

III. Molecular Pathways

This thesis elucidates one of the pathways leading to nuclear movement to the periphery and transversal triad formation in skeletal muscle. By starting with *BIN1*, gene mutated in CNMs, we established that nuclear movement and transversal triad formation was an actin-dependent processes stemming from the same pathway but bifurcating at the Arp2/3 complex level. Nuclear movement and triad formation are therefore independent processes despite the involvement of similar proteins which explain the joint nuclear and triadic phenotype observed in CNMs.

III.1 Amphiphysin 2 and N-WASP: membrane shapers.

Amphiphysin2 (BIN1) is known to be involved in membrane dynamics. The BAR domain enables BIN1 to bind membranes and form membrane curvatures (Toussaint et al., 2010). Different isoforms of BIN1 exist, of which one containing exon 11 is specific to skeletal muscle and highly expressed (Böhm et al., 2013). This is not surprising considering the complex network of membranes found in muscle. Exon 11 codes for a PI domain which may favor the binding of BIN1 to membrane structures as well as favor interactions with proteins through its SH3 domain. We show here that BIN1 interacts with N-WASP through the SH3 domain of BIN1 suggesting that much of the membrane remodeling in muscle is actin driven. Amphiphysin 1 was already shown to interact with N-WASP in sertoli cells to regulate membrane ruffles (Yamada et al., 2009). These structures are however much simpler than the ones found in skeletal muscle. Moreover, we show that the proper localization of N-WASP to triads is dependent on BIN1. As such, BIN1 is important for membrane remodeling to bend membranes but it also acts as an anchor for actin regulators such as N-WASP. This role could be enhanced in skeletal muscle due to the PI domain of BIN1 which would also

promote N-WASP activity. The actin structures that result from N-WASP activation may be essential to reinforce and maintain membrane shape in support to the bending capabilities of BIN1.

We found that N-WASP was a downstream effector of BIN1 to drive actin-driven process. Analyzing the involvement of N-WASP over other NPFs may provide insight into the actin dynamics for membrane remodeling in muscle. The WASP family of proteins differs mostly from other NPF family proteins in their N-terminus. The EVH1 domain of WASPs and the SHD domain of the WAVEs determine binding partners. As such, N-WASP is the preferential binding partner of BIN1. In contrast to WAVEs, WASPs possess a CRIB region allowing them to be directly regulated by small GTPases (Takenawa and Suetsugu, 2007). This difference may be important for a tighter regulation of actin dynamics as well as forming smaller complexes in between the tight membrane junctions. Moreover, N-WASP is preferentially regulated by Cdc42 whereas WAVEs are indirectly linked with Rac1. This could be important for the dynamicity of membrane remodeling in skeletal muscle.

III.2 Arp2/3 complex and actin fine tune actin dynamics

The downstream effector of N-WASP in driving nuclear movement to the periphery and transversal triad formation is Arp2/3. The Arp2/3 complex has become a central player in actin dynamics for its involvement in endo- and exocytosis as well as filopodial and lamellipodial-based cell migration (Goley and Welch, 2006). We show here that the Arp2/3 complex is involved in triad formation thereby underlying its role for membrane remodeling. We also show that the Arp2/3 complex organizes stable actin architecture in skeletal muscle. This is a novel function for the Arp2/3 complex and is important for desmin recruitment at z-lines to crosslink myofibrils. N-WASP was previously shown to be involved in z-line formation. This is however mediated by Nebulin and not the Arp2/3 complex which was found absent of myofibrils both in staining and protein extracts (Takano et al., 2010). Our results confirm that Arp2/3 is not involved in z-line formation however, we do observe the complex to be located at z-lines and involved in myofibril crosslinking. The differences may stem from the fact that the involvement of the Arp2/3 complex was addressed in adult and not developing myofibers. Moreover, the Arp2/3 antibody and the concentration used are not specified

in the methods. In vitro cells are used as a control staining but concentrations must usually be raised to stain isolated myofibers.

The Arp2/3 complex is the stage where the pathway divides to induce nuclear movement to the periphery and transversal triad formation. It has recently been shown that Arp2/3 complexes have different actin kinetics based on their subunit composition (Abella et al., 2016a). As such we found that distinct populations of Arp2/3 complexes mediate different functions in muscle. Namely, Arpc5L is involved in nuclear movement and Arpc5 is involved in triad formation. Abella et al.'s work shows that Arpc5L-containing Arp2/3 complexes promote longer actin tails in motile vaccina viruses in contrast to Arpc5-containing Arp2/3 complexes. This is due to slower disassembly kinetics. As such, the Arpc5L subunit creates more robust actin networking which would explain why this isoform is preferred for crosslinking myofibrils in which actin is used as a scaffold for desmin recruitment. Inversely, Arpc5's rapid kinetics would be useful for the formation of triads, a potentially highly dynamic process. We found that isoforms for the Arpc1 subunit are important for both functions.

Interestingly, we find that γ-actin preferentially interacts with Arpc5L-containing Arp2/3 complexes and β-actin with Arpc5-containing Arp2/3 complexes. These two actin isoforms differ by only 4 amino acids in their N-terminus. In contrast to other cell types that have a 2:1 ratio of β-actin to γ-actin, this ratio is inversed in skeletal muscle (Perrin and Ervasti, 2010; Simiczyjew et al., 2013). γ-actin is also found to be more stable in high calcium environments like in contractile myofibers (Bergeron et al., 2010a). Taken together, γ-actin may be preferentially utilized by the cell to perform tasks requiring strength and stability like crosslinking myofibrils. β-actin, which was found to be important for transversal triad formation, is involved in a process necessitating the rapid turnover and change of membrane networks. It must be noted that γ-actin was observed to be present near transversal triads in mature myofibers. β-actin may be the preferential actin isoform for its high dynamicity and flexibility during the formation of transversal triads but is replaced on the long run by γ-actin for triad maintenance. How cells regulate these different affinities of Arp2/3 and actin isoforms remains unknown but could be a result of compartmentalization of proteins or mainly ruled by nucleation or polymerization rates of actin. The versatility of Arp2/3 populations to perform different actin-related function is a testament to the cells' capacity to fine tune cytoskeletal processes.

Conclusion and Contribution

Conclusion

Nuclear positioning at the periphery of cells is a hallmark of skeletal muscle and is perturbed in many muscle disorders or during muscle regeneration. Myonuclei migrate extensively before they are finally anchored at the periphery. All these movements are driven by specific mechanisms involving protein complexes that can generate sufficient amount of force to displace nuclei. Nuclear migration from the center of the myofiber to its periphery is a central step in the journey of myonuclei. Nuclei squeeze greatly in between myofibrils to reach the periphery, a process that involves a considerable amount of force and time as this is the slowest nuclear movement ever described. How nuclear squeezing or the force exerted on nuclei change their nature remains to be studied. Moreover, the function of nuclei at the myofiber periphery is still largely elusive. Nuclear movement to the periphery occurs at a very specfic stage of muscle development when myofibrils are already formed and desmin becomes organized at the z-lines. This suggests that nuclear movement to the periphery of myofibers could be an important event in muscle development. This is reinforced by the lamin reorganization that occurs during nuclear movement which is sometimes associated with chromatin rearrangement and therefore gene expression changes.

Contribution

Result contributions:

1. **N-WASP is required for Amphiphysin-2/BIN1-dependent nuclear positioning and triad organization in skeletal muscle and is involved in the pathophysiology of centronuclear myopathy.**
   Falcone, S.*, Roman, W.*, Hnia, K., Gache, V., Didier, N., Lainé, J., Auradé, F., Marty, I., Nishino, I., Charlet-Berguerand, N., Gomes ER.
   EMBO Mol. Med. *6*, 1455–1475

William Roman is co-first author of this publication. He conceived, designed, and performed experiments. He also helped in writing the manuscript and made figures.
Figures performed by William Roman:
Figure 1: B, E. Partially: F, G.
Figure 2: G, H and I.
Figure 3: F.
Figure 4: B, E, F and G.
Figure 5: C, D, E, F and G.
Figure 6: A – Q.
Figure S1: C, D and E.
Figure S2: M, N, O and P.
Figure S3: A, B, C and J.
Figure S4: A – F.
Figure S5: E.

2. **A mechanism to position nuclei at the periphery of skeletal muscle.**

   Roman W., Voituriez R., Matrins J., Abella J., Cadot B., Way M., Gomes ER.
   Submitted April 2016

William Roman is first author of this publication. He conceived, designed, and performed experiments. He wrote the manuscript with E.G. Gomes. William Roman made the figures.
Raphael Voituriez raised the theoretical model
Joao Martins helped in generating cells.

References

Abella, J.V., Galloni, C., Pernier, J., Barry, D.J., Kjaer, S., Carlier, M.-F., and Way, M. (in press). Isoform diversity in the Arp2/3 complex determines actin filament dynamics. Nat. Cell Biol.

Abella, J.V.G., Galloni, C., Pernier, J., Barry, D.J., Kjær, S., Carlier, M.-F., and Way, M. (2016a). Isoform diversity in the Arp2/3 complex determines actin filament dynamics. Nat. Cell Biol. *18*, 76–86.

Abella, J.V.G., Galloni, C., Pernier, J., Barry, D.J., Kjær, S., Carlier, M.-F., and Way, M. (2016b). Isoform diversity in the Arp2/3 complex determines actin filament dynamics. Nat. Cell Biol. *18*, 76–86.

Aldrich, R.A., Steinberg, A.G., and Campbell, D.C. (1954). Pedigree demonstrating a sex-linked recessive condition characterized by draining ears, eczematoid dermatitis and bloody diarrhea. Pediatrics *13*, 133–139.

Almonacid, M., Ahmed, W.W., Bussonnier, M., Mailly, P., Betz, T., Voituriez, R., Gov, N.S., and Verlhac, M.-H. (2015a). Active diffusion positions the nucleus in mouse oocytes. Nat. Cell Biol. *17*, 470–479.

Almonacid, M., Ahmed, W.W., Bussonnier, M., Mailly, P., Betz, T., Voituriez, R., Gov, N.S., and Verlhac, M.-H. (2015b). Active diffusion positions the nucleus in mouse oocytes. Nat. Cell Biol. *17*, 470–479.

Al-Qusairi, L., and Laporte, J. (2011a). T-tubule biogenesis and triad formation in skeletal muscle and implication in human diseases. Skelet. Muscle *1*, 1–11.

Al-Qusairi, L., and Laporte, J. (2011b). T-tubule biogenesis and triad formation in skeletal muscle and implication in human diseases. Skelet. Muscle *1*, 26.

Amador, F.J., Stathopulos, P.B., Enomoto, M., and Ikura, M. (2013). Ryanodine receptor calcium release channels: lessons from structure–function studies. FEBS J. *280*, 5456–5470.

Amoasii, L., Hnia, K., Chicanne, G., Brech, A., Cowling, B.S., Müller, M.M., Schwab, Y., Koebel, P., Ferry, A., Payrastre, B., et al. (2013). Myotubularin and PtdIns3P remodel the sarcoplasmic reticulum in muscle in vivo. J. Cell Sci. *126*, 1806–1819.

Apel, E.D., Lewis, R.M., Grady, R.M., and Sanes, J.R. (2000). Syne-1, a dystrophin- and Klarsicht-related protein associated with synaptic nuclei at the neuromuscular junction. J. Biol. Chem. *275*, 31986–31995.

Arimura, T., Helbling-Leclerc, A., Massart, C., Varnous, S., Niel, F., Lacène, E., Fromes, Y., Toussaint, M., Mura, A.-M., Keller, D.I., et al. (2005). Mouse model carrying H222P-Lmna mutation develops muscular dystrophy and dilated cardiomyopathy similar to human striated muscle laminopathies. Hum. Mol. Genet. *14*, 155–169.

Auerbuch, V., Loureiro, J.J., Gertler, F.B., Theriot, J.A., and Portnoy, D.A. (2003). Ena/VASP proteins contribute to Listeria monocytogenes pathogenesis by controlling temporal and spatial persistence of bacterial actin-based motility. Mol. Microbiol. *49*, 1361–1375.

Azibani, F., Muchir, A., Vignier, N., Bonne, G., and Bertrand, A.T. (2014a). Striated muscle laminopathies. Semin. Cell Dev. Biol. *29*, 107–115.

Azibani, F., Muchir, A., Vignier, N., Bonne, G., and Bertrand, A.T. (2014b). Striated muscle laminopathies. Semin. Cell Dev. Biol. *29*, 107–115.

Bannister, R.A. (2007). Bridging the myoplasmic gap: recent developments in skeletal muscle excitation-contraction coupling. J. Muscle Res. Cell Motil. *28*, 275–283.

Bär, H., Mücke, N., Ringler, P., Müller, S.A., Kreplak, L., Katus, H.A., Aebi, U., and Herrmann, H. (2006). Impact of Disease Mutations on the Desmin Filament Assembly Process. J. Mol. Biol. *360*, 1031–1042.

Barbet, J.P., Thornell, L.E., and Butler-Browne, G.S. (1991). Immunocytochemical characterisation of two generations of fibers during the development of the human quadriceps muscle. Mech. Dev. *35*, 3–11.

Beam, K.G., and Bannister, R.A. (2010). Looking for answers to EC coupling's persistent questions. J. Gen. Physiol. *136*, 7–12.

Belyantseva, I.A., Perrin, B.J., Sonnemann, K.J., Zhu, M., Stepanyan, R., McGee, J., Frolenkov, G.I., Walsh, E.J., Friderici, K.H., Friedman, T.B., et al. (2009). Gamma-actin is required for cytoskeletal maintenance but not development. Proc. Natl. Acad. Sci. U. S. A. *106*, 9703–9708.

Benesch, S., Polo, S., Lai, F.P.L., Anderson, K.I., Stradal, T.E.B., Wehland, J., and Rottner, K. (2005). N-WASP deficiency impairs EGF internalization and actin assembly at clathrin-coated pits. J. Cell Sci. *118*, 3103–3115.

Berger, P., Berger, I., Schaffitzel, C., Tersar, K., Volkmer, B., and Suter, U. (2006). Multi-level regulation of myotubularin-related protein-2 phosphatase activity by myotubularin-related protein-13/set-binding factor-2. Hum. Mol. Genet. *15*, 569–579.

Bergeron, S.E., Zhu, M., Thiem, S.M., Friderici, K.H., and Rubenstein, P.A. (2010a). Ion-dependent polymerization differences between mammalian beta- and gamma-nonmuscle actin isoforms. J. Biol. Chem. *285*, 16087–16095.

Bergeron, S.E., Zhu, M., Thiem, S.M., Friderici, K.H., and Rubenstein, P.A. (2010b). Ion-dependent Polymerization Differences between Mammalian - and -Nonmuscle Actin Isoforms. J. Biol. Chem. *285*, 16087–16095.

Bertrand, A.T., Renou, L., Papadopoulos, A., Beuvin, M., Lacène, E., Massart, C., Ottolenghi, C., Decostre, V., Maron, S., Schlossarek, S., et al. (2012). DelK32-lamin A/C has abnormal location and induces incomplete tissue maturation and severe metabolic defects leading to premature death. Hum. Mol. Genet. *21*, 1037–1048.

Bitoun, M., Stojkovic, T., Prudhon, B., Maurage, C.-A., Latour, P., Vermersch, P., and Guicheney, P. (2008). A novel mutation in the dynamin 2 gene in a Charcot-Marie-Tooth type 2 patient: clinical and pathological findings. Neuromuscul. Disord. NMD *18*, 334–338.

Bitoun, M., Bevilacqua, J.A., Eymard, B., Prudhon, B., Fardeau, M., Guicheney, P., and Romero, N.B. (2009). A new centronuclear myopathy phenotype due to a novel dynamin 2 mutation. Neurology *72*, 93–95.

Blondeau, F., Laporte, J., Bodin, S., Superti-Furga, G., Payrastre, B., and Mandel, J.L. (2000). Myotubularin, a phosphatase deficient in myotubular myopathy, acts on phosphatidylinositol 3-kinase and phosphatidylinositol 3-phosphate pathway. Hum. Mol. Genet. *9*, 2223–2229.

Böhm, J., Leshinsky-Silver, E., Vassilopoulos, S., Le Gras, S., Lerman-Sagie, T., Ginzberg, M., Jost, B., Lev, D., and Laporte, J. (2012). Samaritan myopathy, an ultimately benign congenital myopathy, is caused by a RYR1 mutation. Acta Neuropathol. (Berl.) *124*, 575–581.

Böhm, J., Vasli, N., Maurer, M., Cowling, B., Shelton, G.D., Kress, W., Toussaint, A., Prokic, I., Schara, U., Anderson, T.J., et al. (2013). Altered Splicing of the BIN1 Muscle-Specific Exon in Humans and Dogs with Highly Progressive Centronuclear Myopathy. PLoS Genet *9*, e1003430.

Bolhy, S., Bouhlel, I., Dultz, E., Nayak, T., Zuccolo, M., Gatti, X., Vallee, R., Ellenberg, J., and Doye, V. (2011). A Nup133-dependent NPC-anchored network tethers centrosomes to the nuclear envelope in prophase. J. Cell Biol. *192*, 855–871.

Bonne, G., Di Barletta, M.R., Varnous, S., Bécane, H.M., Hammouda, E.H., Merlini, L., Muntoni, F., Greenberg, C.R., Gary, F., Urtizberea, J.A., et al. (1999). Mutations in the gene encoding lamin A/C cause autosomal dominant Emery-Dreifuss muscular dystrophy. Nat. Genet. *21*, 285–288.

Borrego-Pinto, J., Jegou, T., Osorio, D.S., Aurade, F., Gorjanacz, M., Koch, B., Mattaj, I.W., and Gomes, E.R. (2012). Samp1 is a component of TAN lines and is required for nuclear movement. J. Cell Sci. *125*, 1099–1105.

Briñas, L., Vassilopoulos, S., Bonne, G., Guicheney, P., and Bitoun, M. (2013). Role of dynamin 2 in the disassembly of focal adhesions. J. Mol. Med. Berl. Ger. *91*, 803–809.

Bruusgaard, J.C., Liestøl, K., Ekmark, M., Kollstad, K., and Gundersen, K. (2003). Number and spatial distribution of nuclei in the muscle fibres of normal mice studied in vivo. J. Physiol. *551*, 467–478.

Bunnell, T.M., and Ervasti, J.M. (2011). Structural and functional properties of the actin gene family. Crit. Rev. Eukaryot. Gene Expr. *21*, 255–266.

Burke, B., and Stewart, C.L. (2012). The nuclear lamins: flexibility in function. Nat. Rev. Mol. Cell Biol. *14*, 13–24.

Butler, M.H., David, C., Ochoa, G.-C., Freyberg, Z., Daniell, L., Grabs, D., Cremona, O., and Camilli, P.D. (1997). Amphiphysin II (SH3P9; BIN1), a Member of the Amphiphysin/Rvs Family, Is Concentrated in the Cortical Cytomatrix of Axon Initial Segments and Nodes of Ranvier in Brain and around T Tubules in Skeletal Muscle. J. Cell Biol. *137*, 1355–1367.

Cadot, B., Gache, V., Vasyutina, E., Falcone, S., Birchmeier, C., and Gomes, E.R. (2012a). Nuclear movement during myotube formation is microtubule and dynein dependent and is regulated by Cdc42, Par6 and Par3. EMBO Rep. *13*, 741–749.

Cadot, B., Gache, V., Vasyutina, E., Falcone, S., Birchmeier, C., and Gomes, E.R. (2012b). Nuclear movement during myotube formation is microtubule and dynein dependent and is regulated by Cdc42, Par6 and Par3. EMBO Rep. *13*, 741–749.

Cadot, B., Gache, V., and Gomes, E.R. (2015a). Moving and positioning the nucleus in skeletal muscle – one step at a time. Nucleus *6*, 01–09.

Cadot, B., Gache, V., and Gomes, E.R. (2015b). Moving and positioning the nucleus in skeletal muscle - one step at a time. Nucl. Austin Tex *6*, 373–381.

Campellone, K.G., and Welch, M.D. (2010). A nucleator arms race: cellular control of actin assembly. Nat. Rev. Microbiol. *11*, 237–251.

Campellone, K.G., Webb, N.J., Znameroski, E.A., and Welch, M.D. (2008). WHAMM is an Arp2/3 complex activator that binds microtubules and functions in ER to Golgi transport. Cell *134*, 148–161.

Capetanaki, Y., Bloch, R.J., Kouloumenta, A., Mavroidis, M., and Psarras, S. (2007). Muscle intermediate filaments and their links to membranes and membranous organelles. Exp. Cell Res. *313*, 2063–2076.

Carlier, M.F. (1990). Actin polymerization and ATP hydrolysis. Adv. Biophys. *26*, 51–73.

Carlier, M.F., Nioche, P., Broutin-L'Hermite, I., Boujemaa, R., Le Clainche, C., Egile, C., Garbay, C., Ducruix, A., Sansonetti, P., and Pantaloni, D. (2000). GRB2 links signaling to actin assembly by enhancing interaction of neural Wiskott-Aldrich syndrome protein (N-WASp) with actin-related protein (ARP2/3) complex. J. Biol. Chem. *275*, 21946–21952.

Casarotto, M.G., Cui, Y., Karunasekara, Y., Harvey, P.J., Norris, N., Board, P.G., and Dulhunty, A.F. (2006). Structural and functional characterization of interactions between the dihydropyridine receptor II-III loop and the ryanodine receptor. Clin. Exp. Pharmacol. Physiol. *33*, 1114–1117.

Chargé, S.B.P., and Rudnicki, M.A. (2004). Cellular and Molecular Regulation of Muscle Regeneration. Physiol. Rev. *84*, 209–238.

Choi, J.C., Muchir, A., Wu, W., Iwata, S., Homma, S., Morrow, J.P., and Worman, H.J. (2012). Temsirolimus activates autophagy and ameliorates cardiomyopathy caused by lamin A/C gene mutation. Sci. Transl. Med. *4*, 144ra102.

Choudhury, P., Srivastava, S., Li, Z., Ko, K., Albaqumi, M., Narayan, K., Coetzee, W.A., Lemmon, M.A., and Skolnik, E.Y. (2006). Specificity of the myotubularin family of phosphatidylinositol-3-phosphatase is determined by the PH/GRAM domain. J. Biol. Chem. *281*, 31762–31769.

Claeys, K.G., van der Ven, P.F.M., Behin, A., Stojkovic, T., Eymard, B., Dubourg, O., Laforêt, P., Faulkner, G., Richard, P., Vicart, P., et al. (2009). Differential involvement of sarcomeric proteins in myofibrillar myopathies: a morphological and immunohistochemical study. Acta Neuropathol. (Berl.) *117*, 293–307.

Claeys, K.G., Maisonobe, T., Böhm, J., Laporte, J., Hezode, M., Romero, N.B., Brochier, G., Bitoun, M., Carlier, R.Y., and Stojkovic, T. (2010). Phenotype of a patient with recessive centronuclear myopathy and a novel BIN1 mutation. Neurology *74*, 519–521.

Clark, K.A., McElhinny, A.S., Beckerle, M.C., and Gregorio, C.C. (2002). Striated muscle cytoarchitecture: an intricate web of form and function. Annu. Rev. Cell Dev. Biol. *18*, 637–706.

Clemen, C.S., Herrmann, H., Strelkov, S.V., and Schröder, R. (2013a). Desminopathies: pathology and mechanisms. Acta Neuropathol. (Berl.) *125*, 47–75.

Clemen, C.S., Herrmann, H., Strelkov, S.V., and Schröder, R. (2013b). Desminopathies: pathology and mechanisms. Acta Neuropathol. (Berl.) *125*, 47–75.

Coffinier, C., Fong, L.G., and Young, S.G. (2010). LINCing lamin B2 to neuronal migration: growing evidence for cell-specific roles of B-type lamins. Nucl. Austin Tex *1*, 407–411.

Colomo, F., Piroddi, N., Poggesi, C., Te Kronnie, G., and Tesi, C. (1997). Active and passive forces of isolated myofibrils from cardiac and fast skeletal muscle of the frog. J. Physiol. *500*, 535.

Coutts, A.S., Weston, L., and La Thangue, N.B. (2009). A transcription co-factor integrates cell adhesion and motility with the p53 response. Proc. Natl. Acad. Sci. U. S. A. *106*, 19872–19877.

Crisp, M. (2006). Coupling of the nucleus and cytoplasm: role of the LINC complex. J. Cell Biol. *172*, 41–53.

Cui, Y., Tae, H.-S., Norris, N.C., Karunasekara, Y., Pouliquin, P., Board, P.G., Dulhunty, A.F., and Casarotto, M.G. (2009). A dihydropyridine receptor alpha1s loop region critical for skeletal muscle contraction is intrinsically unstructured and binds to a SPRY domain of the type 1 ryanodine receptor. Int. J. Biochem. Cell Biol. *41*, 677–686.

D'Alessandro, M., Hnia, K., Gache, V., Koch, C., Gavriilidis, C., Rodriguez, D., Nicot, A.-S., Romero, N.B., Schwab, Y., Gomes, E., et al. (2015). Amphiphysin 2 Orchestrates Nucleus Positioning and Shape by Linking the Nuclear Envelope to the Actin and Microtubule Cytoskeleton. Dev. Cell *35*, 186–198.

van Dam, E.M., and Stoorvogel, W. (2002). Dynamin-dependent transferrin receptor recycling by endosome-derived clathrin-coated vesicles. Mol. Biol. Cell *13*, 169–182.

Dang, I., Gorelik, R., Sousa-Blin, C., Derivery, E., Guérin, C., Linkner, J., Nemethova, M., Dumortier, J.G., Giger, F.A., Chipysheva, T.A., et al. (2013). Inhibitory signalling to the Arp2/3 complex steers cell migration. Nature *503*, 281–284.

Davidson, P.M., and Lammerding, J. (2014). Broken nuclei – lamins, nuclear mechanics and disease. Trends Cell Biol. *24*, 247–256.

Dayel, M.J., and Mullins, R.D. (2004). Activation of Arp2/3 complex: addition of the first subunit of the new filament by a WASP protein triggers rapid ATP hydrolysis on Arp2. PLoS Biol. *2*, E91.

Dayel, M.J., Holleran, E.A., and Mullins, R.D. (2001). Arp2/3 complex requires hydrolyzable ATP for nucleation of new actin filaments. Proc. Natl. Acad. Sci. U. S. A. *98*, 14871–14876.

DeMali, K.A., Barlow, C.A., and Burridge, K. (2002). Recruitment of the Arp2/3 complex to vinculin: coupling membrane protrusion to matrix adhesion. J. Cell Biol. *159*, 881–891.

Denais, C.M., Gilbert, R.M., Isermann, P., McGregor, A.L., te Lindert, M., Weigelin, B., Davidson, P.M., Friedl, P., Wolf, K., and Lammerding, J. (2016). Nuclear envelope rupture and repair during cancer cell migration. Science *352*, 353–358.

Derivery, E., Sousa, C., Gautier, J.J., Lombard, B., Loew, D., and Gautreau, A. (2009). The Arp2/3 activator WASH controls the fission of endosomes through a large multiprotein complex. Dev. Cell *17*, 712–723.

Desai, R.A., Gao, L., Raghavan, S., Liu, W.F., and Chen, C.S. (2009). Cell polarity triggered by cell-cell adhesion via E-cadherin. J. Cell Sci. *122*, 905–911.

Dirksen, R.T. (2002). Bi-directional coupling between dihydropyridine receptors and ryanodine receptors. Front. Biosci. J. Virtual Libr. *7*, d659-670.

Dugina, V., Zwaenepoel, I., Gabbiani, G., Clément, S., and Chaponnier, C. (2009). Beta and gamma-cytoplasmic actins display distinct distribution and functional diversity. J. Cell Sci. *122*, 2980–2988.

Duleh, S.N., and Welch, M.D. (2010). WASH and the Arp2/3 complex regulate endosome shape and trafficking. Cytoskelet. Hoboken NJ *67*, 193–206.

Durieux, A.-C., Prudhon, B., Guicheney, P., and Bitoun, M. (2010). Dynamin 2 and human diseases. J. Mol. Med. Berl. Ger. *88*, 339–350.

Echaniz-Laguna, A., Nicot, A.-S., Carré, S., Franques, J., Tranchant, C., Dondaine, N., Biancalana, V., Mandel, J.-L., and Laporte, J. (2007). Subtle central and peripheral nervous system abnormalities in a family with centronuclear myopathy and a novel dynamin 2 gene mutation. Neuromuscul. Disord. NMD *17*, 955–959.

Eden, S., Rohatgi, R., Podtelejnikov, A.V., Mann, M., and Kirschner, M.W. (2002). Mechanism of regulation of WAVE1-induced actin nucleation by Rac1 and Nck. Nature *418*, 790–793.

Egile, C., Loisel, T.P., Laurent, V., Li, R., Pantaloni, D., Sansonetti, P.J., and Carlier, M.-F. (1999). Activation of the Cdc42 Effector N-Wasp by the Shigella flexneri Icsa Protein Promotes Actin Nucleation by Arp2/3 Complex and Bacterial Actin-Based Motility. J. Cell Biol. *146*, 1319–1332.

Egile, C., Rouiller, I., Xu, X.-P., Volkmann, N., Li, R., and Hanein, D. (2005). Mechanism of filament nucleation and branch stability revealed by the structure of the Arp2/3 complex at actin branch junctions. PLoS Biol. *3*, e383.

Elhanany-Tamir, H., Yu, Y.V., Shnayder, M., Jain, A., Welte, M., and Volk, T. (2012a). Organelle positioning in muscles requires cooperation between two KASH proteins and microtubules. J. Cell Biol. *198*, 833–846.

Elhanany-Tamir, H., Yu, Y.V., Shnayder, M., Jain, A., Welte, M., and Volk, T. (2012b). Organelle positioning in muscles requires cooperation between two KASH proteins and microtubules. J. Cell Biol.

Eriksson, J.E., Dechat, T., Grin, B., Helfand, B., Mendez, M., Pallari, H.-M., and Goldman, R.D. (2009). Introducing intermediate filaments: from discovery to disease. J. Clin. Invest. *119*, 1763–1771.

Fabrizi, G.M., Ferrarini, M., Cavallaro, T., Cabrini, I., Cerini, R., Bertolasi, L., and Rizzuto, N. (2007). Two novel mutations in dynamin-2 cause axonal Charcot-Marie-Tooth disease. Neurology *69*, 291–295.

Falcone, S., Roman, W., Hnia, K., Gache, V., Didier, N., Lainé, J., Auradé, F., Marty, I., Nishino, I., Charlet-Berguerand, N., et al. (2014). N-WASP is required for Amphiphysin-2/BIN1-dependent nuclear positioning and triad organization in skeletal muscle and is involved in the pathophysiology of centronuclear myopathy. EMBO Mol. Med. *6*, 1455–1475.

Ferron, F., Rebowski, G., Lee, S.H., and Dominguez, R. (2007). Structural basis for the recruitment of profilin-actin complexes during filament elongation by Ena/VASP. EMBO J. *26*, 4597–4606.

Fischer, D., Herasse, M., Bitoun, M., Barragán-Campos, H.M., Chiras, J., Laforêt, P., Fardeau, M., Eymard, B., Guicheney, P., and Romero, N.B. (2006). Characterization of the muscle involvement in dynamin 2-related centronuclear myopathy. Brain J. Neurol. *129*, 1463–1469.

Flucher, B.E. (1992). Structural analysis of muscle development: transverse tubules, sarcoplasmic reticulum, and the triad. Dev. Biol. *154*, 245–260.

Flucher, B.E., Takekura, H., and Franzini-Armstrong, C. (1993). Development of the Excitation-Contraction Coupling Apparatus in Skeletal Muscle: Association of Sarcoplasmic Reticulum and Transverse Tubules with Myofibrils. Dev. Biol. *160*, 135–147.

Folker, E.S., Ostlund, C., Luxton, G.W.G., Worman, H.J., and Gundersen, G.G. (2011). Lamin A variants that cause striated muscle disease are defective in anchoring transmembrane actin-associated nuclear lines for nuclear movement. Proc. Natl. Acad. Sci. U. S. A. *108*, 131–136.

Folker, E.S., Schulman, V.K., and Baylies, M.K. (2013). Translocating myonuclei have distinct leading and lagging edges that require Kinesin and Dynein. Development dev.095612.

Friedl, P., Wolf, K., and Lammerding, J. (2011). Nuclear mechanics during cell migration. Curr. Opin. Cell Biol. *23*, 55–64.

Frost, A., Unger, V.M., and De Camilli, P. (2009). The BAR domain superfamily: membrane-molding macromolecules. Cell *137*, 191–196.

Fugier, C., Klein, A.F., Hammer, C., Vassilopoulos, S., Ivarsson, Y., Toussaint, A., Tosch, V., Vignaud, A., Ferry, A., Messaddeq, N., et al. (2011a). Misregulated alternative splicing of BIN1 is associated with T tubule alterations and muscle weakness in myotonic dystrophy. Nat. Med. *17*, 720–725.

Fugier, C., Klein, A.F., Hammer, C., Vassilopoulos, S., Ivarsson, Y., Toussaint, A., Tosch, V., Vignaud, A., Ferry, A., Messaddeq, N., et al. (2011b). Misregulated alternative splicing of BIN1 is associated with T tubule alterations and muscle weakness in myotonic dystrophy. Nat. Med. *17*, 720–725.

Galeotti, N., Quattrone, A., Vivoli, E., Norcini, M., Bartolini, A., and Ghelardini, C. (2008). Different involvement of type 1, 2, and 3 ryanodine receptors in memory processes. Learn. Mem. *15*, 315–323.

Gautreau, A., Ho, H.H., Li, J., Steen, H., Gygi, S.P., and Kirschner, M.W. (2004). Purification and architecture of the ubiquitous Wave complex. Proc. Natl. Acad. Sci. U. S. A. *101*, 4379–4383.

Gerlitz, G., and Bustin, M. (2011). The role of chromatin structure in cell migration. Trends Cell Biol. *21*, 6–11.

Gokhin, D.S., and Fowler, V.M. (2011a). Cytoplasmic gamma-actin and tropomodulin isoforms link to the sarcoplasmic reticulum in skeletal muscle fibers. J. Cell Biol. *194*, 105–120.

Gokhin, D.S., and Fowler, V.M. (2011b). Cytoplasmic γ-actin and tropomodulin isoforms link to the sarcoplasmic reticulum in skeletal muscle fibers. J. Cell Biol.

Gold, E.S., Underhill, D.M., Morrissette, N.S., Guo, J., McNiven, M.A., and Aderem, A. (1999). Dynamin 2 is required for phagocytosis in macrophages. J. Exp. Med. *190*, 1849–1856.

Goldfarb, L.G., and Dalakas, M.C. (2009). Tragedy in a heartbeat: malfunctioning desmin causes skeletal and cardiac muscle disease. J. Clin. Invest. *119*, 1806–1813.

Goldman, R.D., Cleland, M.M., Murthy, S.N.P., Mahammad, S., and Kuczmarski, E.R. (2012). Inroads into the structure and function of intermediate filament networks. J. Struct. Biol. *177*, 14–23.

Goldspink, G. (1970). The Proliferation of Myofibrils During Muscle Fibre Growth. J. Cell Sci. *6*, 593–603.

Goley, E.D., and Welch, M.D. (2006). The ARP2/3 complex: an actin nucleator comes of age. Nat. Rev. Mol. Cell Biol. *7*, 713–726.

Goley, E.D., Rodenbusch, S.E., Martin, A.C., and Welch, M.D. (2004). Critical conformational changes in the Arp2/3 complex are induced by nucleotide and nucleation promoting factor. Mol. Cell *16*, 269–279.

Gomes, E.R., Jani, S., and Gundersen, G.G. (2005). Nuclear movement regulated by Cdc42, MRCK, myosin, and actin flow establishes MTOC polarization in migrating cells. Cell *121*, 451–463.

Gomez, T.S., and Billadeau, D.D. (2009). A FAM21-containing WASH complex regulates retromer-dependent sorting. Dev. Cell *17*, 699–711.

Gournier, H., Goley, E.D., Niederstrasser, H., Trinh, T., and Welch, M.D. (2001a). Reconstitution of human Arp2/3 complex reveals critical roles of individual subunits in complex structure and activity. Mol. Cell *8*, 1041–1052.

Gournier, H., Goley, E.D., Niederstrasser, H., Trinh, T., and Welch, M.D. (2001b). Reconstitution of Human Arp2/3 Complex Reveals Critical Roles of Individual Subunits in Complex Structure and Activity. Mol. Cell *8*, 1041–1052.

Grabner, M., Dirksen, R.T., Suda, N., and Beam, K.G. (1999). The II-III loop of the skeletal muscle dihydropyridine receptor is responsible for the Bi-directional coupling with the ryanodine receptor. J. Biol. Chem. *274*, 21913–21919.

Grady, R.M., Starr, D.A., Ackerman, G.L., Sanes, J.R., and Han, M. (2005). Syne proteins anchor muscle nuclei at the neuromuscular junction. Proc. Natl. Acad. Sci. U. S. A. *102*, 4359–4364.

Gruenbaum, Y., and Foisner, R. (2015). Lamins: Nuclear Intermediate Filament Proteins with Fundamental Functions in Nuclear Mechanics and Genome Regulation. Annu. Rev. Biochem. *84*, 131–164.

Gruenbaum, Y., and Medalia, O. (2015). Lamins: the structure and protein complexes. Curr. Opin. Cell Biol. *32*, 7–12.

Gundersen, G.G., and Worman, H.J. (2013a). Nuclear positioning. Cell *152*, 1376–1389.

Gundersen, G.G., and Worman, H.J. (2013b). Nuclear Positioning. Cell *152*, 1376–1389.

Gundesli, H., Talim, B., Korkusuz, P., Balci-Hayta, B., Cirak, S., Akarsu, N.A., Topaloglu, H., and Dincer, P. (2010). Mutation in exon 1f of PLEC, leading to disruption of plectin isoform 1f, causes autosomal-recessive limb-girdle muscular dystrophy. Am. J. Hum. Genet. *87*, 834–841.

Hall, A. (1998). Rho GTPases and the actin cytoskeleton. Science *279*, 509–514.

Herskovits, J.S., Shpetner, H.S., Burgess, C.C., and Vallee, R.B. (1993). Microtubules and Src homology 3 domains stimulate the dynamin GTPase via its C-terminal domain. Proc. Natl. Acad. Sci. U. S. A. *90*, 11468–11472.

Hetrick, B., Han, M.S., Helgeson, L.A., and Nolen, B.J. (2013). Small molecules CK-666 and CK-869 inhibit actin-related protein 2/3 complex by blocking an activating conformational change. Chem. Biol. *20*, 701–712.

Hnia, K., and Laporte, J. (2011). [The myotubularin-desmin complex regulates mitochondria dynamics]. Médecine Sci. MS *27*, 458–460.

Hnia, K., Vaccari, I., Bolino, A., and Laporte, J. (2012). Myotubularin phosphoinositide phosphatases: cellular functions and disease pathophysiology. Trends Mol. Med. *18*, 317–327.

Hnia, K., Ramspacher, C., Vermot, J., and Laporte, J. (2014). Desmin in muscle and associated diseases: beyond the structural function. Cell Tissue Res. *360*, 591–608.

Ho, H.Y., Rohatgi, R., Ma, L., and Kirschner, M.W. (2001). CR16 forms a complex with N-WASP in brain and is a novel member of a conserved proline-rich actin-binding protein family. Proc. Natl. Acad. Sci. U. S. A. *98*, 11306–11311.

Ho, H.-Y.H., Rohatgi, R., Lebensohn, A.M., Le Ma, null, Li, J., Gygi, S.P., and Kirschner, M.W. (2004). Toca-1 mediates Cdc42-dependent actin nucleation by activating the N-WASP-WIP complex. Cell *118*, 203–216.

Horn, H.F., Brownstein, Z., Lenz, D.R., Shivatzki, S., Dror, A.A., Dagan-Rosenfeld, O., Friedman, L.M., Roux, K.J., Kozlov, S., Jeang, K.-T., et al. (2013). The LINC complex is essential for hearing. J. Clin. Invest.

Huelsmann, S., Ylänne, J., and Brown, N.H. (2013a). Filopodia-like actin cables position nuclei in association with perinuclear actin in Drosophila nurse cells. Dev. Cell *26*, 604–615.

Huelsmann, S., Ylänne, J., and Brown, N.H. (2013b). Filopodia-like Actin Cables Position Nuclei in Association with Perinuclear Actin in Drosophila Nurse Cells. Dev. Cell *26*, 604–615.

Ihalainen, T.O., Aires, L., Herzog, F.A., Schwartlander, R., Moeller, J., and Vogel, V. (2015). Differential basal-to-apical accessibility of lamin A/C epitopes in the nuclear lamina regulated by changes in cytoskeletal tension. Nat. Mater. *advance online publication*.

Jaeger, M.A., Sonnemann, K.J., Fitzsimons, D.P., Prins, K.W., and Ervasti, J.M. (2009). Context-dependent functional substitution of alpha-skeletal actin by gamma-cytoplasmic actin. FASEB J. Off. Publ. Fed. Am. Soc. Exp. Biol. *23*, 2205–2214.

Ji, J.Y., Lee, R.T., Vergnes, L., Fong, L.G., Stewart, C.L., Reue, K., Young, S.G., Zhang, Q., Shanahan, C.M., and Lammerding, J. (2007). Cell nuclei spin in the absence of lamin b1. J. Biol. Chem. *282*, 20015–20026.

Jiu, Y., Lehtimäki, J., Tojkander, S., Cheng, F., Jäälinoja, H., Liu, X., Varjosalo, M., Eriksson, J.E., and Lappalainen, P. (2015). Bidirectional Interplay between Vimentin Intermediate Filaments and Contractile Actin Stress Fibers. Cell Rep. *11*, 1511–1518.

Jones, S.M., Howell, K.E., Henley, J.R., Cao, H., and McNiven, M.A. (1998). Role of dynamin in the formation of transport vesicles from the trans-Golgi network. Science *279*, 573–577.

Jung, H.-J., Coffinier, C., Choe, Y., Beigneux, A.P., Davies, B.S.J., Yang, S.H., Barnes, R.H., Hong, J., Sun, T., Pleasure, S.J., et al. (2012). Regulation of prelamin A but not lamin C by miR-9, a brain-specific microRNA. Proc. Natl. Acad. Sci. U. S. A. *109*, E423–E431.

Jungbluth, H., Wallgren-Pettersson, C., and Laporte, J. (2008). Centronuclear (myotubular) myopathy. Orphanet J. Rare Dis. *3*, 26.

Kaksonen, M., Toret, C.P., and Drubin, D.G. (2006). Harnessing actin dynamics for clathrin-mediated endocytosis. Nat. Rev. Mol. Cell Biol. *7*, 404–414.

Kee, A.J., Schevzov, G., Nair-Shalliker, V., Robinson, C.S., Vrhovski, B., Ghoddusi, M., Qiu, M.R., Lin, J.J.-C., Weinberger, R., Gunning, P.W., et al. (2004). Sorting of a nonmuscle tropomyosin to a novel cytoskeletal compartment in skeletal muscle results in muscular dystrophy. J. Cell Biol. *166*, 685–696.

Kee, A.J., Gunning, P.W., and Hardeman, E.C. (2009). Diverse roles of the actin cytoskeleton in striated muscle. J. Muscle Res. Cell Motil. *30*, 187–197.

Kim, A.S., Kakalis, L.T., Abdul-Manan, N., Liu, G.A., and Rosen, M.K. (2000). Autoinhibition and activation mechanisms of the Wiskott-Aldrich syndrome protein. Nature *404*, 151–158.

Kim, N., Stiegler, A.L., Cameron, T.O., Hallock, P.T., Gomez, A.M., Huang, J.H., Hubbard, S.R., Dustin, M.L., and Burden, S.J. (2008). Lrp4 is a receptor for Agrin and forms a complex with MuSK. Cell *135*, 334–342.

Kim, Y., Sharov, A.A., McDole, K., Cheng, M., Hao, H., Fan, C.-M., Gaiano, N., Ko, M.S.H., and Zheng, Y. (2011). Mouse B-type lamins are required for proper organogenesis but not by embryonic stem cells. Science *334*, 1706–1710.

Kimura, T., Pace, S.M., Wei, L., Beard, N.A., Dirksen, R.T., and Dulhunty, A.F. (2007). A variably spliced region in the type 1 ryanodine receptor may participate in an inter-domain interaction. Biochem. J. *401*, 317–324.

King, S.J., Nowak, K., Suryavanshi, N., Holt, I., Shanahan, C.M., and Ridley, A.J. (2014). Nesprin-1 and nesprin-2 regulate endothelial cell shape and migration. Cytoskelet. Hoboken NJ *71*, 423–434.

Konieczny, P., Fuchs, P., Reipert, S., Kunz, W.S., Zeöld, A., Fischer, I., Paulin, D., Schröder, R., and Wiche, G. (2008a). Myofiber integrity depends on desmin network targeting to Z-disks and costameres via distinct plectin isoforms. J. Cell Biol. *181*, 667–681.

Konieczny, P., Fuchs, P., Reipert, S., Kunz, W.S., Zeöld, A., Fischer, I., Paulin, D., Schröder, R., and Wiche, G. (2008b). Myofiber integrity depends on desmin network targeting to Z-disks and costameres via distinct plectin isoforms. J. Cell Biol. *181*, 667–681.

Korobova, F., and Svitkina, T. (2008). Arp2/3 Complex Is Important for Filopodia Formation, Growth Cone Motility, and Neuritogenesis in Neuronal Cells. Mol. Biol. Cell *19*, 1561–1574.

Kovacs, E.M., Goodwin, M., Ali, R.G., Paterson, A.D., and Yap, A.S. (2002). Cadherin-directed actin assembly: E-cadherin physically associates with the Arp2/3 complex to direct actin assembly in nascent adhesive contacts. Curr. Biol. CB *12*, 379–382.

Kreishman-Deitrick, M., Goley, E.D., Burdine, L., Denison, C., Egile, C., Li, R., Murali, N., Kodadek, T.J., Welch, M.D., and Rosen, M.K. (2005). NMR analyses of the activation of the Arp2/3 complex by neuronal Wiskott-Aldrich syndrome protein. Biochemistry (Mosc.) *44*, 15247–15256.

Krueger, E.W., Orth, J.D., Cao, H., and McNiven, M.A. (2003). A dynamin-cortactin-Arp2/3 complex mediates actin reorganization in growth factor-stimulated cells. Mol. Biol. Cell *14*, 1085–1096.

Lambrechts, A., Gevaert, K., Cossart, P., Vandekerckhove, J., and Van Troys, M. (2008). Listeria comet tails: the actin-based motility machinery at work. Trends Cell Biol. *18*, 220–227.

Lammerding, J., Schulze, P.C., Takahashi, T., Kozlov, S., Sullivan, T., Kamm, R.D., Stewart, C.L., and Lee, R.T. (2004a). Lamin A/C deficiency causes defective nuclear mechanics and mechanotransduction. J. Clin. Invest. *113*, 370–378.

Lammerding, J., Schulze, P.C., Takahashi, T., Kozlov, S., Sullivan, T., Kamm, R.D., Stewart, C.L., and Lee, R.T. (2004b). Lamin A/C deficiency causes defective nuclear mechanics and mechanotransduction. J. Clin. Invest. *113*, 370–378.

Lammerding, J., Fong, L.G., Ji, J.Y., Reue, K., Stewart, C.L., Young, S.G., and Lee, R.T. (2006). Lamins A and C but Not Lamin B1 Regulate Nuclear Mechanics. J. Biol. Chem. *281*, 25768–25780.

Laporte, J., Blondeau, F., Gansmuller, A., Lutz, Y., Vonesch, J.-L., and Mandel, J.-L. (2002). The PtdIns3P phosphatase myotubularin is a cytoplasmic protein that also localizes to Rac1-inducible plasma membrane ruffles. J. Cell Sci. *115*, 3105–3117.

Le Clainche, C., Didry, D., Carlier, M.F., and Pantaloni, D. (2001). Activation of Arp2/3 complex by Wiskott-Aldrich Syndrome protein is linked to enhanced binding of ATP to Arp2. J. Biol. Chem. *276*, 46689–46692.

Le Clainche, C., Pantaloni, D., and Carlier, M.-F. (2003). ATP hydrolysis on actin-related protein 2/3 complex causes debranching of dendritic actin arrays. Proc. Natl. Acad. Sci. U. S. A. *100*, 6337–6342.

Lecompte, O., Poch, O., and Laporte, J. (2008). PtdIns5P regulation through evolution: roles in membrane trafficking? Trends Biochem. Sci. *33*, 453–460.

Lei, K., Zhang, X., Ding, X., Guo, X., Chen, M., Zhu, B., Xu, T., Zhuang, Y., Xu, R., and Han, M. (2009). SUN1 and SUN2 play critical but partially redundant roles in

anchoring nuclei in skeletal muscle cells in mice. Proc. Natl. Acad. Sci. U. S. A. *106*, 10207–10212.

Leng, Y., Zhang, J., Badour, K., Arpaia, E., Freeman, S., Cheung, P., Siu, M., and Siminovitch, K. (2005). Abelson-interactor-1 promotes WAVE2 membrane translocation and Abelson-mediated tyrosine phosphorylation required for WAVE2 activation. Proc. Natl. Acad. Sci. U. S. A. *102*, 1098–1103.

Loisel, T.P., Boujemaa, R., Pantaloni, D., and Carlier, M.F. (1999). Reconstitution of actin-based motility of Listeria and Shigella using pure proteins. Nature *401*, 613–616.

Ludtke, S.J., Serysheva, I.I., Hamilton, S.L., and Chiu, W. (2005). The Pore Structure of the Closed RyR1 Channel. Struct. Lond. Engl. 1993 *13*, 1203–1211.

Luxton, G.W.G., Gomes, E.R., Folker, E.S., Vintinner, E., and Gundersen, G.G. (2010). Linear arrays of nuclear envelope proteins harness retrograde actin flow for nuclear movement. Science *329*, 956–959.

Machesky, L.M., and Insall, R.H. (1998). Scar1 and the related Wiskott-Aldrich syndrome protein, WASP, regulate the actin cytoskeleton through the Arp2/3 complex. Curr. Biol. CB *8*, 1347–1356.

Machesky, L.M., Atkinson, S.J., Ampe, C., Vandekerckhove, J., and Pollard, T.D. (1994). Purification of a cortical complex containing two unconventional actins from Acanthamoeba by affinity chromatography on profilin-agarose. J. Cell Biol. *127*, 107–115.

Machesky, L.M., Reeves, E., Wientjes, F., Mattheyse, F.J., Grogan, A., Totty, N.F., Burlingame, A.L., Hsuan, J.J., and Segal, A.W. (1997). Mammalian actin-related protein 2/3 complex localizes to regions of lamellipodial protrusion and is composed of evolutionarily conserved proteins. Biochem. J. *328 (Pt 1)*, 105–112.

Machesky, L.M., Mullins, R.D., Higgs, H.N., Kaiser, D.A., Blanchoin, L., May, R.C., Hall, M.E., and Pollard, T.D. (1999). Scar, a WASp-related protein, activates nucleation of actin filaments by the Arp2/3 complex. Proc. Natl. Acad. Sci. *96*, 3739–3744.

Martin, A.C., Xu, X.-P., Rouiller, I., Kaksonen, M., Sun, Y., Belmont, L., Volkmann, N., Hanein, D., Welch, M., and Drubin, D.G. (2005). Effects of Arp2 and Arp3 nucleotide-binding pocket mutations on Arp2/3 complex function. J. Cell Biol. *168*, 315–328.

Martin, A.C., Welch, M.D., and Drubin, D.G. (2006). Arp2/3 ATP hydrolysis-catalysed branch dissociation is critical for endocytic force generation. Nat. Cell Biol. *8*, 826–833.

Martinez-Quiles, N., Rohatgi, R., Antón, I.M., Medina, M., Saville, S.P., Miki, H., Yamaguchi, H., Takenawa, T., Hartwig, J.H., Geha, R.S., et al. (2001). WIP regulates N-WASP-mediated actin polymerization and filopodium formation. Nat. Cell Biol. *3*, 484–491.

Merlie, J.P., and Sanes, J.R. (1985). Concentration of acetylcholine receptor mRNA in synaptic regions of adult muscle fibres. Nature *317*, 66–68.

Merrifield, C.J., Qualmann, B., Kessels, M.M., and Almers, W. (2004). Neural Wiskott Aldrich Syndrome Protein (N-WASP) and the Arp2/3 complex are recruited to sites of clathrin-mediated endocytosis in cultured fibroblasts. Eur. J. Cell Biol. *83*, 13–18.

Merrifield, C.J., Perrais, D., and Zenisek, D. (2005). Coupling between clathrin-coated-pit invagination, cortactin recruitment, and membrane scission observed in live cells. Cell *121*, 593–606.

Metzger, T., Gache, V., Xu, M., Cadot, B., Folker, E.S., Richardson, B.E., Gomes, E.R., and Baylies, M.K. (2012a). MAP and kinesin-dependent nuclear positioning is required for skeletal muscle function. Nature *484*, 120–124.

Metzger, T., Gache, V., Xu, M., Cadot, B., Folker, E.S., Richardson, B.E., Gomes, E.R., and Baylies, M.K. (2012b). MAP and kinesin-dependent nuclear positioning is required for skeletal muscle function. Nature *484*, 120–124.

Metzger, T., Gache, V., Xu, M., Cadot, B., Folker, E.S., Richardson, B.E., Gomes, E.R., and Baylies, M.K. (2012c). MAP and kinesin-dependent nuclear positioning is required for skeletal muscle function. Nature *484*, 120–124.

Miki, H., Miura, K., and Takenawa, T. (1996). N-WASP, a novel actin-depolymerizing protein, regulates the cortical cytoskeletal rearrangement in a PIP2-dependent manner downstream of tyrosine kinases. EMBO J. *15*, 5326–5335.

Miki, H., Sasaki, T., Takai, Y., and Takenawa, T. (1998). Induction of filopodium formation by a WASP-related actin-depolymerizing protein N-WASP. Nature *391*, 93–96.

Mooren, O.L., Kotova, T.I., Moore, A.J., and Schafer, D.A. (2009). Dynamin2 GTPase and cortactin remodel actin filaments. J. Biol. Chem. *284*, 23995–24005.

Muchir, A., Bonne, G., Kooi, A.J. van der, Meegen, M. van, Baas, F., Bolhuis, P.A., Visser, M. de, and Schwartz, K. (2000). Identification of mutations in the gene encoding lamins A/C in autosomal dominant limb girdle muscular dystrophy with atrioventricular conduction disturbances (LGMD1B). Hum. Mol. Genet. *9*, 1453–1459.

Muchir, A., Pavlidis, P., Decostre, V., Herron, A.J., Arimura, T., Bonne, G., and Worman, H.J. (2007). Activation of MAPK pathways links LMNA mutations to cardiomyopathy in Emery-Dreifuss muscular dystrophy. J. Clin. Invest. *117*, 1282–1293.

Mullins, R.D., Heuser, J.A., and Pollard, T.D. (1998). The interaction of Arp2/3 complex with actin: nucleation, high affinity pointed end capping, and formation of branching networks of filaments. Proc. Natl. Acad. Sci. U. S. A. *95*, 6181–6186.

Nakai, J., Tanabe, T., Konno, T., Adams, B., and Beam, K.G. (1998). Localization in the II-III loop of the dihydropyridine receptor of a sequence critical for excitation-contraction coupling. J. Biol. Chem. *273*, 24983–24986.

Nicot, A.-S., Toussaint, A., Tosch, V., Kretz, C., Wallgren-Pettersson, C., Iwarsson, E., Kingston, H., Garnier, J.-M., Biancalana, V., Oldfors, A., et al. (2007a). Mutations in

amphiphysin 2 (BIN1) disrupt interaction with dynamin 2 and cause autosomal recessive centronuclear myopathy. Nat. Genet. *39*, 1134–1139.

Nicot, A.-S., Toussaint, A., Tosch, V., Kretz, C., Wallgren-Pettersson, C., Iwarsson, E., Kingston, H., Garnier, J.-M., Biancalana, V., Oldfors, A., et al. (2007b). Mutations in amphiphysin 2 (BIN1) disrupt interaction with dynamin 2 and cause autosomal recessive centronuclear myopathy. Nat. Genet. *39*, 1134–1139.

Niebuhr, K., Ebel, F., Frank, R., Reinhard, M., Domann, E., Carl, U.D., Walter, U., Gertler, F.B., Wehland, J., and Chakraborty, T. (1997). A novel proline-rich motif present in ActA of Listeria monocytogenes and cytoskeletal proteins is the ligand for the EVH1 domain, a protein module present in the Ena/VASP family. EMBO J. *16*, 5433–5444.

Nolen, B.J., Tomasevic, N., Russell, A., Pierce, D.W., Jia, Z., McCormick, C.D., Hartman, J., Sakowicz, R., and Pollard, T.D. (2009). Characterization of two classes of small molecule inhibitors of Arp2/3 complex. Nature *460*, 1031–1034.

Nowak, K.J., Ravenscroft, G., Jackaman, C., Filipovska, A., Davies, S.M., Lim, E.M., Squire, S.E., Potter, A.C., Baker, E., Clément, S., et al. (2009). Rescue of skeletal muscle alpha-actin-null mice by cardiac (fetal) alpha-actin. J. Cell Biol. *185*, 903–915.

Nozumi, M., Nakagawa, H., Miki, H., Takenawa, T., and Miyamoto, S. (2003). Differential localization of WAVE isoforms in filopodia and lamellipodia of the neuronal growth cone. J. Cell Sci. *116*, 239–246.

Ochs, H.D., and Notarangelo, L.D. (2005). Structure and function of the Wiskott-Aldrich syndrome protein. Curr. Opin. Hematol. *12*, 284–291.

Okamoto, P.M., Gamby, C., Wells, D., Fallon, J., and Vallee, R.B. (2001). Dynamin isoform-specific interaction with the shank/ProSAP scaffolding proteins of the postsynaptic density and actin cytoskeleton. J. Biol. Chem. *276*, 48458–48465.

Osborne, J.P., Murphy, E.G., and Hill, A. (1983). Thin ribs on chest X-ray: a useful sign in the differential diagnosis of the floppy newborn. Dev. Med. Child Neurol. *25*, 343–345.

Ostlund, C., Folker, E.S., Choi, J.C., Gomes, E.R., Gundersen, G.G., and Worman, H.J. (2009). Dynamics and molecular interactions of linker of nucleoskeleton and cytoskeleton (LINC) complex proteins. J. Cell Sci. *122*, 4099–4108.

Owen, D.J., Wigge, P., Vallis, Y., Moore, J.D., Evans, P.R., and McMahon, H.T. (1998). Crystal structure of the amphiphysin-2 SH3 domain and its role in the prevention of dynamin ring formation. EMBO J. *17*, 5273–5285.

Palazzo, A.F., Joseph, H.L., Chen, Y.J., Dujardin, D.L., Alberts, A.S., Pfister, K.K., Vallee, R.B., and Gundersen, G.G. (2001). Cdc42, dynein, and dynactin regulate MTOC reorientation independent of Rho-regulated microtubule stabilization. Curr. Biol. CB *11*, 1536–1541.

Paluch, E.K., and Raz, E. (2013a). The role and regulation of blebs in cell migration. Curr. Opin. Cell Biol. *25*, 582–590.

Paluch, E.K., and Raz, E. (2013b). The role and regulation of blebs in cell migration. Curr. Opin. Cell Biol. *25*, 582–590.

Panchal, S.C., Kaiser, D.A., Torres, E., Pollard, T.D., and Rosen, M.K. (2003). A conserved amphipathic helix in WASP/Scar proteins is essential for activation of Arp2/3 complex. Nat. Struct. Biol. *10*, 591–598.

Perrin, B.J., and Ervasti, J.M. (2010). The actin gene family: function follows isoform. Cytoskelet. Hoboken NJ *67*, 630–634.

Peter, B.J., Kent, H.M., Mills, I.G., Vallis, Y., Butler, P.J.G., Evans, P.R., and McMahon, H.T. (2004). BAR domains as sensors of membrane curvature: the amphiphysin BAR structure. Science *303*, 495–499.

Petrie, R.J., Koo, H., and Yamada, K.M. (2014). Generation of compartmentalized pressure by a nuclear piston governs cell motility in a 3D matrix. Science *345*, 1062–1065.

Pizarro-Cerdá, J., and Cossart, P. (2006). Subversion of cellular functions by Listeria monocytogenes. J. Pathol. *208*, 215–223.

Pollard, T.D., and Borisy, G.G. (2003). Cellular motility driven by assembly and disassembly of actin filaments. Cell *112*, 453–465.

Prehoda, K.E., Scott, J.A., Mullins, R.D., and Lim, W.A. (2000). Integration of multiple signals through cooperative regulation of the N-WASP-Arp2/3 complex. Science *290*, 801–806.

Previtali, S.C., Zerega, B., Sherman, D.L., Brophy, P.J., Dina, G., King, R.H.M., Salih, M.M., Feltri, L., Quattrini, A., Ravazzolo, R., et al. (2003). Myotubularin-related 2 protein phosphatase and neurofilament light chain protein, both mutated in CMT neuropathies, interact in peripheral nerve. Hum. Mol. Genet. *12*, 1713–1723.

Prins, K.W., Call, J.A., Lowe, D.A., and Ervasti, J.M. (2011). Quadriceps myopathy caused by skeletal muscle-specific ablation of β(cyto)-actin. J. Cell Sci. *124*, 951–957.

Quijano-Roy, S., Mbieleu, B., Bönnemann, C.G., Jeannet, P.-Y., Colomer, J., Clarke, N.F., Cuisset, J.-M., Roper, H., De Meirleir, L., D'Amico, A., et al. (2008). De novo LMNA mutations cause a new form of congenital muscular dystrophy. Ann. Neurol. *64*, 177–186.

Ralston, E., Lu, Z., Biscocho, N., Soumaka, E., Mavroidis, M., Prats, C., Lømo, T., Capetanaki, Y., and Ploug, T. (2006). Blood vessels and desmin control the positioning of nuclei in skeletal muscle fibers. J. Cell. Physiol. *209*, 874–882.

Ramesh, N., Antón, I.M., Hartwig, J.H., and Geha, R.S. (1997). WIP, a protein associated with wiskott-aldrich syndrome protein, induces actin polymerization and redistribution in lymphoid cells. Proc. Natl. Acad. Sci. U. S. A. *94*, 14671–14676.

Rebbeck, R.T., Karunasekara, Y., Board, P.G., Beard, N.A., Casarotto, M.G., and Dulhunty, A.F. (2014). Skeletal muscle excitation-contraction coupling: who are the dancing partners? Int. J. Biochem. Cell Biol. *48*, 28–38.

Renganathan, M., Messi, M.L., and Delbono, O. (1997). Dihydropyridine receptor-ryanodine receptor uncoupling in aged skeletal muscle. J. Membr. Biol. *157*, 247–253.

Rodal, A.A., Sokolova, O., Robins, D.B., Daugherty, K.M., Hippenmeyer, S., Riezman, H., Grigorieff, N., and Goode, B.L. (2005). Conformational changes in the Arp2/3 complex leading to actin nucleation. Nat. Struct. Mol. Biol. *12*, 26–31.

Rogers, S.L., Wiedemann, U., Stuurman, N., and Vale, R.D. (2003). Molecular requirements for actin-based lamella formation in Drosophila S2 cells. J. Cell Biol. *162*, 1079–1088.

Rohatgi, R., Ho, H.Y., and Kirschner, M.W. (2000). Mechanism of N-WASP activation by CDC42 and phosphatidylinositol 4, 5-bisphosphate. J. Cell Biol. *150*, 1299–1310.

Romero, N.B. (2010). Centronuclear myopathies: A widening concept. Neuromuscul. Disord. *20*, 223–228.

Romero, N.B., and Bitoun, M. (2011). Centronuclear Myopathies. Semin. Pediatr. Neurol. *18*, 250–256.

Rottner, K., Hänisch, J., and Campellone, K.G. (2010). WASH, WHAMM and JMY: regulation of Arp2/3 complex and beyond. Trends Cell Biol. *20*, 650–661.

Rotty, J.D., Wu, C., and Bear, J.E. (2012). New insights into the regulation and cellular functions of the ARP2/3 complex. Nat. Rev. Mol. Cell Biol.

Rouiller, I., Xu, X.-P., Amann, K.J., Egile, C., Nickell, S., Nicastro, D., Li, R., Pollard, T.D., Volkmann, N., and Hanein, D. (2008). The structural basis of actin filament branching by the Arp2/3 complex. J. Cell Biol. *180*, 887–895.

Rousset, M., Charnet, P., and Cens, T. (2005). [Structure of the calcium channel beta subunit: the place of the beta-interaction domain]. Médecine Sci. MS *21*, 279–283.

Rybakova, I.N., Patel, J.R., and Ervasti, J.M. (2000). The Dystrophin Complex Forms a Mechanically Strong Link between the Sarcolemma and Costameric Actin. J. Cell Biol. *150*, 1209–1214.

Sakamuro, D., Elliott, K.J., Wechsler-Reya, R., and Prendergast, G.C. (1996). BIN1 is a novel MYC-interacting protein with features of a tumour suppressor. Nat. Genet. *14*, 69–77.

Sakar, M.S., Neal, D., Boudou, T., Borochin, M.A., Li, Y., Weiss, R., Kamm, R.D., Chen, C.S., and Asada, H.H. (2012). Formation and optogenetic control of engineered 3D skeletal muscle bioactuators. Lab. Chip *12*, 4976–4985.

Schaerer-Brodbeck, C., and Riezman, H. (2000). Functional interactions between the p35 subunit of the Arp2/3 complex and calmodulin in yeast. Mol. Biol. Cell *11*, 1113–1127.

Shawlot, W., Deng, J.M., Fohn, L.E., and Behringer, R.R. (1998). Restricted beta-galactosidase expression of a hygromycin-lacZ gene targeted to the beta-actin locus and embryonic lethality of beta-actin mutant mice. Transgenic Res. *7*, 95–103.

Shekhar, S., Pernier, J., and Carlier, M.-F. (2016). Regulators of actin filament barbed ends at a glance. J. Cell Sci.

Shikama, N., Lee, C.W., France, S., Delavaine, L., Lyon, J., Krstic-Demonacos, M., and La Thangue, N.B. (1999). A novel cofactor for p300 that regulates the p53 response. Mol. Cell *4*, 365–376.

Shimi, T., Pfleghaar, K., Kojima, S., Pack, C.-G., Solovei, I., Goldman, A.E., Adam, S.A., Shumaker, D.K., Kinjo, M., Cremer, T., et al. (2008). The A- and B-type nuclear lamin networks: microdomains involved in chromatin organization and transcription. Genes Dev. *22*, 3409–3421.

Simiczyjew, A., Malicka-Błaszkiewicz, M., and Nowak, D. (2013). [Functional diversification of cytoplasmic actin isoforms]. Postepy Biochem. *59*, 285–294.

Simon, D.N., and Wilson, K.L. (2013). Partners and post-translational modifications of nuclear lamins. Chromosoma *122*, 13–31.

Solecki, D.J., Trivedi, N., Govek, E.-E., Kerekes, R.A., Gleason, S.S., and Hatten, M.E. (2009). Myosin II motors and F-actin dynamics drive the coordinated movement of the centrosome and soma during CNS glial-guided neuronal migration. Neuron *63*, 63–80.

Sonnemann, K.J., Fitzsimons, D.P., Patel, J.R., Liu, Y., Schneider, M.F., Moss, R.L., and Ervasti, J.M. (2006a). Cytoplasmic γ-Actin Is Not Required for Skeletal Muscle Development but Its Absence Leads to a Progressive Myopathy. Dev. Cell *11*, 387–397.

Sonnemann, K.J., Fitzsimons, D.P., Patel, J.R., Liu, Y., Schneider, M.F., Moss, R.L., and Ervasti, J.M. (2006b). Cytoplasmic [gamma]-Actin Is Not Required for Skeletal Muscle Development but Its Absence Leads to a Progressive Myopathy. Dev. Cell *11*, 387–397.

Soulet, F., Schmid, S.L., and Damke, H. (2006). Domain requirements for an endocytosis-independent, isoform-specific function of dynamin-2. Exp. Cell Res. *312*, 3539–3545.

Splinter, D., Tanenbaum, M.E., Lindqvist, A., Jaarsma, D., Flotho, A., Yu, K.L., Grigoriev, I., Engelsma, D., Haasdijk, E.D., Keijzer, N., et al. (2010). Bicaudal D2, Dynein, and Kinesin-1 Associate with Nuclear Pore Complexes and Regulate Centrosome and Nuclear Positioning during Mitotic Entry. PLoS Biol *8*, e1000350.

Stamnes, M. (2002). Regulating the actin cytoskeleton during vesicular transport. Curr. Opin. Cell Biol. *14*, 428–433.

Starr, D.A., and Fridolfsson, H.N. (2010). Interactions Between Nuclei and the Cytoskeleton Are Mediated by SUN-KASH Nuclear-Envelope Bridges. Annu. Rev. Cell Dev. Biol. *26*, 421–444.

Starr, D.A., and Han, M. (2002). Role of ANC-1 in tethering nuclei to the actin cytoskeleton. Science *298*, 406–409.

Staszewska, I., Fischer, I., and Wiche, G. (2015). Plectin isoform 1-dependent nuclear docking of desmin networks affects myonuclear architecture and expression of mechanotransducers. Hum. Mol. Genet. *24*, 7373–7389.

Steffen, A., Faix, J., Resch, G.P., Linkner, J., Wehland, J., Small, J.V., Rottner, K., and Stradal, T.E.B. (2006). Filopodia formation in the absence of functional WAVE- and Arp2/3-complexes. Mol. Biol. Cell *17*, 2581–2591.

Stovold, C.F., Millard, T.H., and Machesky, L.M. (2005). Inclusion of Scar/WAVE3 in a similar complex to Scar/WAVE1 and 2. BMC Cell Biol. *6*, 11.

Suetsugu, S., Kurisu, S., Oikawa, T., Yamazaki, D., Oda, A., and Takenawa, T. (2006). Optimization of WAVE2 complex-induced actin polymerization by membrane-bound IRSp53, PIP(3), and Rac. J. Cell Biol. *173*, 571–585.

Svitkina, T.M., and Borisy, G.G. (1999). Arp2/3 complex and actin depolymerizing factor/cofilin in dendritic organization and treadmilling of actin filament array in lamellipodia. J. Cell Biol. *145*, 1009–1026.

Swift, J., Ivanovska, I.L., Buxboim, A., Harada, T., Dingal, P.C.D.P., Pinter, J., Pajerowski, J.D., Spinler, K.R., Shin, J.-W., Tewari, M., et al. (2013). Nuclear lamin-A scales with tissue stiffness and enhances matrix-directed differentiation. Science *341*, 1240104.

Takano, K., Watanabe-Takano, H., Suetsugu, S., Kurita, S., Tsujita, K., Kimura, S., Karatsu, T., Takenawa, T., and Endo, T. (2010). Nebulin and N-WASP Cooperate to Cause IGF-1-Induced Sarcomeric Actin Filament Formation. Science *330*, 1536–1540.

Takekura, H., Flucher, B.E., and Franzini-Armstrong, C. (2001). Sequential docking, molecular differentiation, and positioning of T-Tubule/SR junctions in developing mouse skeletal muscle. Dev. Biol. *239*, 204–214.

Takenawa, T., and Miki, H. (2001). WASP and WAVE family proteins: key molecules for rapid rearrangement of cortical actin filaments and cell movement. J. Cell Sci. *114*, 1801–1809.

Takenawa, T., and Suetsugu, S. (2007). The WASP–WAVE protein network: connecting the membrane to the cytoskeleton. Nat. Rev. Mol. Cell Biol. *8*, 37–48.

Tang, W., Sencer, S., and Hamilton, S.L. (2002). Calmodulin modulation of proteins involved in excitation-contraction coupling. Front. Biosci. J. Virtual Libr. *7*, d1583-1589.

Taylor, G.S., Maehama, T., and Dixon, J.E. (2000). Myotubularin, a protein tyrosine phosphatase mutated in myotubular myopathy, dephosphorylates the lipid second messenger, phosphatidylinositol 3-phosphate. Proc. Natl. Acad. Sci. U. S. A. *97*, 8910–8915.

Teeuw, A.H., Barth, P.G., van Sonderen, L., and Zondervan, H.A. (1993). [3 examples of fetal genetic neuromuscular disorders which lead to hydramnion]. Ned. Tijdschr. Geneeskd. *137*, 908–913.

Thiam, H.-R., Vargas, P., Carpi, N., Crespo, C.L., Raab, M., Terriac, E., King, M.C., Jacobelli, J., Alberts, A.S., Stradal, T., et al. (2016). Perinuclear Arp2/3-driven actin polymerization enables nuclear deformation to facilitate cell migration through complex environments. Nat. Commun. *7*, 10997.

Thrasher, A.J. (2002). WASp in immune-system organization and function. Nat. Rev. Immunol. *2*, 635–646.

Toussaint, A., Cowling, B.S., Hnia, K., Mohr, M., Oldfors, A., Schwab, Y., Yis, U., Maisonobe, T., Stojkovic, T., Wallgren-Pettersson, C., et al. (2010). Defects in amphiphysin 2 (BIN1) and triads in several forms of centronuclear myopathies. Acta Neuropathol. (Berl.) *121*, 253–266.

Tran, P.T., Marsh, L., Doye, V., Inoué, S., and Chang, F. (2001). A mechanism for nuclear positioning in fission yeast based on microtubule pushing. J. Cell Biol. *153*, 397–411.

Tsai, J.-W., Lian, W.-N., Kemal, S., Kriegstein, A.R., and Vallee, R.B. (2010). Kinesin 3 and cytoplasmic dynein mediate interkinetic nuclear migration in neural stem cells. Nat. Neurosci. *13*, 1463–1471.

Tsujita, K., Itoh, T., Ijuin, T., Yamamoto, A., Shisheva, A., Laporte, J., and Takenawa, T. (2004). Myotubularin regulates the function of the late endosome through the gram domain-phosphatidylinositol 3,5-bisphosphate interaction. J. Biol. Chem. *279*, 13817–13824.

Vajsar, J., Becker, L.E., Freedom, R.M., and Murphy, E.G. (1993). Familial desminopathy: myopathy with accumulation of desmin-type intermediate filaments. J. Neurol. Neurosurg. Psychiatry *56*, 644–648.

Vander, A.J. (2011). Vander's Human Physiology: The Mechanisms of Body Function (McGraw-Hill).

Vernengo, L., Chourbagi, O., Panuncio, A., Lilienbaum, A., Batonnet-Pichon, S., Bruston, F., Rodrigues-Lima, F., Mesa, R., Pizzarossa, C., Demay, L., et al. (2010). Desmin myopathy with severe cardiomyopathy in a Uruguayan family due to a codon deletion in a new location within the desmin 1A rod domain. Neuromuscul. Disord. NMD *20*, 178–187.

Volkman, B.F., Prehoda, K.E., Scott, J.A., Peterson, F.C., and Lim, W.A. (2002). Structure of the N-WASP EVH1 domain-WIP complex: insight into the molecular basis of Wiskott-Aldrich Syndrome. Cell *111*, 565–576.

Vos, W.H.D., Houben, F., Kamps, M., Malhas, A., Verheyen, F., Cox, J., Manders, E.M.M., Verstraeten, V.L.R.M., Steensel, M.A.M. van, Marcelis, C.L.M., et al. (2011). Repetitive disruptions of the nuclear envelope invoke temporary loss of cellular compartmentalization in laminopathies. Hum. Mol. Genet. *20*, 4175–4186.

Wada, K.-I., Katsuta, S., and Soya, H. (2008). Formation process and fate of the nuclear chain after injury in regenerated myofiber. Anat. Rec. Hoboken NJ 2007 *291*, 122–128.

Warnock, D.E., Baba, T., and Schmid, S.L. (1997). Ubiquitously expressed dynamin-II has a higher intrinsic GTPase activity and a greater propensity for self-assembly than neuronal dynamin-I. Mol. Biol. Cell *8*, 2553–2562.

Weaver, A.M., Heuser, J.E., Karginov, A.V., Lee, W., Parsons, J.T., and Cooper, J.A. (2002). Interaction of cortactin and N-WASp with Arp2/3 complex. Curr. Biol. CB *12*, 1270–1278.

Weiss, R.G., O'Connell, K.M.S., Flucher, B.E., Allen, P.D., Grabner, M., and Dirksen, R.T. (2004). Functional analysis of the R1086H malignant hyperthermia mutation in the DHPR reveals an unexpected influence of the III-IV loop on skeletal muscle EC coupling. Am. J. Physiol. Cell Physiol. *287*, C1094-1102.

Welch, M.D., DePace, A.H., Verma, S., Iwamatsu, A., and Mitchison, T.J. (1997). The human Arp2/3 complex is composed of evolutionarily conserved subunits and is localized to cellular regions of dynamic actin filament assembly. J. Cell Biol. *138*, 375–384.

Welch, M.D., Rosenblatt, J., Skoble, J., Portnoy, D.A., and Mitchison, T.J. (1998). Interaction of human Arp2/3 complex and the Listeria monocytogenes ActA protein in actin filament nucleation. Science *281*, 105–108.

Wilson, M.H., and Holzbaur, E.L.F. (2015a). Nesprins anchor kinesin-1 motors to the nucleus to drive nuclear distribution in muscle cells. Dev. Camb. Engl. *142*, 218–228.

Wilson, M.H., and Holzbaur, E.L.F. (2015b). Nesprins anchor kinesin-1 motors to the nucleus to drive nuclear distribution in muscle cells. Development *142*, 218–228.

Winter, L., and Wiche, G. (2013). The many faces of plectin and plectinopathies: pathology and mechanisms. Acta Neuropathol. (Berl.) *125*, 77–93.

Xu, X.-P., Rouiller, I., Slaughter, B.D., Egile, C., Kim, E., Unruh, J.R., Fan, X., Pollard, T.D., Li, R., Hanein, D., et al. (2012). Three-dimensional reconstructions of Arp2/3 complex with bound nucleation promoting factors. EMBO J. *31*, 236–247.

Yamada, H., Padilla-Parra, S., Park, S.-J., Itoh, T., Chaineau, M., Monaldi, I., Cremona, O., Benfenati, F., De Camilli, P., Coppey-Moisan, M., et al. (2009). Dynamic Interaction of Amphiphysin with N-WASP Regulates Actin Assembly. J. Biol. Chem. *284*, 34244–34256.

Yarar, D., To, W., Abo, A., and Welch, M.D. (1999). The Wiskott–Aldrich syndrome protein directs actin-based motility by stimulating actin nucleation with the Arp2/3 complex. Curr. Biol. *9*, 555-S1.

Yoshikawa, Y., Yasuike, T., Yagi, A., and Yamada, T. (1999). Transverse elasticity of myofibrils of rabbit skeletal muscle studied by atomic force microscopy. Biochem. Biophys. Res. Commun. *256*, 13–19.

Yu, H., Chen, J.K., Feng, S., Dalgarno, D.C., Brauer, A.W., and Schreiber, S.L. (1994). Structural basis for the binding of proline-rich peptides to SH3 domains. Cell *76*, 933–945.

Zalevsky, J., Grigorova, I., and Mullins, R.D. (2001a). Activation of the Arp2/3 complex by the Listeria acta protein. Acta binds two actin monomers and three subunits of the Arp2/3 complex. J. Biol. Chem. *276*, 3468–3475.

Zalevsky, J., Lempert, L., Kranitz, H., and Mullins, R.D. (2001b). Different WASP family proteins stimulate different Arp2/3 complex-dependent actin-nucleating activities. Curr. Biol. CB *11*, 1903–1913.

Zhang, J., Felder, A., Liu, Y., Guo, L.T., Lange, S., Dalton, N.D., Gu, Y., Peterson, K.L., Mizisin, A.P., Shelton, G.D., et al. (2010). Nesprin 1 is critical for nuclear positioning and anchorage. Hum. Mol. Genet. *19*, 329–341.

Zhang, Q., Ragnauth, C.D., Skepper, J.N., Worth, N.F., Warren, D.T., Roberts, R.G., Weissberg, P.L., Ellis, J.A., and Shanahan, C.M. (2005). Nesprin-2 is a multi-isomeric protein that binds lamin and emerin at the nuclear envelope and forms a subcellular network in skeletal muscle. J. Cell Sci. *118*, 673–687.

Zhang, X., Xu, R., Zhu, B., Yang, X., Ding, X., Duan, S., Xu, T., Zhuang, Y., and Han, M. (2007). Syne-1 and Syne-2 play crucial roles in myonuclear anchorage and motor neuron innervation. Dev. Camb. Engl. *134*, 901–908.

Zhao, T., Graham, O.S., Raposo, A., and St. Johnston, D. (2012). Growing Microtubules Push the Oocyte Nucleus to Polarize the Drosophila Dorsal-Ventral Axis. Science.

Zhao, X., Yang, Z., Qian, M., and Zhu, X. (2001). Interactions among subunits of human Arp2/3 complex: p20-Arc as the hub. Biochem. Biophys. Res. Commun. *280*, 513–517.